Traitement automatique du signal pour la surveillance vibratoire des éoliennes : recadrage temps-fréquence, association cinématique et démodulation multi-bandes

Marcin Firla

Communauté
UNIVERSITÉ Grenoble Alpes

THÈSE

Pour obtenir le grade de

DOCTEUR DE LA COMMUNAUTÉ UNIVERSITÉ GRENOBLE ALPES

Spécialité : **Signal, Image, Parole, Télécoms (SIPT)**

Arrêté ministériel : 7 août 2006

Présentée par
Marcin FIRLA

Thèse dirigée par **Nadine MARTIN** et
codirigée par **Tomasz BARSZCZ**

préparée au sein du **laboratoire Grenoble Images Parole Signal Automatique (GIPSA-Lab)**
dans **l'école doctorale Electronique, Electrotechnique, Automatique, Traitement du Signal (EEATS)**

Automatic Signal Processing for Wind Turbine Condition Monitoring. Time-Frequency Cropping, Kinematic Association, and All-Sideband Demodulation.

Thèse soutenue publiquement le **21 janvier 2016**,
devant le jury composé de :

Jérôme MARS
Professeur, G-INP, Grenoble, Examinateur, Président du jury
Radoslaw ZIMROZ
Professeur, Wroclaw University of Technology, Pologne, Rapporteur
Mohamed EL BADAOUI
Professeur, Saint Etienne University, Roanne, Rapporteur
Fabien MILLIOZ
Maître de conférences, Lyon 1 University, Lyon, Examinateur
Nadine MARTIN
Directeur de recherche, CNRS, Grenoble, Directrice de thèse
Tomasz BARSZCZ
Professeur, AGH University of Science and Technology, Pologne, Co-directeur de thèse

Acknowledgements

The Innovation Project 'KAStrion' was supported by KIC InnoEnergy, which is a company supported by the European Institute of Innovation and Technology (EIT), which has the mission of delivering commercial products and services, new businesses, innovators and entrepreneurs in the field of sustainable energy through the integration of higher education, research, entrepreneurs and business companies.

This study was been supported by French Research National Agency (ANR) through the EITE program (project KAStrion ANR-12-EITE-0002-01).

After these official acknowledgements I would like to thank all the people who made my thesis possible.

First of all, I would like to thank Nadine MARTIN and Tomasz BARSZCZ, my supervisors, for their work during the last three years. They enabled me lots of possibilities and help me to reach the place where I am now. I would like to thank Radosław ZIMROZ and Mohamed EL BADAOUI, the reviewers, for their precise analysis of the manuscript and valuable comments. Moreover, I would like to thank Jérôme MARS for accepting the role of the chief examiner and the examiner Fabien MILLIOZ for the interesting questions and remarks. It is my pleasure that all those exceptional researchers were part of my PhD thesis and helped it to come into existence.

I would like to say "thank you" to everyone in GIPSA-Lab including SAIGA team and people whom I had pleasure to work with during my thesis, including Timothée GERBER, Zhongyang LI, Pascal BELLEMAIN, Georgia CABLEA, Pierre GRANJON, Xavier LAVAL, and Guanghan SONG.

I would also like to thank all the industrial partners involved in the Innovation Project KAStrion. This list includes Sophie SIEG-ZIEBA and Nicolas BÉDOUIN who represented CETIM, French research and development unit (`http://www.cetim.fr/en`), Frédéric PREVOST and Alexis LEBRANCHU who worked at French wind turbine operation and maintenance company VALEMO (`http://www.valemo.fr/`), Ceriel TIEMESSEN and Harmen LINKS from MECAL, company providing wind turbine's diagnostic services from the Netherlands (`http://www.mecal.eu/`), and Szczepan POPIELARZ, Adam JABŁOŃSKI, Tomasz MIKOŁAJCZYK, Jarosław PRZYWIECZERSKI, and Tomasz POTACZAŁA who worked at EC Systems, Polish condition monitoring systems producer (`http://www.ec-systems.pl/en/`, as well as an academic companionship in the project including Corinne MAILHES who represented INP Toulouse.

Moreover, I would like to thank the entire KIC community. The list of people that I would like to mention here who were involved in the KIC InnoEnergy PhD School and the

accompanying events is very long and I would not like to omit anybody so I decided not to list the names, but thank all of them together. The KIC activities and people that I have met enriched me in numerous aspects.

Also I would like to thank all the people who supported me during my thesis and are not listed above. Especially a great word of appreciation to all new friends I've made in the laboratory and around it during my thesis. I would not list them since I would like to avoid classifying all those important people, but I believe that they will know that this part is to thank them.

For Natalia and my family.

"Change is the only constant"

Contents

Introduction **1**

1 Synopsis of the Subject **5**

1.1 Motivation 5

1.2 Vibration Signals 9

1.3 Wind Turbine 10

1.4 The State of the Art in the Monitoring of Rotating Machinery Including Wind Turbines 11

1.5 Selected Signal Processing Techniques 16

1.6 Typical Faults 18

1.7 Diagnostic Features 22

1.8 Reliability Analysis 27

1.9 Standards and Regulations 27

1.10 CMS Installation 30

2 AStrion Approach **33**

2.1 System Architecture 33

2.2 Details on Selected AStrion Modules 34

2.3 Outlook of AStrion 38

2.4 Innovation Project KAStrion 39

3 Non-Stationarity of Inputs – AStrion-C **41**

3.1 State of the Art 41

3.2 Stationary Signals 42

3.3 Cropping out a Time-Frequency Representation 43

3.4 Validation on a Simulated Signal 47

3.5 Conclusions and Perspectives 51

4 Integration with Kinematic Information – AStrion-K 53

4.1 State of the Art 53

4.2 Characteristic Fault Frequency Association 56

4.3 Validation 60

4.4 Conclusions and Perspectives 64

5 All-Sidebands Demodulation – AStrion-M 67

5.1 State of the Art 67

5.2 Details of Algorithm 69

5.3 Validation on Simulated Signal 76

5.4 Conclusions and Perspectives 81

6 Validation of Methods on Real-world Signals 83

6.1 Test Rig Data – CETIM 83

6.2 Wind Turbine Data – Arfons 88

6.3 Case Study 1 – AStrion-C on Non-stationary CETIM Data 91

6.4 Case Study 2 – AStrion-C on Highly Non-stationary Arfons Data 94

6.5 Case Study 3 – AStrion-K on CETIM Data 100

6.6 Case Study 4 – AStrion-K on WT's Vibration Signals 103

6.7 Case Study 5 – AStrion-K on Electrical Data 105

6.8 Case Study 6 – AStrion-KM on Arfons Data 110

6.9 Case Study 7 – AStrion-M on CETIM High Degradation Test 114

Conclusions and Perspectives 123

List of Acronyms 127

List of Figures 129

List of Tables **135**

Bibliography **139**

A List of Publications **157**

B French Summary – Résumé en français (French) **159**

B.1 Introduction 159

B.2 Proposition des 3 méthodes automatiques pour le traitement du signal 161

B.3 Présentation des résultats 168

B.4 Conclusions et perspectives 182

Introduction

The rapid development of information technology is omnipresent. It concerns also the abilities for signal processing. Thanks to the ongoing development of digital techniques the analogue signal processing is improved in the digitalized form. The usage of numerical methods has allowed for the introduction of complex post-processing techniques. What is more, the state of the current technology makes possible the usage of compound and CPU demanding algorithms in real time signal processing systems. These circumstances open up the possibility for the implementation of advanced signal processing methods in the practical application and not only for academic considerations. This work presents an attempt to use the advanced signal processing algorithms in monitoring the health of machinery.

One of the basic operations needed for machines' monitoring and diagnostics purposes is a spectrum estimation. It is well known that there is a variety of methods for computing power spectral density (PSD) of the signal. The main groups contain the non-parametric or classical methods and parametric or modern ones. The non-parametric methods are robust because they do not use any model of the signal. This method is based on the computation of fast Fourier transform (FFT) of the signal and different approaches were proposed [NH92]. The more popular PSD estimation techniques in this group include Periodogram, Correlogram, and combined methods as e.g. Nuttall-Carter. The second group, parametric techniques, assumes a model of the signal which allows to obtain a high resolution of PSD, but is also burden with issues due to modelling errors, namely the value of signal-to-noise ratio (SNR), and high computational requirements.

The presented work concerns a new approach for vibration signal processing with the aim of helping the machinery operators with surveillance of the crucial mechanical components at a plant. Sometimes, it turns out to be necessary to monitor numerous systems or components as it is in the case of big wind farms. These circumstances require a high level of automatization of the monitoring systems. It is already implemented at a simple level by supervisory control and data acquisition (SCADA) systems or condition monitoring systems (CMSs), but usually only the simplest diagnosis methods are adopted. The aim of this thesis is to propose an extension to the abilities of the current CMS by combining it with advanced signal processing methods. It brings the possibility of performing an accurate vibration diagnosis without the help of vibration experts. The implementation of complex and adaptive signal processing algorithms in a present-day CMS opens up the possibility of performing a sophisticated analysis without increasing the workload for the operators and maintenance teams.

In the industry three main strategies of maintenance techniques can be distinguished: breakdown maintenance, time-based preventive maintenance, and condition-based maintenance [Ran11]. This order preserves the historical appearance of each strategy. The first one is also referred to as an unplanned maintenance or run-to-failure maintenance and it is characterised by taking the maintenance action only in the case of the failure of a system. It is still effective for small, simple to repair, and not significant parts of the system. Later,

the strategy of planned maintenance has been introduced. This approach features in periodic replacement of the components without taking into account other factors. The time-based preventive maintenance strategy has a goal of assuring the continuity in the good condition of the system. It is a difficult task to select a proper time intervals for this type of maintenance, since often healthy components are replaced as a result of the application of this approach. Moreover, with the development of modern technology, components became more complex and expensive. Together with the required increase of reliability it causes that the time-based maintenance turns out to be a major expense of many industrial companies [BLJ06]. The third strategy, condition-based maintenance, has a goal to improve the earlier approaches and replace the components based on their health status. It is performed in three main steps: data acquisition, data processing, and maintenance decision making. If all the steps are well designed and correctly implemented, this strategy can bring a significant maintenance cost reduction. Although the condition-based maintenance has been under ongoing development for many years, the surveillance of wind turbines (WTs) is still a challenge. In the case of a WT there is a room for improvement of its lifetime by a better CMS used for condition-based maintenance. More details on this approach are presented in chapter 1. The major focus of this thesis is to propose algorithms for data processing step of the condition-based maintenance strategy.

The applicability of its results constitutes an important aspect of a scientific research. The link between the university and the industry is crucial for providing useful solutions that industry needs and is interested in using. Thanks to such a link the need for an improvement of CMSs has been identified. This research is focused on a particular case of CMS, which is dedicated to WTs. The WT industry has very small financial margins, so it is in constant need to decrease the cost of energy production. One of the aspects to be improved is the maintenance and operational costs of WTs. Thanks to technical possibilities and advanced signal processing algorithms, it is now feasible to detect early stages of some faults, including mainly the defects of mechanical components as rolling-element bearings (REBs) and gearboxes. The sooner the information about upcoming faults is provided to the WT operators, the better preparation for fast repair is feasible. It brings the economical benefits, which is the reason for interest in the technology development from the industry. The academic world is able to propose solutions for this problem and this thesis offers an answer to the needs of the industry.

From the academic point of view the WTs are interesting machines for diagnosis and monitoring. In their case the fault detection task is very challenging due to the nature of their operation. Unlike the majority of machines the WT works under highly non-stationary operational conditions and what is more the exciting force is random and not possible to predict, since it is a blowing wind. The constant changes of the wind speed are the main difficulty for CMS. Thus, this thesis addresses the issue of the non-stationarity in vibration signals.

This thesis proposes the development of advanced signal processing techniques in three aspects, all dedicated but not limited to the diagnosis and condition monitoring of mechanical systems. The automatic and data-driven operation is the common points of proposed methods.

Each algorithm has been designed as a user friendly and features in the self-configuration with a minimal number of parameters possible to adjust, so each method can be used even by a layman in the signal processing.

The first proposed method intends to aid the diagnosis and the condition monitoring of machines working under non-stationary condition. It is always needed for machines operating with constantly varying conditions. As a solution a new approach for cropping out the time-frequency plane based on the non-stationarity detection is proposed. The approach is grounded on the iterative searching through the time-frequency representation of the signal and it is adopted for vibration signals. This method enables the selection of the stationary part of the vibration signals and can be applied in diagnosis and condition monitoring systems.

A knowledge of characteristic frequencies of an investigated system is invariably an advantage in monitoring and diagnostics of the system. Hence, there is a need for automatic usage of this information when available. Therefore, the second proposed algorithms is the automatic association of characteristic fault frequencies according to a kinematic configuration of investigated machine with the detected peaks. The proposed approach is adaptive and features in a unique association of kinematic data with detected pattern in a spectrum of the signal. Moreover, the method has the advantage of taking into account a possible slip of the REBs which is an issue of CMSs that has not yet been addressed.

Demodulation is a powerful tool for machine health diagnostics. However, the existing solutions of its usage in CMSs are not adaptive to the content of the signal. Thus, this thesis proposes the third signal processing technique which is a all-sidebands demodulation process. For each detected sidebands series in the investigated signal the automatic procedure of demodulation is proposed and finally a full-band of the signal is demodulated. This method consists of a multi-rate filtering process, a synchronous averaging, and calculation of the amplitude and frequency modulation functions as well as the computation of features describing the condition of investigated system which has the goal to reveal the faults.

This thesis is organised in such a way to be comprehensible for everyone. Thus, chapter 1 gives a broad overview of topics related to vibration-based condition monitoring and diagnosis of machines focusing mainly on the application to WT's mechanical components as REBs, gearboxes, and shafts. Chapter 2 presents the approach for the signal processing under development for years in GIPSA-lab. It is called AStrion and features in data-driven algorithms, which are universal for diagnosis and condition monitoring. This chapter emphasises the results of the signal interpretation which are used as inputs for proposed signal processing techniques. The first proposed algorithm, cropping out the time-frequency representation, is presented in chapter 3. The second one, kinematic association, is detailed in chapter 4. The last signal processing method, all-sidebands demodulation, is proposed in chapter 5. All the proposed signal processing methods are validated on real-world signals from various sources. Those validations are presented in chapter 6. The thesis is concluded with a summary of the results presented in chapter Conclusions and Perspectives. The advantages of proposed algorithms are listed along with the perspectives for future work.

Chapter 1

Synopsis of the Subject

Contents

1.1 Motivation . . . 5
1.2 Vibration Signals . . . 9
1.3 Wind Turbine . . . 10
1.4 The State of the Art in the Monitoring of Rotating Machinery Including Wind Turbines . . . 11
1.4.1 Vibration of Rotating Machinery . . . 14
1.4.2 Methods of Vibration Spectrum Estimation . . . 16
1.5 Selected Signal Processing Techniques . . . 16
1.5.1 Order Tracking . . . 16
1.5.2 Time Synchronous Averaging . . . 17
1.6 Typical Faults . . . 18
1.6.1 Shaft Problems . . . 18
1.6.2 Rolling-Element Bearing Defects . . . 19
1.6.3 Gear Defects . . . 21
1.7 Diagnostic Features . . . 22
1.7.1 Wide-band Features . . . 22
1.7.2 Narrow-band Features . . . 24
1.7.3 Features of Demodulation Analysis . . . 25
1.8 Reliability Analysis . . . 27
1.9 Standards and Regulations . . . 27
1.10 CMS Installation . . . 30

1.1 Motivation

The amount of WTs is constantly increasing together with installed capacity of electric energy which can be provided by wind energy industry. According to [WWE14a] all wind turbines installed worldwide by mid-2014 can generate around 4% of the world's electricity demand. As it is depicted in Figure 1.1 it is over 336 GW of the energy capacity. New WTs keep being added to the existing ones. The new installed capacity of WTs is presented in Figure 1.2. It

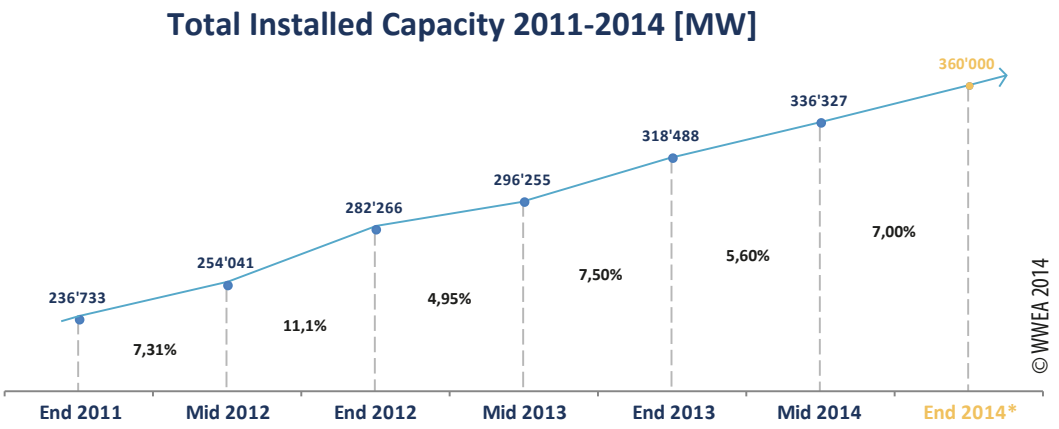

Figure 1.1: The total installed capacity of WT worldwide in the years 2011-2014 [WWE14a].

means that the number of operating WTs is constantly increasing. Moreover, thanks to technology progress the WTs become bigger and more efficient, thus their maintenance becomes more costly.

The wind energy industry is already big and continues to grow. At the end of 2013 there were 241 100 WTs spinning around the world [GWE15]. Although the nominal power of WT increases, the number of commissioned WTs raises faster. As experts from the wind industry predict, the trend of the sector's growth will continue. Figure 1.3 presents the historical data and foreseen total installed capacity of WTs. For the predictions to come true it is required to increase the workload in the sector, including the maintenance of the operating WTs. The costs of operation and maintenance continue to augment and the WT's owners and operators are likely to be more interested in exploring the possibilities for decreasing those costs. It will be even easier to justify the cost of predictive maintenance for bigger wind farms with higher number of operating WTs. The application of CMS is in line with the current situation in the wind industry where more and more machines have to be under supervision with respect to their health to be able to produce the maximal amount of energy. In author's opinion, more owners of the wind parks will decide to install a CMS and it will become a worldwide standard to have a CMS. In some countries it is already the case, since some insurance companies require a CMS to be installed for economical reasons.

There are calculations which say that the potential of offshore wind is enormous [GWE15]. There is enough energy to exceed Europe's demand sevenfold and the United States' energy demand – fourfold. Although the currently deployed offshore wind energy is still minor, the interest in its usage is expressed by many countries. Europe is the leader of offshore wind energy. In each year from 2012 to 2014 more than 1 GW offshore WTs have been installed [EWE15]. For Europe the offshore wind is an essential component of the renewable energy target set on 20% by 2020. Moreover, by the same year China has set itself a target to install 30 GW of WT off its coast. There are also many ongoing projects in the United States, because there are very good resources. The trend of moving WTs onto off-shore locations has

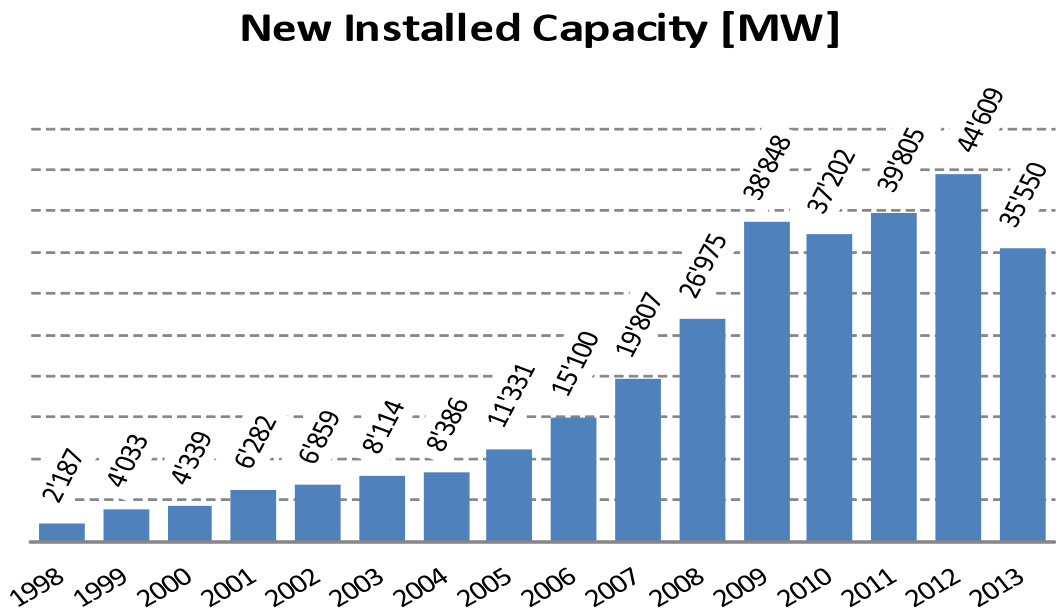

Figure 1.2: The yearly installed capacity of WT worldwide [WWE14b].

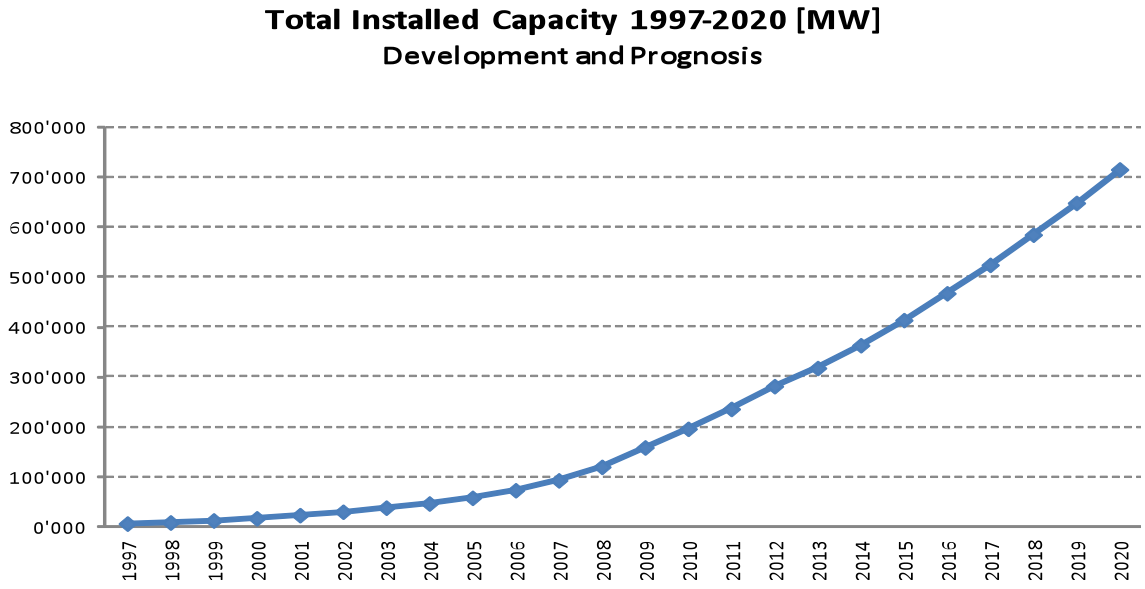

Figure 1.3: The total installed capacity of WT worldwide, the development and prognosis until 2020 [WWE14b].

many pros, like more wind resources and more stable wind conditions [GWE15]. On the other hand there are also cons, like harsh environmental conditions and limited accessibility to WTs placed offshore. To overcome negative aspects of placing wind turbines off-shore more reliable machines and better maintenance is required.

The above-mentioned arguments show that the wind energy has a big potential. The important factor for the further development of wind energy industry is the reliable operation of WTs. This is one of the key factors for the success of existing wind energy companies and it can be improved by deploying the quality CMS. The use of a CMS could decrease the appearance of unpredicted events and make the future of the WT's operators more predictable while the environment of all of us will be less polluted. The stability of the industry can be improved by applying advanced signal processing methods in algorithms used in WT CMS.

This thesis proposes an attempt for improvement of the algorithms used in CMS as mentioned in the introduction. The WT is a challenging object for monitoring. Constant and unpredictable changes of speed and direction of wind make the WT work under highly non-stationary conditions. This thesis is focused on the development of signal processing techniques which can overcome some difficulties of a standard CMS. The above-mentioned arguments are also the justification of this work.

The goal of the thesis is to propose signal processing methods suited for a data-driven CMS which is under development in GIPSA-Lab and which is called AStrion. This CMS by definition works without any additional information about the investigated signal. Moreover, it is a fully automatic tool which provides automatic and detailed signal interpretation and operates in a user-friendly manner. The general scope of this dissertation can be shortly closed in three following points:

- Cropping of time-frequency (TF) representation;
- Kinematic association;
- All-sideband demodulation.

The cropping TF representation of a signal is proposed to select the most stationary part of the signal. The idea behind this concept is to facilitate the diagnosis and monitoring of the mechanical system by considering only the part of the signal which is the easiest to be correctly interpreted. This is a way proposed to deal with the high non-stationarity of the vibration signals measured on WTs. Moreover, one can conceive the proposed method in the context of a continuous acquisition for data selection.

The kinematic association is proposed to use available characteristic fault frequencies of investigated machines by AStrion. The usage of the kinematic data allows us to make a link between AStrion results and physical origin of detected spectral components, which provides additional information for results interpretation. The main goal of this method is to perform a unique association of the kinematic components with the spectral content of the investigated signal.

The all-sideband demodulation method is proposed to reveal information concealed in the modulations present in a vibration signal. This technique is designed to obtain the maximum amount of information on the nature of the signal generated by the rotating components by estimating all the amplitude and frequency demodulation function. Statistical features are proposed for an automatic evaluation of the modulations. These indicators aim to give accurate information about component health and fault detection.

1.2 Vibration Signals

Vibration is an effect of oscillatory motion in solid bodies. This oscillatory motion is linked with body inertia and elasticity. Inertia is related to density and permits to transfer momentum between adjacent elements. Elasticity is the property that exerts a force on a displaced element, which causes it to return to its equilibrium position [NK03].

Vibrations are generated by all operating machines and can be captured by a vibration sensor. Lateral vibration can be described by displacement, velocity, and acceleration. There are transducers to measure each of the mentioned vibration parameters. Nowadays, acceleration sensors are the most popular in CMS [Ran11]; they measure vibration in a unit of meter per second square. After the acquisition of acceleration signal it is possible to compute a velocity by integration of this signal. A displacement can be obtained by evaluation of the second integration of acceleration. Piezoelectric accelerometers are used in most CMS applications since these transducers are reliable and relatively cheap.

A time history of acceleration signal, representing vibrations and commonly called a vibration signal, can be transformed into frequency domain by computing the Fourier Transform. This is refereed to as a spectrum of the signal. A spectrum is a powerful diagnostic tool which gives an insight into the investigated system by a vibration signature of mechanical components. More details about the characteristic frequencies of mechanical components in rotating machinery are given in section 1.6.

Wind turbines produce vibrations during operation as any other machine, but contrary to a vast number of industrial cases a wind turbine operates thanks to a non-controllable input. Wind turbines are excited by random force of wind, thus the output vibrations in general can be seen as random vibrations. It means that it is not possible to model the input signal to a wind turbine system by an explicit mathematical relationship. The input signal can be only described with probability and statistical tools, since the time history of the signal is continuous and does not repeat. Therefore a time history of a typical random signal, like wind turbine vibration signal, contains a vast number of frequency components.

Moreover, in the case of real-world applications, vibration signals are always embedded in a noise. It is important to remember this fact while performing vibration-based condition monitoring or diagnosis.

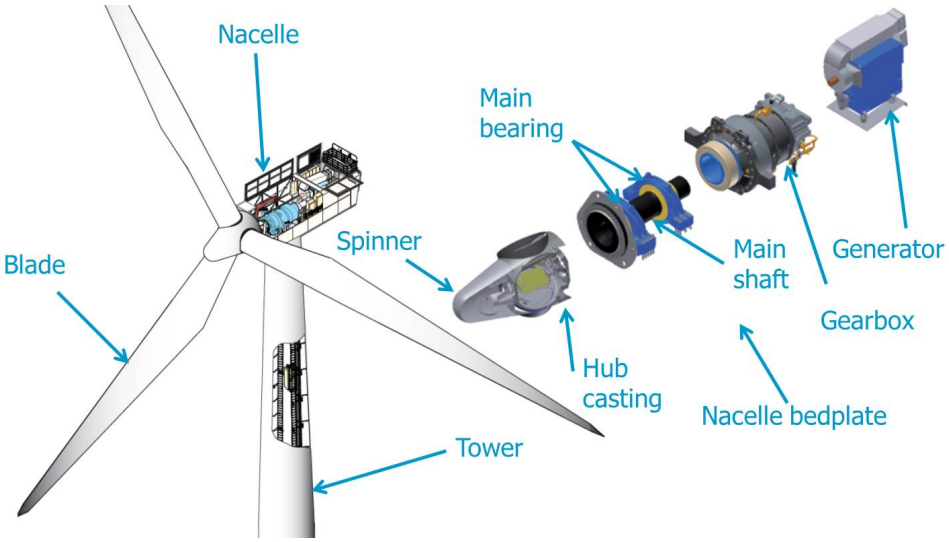

Figure 1.4: Typical configuration of a horizontal axis WT with a gearbox [Ken15].

.

1.3 Wind Turbine

There is a vast number of possible WT configurations. The main two groups are the horizontal and the vertical axes WTs. The more popular configuration of rotational axis is a horizontal one, which could be divided into WTs with a gearbox or direct drive (gearless). According to the position of the generator and the gearbox, there is another division [Hau06]:

- Generator and gearbox inline in the nacelle, which is a standard configuration;
- Generator vertical in the towerhead;
- Generator and gearbox in the towerfoot;
- Gearbox in the nacelle, generator in the towerfoot;
- Generator in the towerfoot, two separate gearboxes.

Apart from the above-mentioned divisions, WTs are also classified according to the localisation of the turbines. There are onshore WTs, placed inland, and offshore WTs, which are located in water.

The most common mechanical configuration of a WT is presented in Figure 1.4. This picture shows a general overview of the WT parts and a 3D assembly model of the main components of the drive train on the right-hand side of Figure 1.4. It is a popular type of an upwind horizontal axis WT with a gearbox and generator inline.

Figure 1.5 shows in details two rotating machine components. A one-stage planetary gearbox with two-stage parallel shaft gearbox popular in a big WT is presented in Figure 1.5 (a).

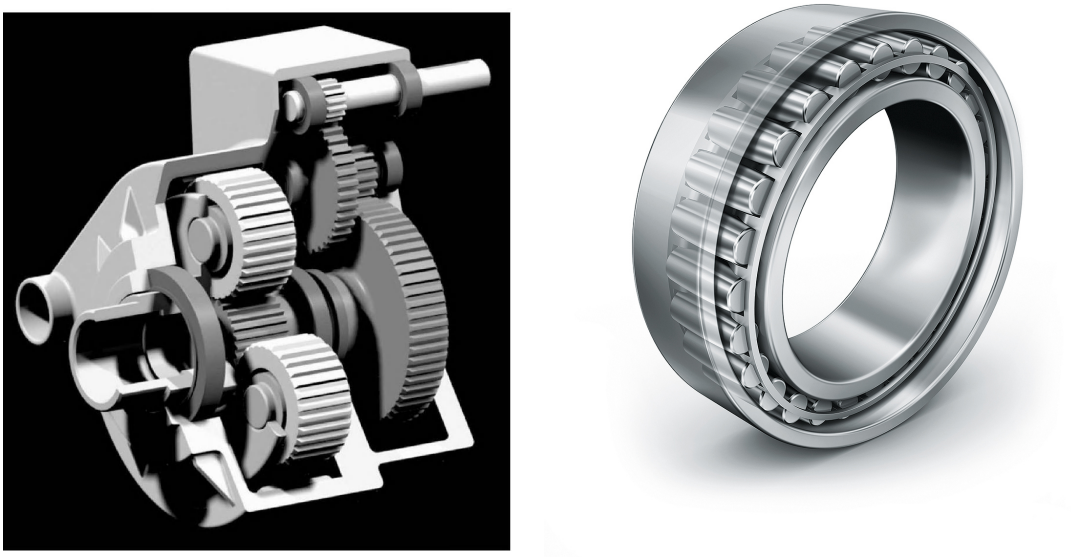

(a) Gearbox (b) Bearing

Figure 1.5: Examples of basic WT's drive train component models: (a) an one-stage planetary with two-stage parallel shaft gearbox [Hau06] and (b) a main bearing [Sch15].

Starting from the left-hand side a planetary gearbox is presented with three planetary gears rotating over a ring gear which is fixed with the gearbox casing. The three planetary gears are connected by a carrier which is fixed on an input shaft and thus driven by WT blades. The planetary gears drive a small sun gear in the center which transfers a rotational motion to two-stage spur gear. A gearbox in a WT works as a multiplier which typically has a ratio around 1:100. A rolling-element bearing (REB) is presented in Figure 1.5 (b). This component is used to reduce the friction between moving parts. Thus it is a very important element of the drive train. Various types of REBs are utilized in a WT and, apart from main bearing, REBs are located in the gearbox and in the generator to support all shafts.

1.4 The State of the Art in the Monitoring of Rotating Machinery Including Wind Turbines

CMSs are widely used in industry and bring considerable benefits in mechanical components surveillance [GM+12]; [Liu+15]. The CMS name is commonly used for condition monitoring and diagnostic systems. These systems are composed of a data acquisition part followed by a post-processing in order to reveal abnormalities in the state of the investigated system as well as a maintenance decision making. There are several techniques to perform this task such as the vibration analysis, the acoustic emission, the lubricant analysis, and others. Each of them has its own advantages and disadvantages.

Table 1.1: Summary of condition monitoring techniques in WT, where a: Statistical methods; b: Time domain analysis; c: Cepstrum analysis; d: Fast Fourier Transformation (FFT); e: Amplitude demodulation; f: Wavelet transformation; g: Hidden Markov models; h: Novel techniques; i: Other.

Technique	Blades	Rotor	Gearbox	Generator	Bearings	Tower
Vibration	a: [Gho+00] f: [Hon+02] i: [Gie+06]	a: [CG05] c: [CG03]; [ZW01]; [Wis94]; [BP06] i: [YT09]	a: [CG03] b: [Fut95]; [McF87b] bef: [Mil99] c: [CGM94]; [Cas+97] cdefi: [DRR00] d: [NPLAFK]; [CW03]; [WST07] e: [McF86] eb: [CYY10] f: [LM95]; [WM96]; [BB03] fg: [MM07]; [RCP96] fi: [Raf+07] i: [Ant09]; [BZ09b]; [RSC12]		a: [CG03]; [DS78]; [ST02] c: [CGM94]; [Cas+97] d: [NPLAFK]; [IH82]; [IY83] e: [MS84] df: [TPY01] f: [LOI03]; [PCT07]; [Hon+02]; [Sun+05]; [NA02] fi: [YSM03]; [Raf+07] g: [OL01] i: [HR00]; [Ant09]; [RSC12]; [BS12]; [Zim+14]; [Zha+14]	d: [NPLAFK]
Acoustic emission	a: [Ana+02]; [Sor+02]; [GR97b]; [GR97a]; [WM93]; [BD03]; [Jun08]; [Joo+02]; [Dut+01] i: [Gie+06]	f: [Men+00]	a: [BR99]; [TTM05] f: [BB03]		a: [TN90]; [Kim+99]; [EM10] b: [LL95]; [HM96] de: [TN92] i: [JL95]	
Ultrasonic technique	a: [RJv08]; [Jas+08]; [Jas+09]; [Rai+08] f: [Cas+98]; [GR97b]					
Oil analysis			a: [BR99]; [PKC05] b: [LK06]	i: [PJ99]	a: [Tom98]	
Strain	a: [Sor+02] c: [Wer+04] i: [Gie+06]; [MPP00]; [VPD05]; [ES08]	i: [MB96]				

Continued on next page

Table 1.1 – continued from previous page

Technique	Blades	Rotor	Gearbox	Generator	Bearings	Tower
Electrical effects	i: [SL99]; [MT06]			a: [Smi+93]; [YTC13]; [Dju+12]	i: [CGB14]	i: [TT02]
Shock Pulse methods					a: [But73] de: [TN92] f: [GMRT10]; [Zhe+08]	
Process parameters	a: [ZM07]			a: [Mü+06]		
Performance monitoring	i: [Sor+02]			a: [Mü+06] b: [DL05]	cd: [Hat04]	
Radiographic inspections	i: [Jas+09]; [FPB11]					
Thermography	i: [RM01]; [Smi+93]; [BR99]		h: [ZM07]	h: [ZM07]		
Other	i: [BR99]; [NS96]; [DG07]; [YCJ13]		i: [YCJ13]	i: [YCJ13]	i: [IH82]; [IY83]; [DG07]	i: [YCJ13]

In the case of the wind energy sector, CMSs are widely used to monitor the state of the mechanical components of WTs due to the increasing number of machines often located in remote places. As [Hau06] points out, the usage of CMSs is especially crucial for offshore wind farms due to restricted human accessibility and harsh environmental conditions. A robust CMS is very beneficial for the wind energy industry and in particular for offshore farms.

Various aspects of a CMS could still be improved thus it is an active research domain [Yan+08]; [TJ11]; [MBM12]; [Tch+13]; [BS13]. The overview of diverse techniques used for condition monitoring of WTs' components is presented in Table 1.1 with a division according to the signal processing method applied. The table is based on [GM+12] and is complemented with more examples.

Table 1.1 is not exhaustive and some approaches and methods used in a CMS are missing. Among the most important it is worth adding the following:

- Data validation;
- Operational state control;
- Order tracking.

It is important for any further analysis to assure a good quality of the measures, thus a data validation is advised to execute in the case of each technique and component listed in Table 1.1. There are various approaches to data validation. One is based on the evaluation of the correctness of the vibration signal acquisition process [JBB11]; [JB13]. Another one is based on the detection of the non-stationarity in the vibration signals based only on the information contained in the signal itself [HM06]; [Mar07]; [MM09].

As pointed out in [BZ09a]; [Cha+12], it is very important to take into account the changes of load of the machinery being diagnosed. The operational states can be utilized in CMSs of machines working under constantly changing conditions. In such a case this signal processing approach enables the usage of relatively simple tools to compare data. It is applied to analyse measurements taken under similar operational conditions of the investigated machine. An example of this aspect of CMS can be found in [BJB12]; [JB12]; [Str+15].

In Table 1.1 it lacks the so called order tracking technique used for condition monitoring and diagnosis of rotating machinery. It can be applied to gearbox, generator, and bearing. This method is also referred to as an angular resampling and the basis are well explained in [FM97]. The more recent applications for condition monitoring and proposed enhancements can be found in [Bon+05]; [Wu+09]; [RSC12]; [UBA13].

A distinctive picture of the status of CMSs dedicated to WTs is presented in [CZT14]. In this report authors present an up-to-date and comprehensive comparison of commercially available WT's CMSs. One of the conclusions in this report mentions that 'Successful CMSs must be able to adapt to the non-stationary, variable speed nature of WTs' what is a very accurate remark.

Above all, the usage of a CMS has to be justified from an economical point of view. The financial margins of the wind energy business are very low, so a prolonged down-time of a WT could generate high economical losses [GWE14]. Some examples of the considerations of a CMS from economical aspect can be found e.g. in [ANA04]; [MA08]. The mentioned papers prove that it is possible to achieve considerable financial benefits by a proper employment of a CMS.

As it could be spotted from Table 1.1, the most common technique used nowadays is a vibration-based condition monitoring. The vibration technique has wide abilities and there is a big interest in its development. Moreover, a vibration-based condition monitoring is often the key component of a predictive maintenance since it provides indicators related to the evolution of potential faults and failures [APC13]; [LCB14]; [Egu+15]. This is the reason for focusing mainly on this method of CMSs throughout this thesis. The next subsection elaborates more on vibration monitoring for rotating machinery.

1.4.1 Vibration of Rotating Machinery

The rotating machinery generates vibrations during its operation. In the majority of cases there is a possibility to recognize specific patterns of the signal and to link it to a mechanical

component. Some of generated vibrations are always present in the signal and are not an evidence of any fault, but just a part of a normal operation. On the other hand, specific patterns present in the signal are the sign of damages of a mechanical component.

The basic examples of normally present patterns in the vibration signals of a rotating machinery are shaft frequency and gear mesh frequency (GMF). These components generate vibrations which can be identified as harmonics (integer multiples) of the associated shaft rotation speed where the shaft frequency is the fundamental. In the case of gearboxes, the fundamental frequency of the harmonic family is equal to the GMF. The harmonic pattern can be usually easily found on the spectrum of a signal. On the contrary, the rolling-element bearings (REBs) generate cyclic vibrations which are not harmonics of the associated shaft speed.

Gearboxes generate also another easily identifiable vibration pattern to be seen on a spectrum. In the case of a simple gearbox consisting of two gears, each of them is mounted on a shaft. Due to a tooth deflation and a dynamic transmission error of the gearbox fluctuations, the torque transmitted by the gearbox is varying. This can be considered as an amplitude modulation effect [Ran11]. Gearbox wear causes a change in the geometry of the tooth surface. It is the reason for variation of the tooth contact point. This change in the gearbox operation is considered as a source of frequency modulation of the GMF. The above-mentioned amplitude and frequency modulations are easy to be seen in the frequency domain of a gearbox vibration signal and they are manifested as sidebands around the GMF and its harmonics. For a pair of operating gears it is normally possible to distinguish the two families of sidebands. Each one corresponds to the rotational speed of the shaft on which the gear is mounted. Moreover, to distinguish the shaft being the source of modulation it is enough to verify the distance between the peaks corresponding to the GMF (or its harmonics) and its modulation, which equals to the frequency of rotating shaft.

From a broader perspective, the classical approach of signal analysis offers a wide selection of diagnostic tools. In general, each tool is proper for a specific type of signal. E.g. if a steady-state signal is to be analysed, the Fourier Transform is suited to precisely estimate its frequency content. For determining the rotational speed values which excite the resonances of machinery, a time-frequency analysis would be an appropriate technique for the investigation of a signal acquired during a run-up test.

The fact that the change in the machine health manifests itself as the change in the vibration signature of the supervised machinery allows for the implementation of a CMS. However, the vibration signature of a rotating machinery changes also with the change of load or speed of the machinery [MHB04]. This fact makes the comparison of signals generated under changing operational conditions difficult. That is why the CMS of machines working under varying operational conditions is challenging and one way to overcome these difficulties is an employment of more sophisticated data validation algorithms. For condition monitoring purposes, the main interest is to use the signals acquired under the same, or as similar as possible, operational conditions including load and rotational speed. Because of the mentioned difficulties, section 1.6, dedicated to the description of typical faults of rotating machinery,

is restricted to the case of signals generated by machinery working with constant speed and load. Such signals are stationary or cyclostationary.

1.4.2 Methods of Vibration Spectrum Estimation

A lot of methods used in vibration diagnosis use the Fourier Transform. Its basic concept is to represent the signal as a summation of sine waves. Primary application of Fourier series in machine vibration analysis was to capture periodic signals generated by a rotating machinery under constant rotational speed [Ran11].

The Fourier Transform $X(f)$ of a continuous signal $x(t)$ at frequency f can be written as a complex number

$$X(f) = \int_{-\infty}^{\infty} x(t) \cdot e^{-j2\pi ft} dt. \tag{1.1}$$

When the signal $\tilde{x}[n]$ is a discrete and periodic sequence with period N, the Fourier series representation can be expressed as

$$\tilde{x}[n] = \frac{1}{N} \sum_{k} \tilde{X}[k] \cdot e^{-j(2\pi/N)kn}, \tag{1.2}$$

where n is an integer number corresponding to a time moment, $1 < n < N$, k is an integer, and the Fourier series coefficients $\tilde{X}[k]$ can be computed as

$$\tilde{X}[k] = DFT(\tilde{x}[n]) = \sum_{n=0}^{N-1} \tilde{x}[n] \cdot e^{-j(2\pi/N)kn}. \tag{1.3}$$

This representation is called the Discrete Fourier Transform (DFT). A detailed explanation of the theory of Fourier Transform can be found in vast number of signal processing publications as [OSB98].

1.5 Selected Signal Processing Techniques

1.5.1 Order Tracking

The measured signals are rarely acquired under perfectly constant speed and load conditions, as assumed for the presentation of typical faults in Section 1.6. Any change of those operational parameters during the record of an acceleration signal causes the effect of smearing energy in the frequency domain, which means that energy corresponding to a mechanical component is distributed in some narrow-band range instead of one peak. In order to get rid of this phenomenon, the order tracking technique has been developed [FM97]. Instead of a fixed time sampling period, the signal is sampled on the basis of equidistant angle position of a reference shaft. The effect of applying this technique on a signal acquired under varying speed

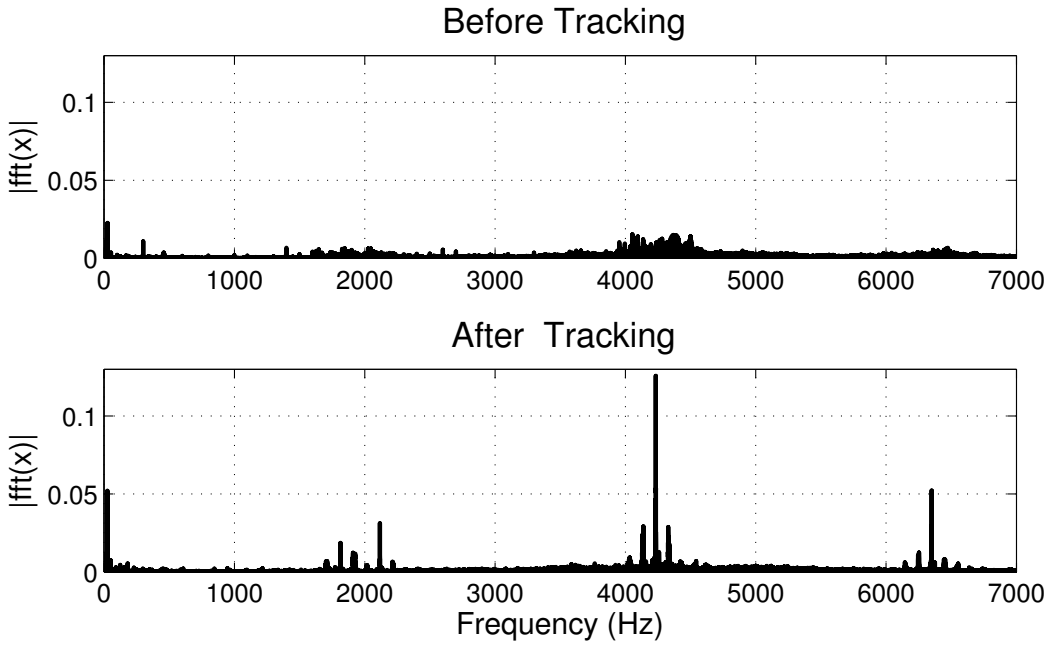

Figure 1.6: Spectrum of the signal before and after order tracking which is applied to avoid effect of changing operation parameters during data acquisition.

is presented in Figure 1.6. This technique allows for more precise narrow-band analysis and is widely applied in CMSs.

It is worth mentioning that after performing the order tracking on the signal the rectangular windowing for filter can be used. Thanks to integer number of samples per each revolution the effect of energy leakage is not present at estimated PSD [Ran11].

1.5.2 Time Synchronous Averaging

The time synchronous averaging of a signal has been applied over many years for the extraction of vibration information corresponding to a particular gear of a gearbox. This operation has a goal to intensify or even separate the deterministic part of the signal and reduce the random content, as well as the content not related with the averaging period of vibration signal [Bra11].

By definition the time synchronous average of a signal y(t) is expressed as [McF87a]

$$y_a(t) = \frac{1}{N} \sum_{n=0}^{N-1} y(t + nT_R), \tag{1.4}$$

where N is a number of periodic sequences shifted by integer multiples of the periodic time T_R.

The time synchronous averaging is performed by averaging together the series of signal segments corresponding to one period of a synchronising signal. In frequency domain, this

operation can be seen as the application of a comb filter selecting the harmonics of the periodic frequency. In the case of finite length and discrete signals the remove of the entire discrete masking signal is not always possible, but often it is possible to adjust the number of averages to obtain this goal [McF87a].

From the practical point of view, it is important to average the signal which constitutes samples identically distributed for each period to be averaged. Even a slightest speed fluctuation in the recorded signal would cause a jitter after a number of averages. The solution for this problem is the usage of order tracking performed on the original signal and the selection of an integer number of samples per period to be used for averaging. This technique allows even for the separation of the individual planet gears in a planetary gearbox [McF94].

1.6 Typical Faults

This section describes the most common problems of the components which are objective of a CMS fault detection. The following sections cover such a components as shafts, rolling-element bearings, and gearboxes. The rotating machinery faults are described based mainly on [Ran11].

1.6.1 Shaft Problems

A vast number of faults manifest themselves at frequencies corresponding to the speed of the investigated shaft (shaft rotational speed expressed in revolution per minute – RPM), or its low harmonics and sub-harmonics. According to [Bus02] the most common vibration trouble sources are unbalance and misalignment. Each of them are identified to occur half the time when a problem with a rotating machinery is investigated. This section describes the most often encounter shaft-related problems as unbalance, misalignment, and looseness.

1.6.1.1 Unbalance

Unbalance (imbalance) occurs when the local centre of mass of the cross-section of the shaft differs from the centre of rotation, resulting in a heavy spot on a rotor. This heavy spot produces a centrifugal force which is the cause of high vibration amplitudes at a frequency equal to $1 \times$ RPM in frequency domain. So it can be modelled as a sinusoidal waveform in the time domain. In the case of rigidly mounted machines, a raise of the vibration amplitude in the horizontal direction versus the vertical direction is expected. In the case of overhung rotors, an increase of axial vibrations can occur.

1.6.1.2 Misalignment

Misalignment occurs when the shaft axes of two mating parts create an angle or are offset to each other, the mixture of both types of misalignment is also possible. This fault is typical for couplings and bearing components and is the cause of higher radial or axial vibrations, depending on the misalignment type. In the case of an angular misalignment, the axial vibration amplitudes raise together with a phase difference of 180° axially across couplings. Offset misalignment type typically manifests also in raised axial vibration amplitudes, but a phase difference observed is 180° radially across couplings. Depending on the type and the design of the coupling as well as upon the share of angular versus offset misalignment problems, a raise of the amplitude of the dominant frequencies can be observed at $1 \times$ RPM, $2 \times$RPM, or both together. The time domain signals of vibration measured on a machine with misalignment problems typically show periodic patterns with one or two cycles per revolution of shaft. Moreover, in the case of a fundamental shaft frequency ($1 \times$RPM) being the frequency with a raised amplitude due to a misalignment problem, the comparison of the phases of the signals at different ends of the shaft are necessary to distinguish it from an unbalance problem.

1.6.1.3 Looseness

In the case of rotating components which do not fit correctly, the problem of a mechanical looseness can be observed. This could occur due to a loose or a distorted machine feet (soft feet), a loose foundation, a weak grouting, loose bolts or bedplates. The looseness problem can be modelled in time domain signal as high random impacting patterns and in some instances the waveform may appear truncated. In the frequency domain the spectrum typically shows higher amplitudes of shaft related components up to its high harmonics, $1 \times$ *to* $10 \times$ RPM, and in some cases the sub-harmonics $\frac{1}{2} \times$ RPM and its multiplies can be raised.

1.6.2 Rolling-Element Bearing Defects

There can be various reasons for a fault of a bearing and any combination of following can be a cause: design, manufacture, assembly, operation, maintenance. A common group of rolling-element bearing (REB) fault is caused by a material degradation. [ISO04] presents a classification of bearing failure which is based on the features visible on functional surfaces of a REB. This standard lists failure caused by fatigue, wear, and corrosion which are manifested by a REB's surface damage. There are different types of surface degradation and they can be described as flaking, spalling (pitting), or peeling.

There are four main types of REB characteristic fault frequencies which are related to above-mentioned material degradation. The characteristic fault frequencies depend on the bearing geometry, n_r the number of rolling elements, d_r the diameter of rolling elements, d_p the pitch diameter, and ϕ the angle of the load from the radial plane, as well as speed of shaft f_r. The equations for the REB characteristic fault frequencies are listed below along with

a description of each type of the fault as each of them causes a specific pattern of vibration which is normally not present for a healthy REB.

- Fundamental Train Frequency (FTF)

$$FTF = \frac{f_r}{2}\left\{1 - \frac{d_r}{d_p}cos(\phi)\right\}. \tag{1.5}$$

  Defects of a REB cage are normally present along with other problems, such as rolling element defects described in the following points of this list. Cage problem is frequently a cause of a rapid failure. This defect does not produce a high amplitude of vibration and is mainly detectable as a sideband frequency component, whose value corresponds to Fundamental Train Frequency;

- Ball Spin Frequency (BSF)

$$BSF = \frac{f_r \cdot d_{cr}}{2d_r}\left\{1 - \left(\frac{d_r}{d_p}cos(\phi)\right)^2\right\}. \tag{1.6}$$

  A damage of the surface of a bearing rolling element excites Ball Spin Frequency. The characteristic fault frequency generated by rolling elements with damaged surface can be modelled by Equation (1.6). This problem can appear at the fundamental or second harmonic which are surrounded by sidebands corresponding to the cage characteristic frequency. It is also possible to notice impacts in the time domain signal representation which are at a distance corresponding to the fundamental frequency of the ball spin;

- Ball Passing Frequency – Outer Race (BPFO)

$$BPFO = \frac{n_r f_r}{2}\left\{1 - \frac{d_r}{d_p}cos(\phi)\right\}. \tag{1.7}$$

  The Ball Passing Frequency – Outer Race is excited by a rolling element passing across a defect on the surface of the outer race. This problem is possible to spot by the appearance of several harmonics of the fundamental BPFO, which raises in amplitude. In the case of a rotating outer race and a fixed inner race, BPFO frequencies can be modulated by the shaft speed which results in the appearance of sidebands around the BPFO defect. The time domain signal typically shows high impacts with a period corresponding to the fundamental BPFO or related dominant harmonic;

- Ball Passing Frequency – Inner Race (BPFI)

$$BPFI = \frac{n_r f_r}{2}\left\{1 + \frac{d_r}{d_p}cos(\phi)\right\}. \tag{1.8}$$

  The Ball Passing Frequency – Inner Race fault is created similarly to the BPFO one. In the majority of cases, the inner ring of a rolling-element bearing rotates together with the shaft, thus a modulation related to the shaft speed can be observed. This once per revolution modulation can be produced when a BPFI fault passes through the load zone.

Generally, four stages of rolling-element bearing (REB) faults are distinguished. It is established and agreed that the early stage of a REB problem appears in the ultrasonic range (e.g. up to 20kHz and even higher). The second stage is characterised by an increase of ultrasonic frequencies as well as the natural frequencies which are excited by a very minor REB defect. It is possible to distinguish the harmonics of the fundamental bearing characteristic fault frequencies. The next stage of REB problem is when the number of characteristic fault frequency harmonics increases and when sidebands appear around those frequencies. Ultrasonic levels also continue to rise. The bearing should be replaced at this stage. The fourth stage of a REB fault is characterised by a random and broadband high frequency noise which can replace characteristic fault frequencies.

1.6.3 Gear Defects

Gearbox problems include wear, which is visible on a tooth surface as pitting, spalling, scratching, or scraping, corrosion, permanent deformation, chipped or broken teeth, or misalignment. Some of this problems are further defined in following subsections and a detailed description of the mentioned and more gear degradation patterns is given in [ISO95].

The gear mesh frequency (GMF) is a characteristic frequency crucial in monitoring and diagnosis of a gear-set and can be computed as

$$GMF = f_r \cdot z, \tag{1.9}$$

where z corresponds to the number of teeth of the gear. There is always one GMF present per each pair of gears and it is always present regardless of gear condition. The amplitude of the GMF may increase due to load or gear condition. Sidebands related to each shaft of gearbox are considered as the key to diagnose gear faults and the spacing of sidebands shows which shaft the faulty gear is on.

1.6.3.1 Worn Gears

A distributed lack of material without any local damage of the tooth surface is caused by a wear phenomenon. This problem appears on the spectrum as the raised sideband amplitude which are equally spaced on both sides of the fundamental GMF and its harmonics. The presence of sidebands is not a good enough fault indicator since the healthy gearbox also generates this pattern, the key factor is the amplitude of those sidebands. Worn gears can also excite the natural frequencies of the gears, casing, or both.

1.6.3.2 Chipped / Broken Gear Teeth

A single chipped or broken gear tooth generates vibration corresponding to one impact per revolution of the shaft with gear mounted on and corresponds to the frequency equal to fundamental shaft speed $1 \times$ RPM. It is easy to confuse this fault with other shaft related

problems. The chipped or broken gear teeth can be identified using a time domain signal where a once-per-revolution impact is followed by a ring down from the shaft with the defective gear tooth on.

1.6.3.3 Misaligned Gears

Misaligned gears occur once the shaft with mounted gears are badly oriented. This fault is generally visible in frequency domain as an increase of the level of the vibrations corresponding to harmonics of GMF, $2 \times$ GMF, and $3 \times$ GMF as well as its shaft related sidebands. The diagnosis of this problem can be facilitated by the inspection of the time domain signal. If the misaligned gear problem last for sometimes it is typical that the gear is also worn.

1.7 Diagnostic Features

In order to detect the above-mentioned defects, this section shortly describes the more popular techniques and generated features according to the following division:

- Wide-band features;
- Narrow-band features;
- Demodulation analysis.

1.7.1 Wide-band Features

Wide-band features in the majority of cases are computed with the usage of the entire length and frequency range of the investigated signal. These features are simple and mostly based on statistical properties of the signal. In traditional CMS, these general indicators are always employed. The basic list of wide-band features includes [SF84]

- Mean value $\bar{x}$ – the first order arithmetic mean of a vibration signal $x[n]$ for a defined range from first to last sample N computed according to equation

$$\bar{x} = \frac{\sum_{n=1}^{N} x[n]}{N}; \tag{1.10}$$

- Root mean square (RMS) x_{rms} – the second order statistical measure of the energy of vibration signal computed according to equation

$$x_{rms} = \sqrt{\frac{\sum_{n=1}^{N} x^2[n]}{N}}; \tag{1.11}$$

- Velocity root mean square (VRMS) x_{vrms} – unlike other wide-band features the VRMS is computed from a specified frequency range, the one which is available from velocity transducers, usually assumed to be from 10 Hz to 1 kHz. This diagnostic feature originates from the history of the vibro-diagnostic development where the sensors for velocity measurement were widely applied and is still present in formal requirements like ISO standards. It is easy to compute this feature also from acceleration signal by filtering the frequency content of signal. After obtaining signal x_v in the required frequency range, the VRMS can be computed in the same manner as RMS

$$x_{vrms} = \sqrt{\frac{\sum_{n=1}^{N} {x_v}^2[n]}{N}}; \tag{1.12}$$

- Peak to peak (PP) – the biggest difference between positive and negative amplitudes of the signal

$$PP = \max_{0<t<T} x[t] - \min_{0<t<T} x[t]; \tag{1.13}$$

- Zero to peak (ZP) – the highest absolute amplitude of the vibration signal

$$ZP = \max_{0<t<T} |x[t]|; \tag{1.14}$$

- Crest factor (CF)– the ratio of the highest value to the effective value of signal

$$CF = \frac{PP}{x_{rms}}; \tag{1.15}$$

- Skewness (Sk) – the third order statistical moment

$$Sk = \frac{\sum_{n=1}^{N} \left(x[n] - \bar{x}\right)^3 / N}{\left(\sqrt{\sum_{n=1}^{N} \left(x[n] - \bar{x}\right)^2 / N}\right)^3}; \tag{1.16}$$

- Kurtosis (K) – the fourth order statistical moment normalized by the variance. Commonly it is described as the statistical measurement of the 'peakedness' of a signal and computed with the formula

$$K = \frac{\mu_4}{\sigma^4} = \frac{\sum_{n=1}^{N} \left(x[n] - \bar{x}\right)^4 / N}{\left(\sqrt{\sum_{n=1}^{N} \left(x[n] - \bar{x}\right)^2 / N}\right)^4}, \tag{1.17}$$

  where μ_4 is the 4^{th} momentum about the mean value and σ is a standard deviation of the signal. It is a common practice to subtract the value 3 from the result obtained with usage of Equation (1.17) which is explained by the fact that after this operation the kurtosis of a normal distribution equals zero.

1.7.2 Narrow-band Features

The next group of diagnostic indicators popular in CMS are narrow-band features. This group is dedicated to compute energy in bands which are selected according to the kinematic configuration of the system. This group of analysis could be used for most kinematic components including shafts, gearboxes, and bearings. Depending on the CMS the width of the band used for the definition of narrow-band features can vary. One of popular approaches is to set a bandwidth as a percentage of characteristic fault frequency, e.g. band-width equal to 3% of this frequency. Although it is possible to compute a precise value of the frequency corresponding to a kinematic component, provided the rotational speed is measured correctly, the band for narrow-band energy computation is usually selected as a much wider one. It is due to the approximations in signal processing as well as the slippage phenomena observed during contact of machine elements.

One approach for computing the energy in a band is to filter the signal in time domain x_{NB} and compute its RMS as defined in Equation (1.11). Another methodology makes usage of Parseval's theorem which allows the computation of RMS directly from a vibration spectrum X according to the equation

$$x_{NB,rms} = \sqrt{\frac{\sum_{n=1}^{N} {x_{NB}}^2[n]}{N}} = \sqrt{\frac{\sum_{k=f_L}^{f_H} |X[k]|^2}{M^2}}, \tag{1.18}$$

where f_L represents a lower frequency of a filter, f_H is its upper frequency, and both have integer values. M corresponds to the number of samples in the bandwidth from f_L to f_H.

Any of the statistical indicators mentioned in section 1.7.1 can be computed from a narrow-band filtered signal, but it is not very popular in CMS.

1.7.2.1 Gearbox Specific Features

Apart from the above-mentioned features, there are some indicators proposed specifically to detect a gearbox fault [Tow97]; [SP05]; [VKŠ05]; [SSE11]. Some examples are listed below.

- Energy ratio (ER) – the ratio between the energy of a difference signal, being the remainder of the vibration signal after removing the components excited by a gearbox, and the energy of the regular meshing component expressed as [DL03]

$$ER = \frac{RMS(d)}{RMS(r)}, \tag{1.19}$$

  where $RMS(d)$ is the standard deviation of the difference signal and $RMS(r)$ is the standard deviation of the mesh frequency and its harmonics;

- Zero-order figure of merit $FM0$ – the parameter defined as the division of the peak-to-peak value PP and the energy of the mesh frequency and its harmonics $A(i)$ [DL03]

$$FM0 = \frac{PP}{\sum_{i=0}^{N} A(i)}, \tag{1.20}$$

  where i is the number of GMF harmonics;

- Sideband Energy Ratio$^{\text{TM}}$ (SER) – the indicator which gives a ratio between the sum of amplitudes of sidebands and the amplitude of mesh frequency [Han+]

$$SER = \frac{\sum_{i=-6}^{6} A_{S,i}}{A_{GMF}} \tag{1.21}$$

  where $A_{S,i}$ is the amplitude of $i-th$ sideband and A_{GMF} is the amplitude of the center mesh frequency. This indicator can be separately calculated for fundamental gear mesh frequency and its harmonics.

The list of dedicated features for gearbox diagnosis is much longer. It could be extended by examples as a sideband level factor [VKŠ05] or sidebands index computed from the signal after the time synchronous averaging [Szc89], and many more [SSE11].

1.7.3 Features of Demodulation Analysis

The fault detection methods based on the demodulation of a signal are called envelope analysis. This group of techniques takes advantage of the fact that the vibration of one element of a rotating machinery influences other components. This phenomenon is sometimes easy to be noticed in the frequency domain of a signal, like in the case of the GMF with visible sidebands which are due to modulation by high and low speed shafts. The modulation is not always as easy to spot and can be hidden in a wide-band noise, like in the case of REB faults which are detectable in the resonance frequencies of the machine. In order to achieve that separation of low frequency components related to impacts of REB from high frequency signal, typically above 4 kHz, the envelope analysis is used. This procedure for detection of a REB fault is presented in Figure 1.7.

The envelope analysis method consists respectively of a band-pass filter of a signal carrying information on a bearing fault, a demodulation, and Fourier transform computation of the envelope signal. More details on the methodology are given in chapter 5. Some CMSs use the envelope analysis and compute features based on results of this technique. An example of feature is the narrow-band RMS computed from the envelope spectrum at the frequency corresponding to the characteristic fault frequency.

It is important to note that rotating machinery components such a REB and gear defects excite resonance frequencies [Bra86]. Thus the fault changes the modulation of the signal

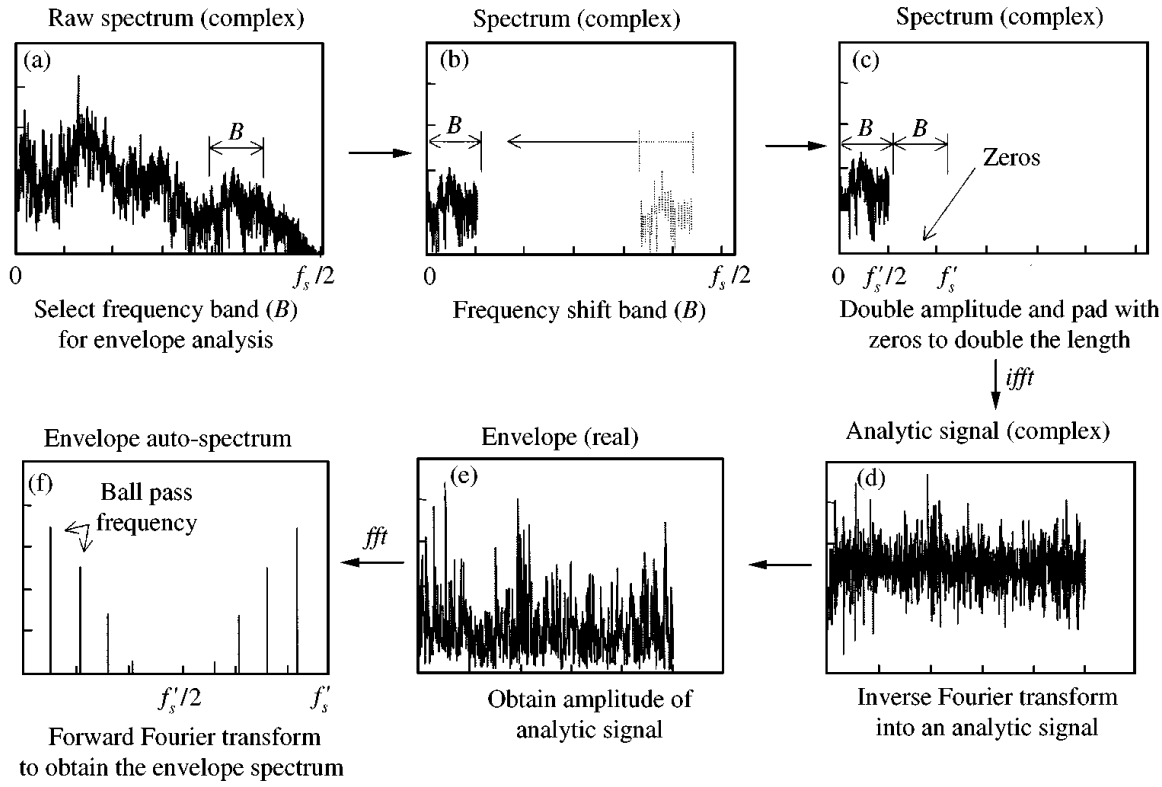

Figure 1.7: Procedure for envelope analysis using Hilbert transform technique [HR00].

related to these components. In the case of REB diagnosis the demodulation is performed to find characteristic fault frequencies in the envelope spectrum, but tracking the changes of demodulation signal also brings the information of changes in the machinery health, so the modulation could be used to spot and evaluate fault development and condition of the rotating machinery.

Apart from this, the modulation phenomenon is also used for gearbox diagnosis. An example is the feature called $NB4$ computed from the envelope of the analytic signal E

$$E = |\overline{a}[\tau]| = \sqrt{a^2[\tau] + \mathcal{H}\{a^2[\tau]\}}, \tag{1.22}$$

where $a[\tau]$ is an input analogue band-passed signal and $\mathcal{H}\{\cdot\}$ is the Hilbert transform. $NB4$ is calculated as the time averaged kurtosis of the envelope of the signal E that is band-pass filtered about the mesh frequency [DL03]. $NB4$ is determined by dividing the 4^{th} statistical moments of the envelope signal, raised to the second power

$$NB4 = \frac{N \sum_{i=1}^{N} (E_i - \bar{E})^4}{\left\{ \frac{1}{M} \sum_{j=1}^{M} \left[\sum_{i=1}^{N} (E_{ij} - \bar{E}_j)^2 \right] \right\}^2}, \tag{1.23}$$

where $\bar{E}$ is the mean value of the enveloped signal, N the total number of data points in time record, M the number of averages, i the index of data points in time domain, and j the index of time record in averaged period.

1.8 Reliability Analysis

The important aspect and capability of a CMS is the possibility of the time prediction concerning the safe and reliable operation of the machine. It is among the biggest benefits delivered by a CMS. As pointed out in [Hen+09] the phase of the maintenance decision making is the least developed in CMS. One way to perform this step is a trend analysis which is based mostly on engineering experience. Another popular way for this prediction is the calculation of the remaining useful life (RUL) of mechanical components.

[Hen+09] describes two basic approaches for the evaluation of the RUL. One is 'model-based' which means that the model of failure is created. It could be done by physical or mathematical means, e.g. the crack growth is simulated and by measuring the size of the crack it is possible to calculate the RUL. This approach needs a reliable information on the state of machinery which is not always available. The other technique is called 'data-driven' and is based on a statistical processing of historical data. It could either use multiple historical cases if available or extrapolate the health indicators of the monitored component into the future. Each approach needs trends of features resulting from the data processing step of the CMS. A good review of a prognostic implementation is presented in [BLJ06]. Moreover, this subject is of permanent interest of researchers. An example of that is a paper on multi-branch Hidden Markov Models applied on multi-state systems [LCB14] where the novel model for the RUL estimation is proposed. This approach takes into the account multiple degradation mechanisms of a mechanical system.

1.9 Standards and Regulations

As the wind industry matures, the established methods used in WT monitoring are becoming official standards. The two main regulations are International Organization for Standardization (ISO) [ISO15b] and Verein Deutscher Ingenieure (eng. Association of German Engineers) (VDI) [VDI14]. Moreover, it happens that an insurance company requires to meet some internal specifications like Allianz Zentrum für Technik (AZT), that is why this section is focused only on ISO and VDI standards.

VDI is an engineering association and one of its interests is wind turbine industry, thus the VDI 3834 comes into existence. This standard is entitled *Measurement and evaluation of the mechanical vibration of wind turbines and their components* and covers the machines from 100 kW of nominal power. This standard does not foresee the upper limit, since it turned out, that bigger units do not require other zone boundaries. There are separate releases of VDI 3834 dedicated to:

- Wind turbines with gearbox – Part 1;
- Direct drive wind turbines (without a gearbox) – Part 2.

At present only Part 1 of the VDI 3834 is available and in comparison to its first edition from 2009 there is no longer distinction of onshore and offshore wind turbines – both types are covered by one document only. Part 2 is in preparation.

The VDI 3834 series of guidelines provides information about the measurement and the evaluation of the mechanical vibration of wind turbines and their components. Described instructions on measurement and interpretation includes:

- Nacelle and tower;
- Rotor bearing with roller bearings;
- Gearbox;
- Generator;
- Requirements made of the measuring device;
- Mounting and connection of the vibration transducers;
- Operating condition during measurements.

Each subsection concerns wind turbine components and consists of information about characteristic quantities, measuring positions and directions. The document describes the evaluation criteria of vibration. RMS values of vibrations are divided into three amplitude level for each component. The 1^{st} level means a good component condition suitable for running in continuous operation. The 2^{nd} level consists of vibration values that might be tolerated, but continuous operation may cause a wind turbine failure. This level requires the investigation of which excitations are responsible for the increase of that value. The fall within the 3^{rd} level is regarded as dangerous and a damage of wind turbine components could happen. The representation of those thresholds is presented in Figure 1.8.

It is important to notice that VDI 3834 it not mentioned in vibration-based CMS. The document explicitly points out that recommended vibration guide values are not suitable for use as limit values in CMS. It is also noted that individual threshold setting and more advanced analysis is required by vibration-based CMS installed in wind turbines to provide early detection of faults.

The recently published, May 2015, ISO 10816-21 is the international standard, which describes the guides for horizontal axis WT with a mechanical gearbox and output power exceeding 200 kW. The standard is entitled *Mechanical vibration – Evaluation of machine vibration by measurements on non-rotating parts – Part 21: Horizontal axis wind turbines with gearbox*. This standard is in line with [VDI14] and also points out that the vibration-based

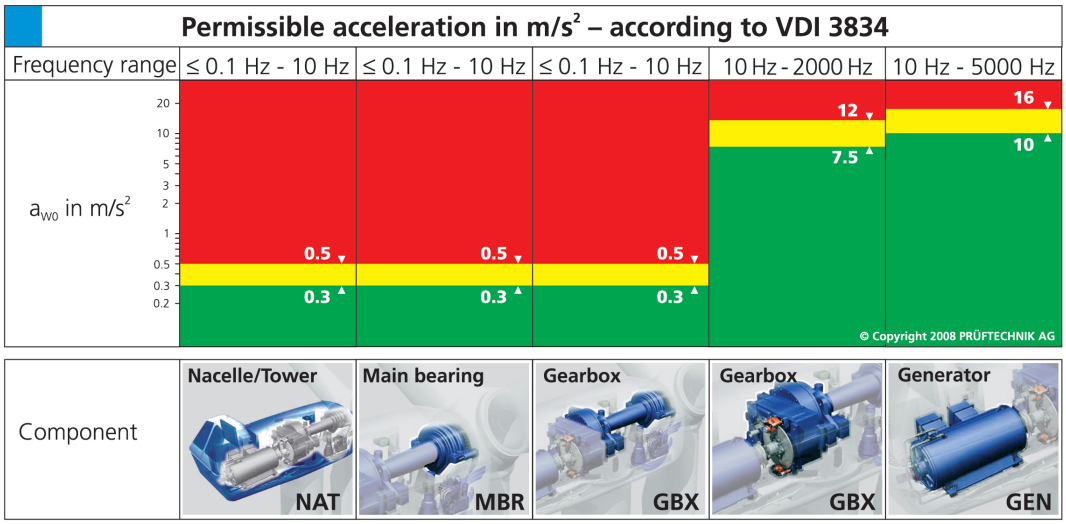

Figure 1.8: The acceleration limits of WT's components according to VDI 3834 [PRÜ15].

condition monitoring systems installed in wind turbines for early faults detection require more advanced analyses than are described in ISO 10816-21. Similarly to VDI standard the ISO document states that given values of limits are not suitable for use in CMSs. Moreover, ISO 10816-21 point out that following documents present requirements for CMSs [ISO02]; [ISO05]; [ISO b].

The ISO 16079-1 is entitled *Condition monitoring and diagnostics of wind turbines – Part 1: General guidelines* and seems to be a standard we are the most interested in, but this document is under development. This leaves us with the international standard ISO 13373 which is entitled *Condition monitoring and diagnostics of machines – Vibration condition monitoring* and has following parts:

- Part 1: General procedures;
- Part 2: Processing, analysis and presentation of vibration data;
- Part 3: Basic techniques for diagnostics (under preparation).

The ISO 13373 is neither dedicated to apply at WT nor indicates that it is the machine which needs other treatment. Thus, this standard can be used by a WT's dedicated CMS. ISO 13373-1 describes guidelines for vibration condition monitoring of machines. While ISO 13373-2, contains guidelines for the processing, presentation and analysis of the vibration data thus obtained, and that can be used for diagnostics to determine the nature or root causes of problems. This standard describes the acquisition part of the system with general information on signal conditioning, analog and digital systems, signal conditioners, and filtering. Afterwards data processing and analysis are characterized including time domain analysis, frequency domain analysis, display of results during operational changes, real-time analysis and real-time bandwidth, order tracking (analog and digital), octave and fractional-octave

analysis, cepstrum analysis, and other techniques. This gives a wide range of tools to select from which are suited for various applications.

Another standard closely related to condition monitoring in more general way, neither the technique is specified nor a list of the machine types addressed is included, is ISO 13379, which is entitled *Condition monitoring and diagnostics of machines – Data interpretation and diagnostics techniques*. This standard consists of three parts:

- Part 1: General guidelines [ISO12];
- Part 2: Data-driven applications [ISO15a];
- Part 3: Knowledge-based applications.

The first part of ISO 13379 describes procedures for the data interpretation and diagnostics of machines. Among others, it is intended to give an appropriate approach to achieve a diagnosis of machine faults. The second part of ISO 13379 contains guidelines that can be used to determine the condition of a machine relative to a set of parameters characterizing the normal behaviour of a machine. A CMS described in this standard presents a modern system which is suited to monitor a specific machine. The technique usually applied by this data-driven CMS is pattern recognition followed by pattern classification. The third part is not published yet.

A parent standard for the above-mentioned is ISO 17359 [ISO11]. It is entitled *Condition monitoring and diagnostics of machines — General guidelines* and applies to all machines. This standard tackles vast number of issues and is not restricted to any technique which can be used in CMS. Thus the ISO 17359 is a good document to start building a condition monitoring of any type of machine.

1.10 CMS Installation

As the major interest of this thesis is the development of WT CMS an example of such an installation is presented in this section. This case is the CMS prototype developed for the European Innovation Project KAStrion which is described in section 2.4.

This thesis considers the most popular nowadays WT type which is a horizontal axis wind turbine with gearbox and rotor operating upwind [The15]. There are also numerous other WT configurations [Hau06] including direct-drive concept.

The main objective of vibration-based CMS is to supervise the health of drive train components including

- Main bearing;
- Gearbox;

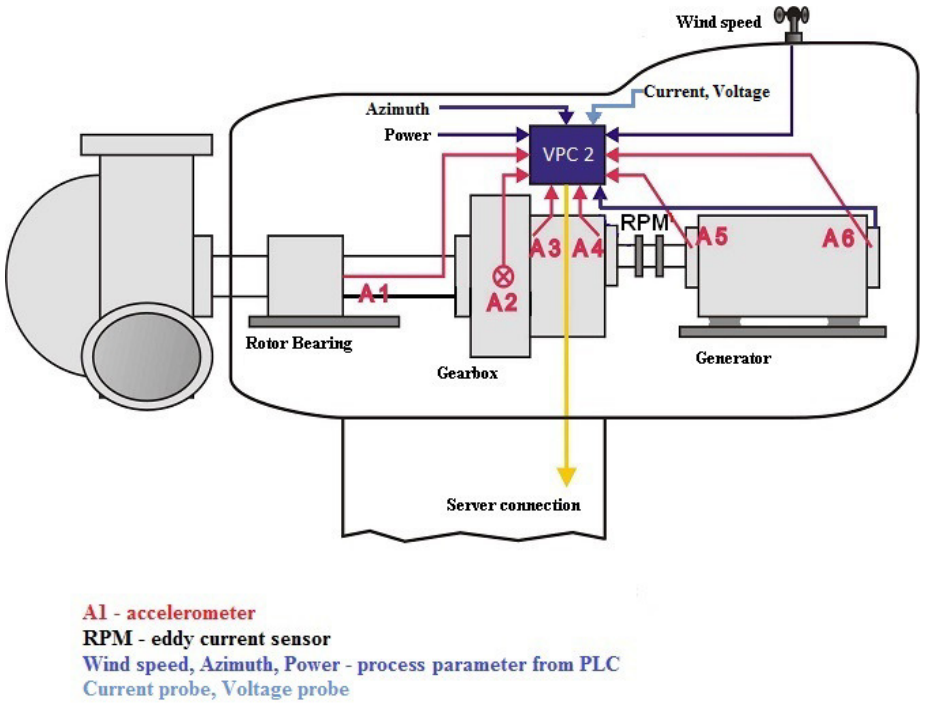

Figure 1.9: Localization of sensors for vibration-based CMS of WT with a planetary gearbox for the Innovation Project KAStrion.

- Generator.

The common approach is to detect faults of these parts and its sub-components by the usage of kinematic information, which allows to compute characteristic fault frequencies of mechanical components.

The vibration-based condition monitoring configuration of the WT drive train used within Innovation Project KAStrion is presented in Figure 1.9. It consists of six sensors for measuring the acceleration on non-rotating parts as well as the measurement of operation parameters. The second group includes the speed of high speed shaft (HSS), output power, orientation of the nacelle, and wind measurement. As [Jab12] points out, a modern CMS requires to conduct an advanced data validation of measured signals. Another advantage of state-of-the-art systems is the possibility of sending to a server and to diagnostics experts not only values of computed features, but also raw data for further analysis. An exhaustive study on the optimal configuration of a CMS is presented in [Jab12].

Chapter 2

AStrion Approach

Contents

2.1 System Architecture 33
2.2 Details on Selected AStrion Modules 34
2.2.1 AStrion-D – Data Validation 35
2.2.2 AStrion-H – Harmonics & Sidebands 36
2.3 Outlook of AStrion 38
2.4 Innovation Project KAStrion 39

AStrion is a data-driven and fully automatic spectrum analyser. This approach for signal processing is under development in GIPSA-Lab. AStrion can serve as a core of a CMS. In this chapter a general introduction to AStrion idea is given. A short explanation on the function of each signal processing step, which is called a module of the AStrion tool, is also presented. The following section contains a deeper explanation on selected modules of AStrion and its results which are used as an input for methods proposed in this thesis. This chapter is concluded by a section on the European Innovation Project KAStrion, which this thesis is a part of.

2.1 System Architecture

As a minimum, AStrion requires a discrete time signal and its sampling frequency to perform the analysis of a single time domain signal. However, by using additional inputs as the rotational speed signal or the kinematic information on the system configuration it is possible to perform additional AStrion analysis. Figure 2.1 shows the way of processing a single time signal. In 2012, the AStrion algorithm consisted of three modules:

- AStrion-D – Data validation module executes a number of test to verify the quality of a measured signal. This module tests time domain as well as time-frequency domain of the inspected signal. Furthermore, a non-stationarity index of the investigated signal is computed. More details on this AStrion step are presented in [MM09]; [MM10] and in section 2.2.1;
- AStrion-I – Identification of peaks in an investigated signal. This module analyses the signal and performs several spectral estimations to classify its spectral content.

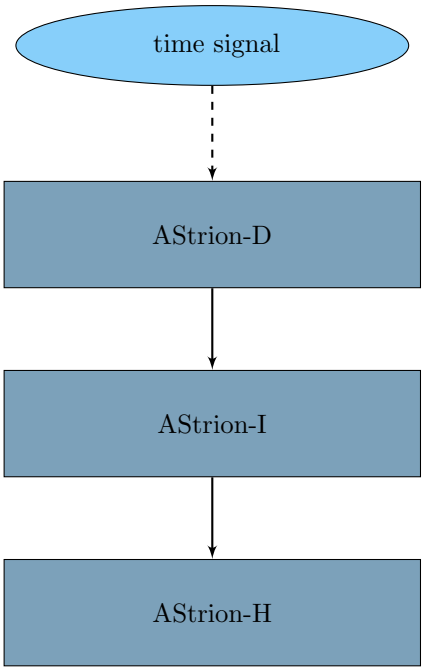

Figure 2.1: Flowchart of the AStrion in 2012 – Processing of a single time signal.

AStrion-I provides the so-called identity cards of each detected frequency pattern. The identity card for each peak among others includes its amplitude, frequency, class (sine wave, narrow band, noise, and alarms, as well as transitional classes), probability of misclassifying, and local signal-to-noise ratio (SNR). This AStrion module is based on the PhD thesis [Dur99];

- AStrion-H – Harmonic and sideband detection module seeks for patterns in the identity cards of an investigated signal. This module groups series of peaks which are harmonics of a fundamental frequency. In the second step, each peak within a detected harmonic series is assumed to be potentially a carrier frequency. The algorithm tries to find frequency peaks which belong to its modulation pattern, such a group is called sideband series. More details on AStrion-H can be found in [GMM13]; [MMG13] as well as in section 2.2.2.

2.2 Details on Selected AStrion Modules

This section covers the aspects of AStrion methodology which are the most important to understand signal processing methods presented in this thesis. The explanation of algorithms includes their outputs, which are simultaneously inputs for the other AStrion modules. Some of these results are also utilized as inputs for the proposed methods.

2.2.1 AStrion-D – Data Validation

The aim of AStrion-D module is to verify the quality of the analysed signal. A number of tests is performed including time saturation test, Shannon sampling test, non-stationarity detection tests, and periodicity tests. A lot of details on the algorithms applied in this module can be found in [HM06]; [MM09]; [MM10]. This section focuses only on the results of AStrion-D module which are essential for the following.

Among other results, AStrion-D computes a spectrogram of the signal and detects non-stationary time-frequency points. The two tests for detection of non-stationarities of the signal are detailed in [Mar05]; [MM09]. The first test detects time and frequency non-stationarity based on the time-frequency representation of the signal. This test is the binary hypothesis test which divides all the time-frequency tiles into one of the following subsets:

- the time-frequency tiles whose process is random and stationary, and eventually added with a deterministic process;
- the time-frequency tiles whose process in non-stationary.

This classification is performed for each frequency and is specified from the Neyman-Pearson criterion. The second test is performed in the frequency domain and it is proposed to avoid an influence of the time and frequency resolution of a time-frequency approach. This test is based on the normalized-variance properties of a spectral estimator. An example of the detected non-stationarities by this tests is shown in Figure 2.2. As it can be spotted from the legend of the right-hand figure, the level of the non-stationarity is evaluated and divided into four groups. The lowest non-stationarity is represented by a blue colour (level 1) while the highest level of detected non-stationarity is represented by a red colour (level 4).

From this thesis point of view, another important output of AStrion-D is a non-stationarity index [MM09]. This feature is computed by the fusion of the algorithm results from the time domain and from the frequency domain. More precisely, the frequency domain test consists of two different non-stationarity detections; the first is the detection of non-stationarities in the frequency projection and the second is the detection by normalized variance test in the TF representation of the signal. In this way a global non-stationarity index of the TF plane is obtained. The following equation shows how this index is evaluated

$$StatIndex = \left\lfloor \frac{t_{Det}}{P} \times \frac{f_{Det} - f_{NonConf} + f_{New}}{K} \times 100 \right\rfloor, \tag{2.1}$$

where $\lfloor\ \rfloor$ represents a floor operation, t_{Det} is the number of the non-stationary time segments, P is the number of all time segments in a spectrogram, f_{Det} is the number of frequency channels with detected non-stationarity obtained in the first frequency domain test, $f_{NonConf}$ is the number of non-confirmed frequency channels with respect to the total number of segments in a spectrogram and also can be seen as a false alarm rate computed in the second frequency domain test, f_{New} is the number of new frequency channels detected in the second frequency domain test, and K is the Fourier channel number.

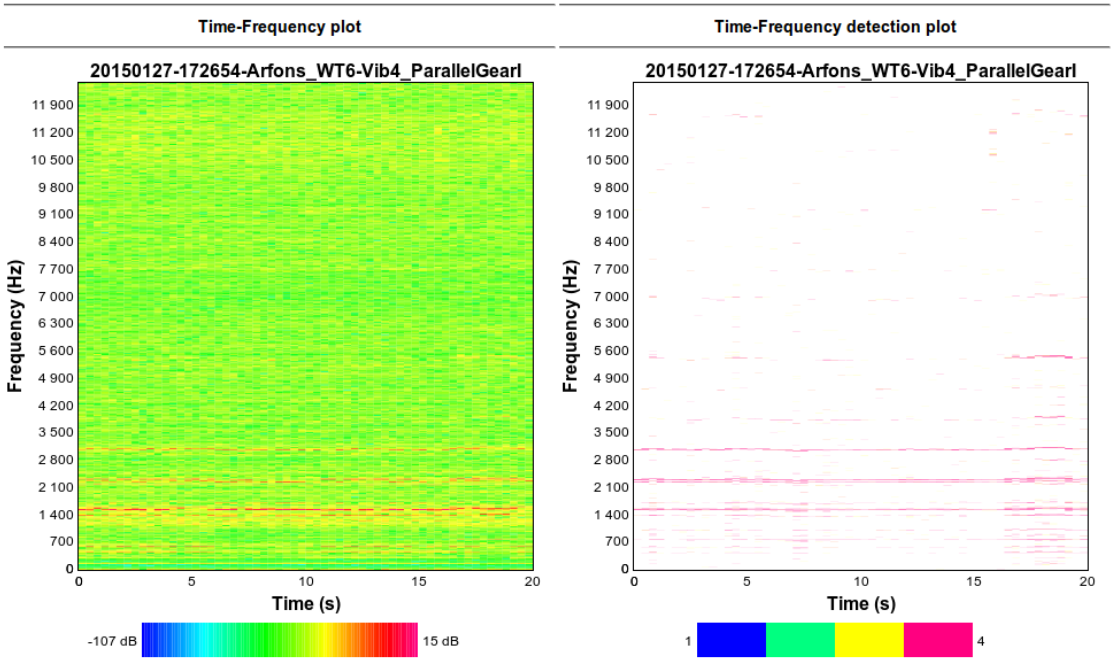

(a) Spectrogram (b) Detected non-stationarities

Figure 2.2: An example of (a) spectrogram computed by AStrion-D and (b) its non-stationarities detected in the signal.

A stationary signal has $StatIndex = 0\%$ whereas $StatIndex = 100\%$ corresponds to a fully non-stationary signal. Based on this value, AStrion-D informs the user that a signal is stationary or raises a warning or alarm, depending on the value of the stationary index.

2.2.2 AStrion-H – Harmonics & Sidebands

The task of this module is to identify and characterise frequency patterns in an investigated signal. As mentioned in section 2.1, AStrion-H uses the identity cards to group the detected peaks into two categories of series. The first one contains harmonics which are integer multiples of a fundamental frequency. The second group contains sideband series which are detected around a peak belonging to a harmonic series. One sideband series is distinguished by a carrier frequency and a modulation frequency, thus, for one harmonic series, AStrion-H can detect separate sideband series for the different peaks of the series. In addition to this multiple sidebands, series can be found for each peak being considered as a carrier frequency. The visualisation of various sideband series corresponding to one harmonic series is presented in Figure 2.3.

The harmonic and sideband pattern detection is performed with certain rules which can be found in [GMM13]; [MMG13], but more important from this thesis point of view is the

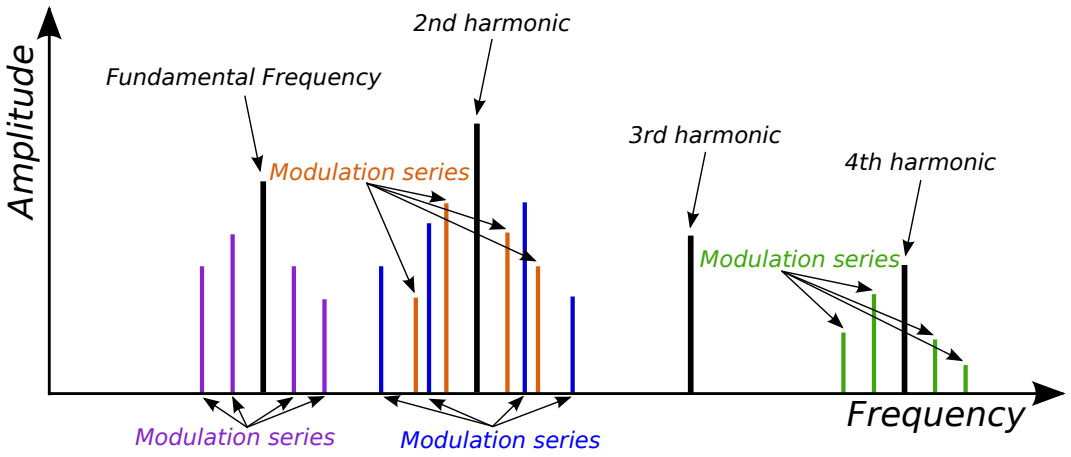

Figure 2.3: Examples of detected series by AStrion-H.

characterisation of detected series by features computed by AStrion-H. For each harmonic series **H**, the following indicators are computed:

- the fundamental frequency of the series **H** expressed in Hz – it is allowed that the fundamental frequency is not present and then the series starts from the second harmonic;
- the number of peaks constituting the series **H** – some gaps in **H** are allowed;
- the energy of the series **H** computed according to

$$E = A_1^2 + A_2^2 + ... + A_n^2, \tag{2.2}$$

  where A_i is the amplitude of peak i present in the series **H**, i is greater than or equal to 1, has integer values up to n, and i equal to 1 corresponds to the fundamental frequency;
- the density of **H** which characterises the number of missing peaks in the series **H**. This feature has a value from 0 to 1 and is expressed as

$$Den = \frac{N(\mathbf{H})}{r_{max}}, \tag{2.3}$$

  where $N(\mathbf{H})$ is the number of peaks in **H** and r_{max} is the rank of the last harmonic in **H**;
- the richness of **H** which indicates the size of the series relative to the entire spectrum of the signal. This indicator can have a value from 0 to 1 and is computed in the following way

$$Rich = \frac{r_{max}}{\left\lfloor \frac{\nu_F}{\nu_i} \right\rfloor}, \tag{2.4}$$

  where $\lfloor\ \rfloor$ is an integer operator, ν_i corresponds to the value of the fundamental frequency of the series **H**, and ν_F is the highest detected frequency in the investigated signal;

- the total harmonic distortion (THD) of the series **H** which expresses the classical measurement of the harmonic distortion [Slo01]. It is computed in the following way

$$THD = \sqrt{\frac{A_2^2 + A_3^2 + ... + A_n^2}{A_1^2}}, \tag{2.5}$$

  where the energy A_i is the amplitude of peak i present in the series **H**, i is greater than or equal to 1, has integer values up to n, and i equal to 1 corresponds to the fundamental frequency.

The features computed for the sidebands series are similar to the ones for harmonic series. The differences are

- Instead of the fundamental frequency, the carrier frequency and the modulation frequency represent the general identification of a sidebands series;
- Each of the above-mentioned features is computed separately for the left- and right-hand side of the carrier frequency.

2.3 Outlook of AStrion

AStrion presented in section 2.1 is the state of the development of this idea in 2012, at the beginning of this thesis. In order to present to the reader the whole idea the research parallel to this thesis is briefly mentioned.

One additional module has been developed to allow AStrion operate on the signal after order tracking. It is called AStrion-A, which stands for the angular resampling module, and it performs resampling from time-frequency domain into angle-order domain before AStrion-DIH modules provided the speed signal is available. This order tracking operation serves to suppress non-stationarities of spectral components which originate in mechanical phenomena and are caused by small speed variation during the signal acquisition. Details of this algorithm can be found in [Fir+14].

Apart from the modules presented throughout this thesis, there are two additional AStrion modules, which work as a core of a data-driven CMS. The first one tracks the time-frequency component module, AStrion-T. It tracks the results produced by all previous modules from time signals which are acquired in different time stamps. AStrion-T produces the trends of all the features computed by AStrion-ADIH modules (in practice it also takes into account the results of modules proposed in this thesis). The second module is AStrion-S which is the surveillance of the system. The goal of it is to fuse all available information in order to detect abnormal trends without setting predefined thresholds. Alarms raised by this module should serve the user as an early information on upcoming failures. A flowchart of AStrion-S operation is presented in Figure 2.4. The details on AStrion-T can be found in [GMM14]; [GMM15]; [Ger15], while AStrion-S module is still under development.

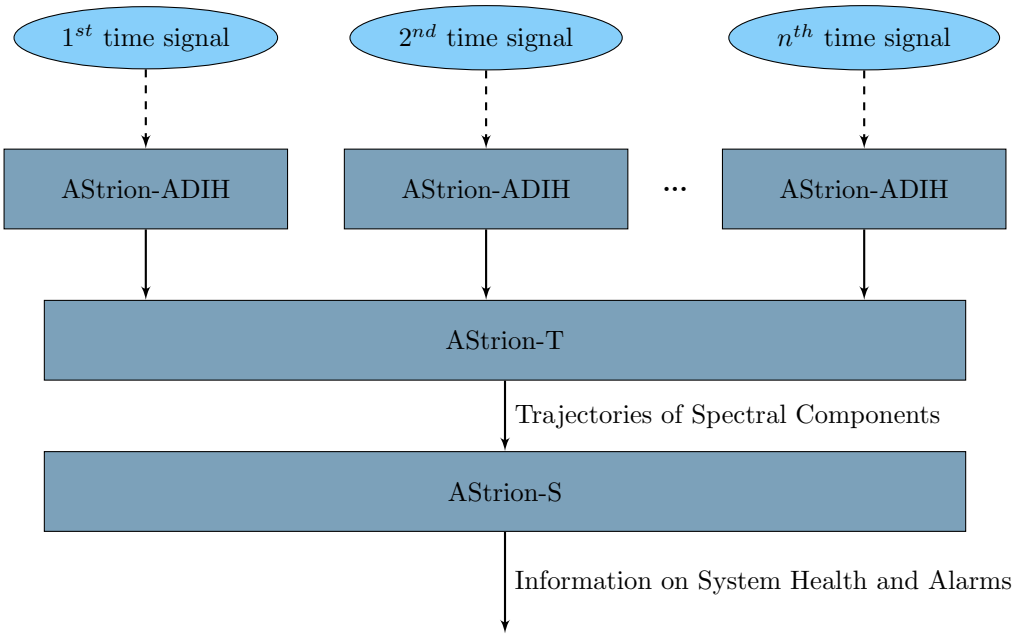

Figure 2.4: Flowchart of the AStrion tracking and surveillance modules – multiple signals usage.

2.4 Innovation Project KAStrion

The Innovation Project KAStrion is entitled *Current and vibration analysis for a preventive and predictive condition based maintenance in offshore wind farms*. It was funded by the European Institute of Innovation and Technology (EIT) through KIC InnoEnergy which is a European company for innovation, business creation and education in sustainable energy. This project is performed by an international consortium of academic and industrial partners which are Grenoble INP, INP Toulouse, EC Systems, CETIM, VALEMO, and MECAL. Further details can be found also on-line at `http://www.gipsa-lab.fr/projet/KASTRION/`.

KAStrion aims at maximizing the production time of offshore wind turbine farms by delivering a complete condition monitoring system. The Innovation Project KAStrion is business oriented and aims to deliver a maintenance system in the wind energy sector. Targeted customers are wind energy operators, expert and service companies in wind energy turbine monitoring, and wind turbine manufacturers. The business opportunity is based on the assumption that the maintenance and condition monitoring of wind farms are key to achieve a reliable prediction of the production capacity as well as to minimise the downtimes of machines. Therefore it is an important factor to maximize the revenue stream of wind farms.

KAStrion's solution to minimize the maintenance cost of wind turbines is twofold. Firstly the KAStrion CMS is built upon a stand-alone analysis system which delivers an innovative on-site pre-diagnostic of the machine based on a multi-modal spectral monitoring technology. Secondly this CMS is connected to a tailored diagnostic center which delivers a periodic

reporting on the technical state of each machine of the farm as well as provides an on-line access to the current information on the state of supervised systems.

The unique concept of the KAStrion CMS is the main differentiator face to systems present on the market. The advantages of KAStrion start at the system prototyping and validation. Thanks to the CETIM test rig designed and built as a small scale imitation of a wind turbine drive train it is possible to create typical faults and check the implemented algorithms on signals captured during the changing health condition of selected components. In addition to CMSs available on the market, KAStrion also offers poly-phase electrical analysis. Moreover, KAStrion is reliable due to maximal possible autonomy of AStrion algorithms with a minimal user dependencies. Most settings are signal dependent and are selected internally. Finally, thanks to cooperation with Valemo the prototype version of the system has been installed on two WTs which provided the possibility of a signal processing algorithm validation on real-world WT signals.

This study is a development of the CMS called KAStrion. Throughout this thesis some signal-processing methods are proposed to fulfil the objectives of KAStrion by improving and completing AStrion methodology presented in section 2.1.

Chapter 3

Non-Stationarity of Inputs – AStrion-C

Contents

3.1 State of the Art 41
3.2 Stationary Signals 42
3.3 Cropping out a Time-Frequency Representation 43
3.3.1 Framework 43
3.3.2 Details of the Cropping Time-Frequency Plane Method 43
3.4 Validation on a Simulated Signal 47
3.5 Conclusions and Perspectives 51

3.1 State of the Art

For reliable operation of CMSs it is important to compare diagnostic features computed from signals acquired under constant load and speed of investigated machine as well as similar operational conditions, as pointed in [BZ09a]; [JB13]. Generally, the established methods used in diagnosis and CMS cope well with stationary signals. However, in the case of a small speed fluctuation, the order tracking method [FM97] is applied and in the majority of cases this is sufficient for a proper diagnosis. The challenge starts in the case of a continuous and high variation of the machine operating conditions or load, as in the case of a WT. That is why even a CMSs supplied with the best post-processing algorithms will have real difficulties working on non-stationary signals. It explains the need for the selection of the best stationary signal for a robust condition monitoring and diagnosis.

An interesting way to deal with the problem of changing operational conditions in a gearbox diagnosis is presented in [BZ09a]. The authors proposed a feature which is plotted against operational parameter, in the presented case it is a rotational speed, that changes linearly in a limited range of operating conditions. However, this paper does not address an issue of a data selection and a rejection of samples with possible external impacts not related to the operation of the machine in the real-world condition.

The diagnosis of rolling-element bearings working under changing operational condition is also of big interest. An example could be [MZ11], where the authors propose to filter out impact signals related to the bearing fault. This approach is oriented to detect a specific type of a fault by taking into account the whole provided signal and thanks to a normalization it is an adaptive method suited for the non-stationary time-series.

There are various approaches to detect a change in the signal stationarity. There are model-based methods [BB83]; [Pop99] and statistical parameters driven [Oli+90]; [BN91]; [WW04], but recently the most popular ones employ a time-frequency (TF) signal representation [LD98a]; [Bor+10]; [Sou+12]; [Mar05].

There are various application domains for the above-mentioned non-stationary detection techniques including speech processing, image processing, vibroacoustic signals, automatic analysis of biomedical signals, or even seismic signals. However, an advantage of applying these methods in fault detection is not well proven and rather they can serve as an auxiliary tool. For fault detection facilitation a feature related to detected non-stationarity has been introduced. In the literature there are also proposals of stationary index estimation which are based on TF plane only, as in [LD98b], or combine time and TF non-stationarity detection, as in AStrion-D described in section 2.2.1.

The selection of a stationary part of a vibration signal by cropping out its TF representation is proposed in this chapter. This technique takes advantage of the method already applied in AStrion and briefly described in section 2.2.1.

This chapter proposes to use the results of non-stationary detection in TF representation and select the biggest possible part of the signal with the lowest non-stationarity. It is called *cropping out time-frequency plane* since the output of this algorithm is a truncated time signal in terms of its time duration as well as frequency range. A similar approach has been presented in [Zil06], but this is applied on low probability of intercept radar data and has a goal to isolate a modulation.

3.2 Stationary Signals

The definition of the stationarity is based on the statistical properties of the signal and it says that a signal is strictly stationary (ergodic) while its statistical properties does not change with time [OSB98]. Moreover, a signal weakly stationary, also described as a wide-sense stationary signal, can be defined if only its first and second order moment meets the above-mentioned condition. If the probability distribution varies with time, the signal is non-stationary.

In an engineering approach it is important to bear in mind that speaking about stationary and non-stationary signals, it is the probability distribution of the signal that is referred to, and not the process which generates this signal [NK03].

3.3 Cropping out a Time-Frequency Representation

3.3.1 Framework

The considerations in this chapter are based on the detection of a non-stationarity in a spectrogram which has been briefly introduced in chapter 2.2.1. More details are given in [MM09]; [Mar05]. The discrete time signal $x[n]$ of the length N and sampling frequency F_s can be represented in a TF plane as the spectrogram

$$S_x[n,k] = \frac{1}{NF_s}\left|\sum_{m=0}^{N-1} x[m]w[m-nD]e^{-2\pi jkm/K}\right|^2, \tag{3.1}$$

where k is the frequency variable, $w[m]$ is the time window, D is the time-shift of the window, and K is the Fourier bin number.

Launching AStrion-D, all the tiles corresponding to non-stationary events in the TF representation of the signal are detected, as illustrated in Figure 2.2 (b). Based on this non-stationarity detection results, this thesis proposes further processing in order to extract a TF area which has a lower stationary index, the index being recalled in Equation (2.1).

The following glossary is adopted:

- *Tile* – a single bin of the TF representation;
- *Time segment (t_{seg})* – a subset of the spectrogram $S_x[n,k]$ which meets the following condition
$$\mathfrak{L}_x[n] = \left\{(n,k) \in \Re^2 / \exists S_x[n,k] \; for \; a \; given \; x[n]\right\}, \tag{3.2}$$
$\mathfrak{L}_x[n]$ is a cross section of $S_x[n,k]$ at constant time n;
- *Frequency segment (f_{seg})* – a subset of the spectrogram $S_x[n,k]$ which meets the following condition
$$\mathfrak{L}_x[k] = \left\{(n,k) \in \Re^2 / \exists S_x[n,k] \; for \; a \; given \; x[n]\right\}, \tag{3.3}$$
$\mathfrak{L}_x[k]$ is a cross section of $S_x[n,k]$ at constant frequency k;
- *Area (A)* – a selected part of the TF representation.

The terminology is also illustrated in Figure 3.1.

3.3.2 Details of the Cropping Time-Frequency Plane Method

To assure a manageable computation time and usability of obtained results, some presumptions on the signal under study have been made. First of all, the selected frequency segments always start from the minimal frequency equal to 0 Hz. This selection is made because of

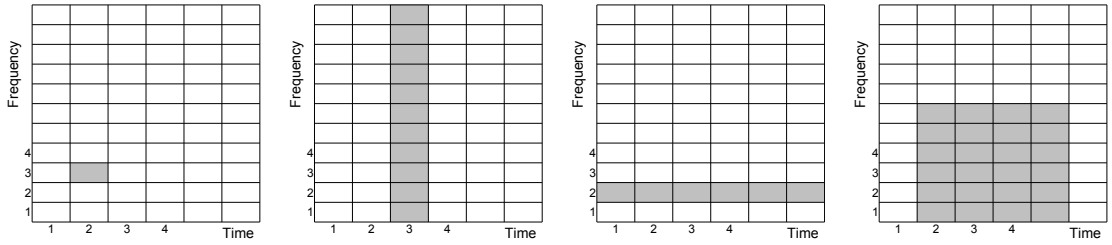

(a) Tile (b) Time Segment (c) Frequency Segment (d) Area

Figure 3.1: Graphical visualisation of the TF subsets.

the nature of vibration signals, which are object of this study. A lot of valuable information is present in the relatively low frequency, that is the frequency corresponding to fundamental characteristic frequency value and its first few harmonics. Moreover, this restriction assures that the computation time is highly reduced for the proposed iterative method. Secondly, the selected area has to be rectangular. It is determined by the further usage of the obtained result, which makes the post-processing of the cropped signal feasible. Thirdly, the minimal number of the time segments has to be determined. This value depends upon the required spectral frequency resolution Δf of the signal, which in turn depends on the mechanical system under investigation. Finally, the minimal number of the frequency segments has to be defined as well. As a general rule we propose to use at least 10% of the original signal length and 5% of the available frequency range (Nyquist frequency divided by two), but these values could be changed according to the user requirements.

The minimal duration of the signal can be adjusted according to the system. It is enough to determine the lowest frequency of interest which is present in the investigated mechanical system. It could be the slowest characteristic shaft frequency or a fault frequency of the rolling-element bearing, let it be f_{min}. Then the minimal signal length to capture this phenomenon is expressed as

$$t_{min} = \frac{1}{f_{min}}. \tag{3.4}$$

In the case of processing a real-world signal it is advised to double the obtained time t_{min} or even multiply it by the factor of 4 since the more full cycles of mechanical related vibration are registered, the easier it is to obtain relevant results.

Similarly, the minimal frequency range could be determined according to the investigated system. Let F_{inv} be the frequency corresponding to the investigated mechanical component, then the minimal frequency range to capture should be at least the double value which is expressed as

$$f_{min} = 2 \cdot F_{inv}. \tag{3.5}$$

The goal of the proposed method is to select the biggest possible area from the TF representation which is stationary up to a certain level. The quantity T_i is used as the measure of

the stationarity of the area and it is inspired by the non-stationarity rate definition proposed for AStrion-D [MM09]. The T_i is defined as

$$T_i = \frac{NST_i}{AT_i} \cdot \frac{NSF_i}{AF_i} \cdot 100\%, \tag{3.6}$$

where NST_i is the number of time segments containing non-stationary tiles in the considered time range AT_i, and NSF_i is the number of frequency segments containing non-stationary tiles in the considered frequency range AF_i. Based on the user needs the accepted level of non-stationarity, referred to as a threshold T_S, can be adapted and only the area which meets the condition

$$T_i \leq T_S \tag{3.7}$$

is considered as an allowable result for further cropping. The selection of the T_S value is important. Please note that $T_S = 0\%$ applied on real-world noisy signals is a too low value, since it is a frequent phenomenon that some non-stationary spectral component appears. Based on tested examples the threshold value T_S is fixed to 4%, which allows to reduce the non-stationrity of the signal after cropping operation as well as to preserve a sufficient time duration of the investigated signal. Moreover, the threshold $T_S = 4\%$ is the beginning of the serious warning on the non-stationarity of the signal proposed in [MM09].

Figure 3.2 presents the detailed flowchart of the iterative algorithm for selecting the stationary part of the signal. It consists of two loops. The first one, the main loop with blocks in light blue colour, is to select the time tile to start with t_0 and preserve the biggest area A_i for the starting conditions. The second loop is executed under the first one and iterates through the TF plane to select the biggest area A_i which fulfills the condition with a selected threshold T_S. The blocks of this loop are in dark blue colour. Finally, the algorithm selects the biggest area A_{max} among all the results kept in the main loop A_i. Afterwards, the A_{max} is used for cropping the signal.

The cropping operation on the signal is executed without any filter application. In the proposed approach the first step to obtain the result is to truncate the signal in the time domain according to the A_{max}. The next step is to make use of the selected frequency band and analyse the signal only up to evaluated frequency, which is possible in AStrion. This method enables the operation only on the specified part of all the frequency segments of the signal spectrum.

An important part of the algorithm is a decision block in the centre of Figure 3.2. ($T_i < 6 \cdot T_S$?) operation has a function of stopping the inner loop of area seeking. This condition uses a multiplied value of the defined threshold T_S in order to allow the algorithm to include in the final result non-stationarities gathered in one region of the TF signal representation in the case of a big stationary area is present after this non-stationary tiles. Thanks to this condition, the algorithm does not stop immediately after encountering an area which does not meet the defined conditions but instead of that it keeps looking for a possible bigger area with the non-stationary tiles below the defined threshold value T_S.

The algorithm presented in Figure 3.2 has a priority to increase the selection area in the frequency direction. Nevertheless, it is proposed to execute the same iterative algorithm the

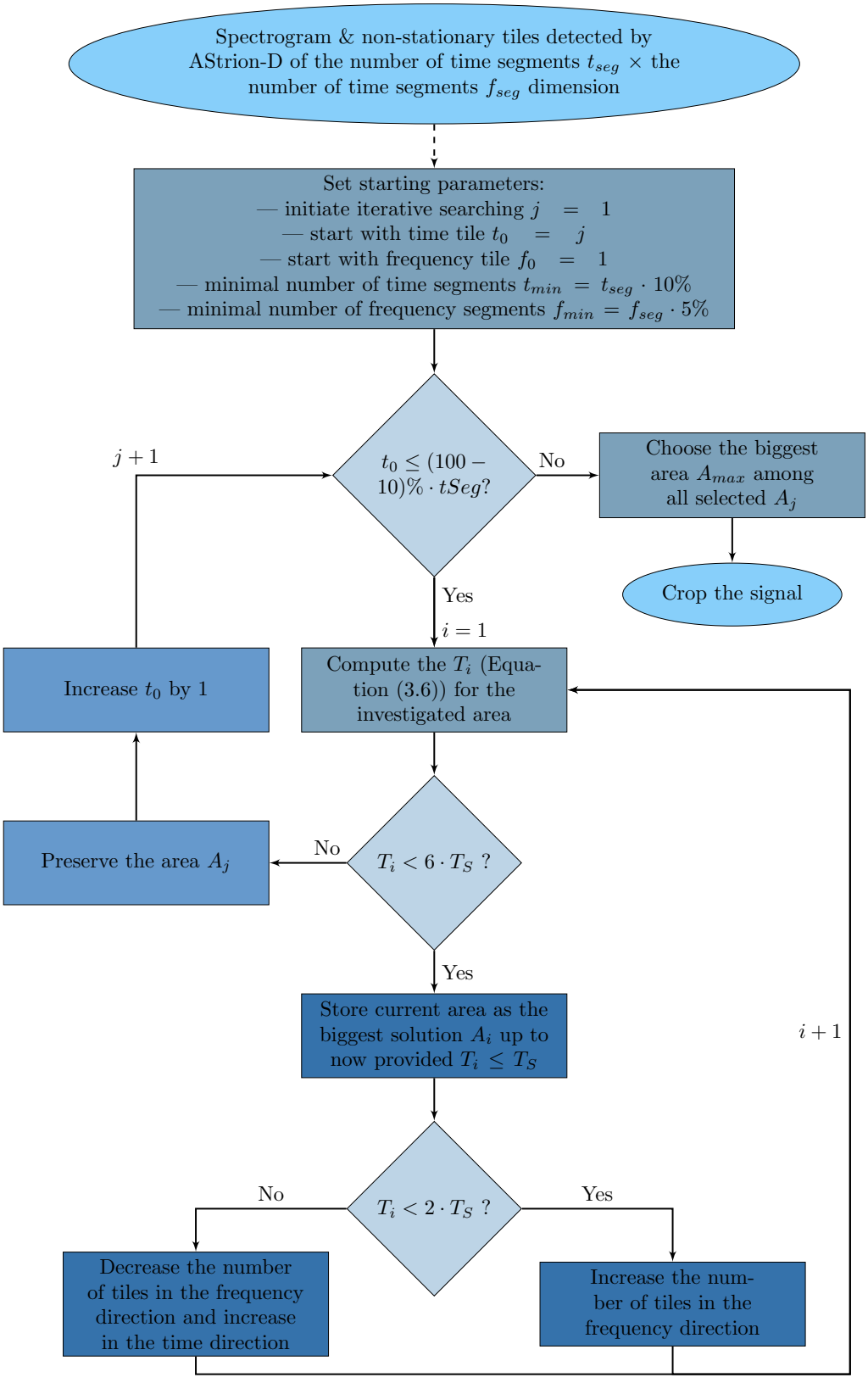

Figure 3.2: Flowchart of cropping, with the frequency priority setting, the TF representation of a signal.

Table 3.1: Changes to perform to blocks in Figure 3.2 to obtain time priority version of AStrion-C algorithm.

Frequency priority	**Time priority**
Decrease the number of tiles in the *frequency* direction and increase in the *time* direction	Decrease the number of tiles in the *time* direction and increase the number of tiles in the *frequency* direction
Increase the number of tiles in the *frequency* direction	Increase the number of tiles in the *time* direction

second time on the signal with a change to time priority. It is simply applied by changing the action performed after checking the condition ($T_i < 2 \cdot T_S$?) in the manner presented in Table 3.1.

The implementation of the block executed in the case that the condition ($T_i < 2 \cdot T_S$?) is not met is more complex than presented in Figure 3.2. Additional parameters are defined and two different scenarios in this situation are possible. The first one is a decrease of the number of frequency segments and increase of the number of time segments by the value of one provided that in the previous iteration $i-1$ the area is not increased in the time direction and in the iteration $i-2$ the area is not decreased in the frequency direction. Otherwise, the second scenario is performed which is the increase in the frequency direction only. In the case of time priority these conditions are defined in the same manner but time and frequency indexes are reversed. This procedure allows to steadily increase the prioritized direction.

3.4 Validation on a Simulated Signal

The above-described signal processing method has been tested on a simulated signal. The signal is prepared to contain strong non-stationarities made of two frequency components. One component has a constantly increasing frequency value from 10 Hz to 30 Hz and another is reversed. The signal has also a pure sine wave component at 15 Hz for a finite duration at the beginning of the signal as well as a wide-band noise at frequency around 33 Hz also during restricted time of the signal duration in the middle of it. To all those pure frequency components a white noise is added with the SNR equal to 15 dB.

The signal has parameters as listed in Table 3.2. The time domain view of the signal is presented in Figure 3.3 and spectrogram of the signal in Figure 3.4 (a) along with non-stationary tiles detected by AStrion-D in Figure 3.4 (b). AStrion-D computed the non-stationarity rate which equals to 48% for this simulated signal.

The time signal has been divided into 96 time segments and 513 frequency segments. Assuming that a minimal signal duration at the input of the algorithm is 10%, t_{min} equals to 10 time segments. Thus, the algorithm has performed 86 iterations as presented in Figure 3.2 starting from time segments t_0 equal to 1 and has the highest value equal to 86 as the following

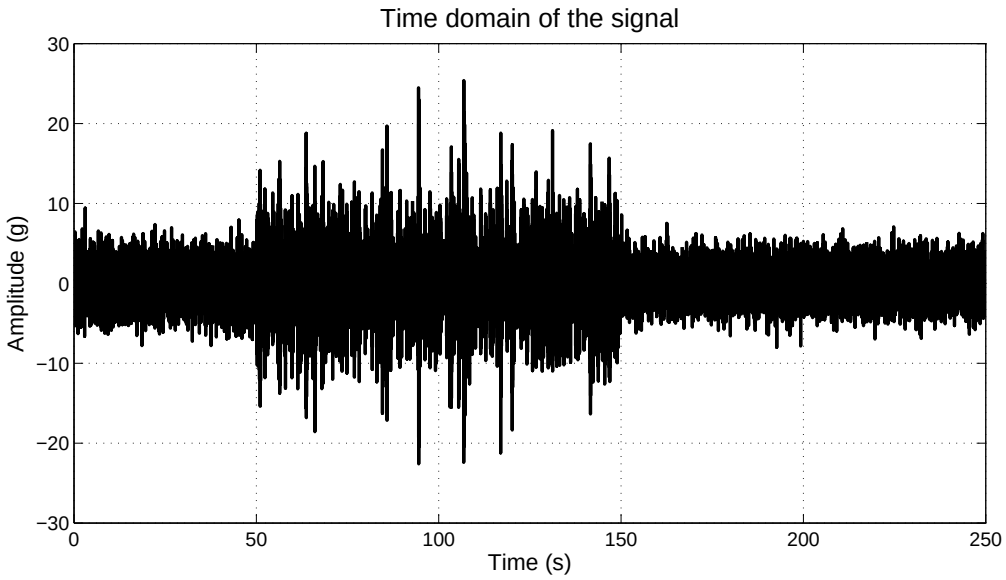

Figure 3.3: Simulated signal in the time domain.

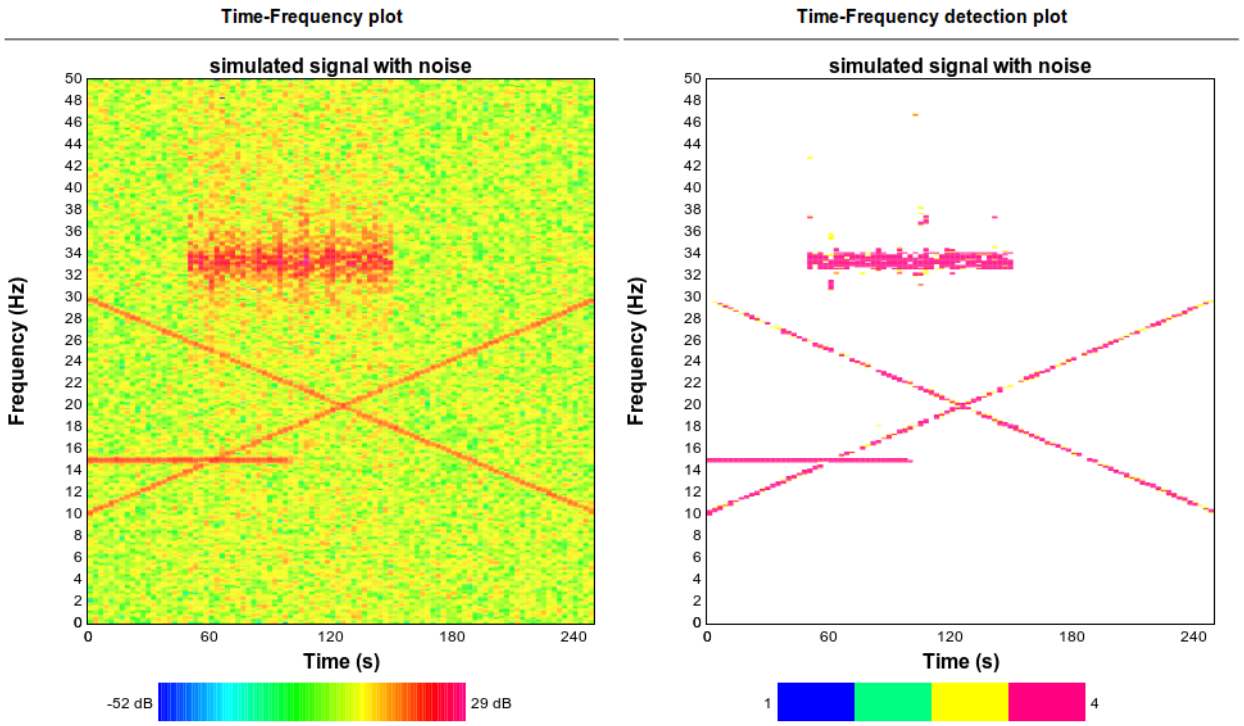

(a) Spectrogram (b) Detected non-stationarities

Figure 3.4: Simulated signal in the frequency domain (a) spectrogram computed by AStrion-D and (b) its non-stationarities detected in the signal. The non-stationarity rate computed by AStrion-D equals to 48%.

Table 3.2: Simulated signal parameters.

Sampling frequency	100 Hz
Number of samples	25,000
Signal duration	250 s

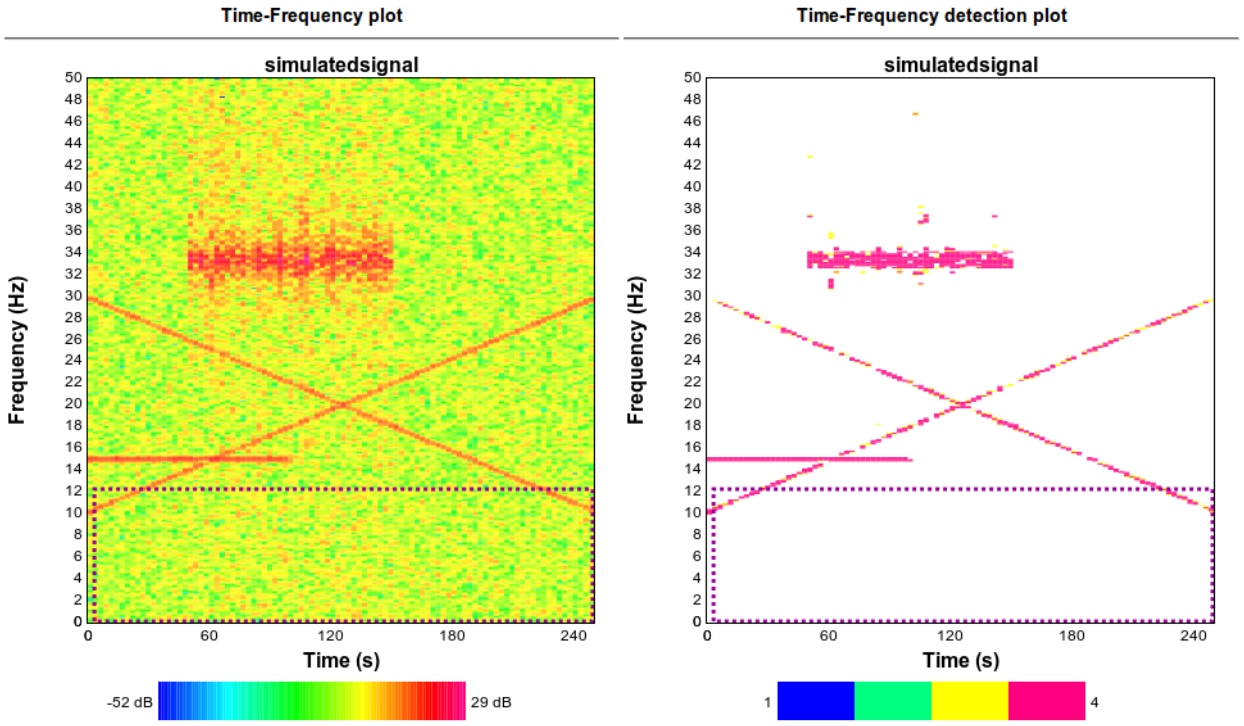

(a) Spectrogram (b) Detected non-stationarities

Figure 3.5: Presentation of AStrion-C result represented by dashed lines; (a) spectrogram and (b) its non-stationarities detected in the signal. The non-stationarity rate for the selected part of the signal computed by AStrion-D equals to 4%.

time segments do not meet the t_{min} condition to start the iterative searching. The last iteration has no chance of growing in the time direction so only the frequency dimension increase is verified. After that the time direction priority version is launched and final selection of the biggest area is made. It occurs that the biggest stationary area A_{max} among results of all performed iterations of the algorithm is found in the second iteration of the time priority version of the algorithm, that corresponds to j equal to 2. The best result found by the proposed algorithm is presented in Figure 3.5.

Moreover, to give an insight view of the inner steps of the proposed algorithm the sub-iterative searching of the biggest area is presented. The result corresponds to the smaller loop of the algorithm presented in Figure 3.2 while the j is equal to 2 and i is iteratively increased. This iteration starts from time segments in a range $2-12$, this can be noted from Figure 3.6 (a), and a range of the frequency segments equal to $1-25$. During this iteration of

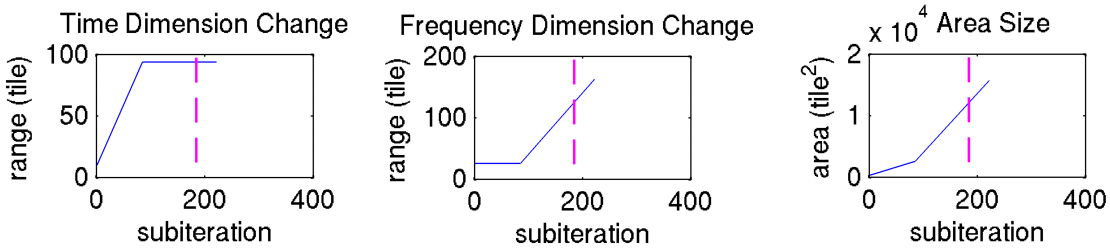

(a) Time segments (b) Frequency segments (c) Area size

Figure 3.6: Evolution of parameters during the iterative searching of the biggest area to be cropped. (a) number of time segments, (b) number of frequency segments, and (c) size of area. The vertical dashed magnet lines show the 185^{th} iteration that corresponds to the biggest area A_{max} selected by AStrion-C.

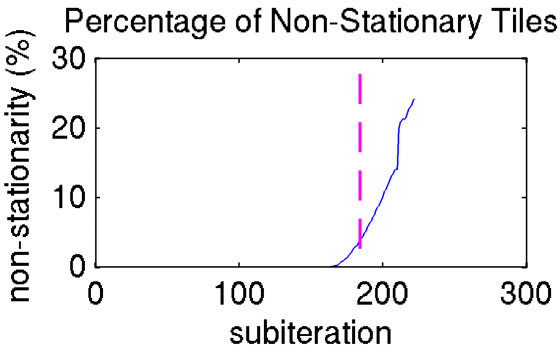

Figure 3.7: Evolution of the T_i during the iterative searching for the biggest area in the iteration corresponding to j equal to 2. The vertical dashed magnet line shows the 185^{th} iteration that corresponds to the biggest area A_{max} selected by AStrion-C for the investigated signal.

the algorithm a 222 sub-iterations are performed and changes of basic parameters are shown in Figure 3.6 as well as a T_i value computed for each verified area is presented in Figure 3.7. In all figures presenting the details of sub-iterations there is a dashed magenta line which represents an iteration with the biggest area meeting the condition $T_i < T_S$, in the presented example it is at 185^{th} sub-iteration. The selected area is depicted by a dashed magenta lines in Figure 3.5 and captures the time segments from 2 to 96 and frequency segments up to 127, which corresponds to the frequency 12.38 Hz.

This result is exploited further on by a cropping operation. This starts from the signal truncation in the time domain for the length corresponding to the time segments which creates the final area. Subsequently, the selection of the frequency range of the cropped signal is applied. This operation is performed without any filter operation but the frequency truncation is managed internally by AStrion – selected percentage of full spectrum is further analysed. The non-stationarity index computed by AStrion-D for selected area equals 4%, which is a significant difference in comparison to the non-stationarity index of an original signal.

3.5 Conclusions and Perspectives

The presented example illustrates that the proposed algorithm is able to select a stationary part of a signal. This result is presented in Figure 3.5 and intuitively one can say that the area marked out by a dashed line is an appropriate selection. For the internal purpose of validation, this algorithm has been used on a vast number of signals, which includes simulated and real-world signals starting on simple examples and finishing on more complex ones, in terms of richness of spectral components. In section 6.3 the application of AStrion-C on a real-world signal measured on the test rig will be described. Another example will be presented in section 6.4 with the use of the proposed algorithm on a WT vibration signal of 60 s length with a significant speed fluctuation.

The validation of the proposed algorithm allows us to integrate it into the whole AStrion methodology. AStrion-C can be thus considered as a means to deal automatically with non-stationary signals, which is a necessity for a usage within an automatic CMS. The presented examples show that it is possible to select more stationary part of the signal relevant for a further analysis.

Apart from its usage presented in this chapter, AStrion-C has a potential to be employed for a signal acquisition and more precisely its validation. The presented method for the stationary signal selection could be used for recording the best possible signals from an on-line measurement by a CMS.

Another perspective for the proposed algorithm is the selection of stationary areas from a signal containing strong impacts. Such a signal could make a diagnosis of a machine very difficult. An example of this situation is a power press, which works with frequently and constantly repeated impacts.

Chapter 4

Integration with Kinematic Information – AStrion-K

Contents

4.1 State of the Art 53
4.2 Characteristic Fault Frequency Association 56
4.2.1 Shafts and Gearboxes Association 57
4.2.2 REB Association 57
4.2.3 Additional Remarks 58
4.3 Validation 60
4.3.1 GOTIX 60
4.3.2 AStrion-K Results 63
4.4 Conclusions and Perspectives 64

This chapter is dedicated to describe a signal-processing methods proposed for automatic usage of the available information on the system within AStrion methodology. This chapter starts with a description of state of the art including the explanation of the dependencies of the components geometry with the characteristic frequency generated by the machinery. The proposed method is then described in section 4.2 and validated on a real-world vibration signal in section 4.3.

4.1 State of the Art

Characteristic fault frequencies arise from the geometry of the mechanical parts of an investigated system and help to find and identify the origin of a fault. These frequencies are easy to estimate for such components as gears, shafts, and rolling-element bearings (REBs), which are important parts of a wind turbine drive train. An overview of the known fault frequencies concerning WTs is given in section 1.6.

In the case of gearboxes, a characteristic pattern of vibrations due to teeth meshing is always generated and its changes indicate a fault. Figure 4.1 (a) presents a technical drawing of a spur gear with its basic dimensions and Figure 4.1 (b) shows a vibration signal model

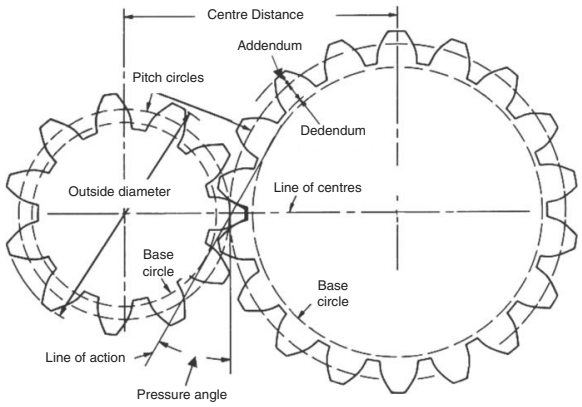

(a) Basic dimensions of a pair of spur gears

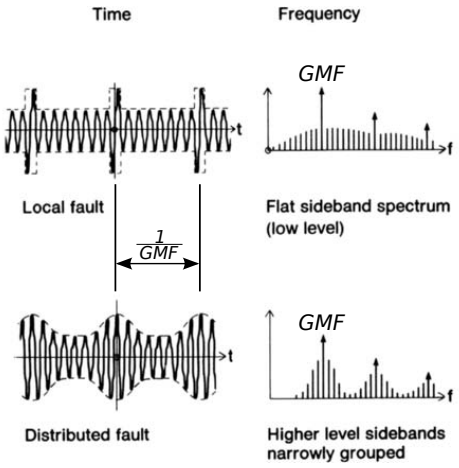

(b) Characteristic pattern of a local and distributed faults in gears in the time and frequency domains

Figure 4.1: Fundamental diagnostics knowledge about gears [Ran11].

of a faulty gearbox for the case of a local damage as well as a distributed one, both figures are cited from [Ran11]. Figure 4.1 (b) presents time domains and frequency domains of both types of faults. Sidebands of the GMF are present in the local and distributed faults, but only the second one presents a clear amplitude modulation pattern in the time domain signal.

REBs do not produce characteristic vibration patterns in a good condition, but in the case of a failure the appearance of certain signal patterns informs about a corresponding type of damage. An established method for REBs diagnosis is the so called envelope analysis [RA11]. Figure 4.2 shows dimensions of a REB in its top part and model vibration signals generated by common fault types. Vibration patterns are presented in time domain as well as an envelope signal is given.

The equations to calculate the values of the characteristic fault frequencies of a rotating machinery are presented in Table 4.1, where f_r is the shaft speed expressed in Hz, z is the number of teeth of a gear, n_r is the number of rolling elements in a bearing, d_r is the diameter of the rolling elements, d_p is the pitch diameter, and ϕ is the angle of the load from the radial plane.

Table 4.1 presents formulae based on theoretical models for calculating the characteristic frequencies of rotating machinery components and are referred to as theoretical values. It is important to notice that in the case of a REB, the characteristic fault frequencies as BPFO, BPFI, FTF, BSF assume no slippage, whereas it must occur when the bearing is running. This is the reason why the actual characteristic frequencies may vary slightly in the real-world applications in comparison to these theoretical values. In practice, it is normal to see a random variation of the theoretical REB characteristic fault frequencies in the order 1–2% [RA11].

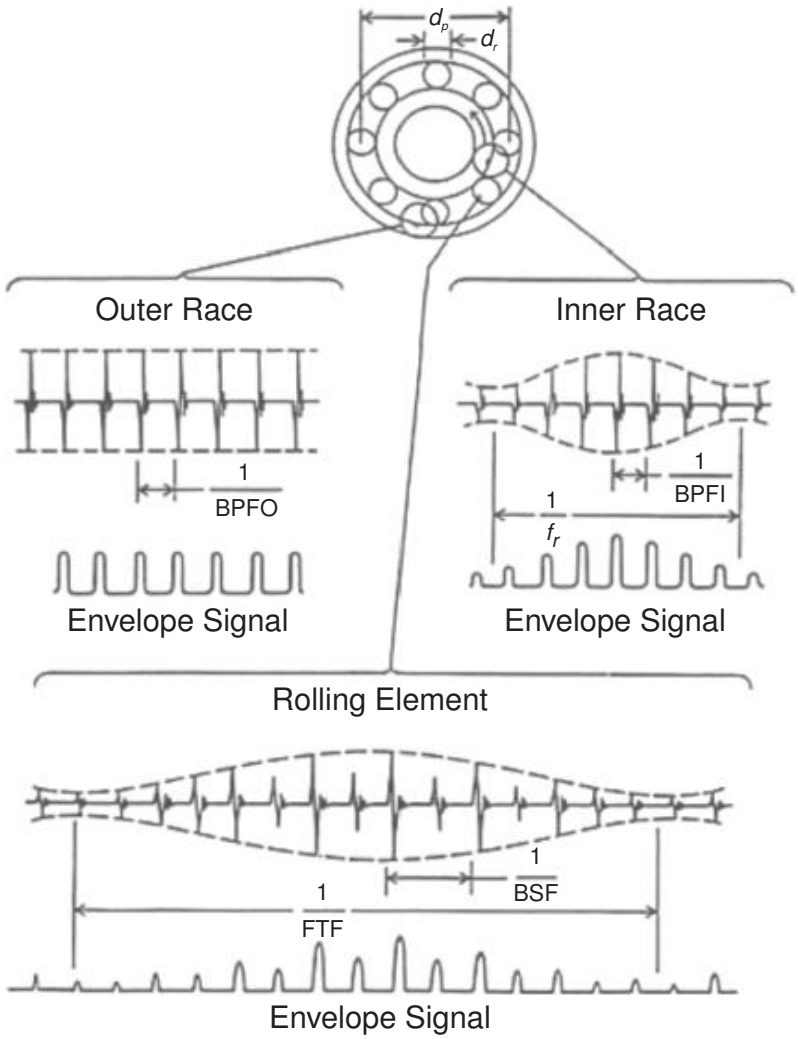

Figure 4.2: A drawing of a REB with its typical faults [RA11].

Usually, rotational frequency f_r is measured only on the high speed shaft (HSS) of a WT. In such a case it is necessary to calculate the relative value of an f_r for each shaft present in the system. This recalculation is executed by using the speed ratio of present gearbox stages in the investigated system.

Moreover, a standard approach in CMS is system-based and characteristic frequencies are directly used to compute health indicators without analysing vibration signals earlier e.g. narrow-band RMS computed according to previously defined band. There is no method which applies kinematic information only for adding information to earlier-obtained harmonic and modulation series as it is presented in the following section.

Therefore an automatic method to associate previously detected patterns in a signal with characteristic fault frequencies is proposed and it is called AStrion-K. The details and challenges of this technique are presented in the next section.

Table 4.1: Selected formulae for calculating characteristic fault frequencies [Ran11].

Fault frequency name	**Formula**
Shaft	
Shaft Speed Frequency	$SSF = f_r$
Gearbox	
Gear Mesh Frequency	$GMF = f_r \cdot z$
Rolling-element bearing	
Ball-Pass Frequency of Outer Race	$BPFO = \frac{n_r f_r}{2}\left\{1 - \frac{d_r}{d_p}cos(\phi)\right\}$
Ball-Pass Frequency of Inner Race	$BPFI = \frac{n_r f_r}{2}\left\{1 + \frac{d_r}{d_p}cos(\phi)\right\}$
Fundamental Train Frequency	$FTF = \frac{f_r}{2}\left\{1 - \frac{d_r}{d_p}cos(\phi)\right\}$
Ball Spin Frequency	$BSF = \frac{f_r \cdot d_p}{2d_r}\left\{1 - \left(\frac{d_r}{d_p}cos(\phi)\right)^2\right\}$

4.2 Characteristic Fault Frequency Association

The proposed method for kinematic information usage is a data-driven approach. It requires an *a-priori* interpretation of a spectral content of a signal as well as a harmonic and sideband pattern recognition which are provided by AStrion-IH performed earlier. The spectrum identification pre-requisite is obtained by AStrion-I briefly described in section 2.1 and more details are given in [Mai+06]. The proposed algorithm assumes also that the harmonic series and modulation sideband series are detected previously with the method described in section 2.2.2. In this section the proposed algorithm associates characteristic fault frequencies with previously detected harmonic and sideband series. It is an iterative method, which performs an association with each characteristic frequency provided by the kinematic information of the system.

In the first step of this method the characteristic frequencies have to be calculated for each mechanical component as shown in Table 4.1. In order to compute it automatically for the investigated signal the measured rotational speed and the list of characteristic frequencies expressed in orders is needed for this operation. The order values originate in the order tracking method mentioned in section 1.5.1 and are equivalent to the characteristic frequencies computed for the rotational speed equal to 1 Hz. The order values are expressed in the unit of *orders*. The order values are popularly used as a reference, since they can be directly applied on a signal after angular resampling, which is also called order tracking. More details on the resampling can be found in [FM97]; [Ran11]; [Fir+14].

In the case of more complex systems, such as a wind turbine drive train, the mechanical components are carried by several shafts. It is popularly done in the case of wind turbines that only a high speed shaft speed is measured, which serves as a reference shaft. As a consequence, the speed of other shafts has to be calculated from the gear ratios. This permits to reduce the cost of sensors for the measurement of the rotational speed.

The association of the characteristic fault frequencies is performed in two steps. Firstly, the harmonic series which meet a criterion are identified as candidates for the association. The second step is the selection of one final candidate. These two steps are executed for the harmonic series and afterwards the same set of operations is performed on the modulation sidebands series. The association details are explained separately for rolling-element bearings and other components in the following subsections.

4.2.1 Shafts and Gearboxes Association

The selection step is based on a relative difference between the theoretical f_t and the detected f_d value of the characteristic fault frequency defined as

$$RFD_i = \left| \frac{f_{d,i} - f_{t,j}}{f_{t,j}} \right| \cdot 100\% < \eta, \tag{4.1}$$

where i is the index of a series, j is the index of a characteristic frequency calculated for the investigated kinematic configuration, $f_{d,i}$ is the fundamental frequency of the detected series, $f_{t,j}$ is the theoretical frequency based on the system kinematics. Only series with a value of RFD_i lower than a threshold η are kept. It is selected that η equals to 1% of the investigated theoretical frequency $f_{t,j}$.

Usually, a real-world signal has so many peaks detected that even in a small range defined by the threshold η there are numerous candidates for the association. The second step is to select only one series for the final association. The association of series with the characteristic fault frequencies corresponding to shafts and gearboxes is intuitive. The proper series S_j to be associated is selected as the one with the lowest RFD_i value among the candidates from the first step of the association

$$S_j := \{b \in RFD : b \leq a \forall a \in RFD\}, \tag{4.2}$$

where RFD is a set of all relative frequency difference values kept from the first step of the association algorithm for the inspected characteristic frequency.

4.2.2 REB Association

The REBs are always subject to the slippage phenomenon mentioned earlier which causes the variation of the measured and the theoretical frequency in the order 1–2% [RA11]. This issue is addressed in AStrion-K module, which has never been attempted before. This is the reason for the proposal of a different association method for REBs.

The first step of the association is similar to the one performed for the other mechanical components and defined in Equation 4.1. The difference is in the threshold η which is proposed to be bigger and equals to $\eta + \delta\eta$. Then the condition for selecting the candidates for the association is the following

$$RFD_i = \left| \frac{f_{d,i} - f_{t,i}}{f_{t,j}} \right| \cdot 100\% < \eta + \delta\eta, \tag{4.3}$$

this change is due to the slippage phenomenon. We propose to use $\eta + \delta\eta$ equal to 2%.

In the case of rolling-element bearings the lowest RFD_i value is not a sufficient indicator because of the slippage phenomenon, which can be random. As a consequence, earlier computed RFD_i is not used at all for the final selection of one candidate and an additional parameter is proposed. It is a bearing series indicator defined as

$$BSI_i = \frac{\frac{E_i}{E_{max,i}} + Den_i}{2}, \tag{4.4}$$

where E_i is the energy of the series under investigation, see Equation (2.2), $E_{max,i}$ is the energy of the series with the highest energy among the series selected in the first step, and Den_i is the density of the series, see Equation (2.3). These features are computed by AStrion-H which is presented in section 2.2.2. BSI_i can have a value from 0 to 1, where the highest value describes a series with the highest energy among selected candidates and without gaps within the peaks constituting a series. Therefore, the series B_j with the highest BSI_i is selected to be associated to a REB characteristic fault frequency

$$B_j := \{b \in BSI : b \geq a \forall a \in BSI\}, \tag{4.5}$$

where BSI is a set of all bearing series indicator values kept from the first step of the association algorithm for the investigated characteristic fault frequency.

The BSI_i factor has been determined after an empirical inspection of numerous examples from real-world signals acquired on different systems.

4.2.3 Additional Remarks

The above explanation gives details on a single iteration of the proposed method to associate one characteristic frequency. Figure 4.3 shows a flowchart of the proposed method and indicates its iterative workflow.

The closest to the proposed method found in literature [Gel+00] uses a different amplitude and frequency estimation of the spectral content and associates a single frequency and not a detected harmonic or sideband series, as well as does not precisely indicate the condition of decision making for harmonic frequency selection. Additionally, a slippage phenomenon which occurs in REB is also considered in this thesis.

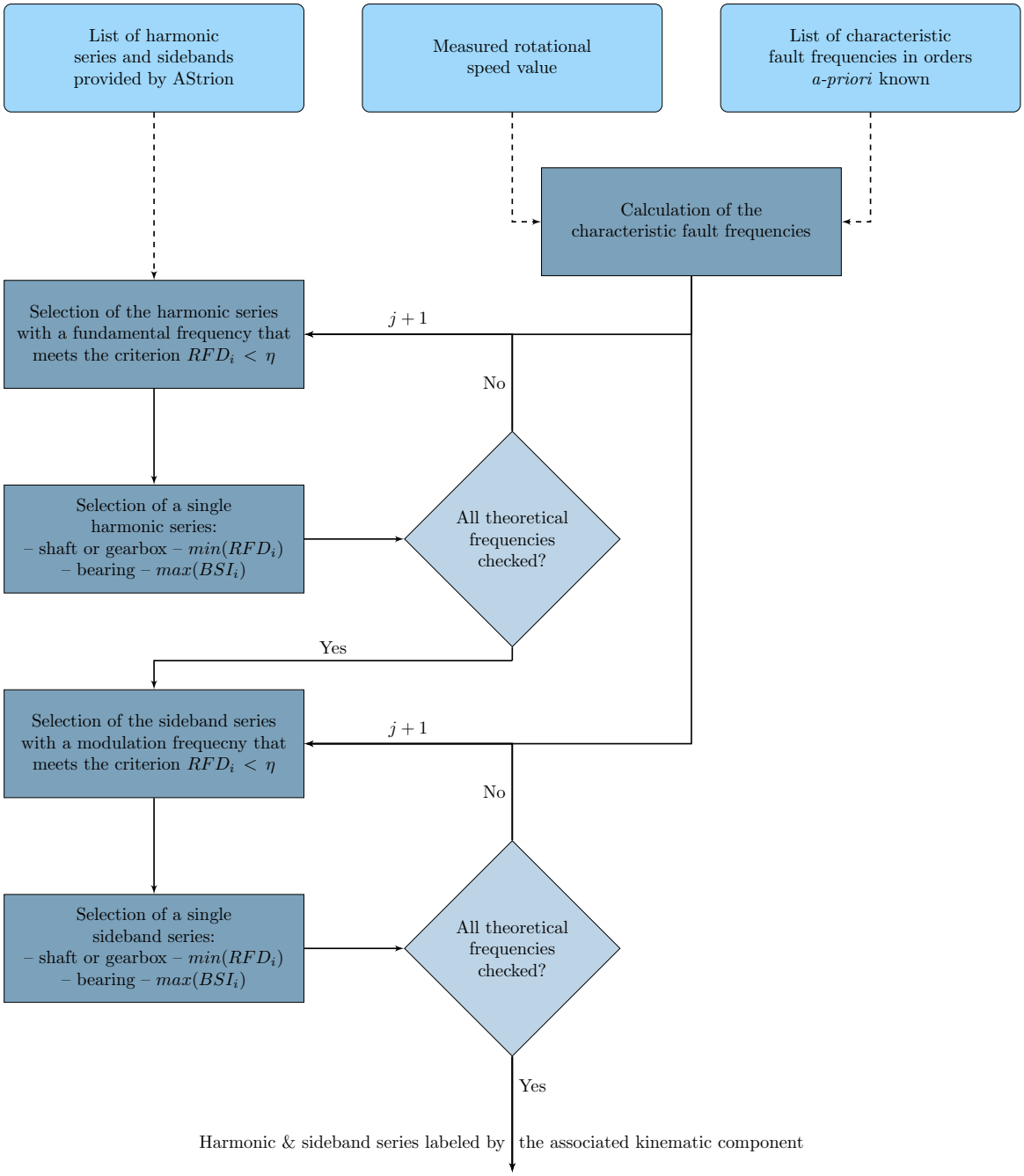

Figure 4.3: Flowchart of the characteristic fault frequency association algorithm.

There is one major difference in the results of the proposed method for harmonic and sideband series. In the first group each occurrence of a characteristic frequency is unique: only one harmonic series can have an association with a particular characteristic frequency. Whereas, in the final result of sideband series association a multiple number of these series can have a label with the same name of a characteristic frequency. It is caused by the fact that for each carrier frequency of a detected modulation series, one characteristic fault frequency can be associated.

Moreover, the kinematic module is optional for AStrion and it is possible to execute all other AStrion modules without kinematic data. Nevertheless, the employment of the kinematic information makes the interpretation of AStrion results easier by highlighting the most relevant patterns detected by AStrion-H in the investigated spectrum which arise from mechanical parts of investigated system.

In section 4.3 a few examples of BSI_i on real-world data are presented. For chosen mechanical components, the RFD_i value of all series selected in the first step as candidates for association are given along with other features that describe harmonic and sideband series.

4.3 Validation

The validation of the proposed method is performed on a real-world signal. This decision has been made because of the nature of the presented algorithm which is dedicated to work on complex signals with a vast number of spectral components. Moreover, with a simple simulated signal it would be too trivial to obtain a good performance of AStrion-K, especially the REB association would be hard to test due to the slippage phenomenon which causes a random variation of the frequency. Therefore, for the validation of the proposed signal-processing method, a single vibration signal originating in GOTIX test rig is used. This section opens with a description of the GOTIX test rig and it is followed by the detailed results of AStrion-K on a selected signal.

4.3.1 GOTIX

The GOTIX test rig is a simple set-up designed for the fault characterisation of an electrically driven mechanical system within 'GOTIX' project (`http://www.gipsa-lab.grenoble-inp.fr/projet/gotix/`).

Figure 4.4 presents the most important kinematic components of this test rig and Figure 4.5 shows the gearbox of the test rig. The GOTIX test rig consists of a single stage of parallel gearbox and bearing supporting its two shafts. It is equipped with a three-phase asynchronous motor of a nominal power equal to 55 kW. The test rig operates at a constant speed and the aim of the 'GOTIX' project is to observe the wearing effect of the gearbox.

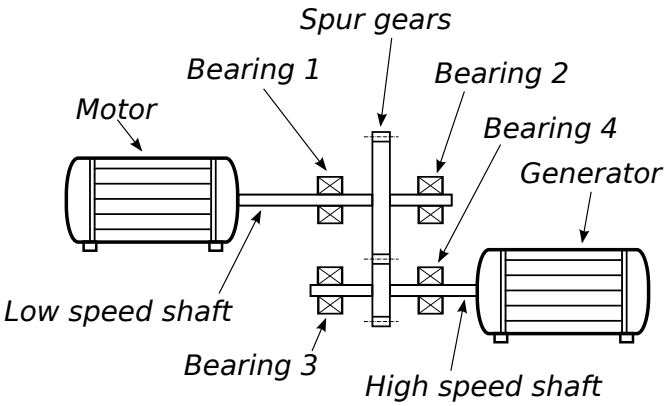

Figure 4.4: Main mechanical components of the GOTIX test rig.

Table 4.2: Characteristic frequencies of the GOTIX test rig gears expressed in *orders*.

Component name	**Order**
GMF	57
High speed shaft = smaller wheel relative frequency	3.8
Low speed shaft = bigger wheel relative frequency	1

The gearbox works as a multiplier which has a ratio equal to 1 : 3.8. The GOTIX test rig is not complicated from the mechanical point of view, henceforth it is used for the purpose of the validation of the proposed method. The list of characteristic fault frequencies which originate in gearbox-related components is given in Table 4.2 and bearing ones in Table 4.3. These two tables contain the theoretical values of the characteristic frequencies computed as defined in Table 4.1. The values in Tables 4.2 and 4.3 are given in orders which means that they are calculated for a shaft speed equal to 1 Hz. Moreover, the frequency of each component is calculated assuming that the test rig works with the speed of low speed shaft equal to 1 Hz. The speed of the high speed shaft is calculated with the application of the gear ratio as well as the characteristics orders of REBs supporting the high speed shaft are recalculated accordingly. Please note, that the GOTIX test rig is equipped with four identical REBs, but in the kinematic list used as an input for AStrion-K their characteristic order values are the same only for the bearings working on the same shaft, see Table 4.3.

The test rig is equipped with the sensors to record various parameters. The installed measurement channels include such sensors as:

- 6 accelerometers;

Table 4.3: Characteristic frequencies of the GOTIX test rig bearings expressed in *orders*.

REB name	**BPFO**	**BPFI**	**FTF**	**BSF2**
NU 206 E = Bearing 1 & 2	5.24	7.76	0.4	4.97
NU 206 E = Bearing 3 & 4	23.48	33.55	1.56	20.56

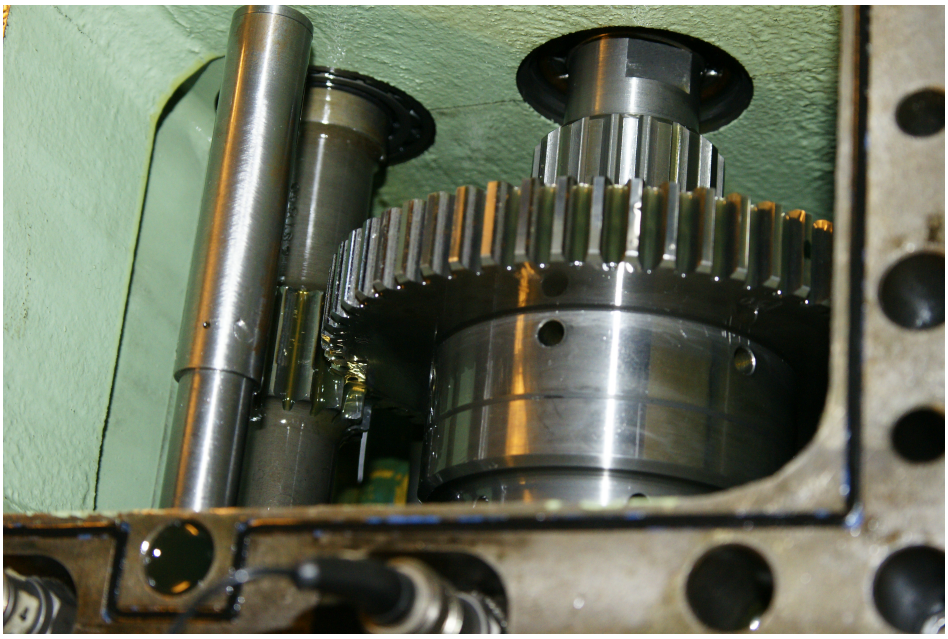

Figure 4.5: The gearbox of the GOTIX test rig.

Table 4.4: The GOTIX test rig signal parameters.

Sampling frequency	$25,600\ Hz$
Number of samples	$2,048,000$
Signal duration	$80\ s$
LSS speed	$\sim 473.75\ RPM$
HSS speed	$\sim 1800\ RPM$
Torque	$\sim 206\ Nm$

- 1 tachometer sensor;
- 2 optical encoders;
- 1 torque-meter;
- 3 current probes;
- 3 voltage probes;
- 4 thermocouples.

The vibration signal used in this section originates in an accelerometer placed on the housing of the gearbox close to the bearing 4, which is the bearing supporting high speed shaft from the generator side. This accelerometer is oriented vertically and it is referenced to as 24RV. The data acquisition parameters along with the operational conditions are presented in Table 4.4.

4.3.2 AStrion-K Results

The signal is processed by AStrion-DIH as described in chapter 2. As a result, 13,573 spectral components are identified and AStrion-H detects 948 harmonic series and 106,841 sideband series. These harmonic and sideband series are used to be associated with the characteristic frequencies listed in Tables 4.2 and 4.3.

Some examples of the proposed method results together with their middle steps are presented in Table 4.5. Each of the examples is separated with a double horizontal line and the series to be selected for the final association is in the highlighted row. A double vertical line divides the data available from the previous AStrion steps on the left-hand side, and AStrion-K information on the right-hand side. The 'Theoretical frequency (Hz)' column contains the values of the characteristic fault frequencies after taking into account the value of the rotational speed. In the investigated case the reference speed equals to 473.75 RPM and after changing the unit it is equal to ~ 7.9 Hz, so as a preparation for association all the values of characteristic orders, presented in Tables 4.2 and 4.3 need to be multiplied by ~ 7.9 Hz. For example, in the GMF frequency it results in a value of 450.065 Hz as a characteristic frequency for further association.

The first two examples show an association of the shaft frequencies with the previously detected harmonic series. In the first case, it occurred to be very easy since only one harmonic series is present in the range of the low speed shaft frequency and AStrion-K labels this harmonic series as corresponding to the frequency of this shaft. The second example shows that two harmonic series are selected as possible candidates for the association, according to Equation (4.1). After that, the series with the lowest RFD_i, as defined in Equation (4.2), is selected to represent the high speed shaft frequency. The BSI_i value is not computed in these cases because it is used only for bearings and this information is available together with the names of the characteristic frequencies.

The third example shows the process of association of the BPFI characteristic fault frequency of the bearings 1 and 2. Because of the fact that exactly the same type of rolling-element bearings is used multiple times and they are operate at the same speed in the investigated system, it is not possible to distinguish between these mechanical components since their characteristic fault frequencies are the same. In the first step of AStrion-K, the algorithm selected four harmonic series that meet the condition given in Equation (4.3). All the selected candidates have the RFD_i value lower than two. In the second step of the proposed algorithm, the values of BSI_i are calculated according to Equation (4.4) and the harmonic series with the highest, as defined in Equation (4.5), BSI_i is selected for final association.

The fourth example presented in Table 4.5 shows the association of the GMF to a harmonic series. In the first step, AStrion-K selected three harmonic series and the final selection is based on the lowest value of RFD_i, which is equal to 0.007. Such a high precision is expected from the gearbox-originating spectral component and to double-check the correctness of this association one can compare the number of peaks and energy of this series with other proximate

series. The high values of these features are an indication that AStrion-K properly associated the GMF frequency.

The last three examples presented in Table 4.5 are very trivial. Each presents the association of the low speed shaft frequency with a modulation series around the fundamental GMF frequency, its 2^{nd}, and 3^{rd} harmonic respectively. In all these cases only one sideband series is selected in the first step of AStrion-K and associated afterwards. This simple example presents the important difference of the proposed method results between harmonic and sidebands series. It illustrates the possibility of association of the same characteristic frequency with multiple sidebands series with a different carrier frequency. In the case of harmonic series each characteristic frequency could be associated only once for all the harmonic series detected in the investigated signal. For these examples a sign '|' in some cells is used to distinguish the feature values between left-hand and right-hand side of the carrier frequency.

4.4 Conclusions and Perspectives

The presented example shows step by step the operations of the proposed algorithm for the association of the detected spectral patterns in the signal with the theoretical characteristic frequencies corresponding to the mechanical components of the investigated system. These results show that AStrion-K algorithm can accomplish the research of the characteristic frequencies. The method for selecting a bearing characteristic fault frequency is also proposed and it gives an approach to deal with a slippage phenomenon present in bearings during their operation.

The proposed method can be easily used in an automatic and data-driven CMS. It is ready for an efficient labelling of the spectral component of mechanical origin. What is more, the result of this method could be simply employed to compute a component specific health indicator which could help precisely to identify a problem present in the system. For example the ratio of the first and second harmonic amplitudes of a harmonic series associated with a shaft could inform about a misalignment problem. Such an indicator could be computed for series associated with the characteristic frequency of a shaft only.

Table 4.5: Detailed results of AStrion-K on the example of GOTIX 5797h Track 1 signal. Possible association results selected according to Equatios (4.1) and (4.3) are grouped between double lines and final series to be associated are highlighted.

Type	**Freq. (Hz)**	**Carrier freq. (Hz)**	**Modulation freq. (Hz)**	**Number of peaks**	**Energy (10^{-5})**	**Density**	**Selected component name**	**Theoretical freq. (Hz)**	**RFD_i**	**BSI_i**
Harmonic	7.894	—	—	5	0.2	0.714	Low speed shaft	7.896	0.02	—
Harmonic	30.002	—	—	4	9.2^{-5}	0.6	High speed shaft	30.004	0.006	—
Harmonic	30.261	—	—	3	9.9^{-5}	0.9	High speed shaft	30.004	0.857	—
Harmonic	60.157	—	—	4	0	0.5	Bearing 1 & 2.BPFI	61.272	1.82	0.25
Harmonic	60.708	—	—	3	0.1	0.75	Bearing 1 & 2.BPFI	61.272	0.92	0.475
Harmonic	61.034	—	—	3	0.5	0.5	Bearing 1 & 2.BPFI	61.272	0.388	0.75
Harmonic	61.717	—	—	3	0.3	0.75	Bearing 1 & 2.BPFI	61.272	0.726	0.675
Harmonic	446.806	—	—	3	76	0.75	Gearbox.GMF	450.065	0.724	—
Harmonic	450.032	—	—	15	2,749,000	1	Gearbox.GMF	450.065	0.007	—
Harmonic	453.261	—	—	3	62	0.75	Gearbox.GMF	450.065	0.71	—
Sideband	—	450.32	7.895	8 | 11	10 | 10	0.8 | 0.917	Low speed shaft	7.896	0.007	—
Sideband	—	900.063	7.895	17 | 36	3220 | 4020	0.944 | 1	Low speed shaft	7.896	0.007	—
Sideband	—	1350.095	7.895	18 | 17	4160 | 5370	1 | 1	Low speed shaft	7.896	0.007	—

Chapter 5

All-Sidebands Demodulation – AStrion-M

Contents

5.1 State of the Art 67
5.2 Details of Algorithm 69
5.2.1 Signal Model and Method Overview 69
5.2.2 Multi-Rate Filtering Technique 70
5.2.3 Time Synchronous Averaging 75
5.2.4 Demodulation Based on the Synchronous Averaged Signal 75
5.2.5 Features of Modulation Sidebands 76
5.3 Validation on Simulated Signal 76
5.4 Conclusions and Perspectives 81

5.1 State of the Art

The demodulation operation aims to extract the original baseband signal by removing the modulation effect. Compared to the traditional Fourier transform, which assumes that the investigated signal is a sum of a number of sine waves, the Hilbert transform (HT) allows to analyse the signals constituted of a single but modulated sine wave. The vibration signals have multi-component content and this is the reason why HT can be applied only after the filtering of a single component from the signal.

The demodulation is successfully applied in gearbox fault diagnosis for years. [McF86] presents the use of amplitude and frequency demodulation for a fatigue crack in a gear and concludes that a phase modulation detection is important in the early fault detection. [ML96] introduce a model-based demodulation scheme to derive amplitude and phase modulation signals from a gear's vibration signal average. [Bri+97] proposes two methods for adaptive demodulation for the detection of the gear crack. [Cha+12] states that for a gearbox working under changing operational conditions there are amplitude and frequency modulations present simultaneously, which is relevant in the wind turbine application. There is still interest to derive more from the demodulation. [CG11] proposes some new health indicators based on

the amplitude demodulation obtained from the time synchronous averaging of a signal to make the proposed technique adaptive. And a number of other developments about demodulation is proposed in [Tow97]; [SP05]; [Fen+12]; [Mei12]; [CR14]; [RCS14b]; [Fen+15]. Moreover, the demodulation technique is also used on electrical data for gearbox diagnosis [MK06].

The demodulation technique also proved its value for REB fault detection. In this case the amplitude demodulation is widely used and some examples are given in [MD03]; [LS10]; [RCS14a]. An exhaustive description of methods used for REB diagnostics, including the demodulation, is given in [RA11]. The main interest for bearing diagnostics is the so called narrowband envelope analysis. In general, this method performs the amplitude demodulation of a selected bandwidth in order to find the REB fault frequencies. The optimal bandwidth depends on the system, so there is a number of methods for selecting a carrier frequency and its spectral bands for a demodulation [BJ10]; [BJ11]; [OWZ14]; [LLW15]. The need for those techniques arises due to the fact that for bearing diagnosis it is recommended to select the appropriate resonance frequency of bearing for each investigated case separately.

For both, gearboxes and REBs, the demodulation techniques proposed in the above-mentioned papers are focused on the demodulation of one selected band, or the selection of this band. Mostly these techniques are best for separate diagnosis of a case, which is a disadvantage for an automatic CMS.

[Zhu+14] presents statistical condition indicators as RMS, Crest Factor, Kurtosis, and Peak-to-Peak computed from the amplitude and frequency modulation functions. However, there are no details on the technique to obtain the demodulated signal. The narrow-band analysis is mentioned along with the amplitude and frequency modulation, but this paper also points out that these analyses are not limited to narrow-band signals. In [Zhu+14] the band to demodulate is selected arbitrarily.

As mentioned above there are multiple advantages of the demodulation technique used in the fault detection. Therefore, this chapter proposes a data-driven and automatic demodulation method which is referred to as AStrion-M. It proposes to perform the amplitude and frequency demodulation of all-sidebands previously detected by AStrion-H, as described in section 2.2.2. Thanks to the usage of the AStrion-H results, this method does not need a manual selection of the carrier frequency nor the demodulation bandwidth. The advantage of this approach for the demodulation is that this operation is applied according to spectral content of the signal only. Moreover, the proposed method performs demodulation of all the modulation sidebands detected in the investigated signal and does not try to find only one demodulation bandwidth, as it it described in the literature. The health indicators proposed by this method give an insight in the health of the mechanical components which cause a modulation and are automatically computed for all the modulation series detected in an investigated signal.

The details of each step of AStrion-M algorithm are described in the next section and afterwards a validation of this method is presented with the usage of a simulated signal in section 5.3.

5.2 Details of Algorithm

5.2.1 Signal Model and Method Overview

A discrete signal $y[n]$ is considered as the sum of a band-limited deterministic part $s[n]$ and a wide-band random part $e[n]$

$$y[n] = s[n] + e[n]. \tag{5.1}$$

$s[n]$ can be expressed as

$$s[n] = A[n] \cos\left(\Phi[n]\right), \tag{5.2}$$

where $A[n]$ is the amplitude modulation and $\Phi[n]$ is the instantaneous phase modulation.

The amplitude modulation can be written as

$$A[n] = A_0 \left(1 - \alpha \cos(2\pi f_a n)\right), \tag{5.3}$$

where A_0 is the average amplitude, α is the amplitude modulation index, and f_a is the frequency of the amplitude modulation function.

The instantaneous phase $\Phi[n]$ and instantaneous frequency $F[n]$ modulation functions are written as

$$\begin{aligned} \Phi[n] &= 2\pi f_0 n + \beta \sin(2\pi f_\Phi n), \\ F[n] &= f_0 + \beta f_\Phi \cos(2\pi f_\Phi n). \end{aligned} \tag{5.4}$$

where f_0 is the carrier frequency, which depends on the rotational speed and the resolution of the tachometer, β is the frequency modulation index, and f_Φ is the frequency of the phase modulation function. Since the signal is modulated simultaneously in the amplitude and frequency, the Fourier series expansion s[n] of Equation (5.2) is

$$s[n] = A_0 \sum_{k=0}^{+\infty} \left(J_k(\beta) + \alpha J_{k\pm1}(\beta)\right) \cos\left(2\pi(f_0 \pm k f_\Phi)n\right), \tag{5.5}$$

where k is the order of the sideband, $k = 0$ corresponds to the carrier frequency, and $J_k(\cdot)$ is the Jacobian polynomial of order k. β is determined by

$$\beta = \frac{f_0}{f_\Phi} \cdot r_{FM} \cdot \frac{2\pi}{\Delta\phi}, \tag{5.6}$$

where $\frac{2\pi}{\Delta\phi}$ is the tachometer resolution that specifies the number of tachometer samples per revolution, and r_{FM} is the frequency modulation rate, which rarely exceeds 10% for a rotating shaft. As the frequency modulation yields an infinite number of sidebands, the Bedrosian theorem is not respected. However, under the hypotheses [Pac+13] that

- the carrier frequency f_0 is significantly higher than the frequency modulation frequency f_Φ;
- the sideband power becomes negligible at the maximum frequency of $A[n]$;

the amplitude modulation $A[n]$ and the phase modulation $\Phi[n]$ can be recovered from the signal $s[n]$ using the Hilbert transform. The instantaneous frequency modulation $F[n]$ can be obtained from the phase signal $\Phi[n]$.

The demodulation algorithm can be decomposed into two steps. In the first step, the signal is band-pass filtered around the carrier frequency f_0, in order to isolate the spectral components irrelevant to the phenomena to be analyzed. In the second step, the amplitude and frequency modulation functions are calculated after a synchronous averaging. The different steps of the algorithm are described in the following subsections. Figure 5.1 presents a flowchart of the proposed method.

5.2.2 Multi-Rate Filtering Technique

As mentioned in section 1.7.3, the envelope analysis which uses the complex filtering to perform the Hilbert transform (HT) [RA11] based demodulation is among the most popular techniques for the REB fault detection. This approach gives very good results for the amplitude demodulation, although it is not as good in the case of the frequency demodulation. Therefore, in order to obtain the best possible precision of the demodulation the multi-rate filtering is proposed in AStrion-M.

The filtering method aims to preserve all of the spectral information within a frequency band $\mathbf{B}$

$$\mathbf{B} = [f_{inf}, f_{sup}], \tag{5.7}$$

where f_{inf} and f_{sup} are the lower and upper frequency boundaries of the filter, respectively, whereby both should be positive and below the Shannon frequency $\frac{F_{s,y}}{2}$. The filter bandwidth is defined by $\Delta B = f_{sup} - f_{inf}$.

The challenge comes if the bandwidth is very small or if the filter band is very close to the extreme values (0 and/or $\frac{F_{s,y}}{2}$). The design of a stable filter that satisfies the desired performance is difficult, as a filter is stable at very low order only. As a solution, and as originally used for reduction of the amount of data [MB76], based on a multi-rate filter we propose a new filtering technique that automatically decomposes a difficult filtering task into N_q iterations, each of which is comprised of a chain of three essential operations, as described in subsection 5.2.2.2.

5.2.2.1 Choice of the Filter Bandwidth

On the Fourier spectrum of a signal expressed as in Equations (5.2) and (5.5), the phase modulation will create an infinite number of sidebands, at both sides of the carrier frequency f_0, and which are spaced at an even interval f_Φ. The energy of the high-order sideband is often hard to distinguish from the noise level, thus it is decided to demodulate only the frequency bandwidth which carries relevant energy to identify the modulation sideband from the noise. The filter bandwidth is then selected based on the peak identification by AStrion-DI and

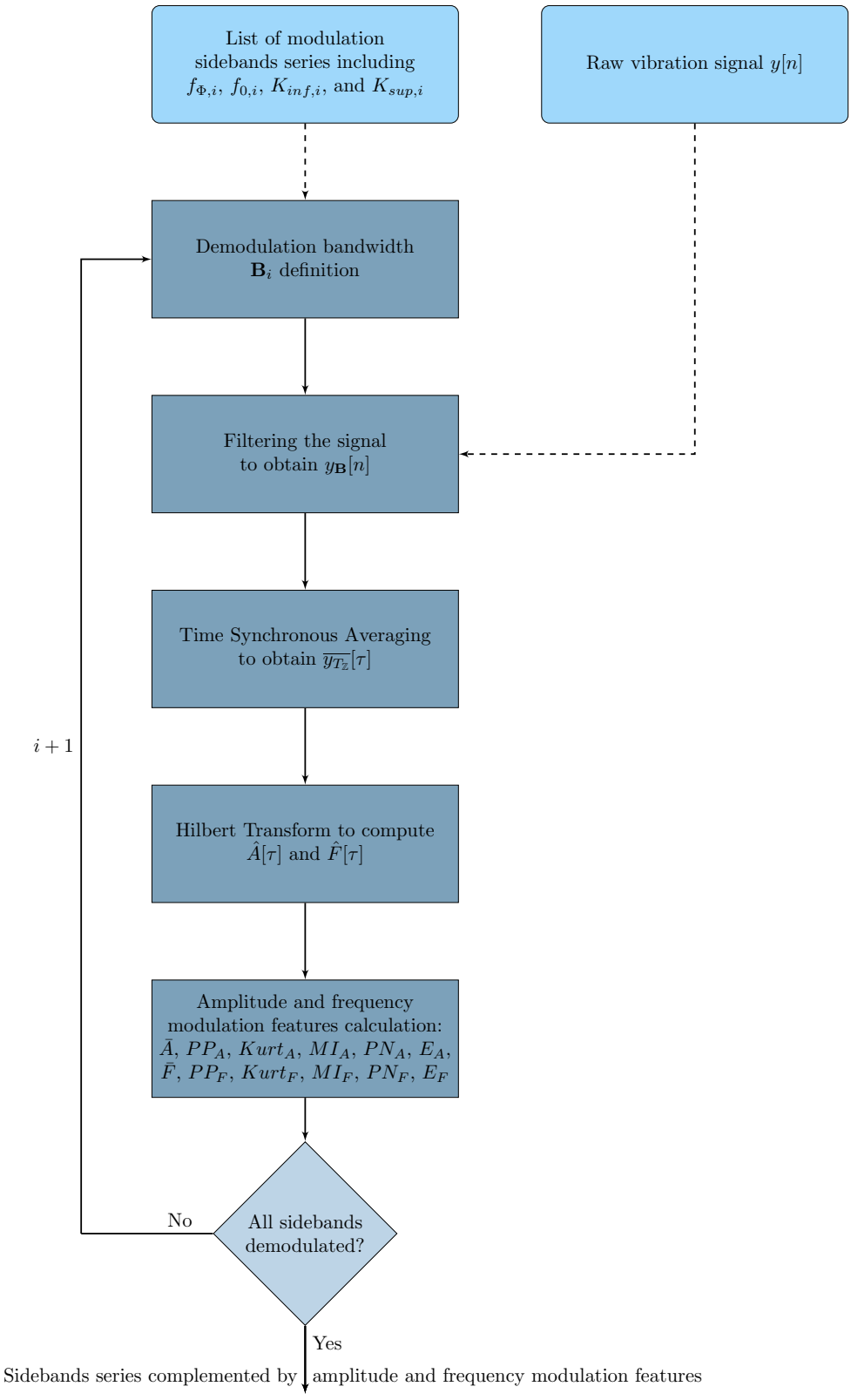

Figure 5.1: Proposed demodulation algorithm.

harmonic and sideband recognition by AStrion-H described in chapter 2. Therefore, the filter bandwidth can be chosen as

$$\begin{aligned} f_{inf} &= f_0 + K_{inf} \times f_\Phi, \qquad K_{inf} \in \mathbb{Z}, K_{inf} < 0, \\ f_{sup} &= f_0 + K_{sup} \times f_\Phi, \qquad K_{sup} \in \mathbb{Z}, K_{sup} > 0, \end{aligned} \tag{5.8}$$

where K_{inf} is the lowest order of the sidebands, and K_{sup} is the highest order of the sidebands. The filter bandwidth is proportional to $(|K_{sup}| - |K_{inf}|)$.

As no preliminary information is available on the modulation, filtering by empirically fixing K_{sup} and K_{inf} might distort the modulated signal, which may degrade the precision and is not the case for the proposed method. The proposed data-driven method uses an automatic algorithm presented in [GMM13]; [Ger15], and described in section 2.2.2. It is initially applied to identify all of the harmonic series and sidebands of the spectrum, and to calculate the important parameters for the filter design, such as f_Φ, f_0, K_{inf}, and K_{sup}, as long as the selected sidebands verify Carson's law [Car22]. Through this approach, all of the detectable sideband orders are taken into account for the demodulation.

5.2.2.2 Methodology of the Multi-Rate Filter

The multi-rate filter consists of three basic operations: a ***frequency shift*** that applies a negative frequency shift $-\Delta f_q$ to the entire frequency contents; a ***filter*** that filters over the target filter band $\mathbf{B}_q$; and a ***down-sampling*** that decimates the signal by a factor D_q.

For the filtering operation, a filter of sharp roll-off is required, and therefore the elliptic filter was selected. Additionally, in the down-sampling operation and the frequency shifting step, a low-pass Butterworth filter is used to avoid the spectrum aliasing, considering its ripple-free feature.

The core operation is the filtering. The other two are preliminary operations that help to carry out the filtering operation under extreme conditions. The down-sampling operation helps to reduce the sampling frequency, and the frequency shifting operation helps to increase the down-sampling ratio to the maximum. Based on these three operations, the iterations of the algorithm are arranged as follows:

- Initialization: $q = 1$, $\mathbf{B}_0 = \mathbf{B}_q$, $y_0[n] = y[n]$, and $F_{s,0} = F_{s,y}$.
- In iteration (q):
  1. Verify if the stability criterion of the elliptic filter is satisfied over the target band $\mathbf{B}_q$. If so, go to the step 2, otherwise skip the next step and go to step 3;
  2. Perform a filtering operation over $\mathbf{B}_q$ on $y_{q-1}[n]$ to get the filtered signal $y_{\mathbf{B}}[n]$, and go to the end;
  3. Perform a frequency shifting operation, which consists of:

— Calculate the negative frequency shift $-\Delta f_q$. Apply a high-pass filter over $\left[\Delta f_q, \frac{F_{s,q-1}}{2}\right]$ on $y_{q-1}[n]$, and carry out frequency shifting to yield

$$y_{shift,q}[n] = \Re\Big\{e^{-2\pi\Delta f_q \frac{n}{F_{s,q-1}}} \times \mathcal{H}\{y_q[n]\}\Big\}, \tag{5.9}$$

where $\Re$ is the operator to take the real part, and $\mathcal{H}\{\cdot\}$ is the Hilbert transform;

— $\mathbf{B}_q = \mathbf{B}_{q-1} - \Delta f_q$.

4 Perform a down-sampling operation;

— Calculate the down-sampling rate D_q. Apply a low-pass filter over $[0, \frac{F_{s,q-1}}{2D_q}]$ on $y_{q-1}[n]$, and down-sample the signal as

$$y_{down,q}[n] = Decimate\Big\{y_{shift,q}[n]; D_q\Big\}; \tag{5.10}$$

— $F_{s,q} = \frac{F_{s,q-1}}{D_q}$;

5 Update the signal for the next iteration $y_{q+1}[n] = y_{down,q}[n]$. Increment the iteration index $q \leftarrow q + 1$, and perform step (2) again.

- End: $F_s = F_{s,q}$, define the filtered signals as $y_{\mathbf{B}}[n]$.

The great advantage of the proposed method is that it is a data-driven approach. The multi-rate filter can automatically choose the optimal number of iterations and the optimal configurations of the operations.

5.2.2.3 Configurations of the Digital Filters

As mentioned in the section 5.2.2.1 the proposed multi-rate filer uses two types of filters. The elliptic filter is employed for the filtering operation and the low-pass Butterworth filter is used for the down-sampling and frequency shifting steps. The specifications of the filters are presented in Table 5.1.

The multi-rate filter algorithm selects the highest order of the filter that satisfies a stability criterion on the maximum of all of the poles. If the selected filter order is below the lowest feasible to execute order, the filter bandwidth is considered too narrow for the filter design. In this situation, the down-sampling and frequency shifting operations are required. The details of the down-sampling rate selection and the frequency shift steps that are applied in the proposed filtering operation are given in 5.2.2.4.

5.2.2.4 Down-sampling Rates and Frequency Shift Steps

The distribution of the down-sampling rates in all of the iterations is an important configuration of this method, and it depends first on the final sampling frequency $F_s = C \cdot \Delta B$, where

Table 5.1: Specification of the digital filters used in the multi-rate filtering.

Type	Butterworth	Elliptic
Nature and operations involved	Low-pass & high-pass	Band-pass
Pass-band ripple	—	0.005 dB
Stop-band ripple	—	−80 dB
Stability criterion on the maximum of all of the poles	< 0.95	< 0.996
Lowest order	10	8

C is a factor between 4 and 10 that ensures a wide filter band and a high sampling frequency at the same time. The overall down-sampling rate D is factorized by $D = 2^{L^{(2)}}3^{L^{(3)}}$ by

$$\begin{aligned} \left\{L^{(2)}, L^{(3)}\right\} = & \underset{\left\{l^{(2)},l^{(3)}\right\}\in\mathbb{Z}^2}{\arg\max} \left\{ \tfrac{F_{s,y}}{F_s} - 2^{l^{(2)}}3^{l^{(3)}} \right\} \\ \text{subject to} \quad & \tfrac{F_{s,y}}{F_s} - 2^{l^{(2)}}3^{l^{(3)}} \geq 0 \end{aligned} \tag{5.11}$$

The factors 2 and 3 are alternatively arranged in a vector $\mathbf{d}$

$$\mathbf{d} = \{d_l\}_{L^{(2)}+L^{(3)}} = [2, 3, 2, 3, \dots]. \tag{5.12}$$

$L_q^{(2)}$ factors of 2 and $L_q^{(3)}$ factors of 3 will be taken from $\mathbf{d}$ in each down-sampling operation, to form the down-sampling factor D_q. At the end of all of the iterations, $\mathbf{d}$ will be empty $\mathbf{d} = \emptyset$. Therefore, the total number of iterations N_q cannot exceed $(L^{(2)} + L^{(3)})$.

In each iteration (q), the algorithm calculates the down-sampling factor D_q by selecting L_q elements from $\mathbf{d}$ according to $D_q = \prod_{l=1}^{L_q+1} d_l$, where L_q defines the narrowest band $[0, (F_{s,q-1})/(2D_q)]$ where a low-pass Butterworth filter satisfies the filter stability criterion. $\mathbf{d}$ is then updated by removing the first L_q factors $\mathbf{d} \leftarrow \mathbf{d}/[d_1, \dots, d_{L_q}]$. If $D_q = 1$, the down-sampling operation will simply be skipped.

The operations aim to down-sample the signal to a sufficiently low sampling frequency to achieve the filter bandwidth ΔB. Hence, the frequency shifting operations will carry the filter band $\mathbf{B}$ to $(\mathbf{B} - f_{inf})$ where the lower frequency boundary is 0. The total frequency shift is therefore $-f_{inf}$ and is divided evenly into M smaller portions. In each iteration (q), the algorithm takes M_q portions to shift the frequency contents of the signal by $-\Delta f_q = -\frac{M_q}{M} f_{inf}$.

In each iteration (q), by finding the narrowest band $\left[\frac{M_q+1}{M} f_{inf}, \frac{F_{s,q-1}}{2}\right]$ where a high-pass Butterworth filter satisfies the stability criterion M_q calculates. Δf is then updated by

$$\Delta f \leftarrow \Delta f - \Delta f_q. \tag{5.13}$$

If the above process returns $\Delta f_q = 0$, the frequency shifting operation will be skipped.

5.2.3 Time Synchronous Averaging

The time synchronous averaging calculates a period-wise average of a periodical signal. It also helps to eliminate all of the spectral content that is incoherent with the period. A review on the available methods for time synchronous averaging is presented in [BK09].

Generally, the period of the signal obtained by the multi-rate filter, which is sampled at $T_{y_\mathbf{B}} = \frac{F_s}{f_\Phi}$ points per period, has not an integer number of points per period. Therefore, the signal $y_\mathbf{B}$ has to be *a-priori* resampled with an interpolation to contain an integer number $T_\mathbb{Z}$ of points per period which is a classical method [McF87a]. The interpolated signal $y_{T_\mathbb{Z}}[n]$ is further processed by

$$\overline{y_{T_\mathbb{Z}}}[\tau] = \frac{\sum_{t=0}^{N_T-1} y_{T_\mathbb{Z}}[tT_\mathbb{Z} + \tau] \times w[t]}{\sum_{t=0}^{N_T-1} w[t]}. \tag{5.14}$$

where τ is the discrete time index, $\overline{y_{T_\mathbb{Z}}}[\tau]$ is the averaged of signal $y_{T_\mathbb{Z}}[n]$, N_T is the total number of periods of $\mathbf{y}_{T_\mathbb{Z}}$, and $w[t], t = 0, \ldots, N_T - 1$ is a window of N_T points. To reduce the border effects of the filtering, we propose to use a Hann window.

5.2.4 Demodulation Based on the Synchronous Averaged Signal

The averaged signal $\overline{y_{T_\mathbb{Z}}}[\tau]$ obtained from Equation (5.14) after the multi-rate filtering can be regarded as band-limited and mono-component, as it contains only one carrier and its associated sidebands. Therefore, a Hilbert transform can be applied to yield an analytical signal [HR00]

$$\overline{y_H}[\tau] = \overline{y_{T_\mathbb{Z}}}[\tau] + j \cdot \mathcal{H}\{\overline{y_{T_\mathbb{Z}}}[\tau]\}, \tag{5.15}$$

where j is the imaginary unit, and $\mathcal{H}\{\cdot\}$ is the Hilbert transform. $\overline{y_H}[\tau]$ can be represented by

$$\overline{y_H}[\tau] = \hat{A}[\tau] e^{j\hat{\Phi}[\tau]}, \tag{5.16}$$

where $\hat{A}[\tau]$ and $\hat{\Phi}[\tau]$ are estimations of the demodulated amplitude $A[\tau]$ and the phase $\Phi[\tau]$, respectively, defined in Equations (5.3) and (5.4), and can be calculated from the modulus and the argument of $\overline{y_H}[\tau]$

$$\hat{A}[\tau] = \left|\overline{y_H}[\tau]\right|, \tag{5.17}$$

$$\hat{\Phi}[\tau] = \arctan\left(\frac{imag(\overline{y_H}[\tau])}{real(\overline{y_H}[\tau])}\right). \tag{5.18}$$

The demodulated frequency $\hat{F}[\tau]$ can be obtained by differentiating $\Phi[\tau]$ [Boa03]

$$\hat{F}[\tau] = \frac{1}{2\pi} \frac{\hat{\Phi}[tau] - \hat{\Phi}[tau - 1]}{F_S}. \tag{5.19}$$

It is worth noting that a frequency domain technique is the most efficient way to obtain an analytical signal, but the time domain method has an advantage of providing an exact linear

Table 5.2: Features calculated from the demodulated amplitude $\hat{A}[\tau]$ and frequency $\hat{F}[\tau]$.

Mean	$\bar{A} = \frac{\sum_{\tau=1}^{T} \hat{A}[\tau]}{T}$	$\bar{F} = \frac{\sum_{\tau=1}^{T} \hat{F}[\tau]}{T}$
Peak-to-Peak	$PP_A = max\hat{A}[\tau] - min\hat{A}[\tau]$	$PP_F = max\hat{F}[\tau] - min\hat{F}[\tau]$
Kurtosis	$Kurt_A = \frac{\left(\sum_{\tau=1}^{T} \hat{A}^4[\tau]\right)/T}{\left[\left(\sum_{\tau=1}^{T} \hat{A}^2[\tau]\right)/T\right]^2}$	$Kurt_F = \frac{\left(\sum_{\tau=1}^{T} \hat{F}^4[\tau]\right)/T}{\left[\left(\sum_{\tau=1}^{T} \hat{F}^2[\tau]\right)/T\right]^2}$
Modulation index	$MI_A = \frac{\max\{\hat{A}[\tau]\} - min\{\hat{A}[\tau]\}}{\bar{A}}$	$MI_F = \frac{\max\{\hat{F}[\tau]\} - min\{\hat{F}[\tau]\}}{\bar{F}}$

phase [Fel11]. Therefore, the time domain based approach is selected in AStrion-M, which allows us to exploit the amplitude and frequency modulations.

5.2.5 Features of Modulation Sidebands

It is proposed to use the demodulated signals in the time domain to compute statistical health indicators. Table 5.2 shows the scalar features that are derived from the demodulated functions $\hat{A}[\tau]$ and $\hat{F}[\tau]$. These values serve as mechanical fault indicators since the detected modulation in a vibration signal often has an origin in the deterioration of mechanical components.

A further run of AStrion [Mai+06]; [GMM13] on $\hat{A}[\tau]$ and $\hat{F}[\tau]$ yields the number of peaks (PN_A and PN_F respectively) and the energy (E_A and E_F respectively) of the harmonic series, which has a fundamental frequency equal to modulation frequency of investigated modulation series. These values contribute to two additional features for $\hat{A}[\tau]$ and $\hat{F}[\tau]$, but they are not always present which is due to the nature of AStrion method described in chapter 2.

5.3 Validation on Simulated Signal

The above-described method is validated on a simulated signal. The signal constitutes of a sine wave modulated in amplitude and frequency simultaneously. In both cases the modulation functions are sine waves. The simulated signal has parameters as listed in Table 5.3. The time domain view of the signal is presented in Figure 5.2. The carrier frequency of the simulated modulation equals to 5000 Hz and the deviation of the modulation equals to 100 Hz. A noise is also added with a SNR = 15 dB. Moreover, two pure sine components are added to the final signal at frequencies equal to 2500 Hz and 7500 Hz to create harmonic series possible to detect by AStrion-H algorithm. More details on AStrion-H can be found in section 2.2.2.

Table 5.3: Amplitude and frequency modulated signal parameters.

Sampling frequency	$25,000\ Hz$
Number of samples	$250,000$
Signal duration	$10\ s$

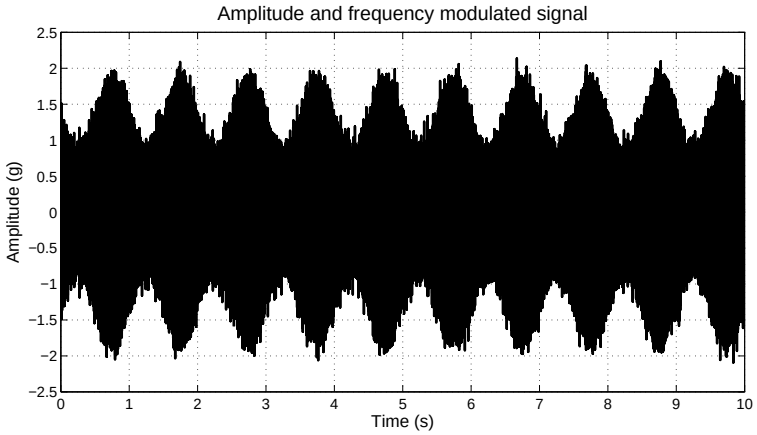

Figure 5.2: Simulated signal in the time domain.

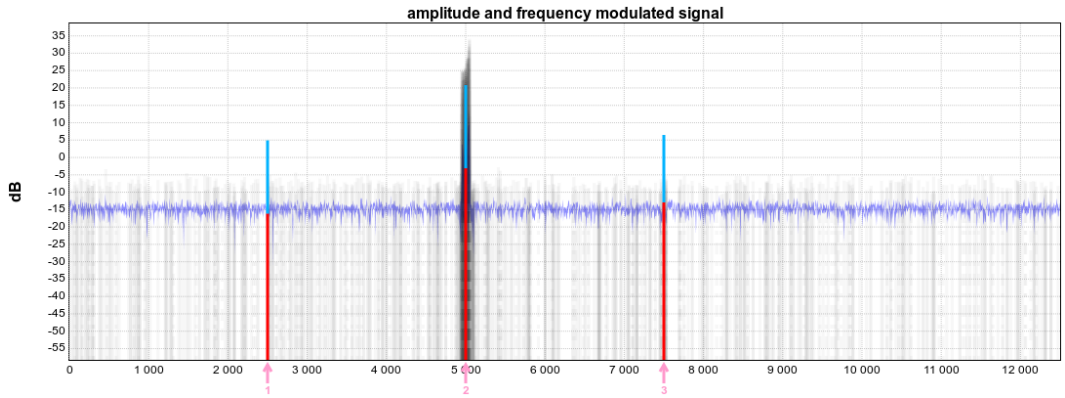

Figure 5.3: Detected harmonic series in the simulated signal. AStrion representation of the spectrum with peaks illustrated by two color lines: the blue part at the top corresponds to very low probability of misclassifying the class of the peak, which in this case corresponds to the pure sine wave depicted by red color.

The signal is processed by AStrion-DIH which results in finding one harmonic series with fundamental frequency equal 2500 Hz and two consecutive harmonic peaks. This result is presented in Figure 5.3.

For further comparison all the features proposed to be calculated on the demodulated functions, as shown in Table 5.2, are also computed for the input simulated amplitude and frequency modulation functions, their values are presented in Table 5.4 in the row described as simulated.

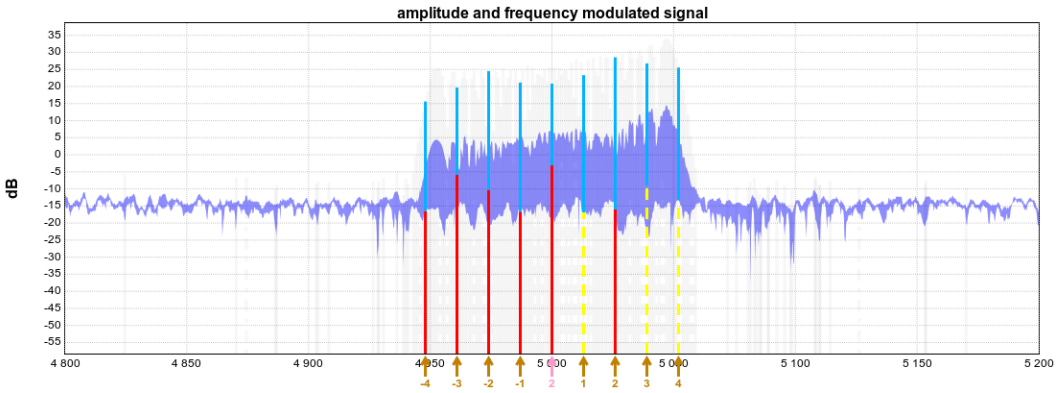

Figure 5.4: Modulation series, detected by AStrion-H, around carrier frequency which is equal to 5000 Hz. AStrion representation of the spectrum with peaks illustrated by two color lines: the blue part at the top corresponds to very low probability of misclassifying the class of the peak, which are sine waves and sine wave / doubt narrow band classes depicted by red line and yellow dashed line respectively. The brown color arrows below the peaks indicate the modulation series and the order of the sideband is marked by the number under the arrow.

Verifying the AStrion-H results on detected modulation sidebands series the bandwidth for proposed algorithm is calculated. Figure 5.4 illustrates detected sideband series for demodulation. This sidebands series has the carrier frequency f_0 estimated to be 5000 Hz, a modulation frequency f_Φ estimated to be 13 Hz, and four sidebands on each side of the carrier frequency without any gaps between them, thus $K_{inf} = -4$ and $K_{sup} = 4$.

The bandwidth is calculated according to Equation (5.8). $f_{inf} = 5000 - 4 \cdot 13 = 4948$ Hz and $f_{sup} = 5000 + 4 \cdot 13 = 5052$ Hz, thus a demodulation bandwidth $\mathbf{B} = 104$ Hz.

The multi-rate filter, as presented in section 5.2.2.2, accomplished the filtering in 2 iterations constituted of an automatic selection of the frequency shift and a signal decimation. In the first step the signal is high-pass filtered from the frequency equal 4948 Hz, then shifted by frequency Δf_q estimated to 4948 Hz and down-sampled by a factor of 6, so its sampling frequency equals 4.166.67 Hz. The second iteration starts from low-pass filtering operation until frequency 104 Hz which is followed by the down-sampling operation with a factor of 9. Finally, the down-sampled signal is sampled at a frequency equal to 462.96 Hz. Figure 5.5 presents the result of the multi-rate filtering. Figure 5.5 (a) shows the time domain of the simulated signal in red and the result of the filter operation in blue. Figure 5.5 (b) presents the zoom of first two seconds. Using the same fashion the frequency domain of the simulated signal and the result of the multi-rate filter is presented in Figures 5.5 (c) and (d).

After a synchronous averaging is done as specified in section 5.2.3 and then a demodulation as in section 5.2.4, the values of the features calculated from the demodulated amplitude and frequency as defined in section 5.2.5 are computed. In this case there are no additional features obtained for this demodulation, since the second run of AStrion on the amplitude $\hat{A}[\tau]$ and frequency $\hat{F}[\tau]$ demodulation functions did not yield the harmonic series corresponding to the modulation frequency.

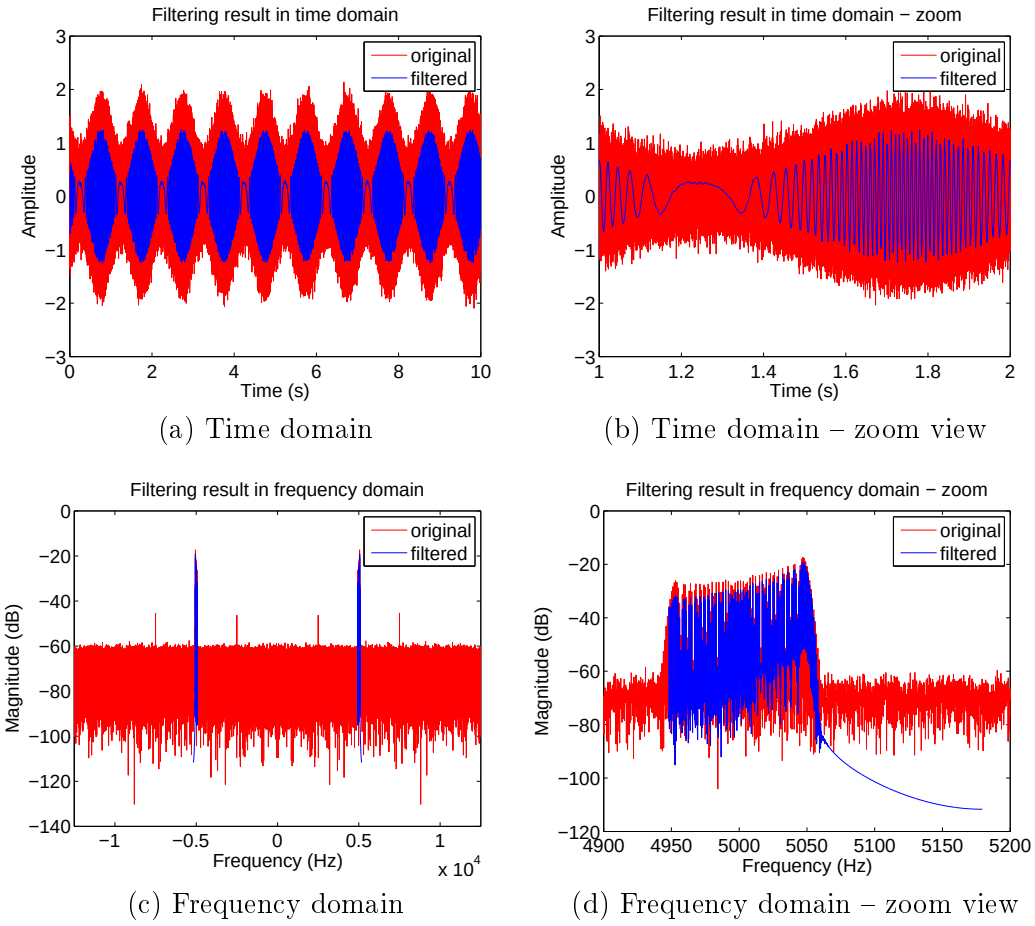

(a) Time domain (b) Time domain – zoom view

(c) Frequency domain (d) Frequency domain – zoom view

Figure 5.5: Filtering results (blue) compared with input simulated signal (red). (a) time domain signal and its zoom (b), (c) frequency domain signal with a zoom of selected frequency range (d).

Furthermore, the final result of the demodulation is compared with the theoretical signals used for creating the simulated signal. This result is presented in Figure 5.6. There is noticeable oscillation of computed demodulation signals which could be caused by the added noise, the filtering, or the Hilbert Transform. This result is considered as a good algorithm performance.

For the purpose of the validation, the whole procedure from signal simulation to features calculation is executed one hundred times to generate signals with a different noise and avoid influence of random component on the results. Table 5.4 presents the final result of the proposed method, which is the mean value of the obtained features from the amplitude $\hat{A}[\tau]$ and frequency $\hat{F}[\tau]$ demodulation functions. The standard deviation σ is also computed for the one hundred simulated signals for each feature. Moreover, the values corresponding to the proposed features are also computed on the simulated amplitude and frequency modulation functions and presented in Table 5.4.

Table 5.4: Comparison of features calculated from the simulated and demodulated amplitude and frequency signals. σ is the standard deviation calculated for 100 simulations.

	$\bar{A}$	PP_A	$Kurt_A$	MI_A	$\bar{F}$	PP_A	$Kurt_F$	MI_F
Simulated	1	1	1.5	1	5000	100	1.5	0.02
Demodulated	0.72	1.048	1.494	1.456	4999.998	110.938	1.511	0.022
σ	4.6^{-4}	8.1^{-3}	2.6^{-3}	1.1^{-2}	8.4^{-4}	1.63	9.12^{-4}	3.26^{-4}

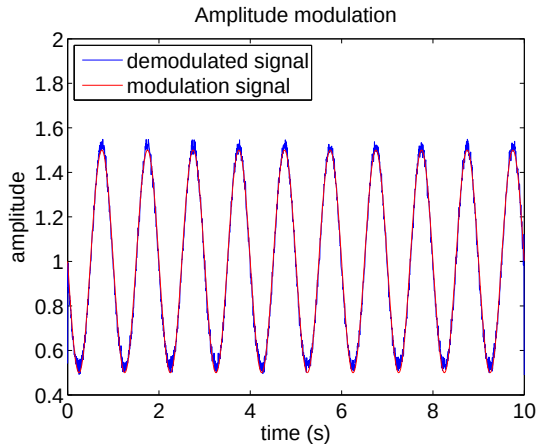

(a) Amplitude modulation

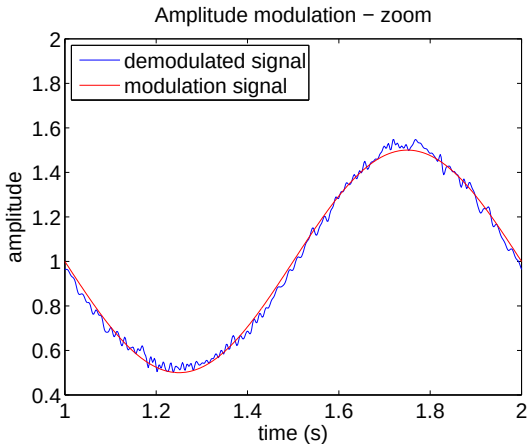

(b) Amplitude modulation – zoom view

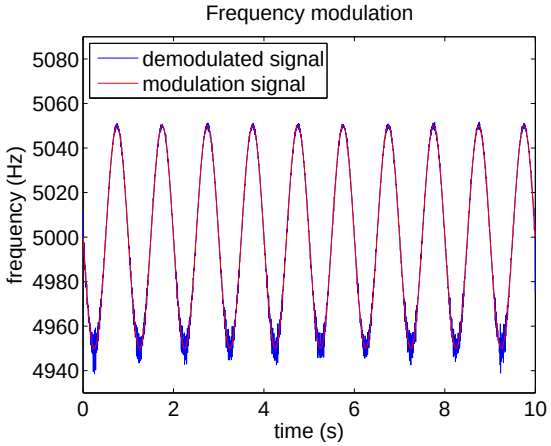

(c) Frequency modulation

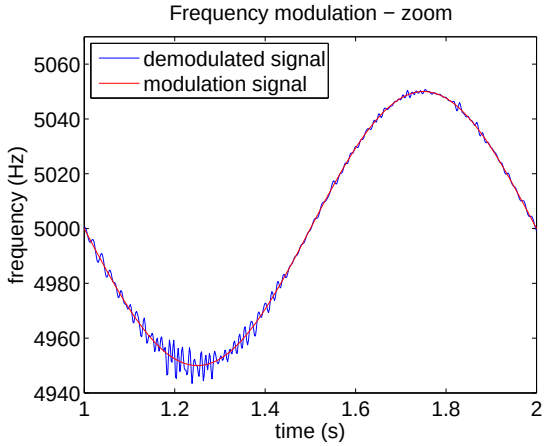

(d) Frequency modulation – zoom view

Figure 5.6: Demodulation results (blue) compared with input modulation signal (red). (a) amplitude modulation and its zoom (b), (c) frequency modulation with a zoom of selected figure part (d).

After comparing the values of the proposed features computed for simulated and demodulated modulation signals, shown in Table 5.4, one can note that in the majority of the cases the results are proximate to each other. The biggest difference is in the case of the $\bar{A}$ and MI_A where the error in the first indicator influenced the result of the second one. As men-

tioned before, several reasons could cause such a difference, including the filtering and Hilbert transform.

5.4 Conclusions and Perspectives

The proposed algorithm is validated on a simulated signal. AStrion-M is able to automatically adjust multiple parameters in order to perform the demodulation and then compute features. It is suited for a precise computation of detected modulations in the investigated signal. The proposed method has the capacity to manage the demodulation of all the detected modulation series whatever is their bandwidth and despite their abundant number, which could be the case for real-world signals.

The proposed method is a good tool for a gearbox problem identification, since these are accompanied with various types of signal modulation. Therefore, an example of AStrion-M results on wind turbine gearbox will be shown in section 6.8.

AStrion-M performance will be illustrated on a real-world signal in section 6.9 as well as on the obtained features during the entire rolling-element bearing life span. This shows an ability of the proposed algorithm to observe a bearing fault by tracking the change in the proposed features.

AStrion-M method is ready to be used with an adaptive and automatic CMS. The proposed method can be used as an advanced signal processing technique able to diagnose mechanical systems. AStrion-M is described in the publications [Fir+14] and has been transferred for the commercial application to a partner of two European projects: Innovation Project KAStrion and SUPREME within European Union Seventh Framework Programme ([FP7/2007-2013] [FP7/2007-2011]).

Chapter 6

Validation of Methods on Real-world Signals

Contents

6.1 Test Rig Data – CETIM 83
6.2 Wind Turbine Data – Arfons 88
6.3 Case Study 1 – AStrion-C on Non-stationary CETIM Data 91
6.4 Case Study 2 – AStrion-C on Highly Non-stationary Arfons Data . . 94
6.5 Case Study 3 – AStrion-K on CETIM Data 100
6.6 Case Study 4 – AStrion-K on WT's Vibration Signals 103
6.7 Case Study 5 – AStrion-K on Electrical Data 105
6.8 Case Study 6 – AStrion-KM on Arfons Data 110
6.8.1 AStrion-K – Association of Kinematics 110
6.8.2 AStrion-M – Sideband Demodulation 112
6.9 Case Study 7 – AStrion-M on CETIM High Degradation Test 114
6.9.1 Single Set of Features for the Sideband Demodulation 115
6.9.2 Features Tracking over Multiple Signals 117
6.9.3 Comparison to Established CMS Techniques 119

This chapter presents and discusses the results of proposed signal processing techniques applied to real-world signals. Data investigated in this thesis originate in the machines used within Innovation Project KAStrion. The CETIM test rig and the wind turbines at Arfons are described in the following sections. Afterwards this chapter presents six real-world cases in separate sections.

6.1 Test Rig Data – CETIM

On behalf of the Innovation Project KAStrion, see section 2.4, a test rig has been designed and installed in CETIM. This test rig simulates a wind turbine drive train configuration at a smaller scale. The detailed description of the CETIM test rig can be found in [SZB15].

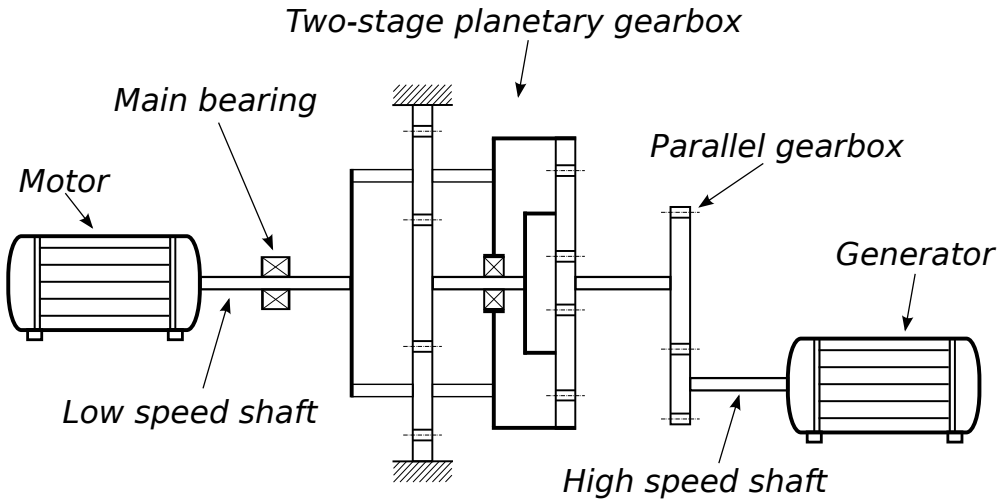

Figure 6.1: The main mechanical components of the CETIM test rig.

Figure 6.1 presents the most important kinematic components of the test rig and Figure 6.2 shows the test rig ready for tests. The test rig is driven by a 10 kW generator. This power was compared with a WT's power and the obtained ratio was used as the scaling factor for the design of the test rig. The test rig is driven by a geared-motor which has the possibility of controlling its input speed. The constant or variable input speed value can be selected according to the conducted tests. Furthermore, the fluctuation of an input speed has been recorded on a real wind turbine and this speed profile can be an input of the geared-motor to simulate real-world wind speed changes.

The two-stage planetary and the one-stage parallel gearbox work as a multiplier which has a ratio equal to 1:100.75. The geared-motor simulates the blades driven by the wind and has a nominal operating speed equal to 18 RPM. This is equal to the speed of the low speed shaft (LSS) which after a transmission via gearboxes gives a rotational speed of the high speed shaft (HSS) equal to 1813.5 RPM.

The CETIM test rig is a complex construction with a big number of mechanical components. The list of characteristic fault frequencies which originate from the gearbox components is given in Table 6.1 and from the bearings in Table 6.2. These two tables contain the theoretical values of the characteristic frequencies computed as defined in Table 4.1. The values in Tables 6.1 and 6.2 are given in orders which means that they are calculated for a shaft speed equal to 1 Hz. Moreover, the frequency of each component is calculated assuming that the test rig works with the speed of the HSS equal to 1 Hz. The speeds of the other shafts are calculated from the gear ratios. This approach enables the possibility to measure only one speed value a speed value that of the HSS.

It is worth mentioning that in the case of WTs the power is transmitted from the blades through gearbox to generator. For the test rig the power is provided by a geared-motor. The consecutive stages of the gearbox are named according to the direction of the power transmission. The calculation of characteristic frequencies starts from the HSS, because of

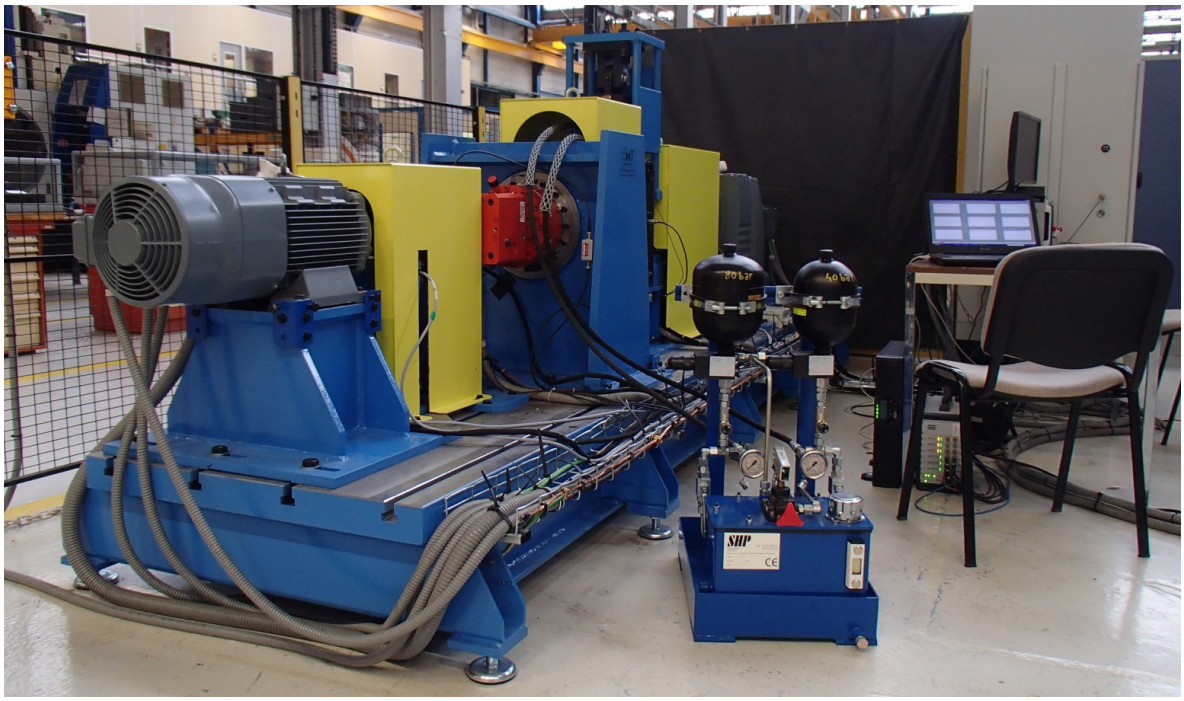

Figure 6.2: The CETIM test rig.

speed measurement taken there, and it has the opposite direction than the stages names of the gearbox. That is why the stage one of the planetary gear has lower characteristic frequencies that the stage two of the planetary gear.

The test rig is also equipped with three additional hydraulic cylinders to enable an accelerated degradation of the selected components by controlling the external forces on the bearings. The cylinders are grouped in two loading units. The first one can load the main bearing in the axial and radial directions and the second one can load a bearing supporting the HSS at the output of the gearbox in the radial direction. The hydraulic cylinders enable also a gearbox deterioration test. Each of those components will be separately damaged by performing a specific test.

A deterioration test consists of specific operation condition periods applied on a cyclic basis which allows us to observe changes in the vibrations of a component up to its degradation. This thesis focuses only on the case of the main bearing defect of the test rig.

The main bearing used in the test rig is a radial spherical roller bearing type. The bearing on the LSS can be loaded axially and radially. This bearing has a 50 mm inside diameter and can be loaded with a maximal radial force equal to 100 kN, a maximal axial force equal to 25 kN, and maximal rotational speed equal to 30 RPM. The main bearing deterioration test has been designed to have a life span of around 24 days.

As each of the deterioration tests conducted on CETIM test rig, the main bearing degradation test consist of two phases which are repeated one after another until the bearing is faulty:

Table 6.1: Characteristic frequencies of the CETIM test rig gears expressed in *orders*.

Component name	**Order**
Parallel gearbox	
GMF	16
HSS = smaller wheel relative frequency	1
Sun shaft of planetary gearbox output = bigger wheel relative frequency	0.307692
Two-stage planetary gearbox	
Planetary gearbox stage 2 – planet frequency	0.091315
Planetary gearbox stage 2 input shaft = planetary gear stage 1 sun shaft	0.069479
GMF	1.07196
Planetary gearbox stage 1 – planet frequency over ring	0.029777
Planetary gearbox stage 1 – planet frequency	0.014437
LSS	0.009926

Table 6.2: Characteristic frequencies of the CETIM test rig bearings expressed in *orders*.

REB name	**BPFO**	**BPFI**	**FTF**	**BSF2**
Generator shaft bearing				
6309-2Z	3.04	4.96	0.38	1.96
High speed shaft bearings				
SKF BS2-2208-2CSK-VT143	6.62	9.36	0.415	2.81
SKF 6407	2.53	4.47	0.361	1.66
Parallel gearbox bearings				
SKF 6307	0.941538	1.52	0.117846	0.618462
Planetary gearbox bearings				
NTN 61910	2.190769	2.732308	0.136923	1.375385
Needle 35	1.012612	1.559991	n/a	0.721481
SKF 61818	0.805955	0.931017	0.032308	0.496079
Needle 5	0.219752	0.296677	n/a	0.148615
NTN 46790	0.197122	0.219752	0.004695	0.176675
Low speed shaft bearings				
SKF 22310E	0.056675	0.082283	0.00405	0.025211
SKF 22210E	0.075732	0.102928	0.00405	0.031464
SKF 21312E	0.089826	0.119107	0.004278	0.034839

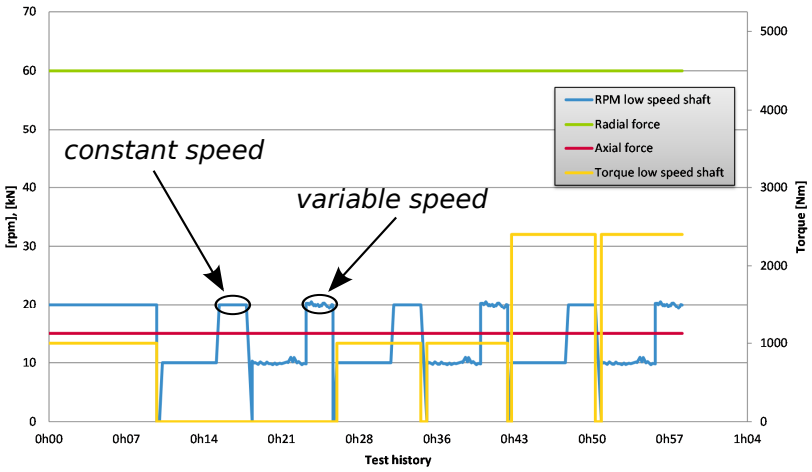

Figure 6.3: A measurement cycle on CETIM test rig.

the degradation phase and the measurement phase. The degradation phase is the operation of the test rig during 5 h 33 min under a constant radial and axial load equal to 60 kN and 15 kN respectively as well as 100 Nm of torque applied on the LSS. The measurement phase lasts for around 1 h and is more complex than the first test phase. The changes of the test rig operational parameters are presented in Figure 6.3. In this study only the part of this measurement phase is used. The signals correspond to the CETIM test rig operating under a constant speed, which is equal to 20 RPM at the LSS, a radial force equal to 60 kN, an axial force equal to 15 kN, and without torque. These measurement segment is around 150 s long and is marked in Figure 6.3 along with the segments corresponding to the variable speed, which simulates real-world wind profile.

The test rig is heavily equipped with sensors:

- accelerometers: 11 single-axis accelerometers with frequency range 0.5 Hz – 10 kHz and 1 tri-axial accelerometer 0.5 Hz – 5 kHz;
- 6 thermocouples;
- 3 tachometer sensors;
- 2 torque-meters, one per LSS and HSS;
- 3 current probes;
- 3 voltage probes.

Moreover, the instrumentation of the test rig comprises two data acquisition systems. One is the National Instrument data acquisition system installed by CETIM and used as a reference and the other one is the prototype of the KAStrion acquisition system installed by EC Systems.

If not indicated differently, all the below-presented CETIM test rig cases originate in National Instrument measurements. The data acquisition parameter along with the operational

Table 6.3: CETIM test rig signal parameters.

Sampling frequency	$39,062.5\ Hz$
Number of samples	$\sim 5,859,375$
Signal duration	$\sim 150\ s$
LSS speed	$\sim 20\ RPM$
HSS speed	$\sim 2015\ RPM$
Radial load	$60\ kN$
Axial force	$15\ kN$

conditions are presented in Table 6.3. During the time between the measurements, the test rig was working with the settings causing deterioration of the main bearing.

All the vibration signals presented in this thesis were acquired by the accelerometers placed on the main bearing where a fault occurred. One accelerometer is placed axially and two others radially on the casing of the main bearing. One radial accelerometer is oriented horizontally and the other one vertically.

6.2 Wind Turbine Data – Arfons

Arfons is a small rural town in southern France where a wind plant called Arfons-Sor is located. This wind farm is owned by Valorem and maintained by Valemo, a partner in the consortium of the Innovation Project KAStrion. At present there are 11 operating wind turbines in Arfons. Figure 6.4 shows the location of the village and of the WTs. A prototype of the KAStrion system is installed on two WTs marked as WT6 and WT8 in Figure 6.4 (b).

An example of WTs operating in Arfons is shown in Figure 6.5 (a). All WTs installed in Arfons are designed by ALSTOM Ecotècnia and are of the same type 80 2.0. Those WTs are 2 MW rated power, 80 m rotor diameter, 70 m hub height, and operate within the range of 3 m/s – 25 m/s for the wind speed at the height of hub. The WTs type can be described as a horizontal axis, upwind, three blades with a gearbox which is in line with the generator. The gearbox of Arfons WTs consists of a planetary gearbox with two parallel stages. The main mechanical components of the drive train are presented in Figure 6.5 (b).

The list of the characteristic fault frequencies which originate from the gearbox is given in Table 6.4 and from the bearings in Table 6.5. These two tables contain the theoretical values of the characteristic frequencies computed as defined in Table 4.1. And again the values are relative to speed of the HSS equal to 1 Hz which makes them *order* values. This is necessary because of the fact that the rotational speed value is measured only on the HSS of a WT.

All data available from Arfons WTs are registered by the prototype of the KAStrion CMS. The parameters of the available vibration signals are presented in Table 6.6.

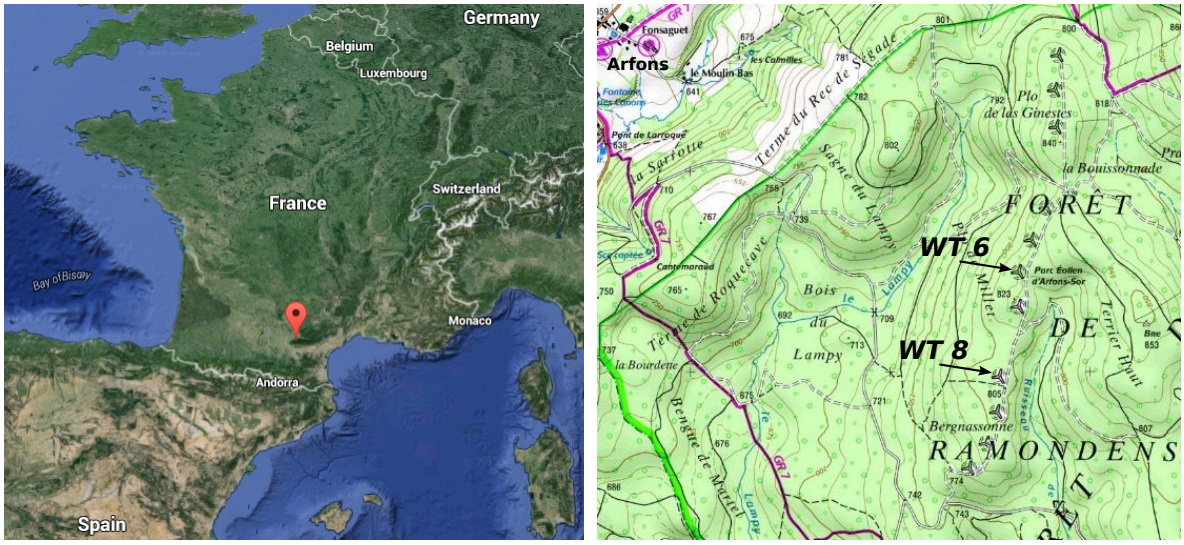

(a) Arfons location [Goo15] (b) Arfons' wind turbines arrangement

Figure 6.4: Arfons wind farm location.

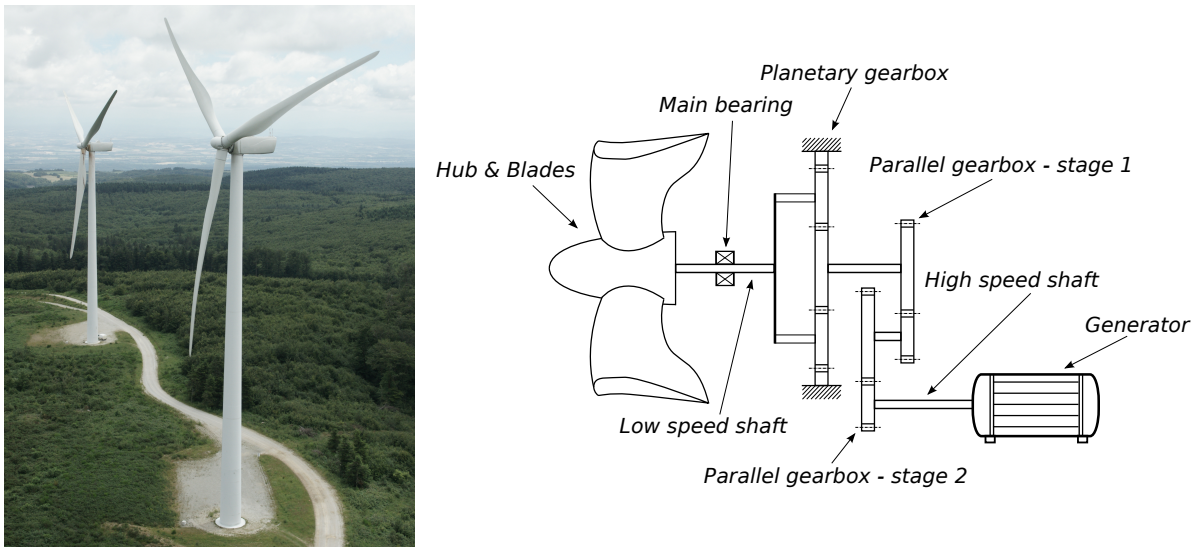

(a) Arfons wind turbines. (b) A drawing of the main mechanical components of the wind turbine drive train in Arfons.

Figure 6.5: Presentation of the wind turbines in Arfons. (a) shows two turbines on site and (b) demonstrates the kinematic configuration of the WTs drive train.

Table 6.4: Characteristic frequencies of Arfons wind turbine gears expressed in *orders*.

Component name	**Order**
Two-stage parallel gearbox	
GMF – stage 2	26
HSS = smaller wheel relative frequency	1
Intermediate shaft = bigger wheel relative frequency for stage 2 and smaller wheel relative frequency of stage 1	0.234234
GMF – stage 1	4.918919
Sun shaft = bigger wheel relative frequency of stage 1	0.056539
Planetary gearbox	
GMF	0.885259
Planetary gear – planet frequency	0.015346
LSS	0.009947

Table 6.5: Characteristic frequencies of Arfons wind turbine bearings expressed in *orders*.

REB name	**BPFO**	**BPFI**	**FTF**	**BSF2**
Generator shaft bearing				
6330-MC3	3.57	5.43	0.4	2.32
High speed shaft bearing				
(59) NSK HR30326	6.15	8.85	0.41	2.64
Parallel gearbox – stage 2				
(58) SKF NU 2328	5.68	8.32	0.405	5.1
(56) SKF NU238	1.909009	2.541441	0.100486	0.810496
Parallel gearbox – stage 1				
(57) NSK HR30334	1.440541	2.072973	0.096036	0.618378
(55) SKF 6026	0.370954	0.477079	0.024708	0.444908
(53) SKF NJ2988	0.830904	0.978130	0.026008	0.701087
Planetary gearbox				
(51) SKF EE243190	1.334327	1.492637	0.972476	0.026687
(52) LB 3U240	0.001048	0.001509	0.000104	0.000686
Low speed shaft bearings				
TIMKEN XC25695C	0.290721	0.316046	0.004765	0.113525
TIMKEN XC2364CA	0.215343	0.242219	0.004685	0.082162

Table 6.6: Arfons signal parameters.

Sampling frequency	$25,000\ Hz$
Signal duration (sensor dependent)	$10\ s$ – $60\ s$
Number of samples	$250,000$ – $1,500,000$

6.3 Case Study 1 – AStrion-C on Non-stationary CETIM Data

This section presents the results of AStrion-C, the signal processing method described in chapter 3, on a real-world signal acquired on the CETIM test rig which is described in section 6.1. The goal of this section is to depict the performance of the proposed method on a relatively simple example.

The investigated vibration signal is recorded by an accelerometer placed on the main bearing of the test rig and oriented horizontally. For the sake of reference this signal is named as '*20140408-171328 Acceleration 5 KAStrionBenchNI Test14T11S4*'. The time domain view of the investigated signal is presented in Figure 6.6. The signal lasts 150.41 s and is sampled at $39,062.5$ Hz.

The data are registered under stationary operational conditions of the test rig which means the constant rotational speed and constant load during the entire time of the signal acquisition. In general all the signals measured at CETIM test rig for these conditions are completely stationary according to AStrion-D test although the selected signal is very particular. In the middle of the measurement there is an extremely strong shock visible in the signal. It is present before the 50^{th} second of the measurement as shown in Figure 6.6. The most probable explanation of this phenomenon is that a particle of the steel from one of the races of the main bearing has detached due to the flaking and has been hit by passing rolling elements. This explanation is plausible because of the fact that the recording corresponds to the 163^{rd} hour of the test and the first indication of the main bearing defect appeared in the 138^{th} hour according to the narrow-band RMS analysis.

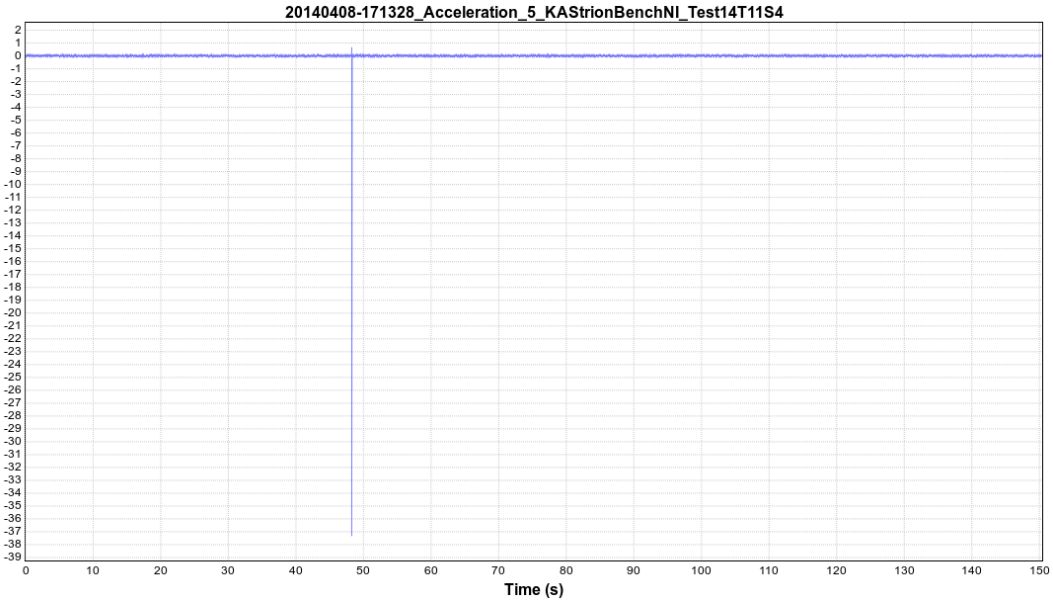

Figure 6.6: The time domain signal registered on 2014.04.08 at 17:13:28 by accelerometer 5 at CETIM test rig.

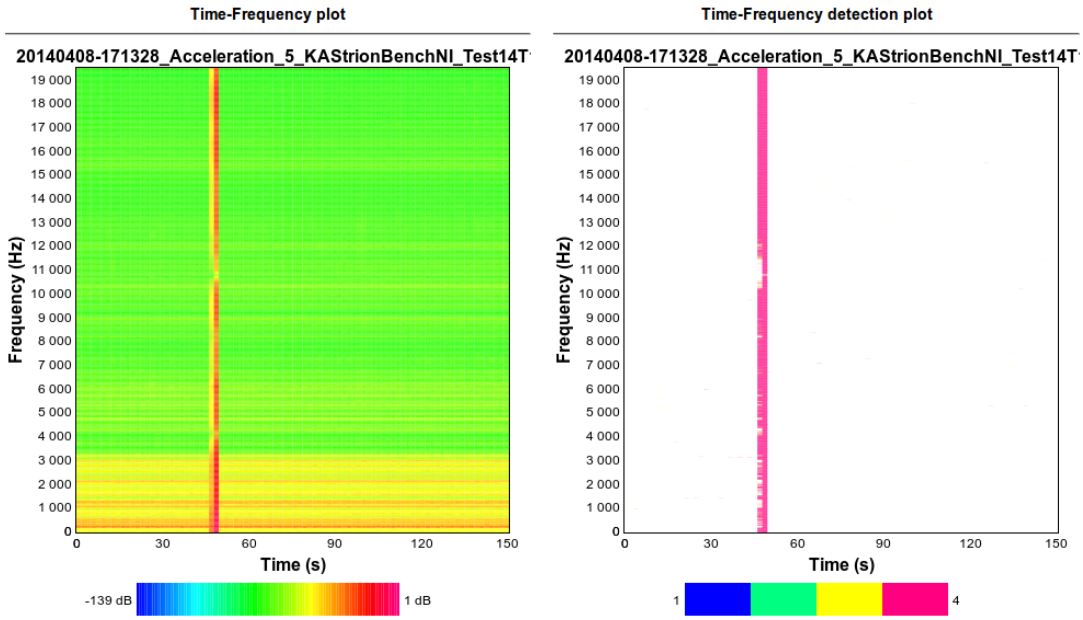

(a) Spectrogram (b) Non-stationarities

Figure 6.7: Time domain signal processed by AStrion-D which computed that the non-stationarity rate equals to 99% for the full signal; (a) spectrogram of the investigated signal and (b) detected non-stationarities on the TF plot.

The first step in processing the signal is to obtain the non-stationary tiles of the signal by applying AStrion-D, earlier developed AStrion module which is briefly described in section 2.2.1. In this example the obtained spectrogram has a dimension of 88 time segments and 131,073 frequency segments. The spectrogram and the results of non-stationarity test are presented in Figure 6.7. The non-stationarity index computed by AStrion-D method is equal to 99% which corresponds to almost maximum non-stationarity rate of the signal.

The high non-stationarity rate computed by AStrion-D could be surprising, but this result originates in the methodology applied in AStrion-D. Similarly to Equation 3.6, AStrion-D separately verifies the number of the time segments and the frequency segments containing any non-stationarity. In the extreme case it could happen that in each time segment there is only one non-stationary tile and also in each frequency segment there is only one non-stationary tile. A combination of these would give a non-stationarity rate equal to 100 % computed by AStrion-D. In fact, the investigated signal is not far away from such a situation. It is easy to notice that probably for each frequency value there is at least one non-stationary tile detected and their position corresponds to the high peak of the signal amplitude presented in Figure 6.6. To perceive the non-stationary tiles distributed along the time segments it is necessary to verify the zoom views of the signal. Figure 6.8 shows that in the frequency range from 2920 Hz to 3150 Hz there are some non-stationarity detections for various time segments of the signal.

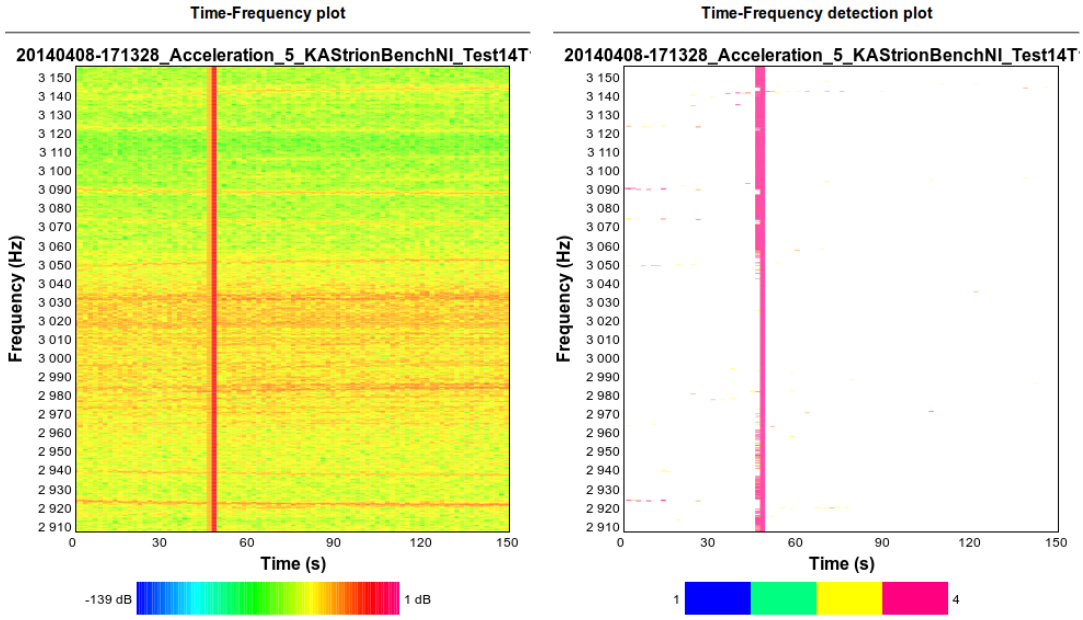

(a) Spectrogram (b) Non-stationarities

Figure 6.8: The zoom of spectrogram and non-stationarity detection test of AStrion-D which shows the non-stationary tiles being the reason for the non-stationarity rate equal to 99%.

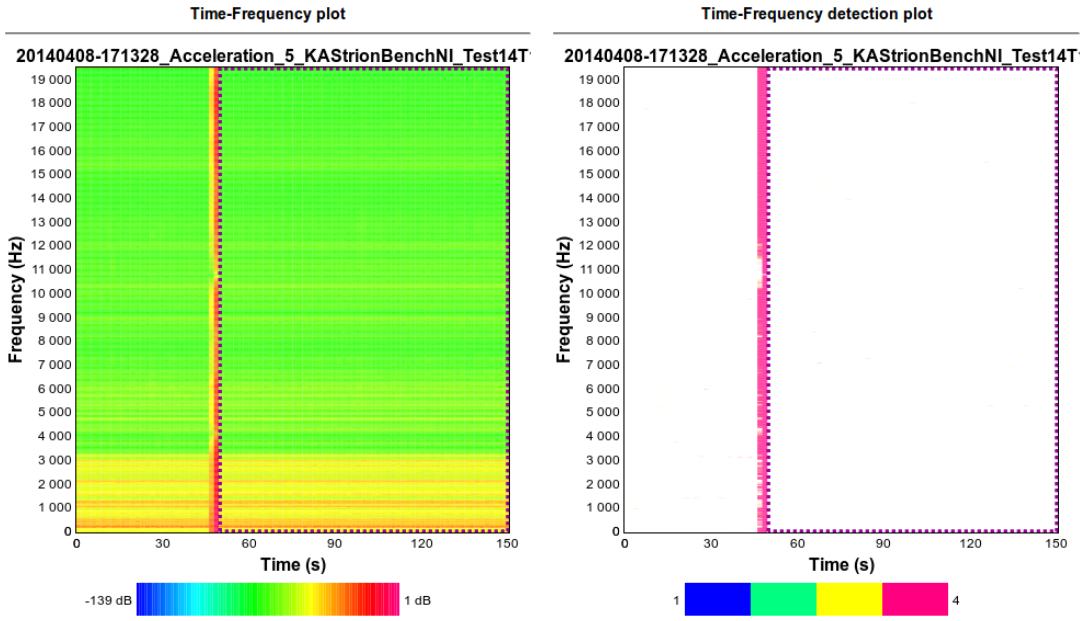

(a) Spectrogram (b) Non-stationarities

Figure 6.9: The result of AStrion-C marked by dotted lines on the (a) spectrogram of the investigated signal and (b) detected non-stationarities on the TF plot. The non-stationarity rate computed by AStrion-D equals to 0% for the selected area.

Based on the AStrion-D result the proposed algorithm searches for the stationary part of the signal. The biggest area is identified in the 30^{th} iteration of the searching. Moreover, the same result is captured twice, for the frequency and the time priority version of the proposed algorithm. These results were then merged into the final one which covers the entire frequency span and time range from 49.57 s to the end of the signal, as presented in Figure 6.9. For the cropped signal the non-stationarity rate computed by AStrion-D equals to 0%, which corresponds to the stationary signal according to AStrion-D definition.

In this section the CETIM test rig signal is used for presenting AStrion-C result. The example showed that the proposed method is suitable for the automatic CMS and copes well with the signal containing a strong wide-band frequency component during a short time. It leads to the conclusion that AStrion-C could be a good proposal for monitoring machines which are exposed to periodic shocks not related to diagnosis, e.g. a power press.

6.4 Case Study 2 – AStrion-C on Highly Non-stationary Arfons Data

This section illustrates AStrion-C again, the signal processing method described in chapter 3, on a real-world signal acquired on one of the Arfons wind turbines.

The investigated vibration data are acquired by an accelerometer placed on the main bearing of a WT6. The signal lasts 60 s and is sampled at $25,000$ Hz. Due to the long measurement time it has been captured with a variable wind speed that decreased which caused the average rotational speed of HSS to decrease as well. The change in the measured shaft speed is significant, during 60 s it drops from almost 1800 RPM to below 1550 RPM at the end of the recording. These signals together with the raw vibration signal are presented in Figure 6.10.

For the purposes of this section the signal is analysed twice, first in the time domain and then in the angle domain after order tracking. Figure 6.11 presents the overlapping signal in the time domain and in the angle domain. The order tracking is executed with AStrion-A module (see chapter 2) and the obtained signal is sampled at 890 *orders* and lasts 1685 $rev.$. Such a type of highly non-stationary signal due to a considerable speed variation is normally analysed with an order-tracking based methods, but too high speed fluctuation may nevertheless prevent a correct diagnosis.

The comparison of the low frequency and low order components on a spectrum view for the investigated signal is presented in Figure 6.12. It is important to highlight that after angular resampling of the signal some components, which were fluctuating beforehand, are stationary after this operation. For example, as shown in Table 6.4, it is the case for the characteristic frequency corresponding to the second stage of the parallel gearbox equal to order 26 and taking into account the average speed of the recorded signal, which is around 30 RPM, it corresponds to 780 Hz in the time domain signal. The second harmonic of this GMF is the easiest to spot in Figure 6.12 and one can see a frequency component in Figure 6.12 (a)

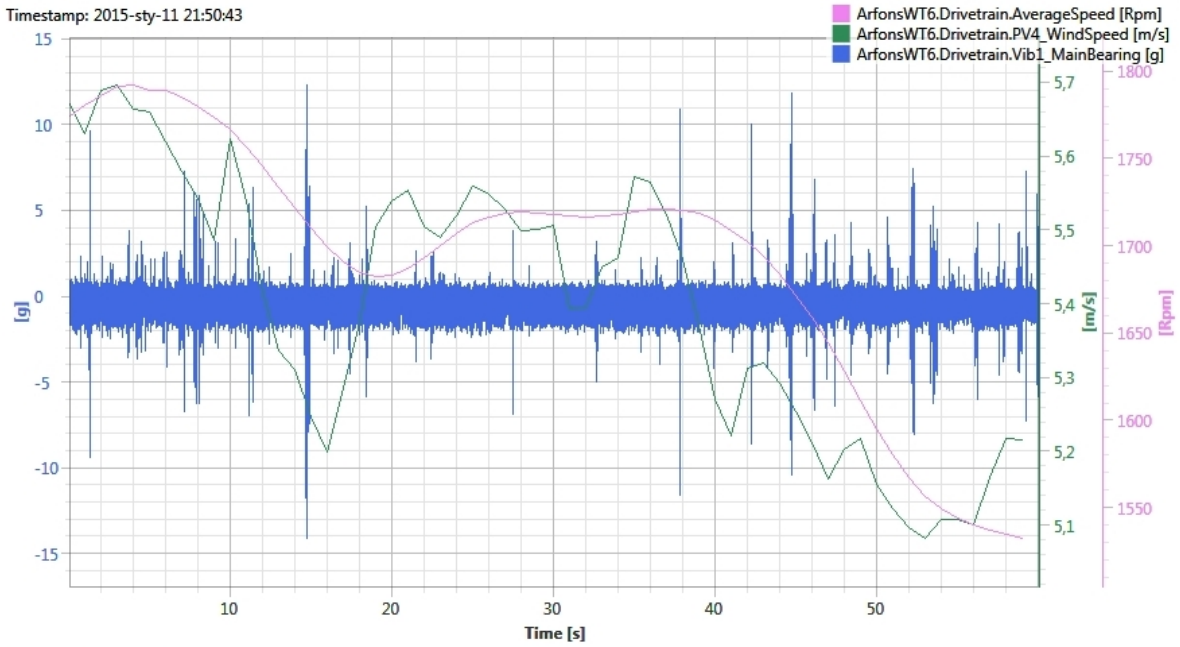

Figure 6.10: The investigated vibration signal in the time domain (blue line), the wind speed (green), and the mean speed of high speed shaft (pink).

starting around 1600 Hz and then changing together with the change of the speed whereas this component corresponds to the straight line in Figure 6.12 (b) which stands for the constant order value equal to order 52.

As one can note pulses in the time signal are visible in the view presented in e.g. Figure 6.10. These shock impulses correspond to the wide-band non-stationarities detected in the signal and are also visible in Figure 6.13 (b) as the vertical red lines. The origin of these shocks is not known. The frequency of their occurrence does not correspond to any mechanical component listed in Tables 6.4 and 6.5, so we are not interested in capturing this phenomenon for further diagnosis in this study. However, AStrion is able to detect the presence of such structures thanks to AStrion-D, briefly presented in section 2.2.1. There is a number of possible causes for these shocks but there is no enough data to find out the true one. It could be due to the control system of the wind turbine which changes the yaw of the nacelle or the pitch of the blades during the changing wind or even a different phenomenon.

The first step in processing the signal is to obtain the non-stationary tiles of the signal by applying AStrion-D, as described in section 2.2.1. In this example the obtained spectrogram has a dimension of 90 time segments and 32,769 frequency segments. The non-stationarity index computed by AStrion-D method is equal to 67% which is considered as a high non-stationarity rate, since 0% corresponds to a stationary signal. Based on this result the proposed algorithm searches for the stationary part of the signal.

The biggest area which meets the condition given in Equation 3.7 for T_S equals to 4% is found in the 43^{th} iteration and has the dimension of 16 overlapping time segments by 32,769

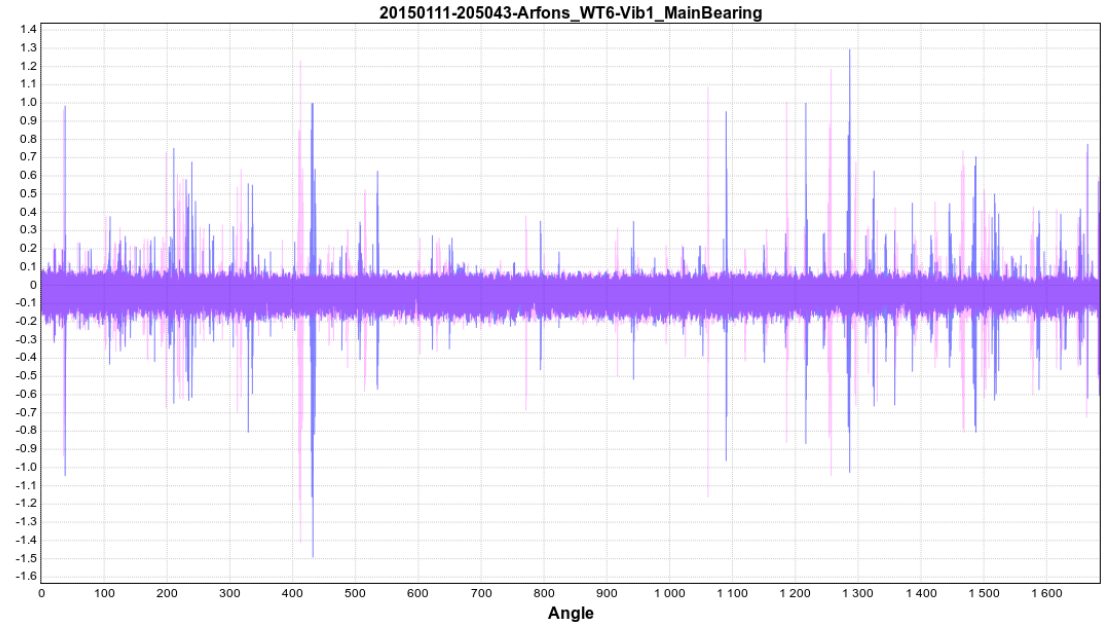

(a) Full view

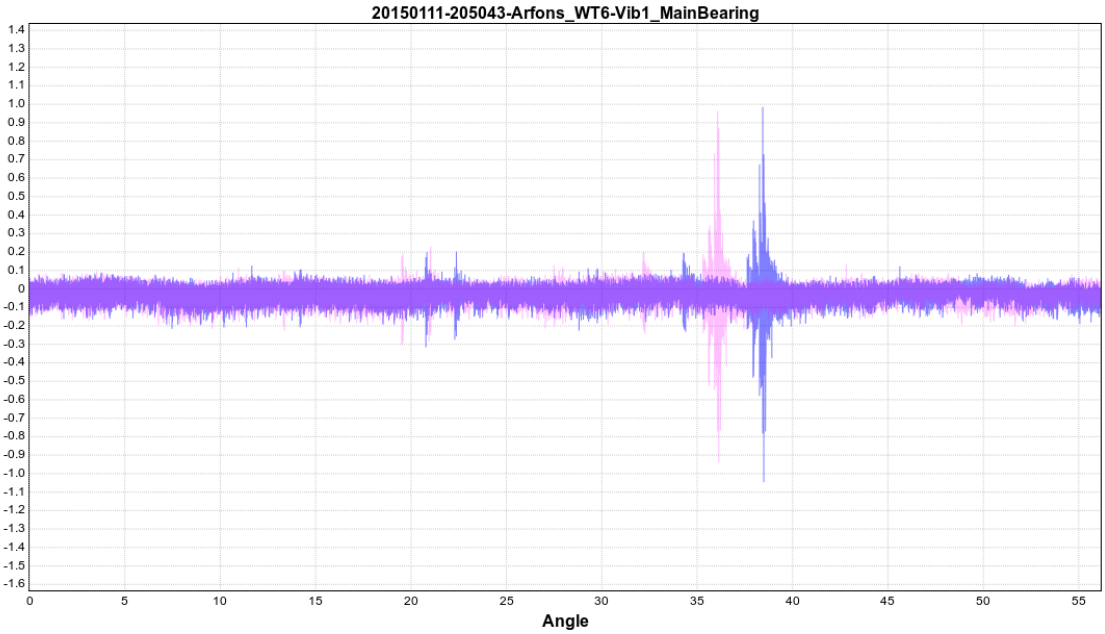

(b) Zoom of the signals in the range of 0 $s - 2$ s corresponding to 0 $rev.-\sim 56$ $rev.$

Figure 6.11: The investigated vibration signal in the time domain (pink line) and in the angle domain (blue line).

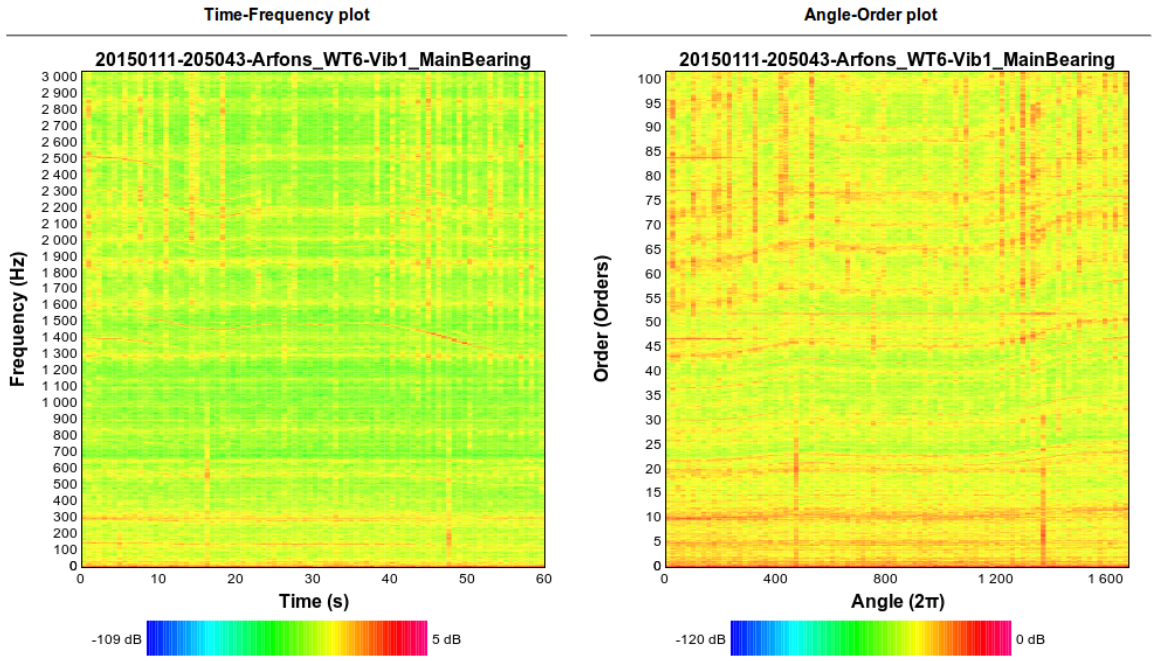

(a) Time domain signal (b) Angle domain signal

Figure 6.12: The zooms (a) in the frequency domain and (b) the corresponding part of the signal in the order domain.

frequency segments, which is the full available frequency range. This means that the selected area lasts 10 s and starts at the 28^{th} second. Figure 6.13 presents the result depicted by dotted lines on the spectrogram as well as on the detected non-stationary tiles on the TF plane of the full-length signal. The selected part of the investigated signal is then processed once again by AStrion-D algorithm. Figure 6.14 shows its result on the TF plane. The non-stationary index computed on the cropped signal equals to 56%, which is a lower value than the one obtained for the full-length signal. This time-frequency representation of the signal consists of 60 time segments and 8193 frequency segments.

The idea is now to test the method after an angular resampling performed by AStrion-A module (see chapter 2). It results in obtaining a signal which is sampled at 890 *orders* and 1685 *rev.* long. This signal is again processed by AStrion-D, see section 2.2.1, to detect non-stationarities. In this step an angle-order representation of the signal is computed which consists of 90 angle segments and 32, 769 order segments. The non-stationarity rate estimated by AStrion-D equals to 88%. This non-stationarity is higher than in the time domain signal due to strong spectral components around 160 *orders* and above 300 *orders*. The change of these spectral components is directly associated with the changing speed of the HSS. In the time domain these spectral components are visible at 4500 Hz and 9000 Hz respectively and can be linked to the inverter frequency.

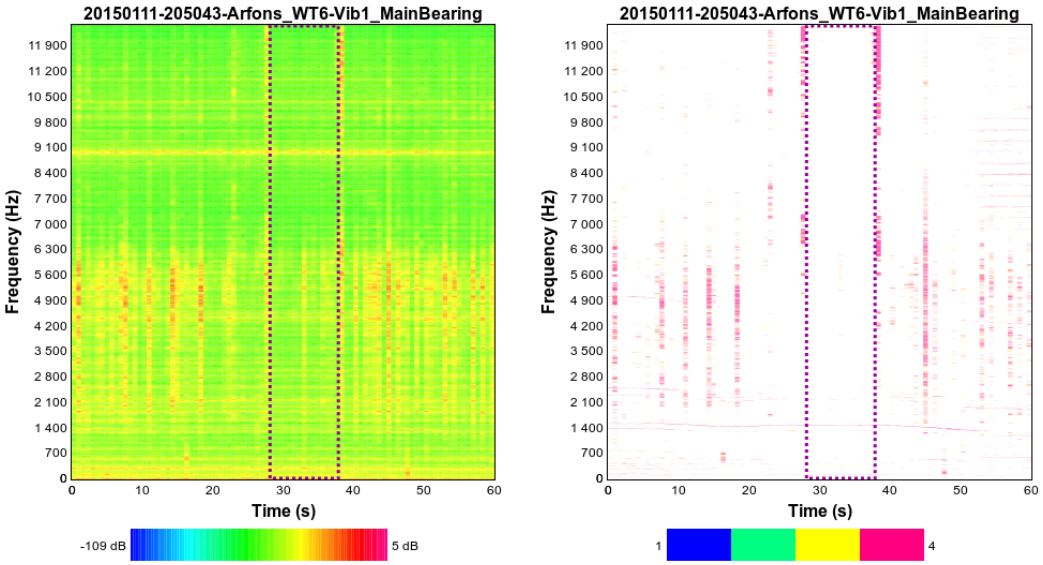

(a) Spectrogram (b) Non-stationarities

Figure 6.13: Time domain signal processed by AStrion-D with the AStrion-C result marked by dotted lines, (a) spectrogram of the investigated signal and (b) detected non-stationarities on the TF plot. The non-stationarity rate for the entire signal equals to 67%.

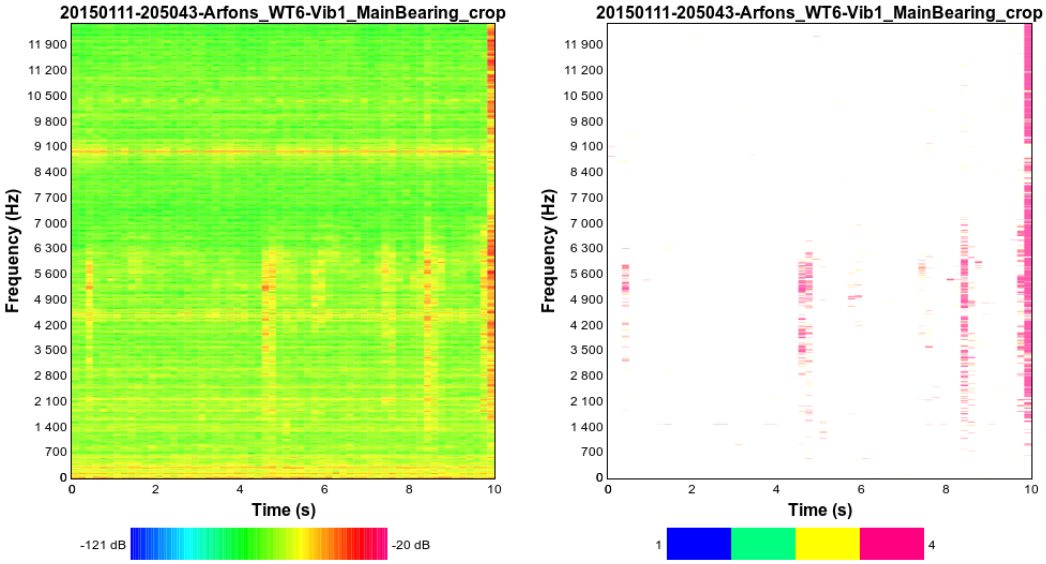

(a) Spectrogram (b) Non-stationarities

Figure 6.14: The part of the time domain signal cropped according to results of AStrion-C and processed by AStrion-D which computed the non-stationarity rate for the cropped signal equals to 56%, (a) spectrogram of the investigated signal and (b) detected non-stationarities on the TF plot.

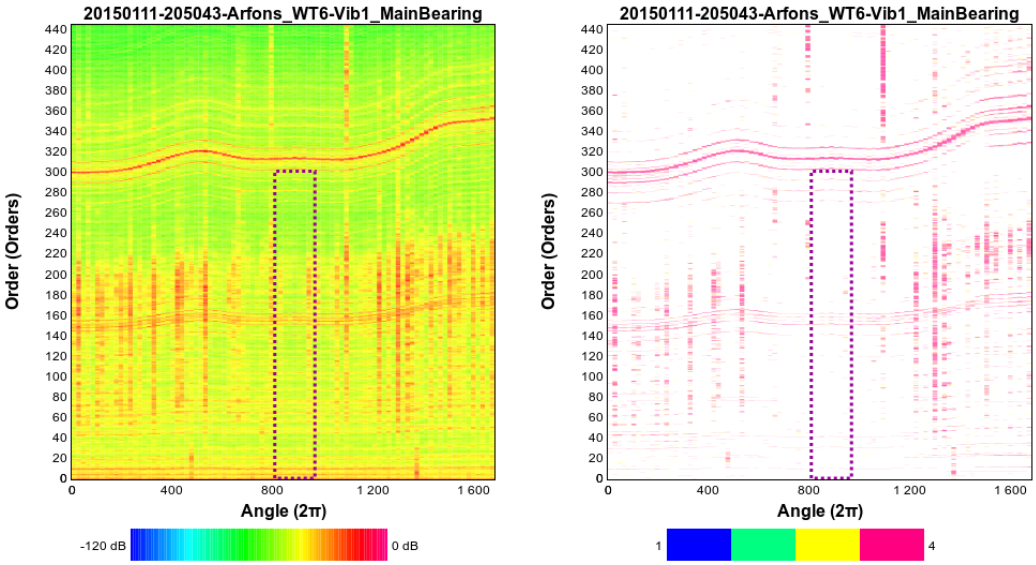

(a) Spectrogram (b) Non-stationarities

Figure 6.15: Angle domain signal processed by AStrion-D with the AStrion-C result marked by dotted lines, (a) spectrogram of the investigated signal and (b) detected non-stationarities on the angle-order plot. The non-stationarity rate for the full signal equals to 88%.

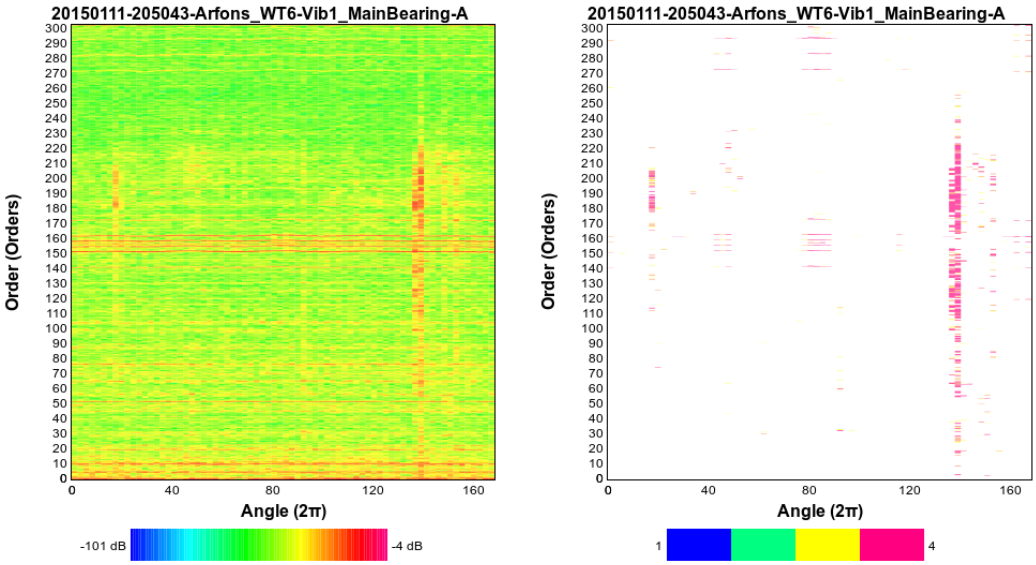

(a) Spectrogram (b) Non-stationarities

Figure 6.16: The part of the angle domain signal cropped according to results of AStrion-C and processed by AStrion-D which computed that the non-stationarity rate equals to 24% for these area, (a) spectrogram of the investigated signal and (b) detected non-stationarities on the angle-order plot.

The proposed AStrion-C algorithm selected the biggest stationary area according to the defined conditions in the 44^{th} iteration. The selected part of the signal has the dimension of 10 angle segments by $22,298$ order segments. This means that the selected area corresponds to the signal 168.45 2π long which starts from the 805^{th} *rev.* of the angle domain signal. In the other direction the signal is restricted to the order corresponding to 605.6 *orders*. Figure 6.15 presents the result of the cropping algorithm depicted by dotted lines on the spectrogram and on the detected non-stationary tiles on the angle-order full-length signal representation. The non-stationary index computed by AStrion-D on the result of AStrion-C equals to 24%. This is a significant decrease of the non-stationarity detected in the signal in comparison to the full-length signal.

Figure 6.16 shows the non-stationarity detection results of AStrion-D on the signal cropped as evaluated by AStrion-C. This new angle-order representation of the signal consists of 72 angle segments and 4097 order segments.

A weakness of the proposed algorithm is revealed by the time-domain signal presented in this section. Due to low time resolution of the spectrogram there is a high non-stationarity present in the AStrion-C result after computing a new spectrogram for the cropped result. It is visible as an almost vertical line the most to the right in Figure 6.14 (b). Another fragility of the proposed algorithm could be pointed out by observing the result of AStrion-C applied on the signal after order tracking. One could suggest that it would be more appropriate to analyse the entire order range, since the detected non-stationarity just above the result of AStrion-C appears to be at the same level, so should not affect much the signal after truncation. However, for the proposed method the number of non-stationary tiles in the area of the signal above the selected one is too high to include this part of the signal in the final result.

Taking into account that the selected signal is highly non-stationary and difficult to interpret for diagnostic purposes this section presents a good performance of the proposed method. AStrion-C managed to select reasonable parts of the time and the angle domain signals as proposals for usage in further processing.

6.5 Case Study 3 – AStrion-K on CETIM Data

This section presents the application of AStrion-K on a single signal measured on the CETIM test rig. For the sake of reference the selected signal is marked as '*20131119-091010 Acceleration 5 KAStrionBenchNI Test12T11S4*', which means that it comes from the accelerometer number 5 placed on the main bearing and its acquisition started on 19^{th} November 2013 at 9:10 a.m.

As explained in chapter 4, the signal is processed by AStrion-DIH. As a result $24,162$ spectral components are identified and AStrion-H detects 535 harmonic series and 7819 sideband series. These harmonic and sideband series should be associated with the characteristic frequencies listed in Tables 6.1 and 6.2.

Some associations provided by AStrion-K are presented in Table 6.7. Each of the examples is separated with a double horizontal line and the series selected for the final association is in the highlighted row. A double vertical line divides the data available from the previous AStrion-DIH steps on the left-hand side, and AStrion-K information on the right-hand side. The 'Theoretical frequency (Hz)' column contains the values of the characteristic fault frequencies after taking into account the value of rotational speed.

The first four associations show the cases of the selected rolling-element bearing frequencies with previously detected harmonic series. As one can notice, there is a various number of series taken into account for each example. This depends on the number of the harmonic series which are detected proximate to the theoretical frequency corresponding to the mechanical component and which meets the condition given in Equation (4.3) which in the case of a REB has a form $RFD_i < \eta + \delta\eta$. In the second step of AStrion-K the final series to be associated is selected based on the highest bearing series indicator (BSI_i) among the selected candidates in the first step as all the first four associations are made for a bearing components. The detailed explanation on the BSI_i is presented in section 4.2.

In the first two examples the series selected for the association, apart from the highest bearing series indicator (BSI_i) value, has also the lowest value of the relative frequency difference (RFD_i) in their groups. For the first association the characteristic fault frequency corresponding to the BPFI of the main bearing, which is described as SKF 22210E, has the biggest number of peaks in the harmonic series, the highest energy and density among the series selected in the first step of the proposed algorithm. In the second association the characteristic fault frequency corresponding to the FTF of a gearbox bearing has the biggest number of peaks consisting of harmonic series and the highest density. Although the energy of the selected series is not the highest one among earlier selected series, this one is chosen to be a representative of the characteristic fault frequency. In the third and fourth associations shown in Table 6.7, one can note that some frequencies are much closer to the theoretical frequency, as their RFD_i is closer to zero, than for the selected series. In the fourth association the difference is very significant, since other series has RFD_i equal to 0.006, while the selected one has a RFD_i equal to 0.684. The difference in the value of the energy of these two series has a major influence on the final selection for the association.

In the fifth association presented in Table 6.7 there is an association of a GMF with a harmonic series. The number of proximate series is high. There are thirteen series which satisfies the condition of Equation (4.1), thus there are thirteen candidates selected in the first step of AStrion-K to be associated. This time we are considering a characteristic frequency of the gearbox, so the final series to be associated is selected based on the lowest value of the RFD_i, as explained in section 4.2. In this case it is the series that has the RFD_i value equal to 0.002. Such a precision is expected of the spectral pattern generated by meshing gears and to double-check this association the number of peaks in the series and its energy can be verified. As it is possible to spot in Table 6.7, these two parameters are the highest in this group of series and what is more important the energy is several orders higher. These confirms the correct result of the proposed method.

Table 6.7: Detailed results of AStrion-K on example of the CETIM signal recorded by accelerometer 5 on 19^{th} November 2013. Selected candidates for association, according to Equations (4.1) and (4.3), are grouped between double lines and final series to be associated are highlighted.

Type	Freq. (Hz)	Carrier freq. (Hz)	Modulation freq. (Hz)	Number of peaks	Energy (10^{-9})	Density	Selected component name	Theoretical freq. (Hz)	RFD_i	BSI_i
Harmonic	3.573	—	—	10	4.3^{-9}	0.417	SKF 22210E.BPFI	3.6	0.743	0.686
Harmonic	3.581	—	—	14	4.5	0.5	SKF 22210E.BPFI	3.6	0.536	0.75
Harmonic	12.601	—	—	6	4.2	0.3	6309-2Z.FTF	12.762	1.257	0.65
Harmonic	12.643	—	—	3	0.2	0.6	6309-2Z.FTF	12.762	0.934	0.324
Harmonic	12.748	—	—	9	3.3	0.9	6309-2Z.FTF	12.762	0.104	0.843
Harmonic	13.678	—	—	3	0.6	0.75	SKF BS2-2208-2CSK.FTF	13.937	1.86	0.44
Harmonic	13.751	—	—	6	5.1	0.3	SKF BS2-2208-2CSK.FTF	13.937	1.334	0.65
Harmonic	14.037	—	—	4	2	0.308	SKF BS2-2208-2CSK.FTF	13.937	0.716	0.35
Harmonic	14.114	—	—	4	0.3	0.667	SKF BS2-2208-2CSK.FTF	13.937	1.272	0.363
Harmonic	20.436	—	—	5	9.2	0.294	SKF 6307.BSF2	20.77	1.61	0.185
Harmonic	20.769	—	—	3	0.7	0.75	SKF 6307.BSF2	20.77	0.006	0.378
Harmonic	20.912	—	—	9	120	0.321	SKF 6307.BSF2	20.77	0.684	0.661
Harmonic	21.064	—	—	4	12	0.333	SKF 6307.BSF2	20.77	1.418	0.217
Harmonic	533.68	—	—	4	42	0.8	GearBox2.GMF	537.333	0.68	—
Harmonic	534.845	—	—	4	430	0.667	GearBox2.GMF	537.333	0.462	—
Harmonic	534.959	—	—	3	20	0.5	GearBox2.GMF	537.333	0.442	—
Harmonic	535.345	—	—	3	34	0.6	GearBox2.GMF	537.333	0.37	—
Harmonic	535.678	—	—	3	27	0.6	GearBox2.GMF	537.333	0.308	—
Harmonic	536.011	—	—	4	120	0.667	GearBox2.GMF	537.333	0.246	—
Harmonic	537.344	—	—	6	18,000	0.857	GearBox2.GMF	537.333	0.002	—
Harmonic	537.679	—	—	4	220	0.571	GearBox2.GMF	537.333	0.064	—
Harmonic	538.345	—	—	6	13	0.857	GearBox2.GMF	537.333	0.188	—
Harmonic	539.679	—	—	5	36	1	GearBox2.GMF	537.333	0.436	—
Harmonic	540.178	—	—	4	15	0.667	GearBox2.GMF	537.333	0.53	—
Harmonic	541.011	—	—	4	5.1	0.8	GearBox2.GMF	537.333	0.68	—
Harmonic	541.178	—	—	3	210	0.428	GearBox2.GMF	537.333	0.716	—
Sideband	—	2686.72	73.002	3 | 3	16 | 6.1	0.75 | 0.6	NTN 61910.BPFO	73.573	0.777	0.838
Sideband	—	2686.72	73.669	3 | 2	8.2 | 1.8	0.75 | 1	NTN 61910.BPFO	73.573	0.13	0.655
Sideband	—	2686.72	74.335	4 | 2	10.3 | 6.5	0.571 | 1	NTN 61910.BPFO	73.573	1.035	0.763

The last association shown in Table 6.7 presents an association of a BPFO frequency of a bearing with detected modulation sideband series. The modulation has a carrier frequency which is also the 5^{th} harmonic of the previously considered GMF frequency. In the case of sideband series the same rules that for the association of the harmonic series are applied. In the first step of the algorithm three series meet the condition on RFD_i, as defined in Equation (4.1), and in the second step only one series is selected based on the highest BSI_i value. In the end, the selected series has not the lowest value of RFD_i, but has the highest energy and considerably high density among the series in the group selected in the first step.

6.6 Case Study 4 – AStrion-K on WT's Vibration Signals

This section presents the results of AStrion-K, the kinematic association proposed in chapter 4. The algorithm is tested on real-world signals acquired on a wind turbine. The mechanical system and installation is featured in section 6.2. The below presented data come from one accelerometer placed on the front side of the generator of WT 8, which is shown in Figure 6.4 (b) whereas the localisation of all the sensors is presented in Figure 1.9.

There are 165 signals between 10^{th} February to 31^{st} December 2014 acquired under similar WT's operational state. The data are chosen based on the HSS rotational speed only. In this case the speed is within the range 1780 RPM – 1795 RPM. The speed values of all the investigated signals are presented in Figure 6.17.

Each of the signals is processed by AStrion-ADIHKMT algorithm, for details please refer to chapter 2. This includes order tracking, data validation, peak identification, harmonic and sideband detection, kinematic association, sideband demodulation, and tracking of the spectral components. Thanks to AStrion-T, the tracking method, it is possible to easily display the evolution of the computed features over multiple signals. The high speed shaft is selected as the component of interest for this case study.

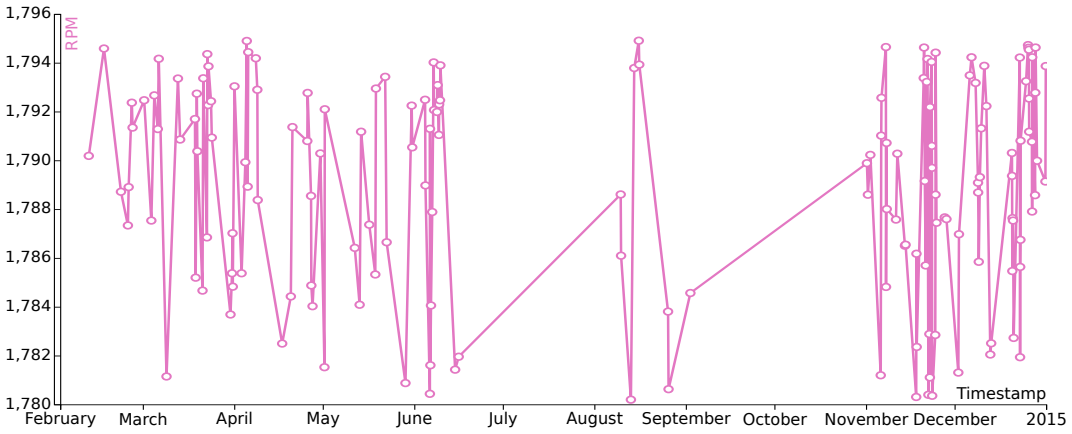

Figure 6.17: Average speed of the high speed shaft displayed for every investigated vibration signal acquired in 2014 by accelerometer located on the generator of the WT8 and during the wind turbine was operating within the range 1780 RPM – 1795 RPM of HSS.

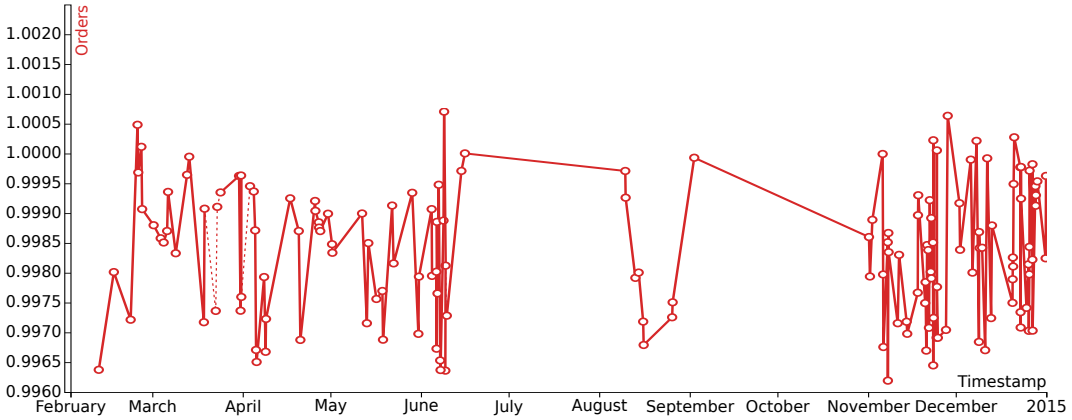

Figure 6.18: Fundamental order of series associated with high speed shaft for the investigated misalignment problem.

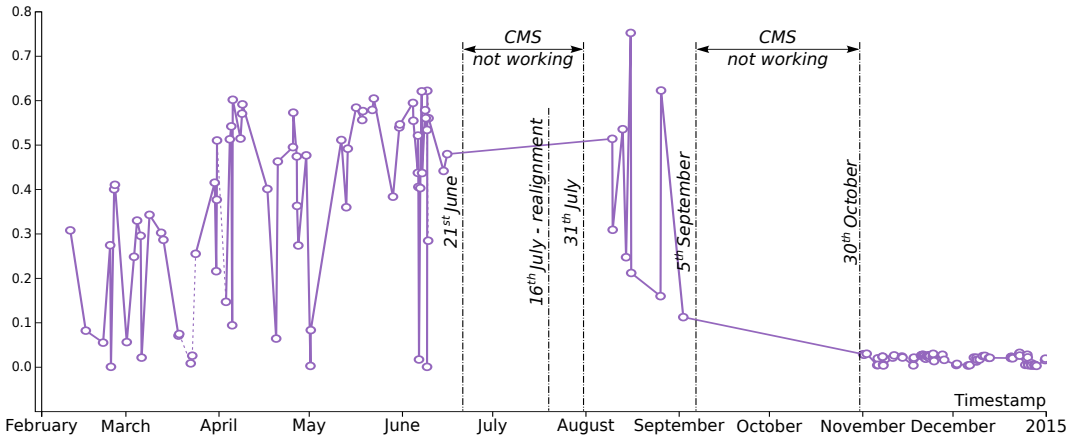

Figure 6.19: Energy computed by AStrion-H of the series associated with the high speed shaft of the WT8 wind turbine.

Among all the signals it was possible to automatically identify the harmonic series associated to HSS characteristic frequency. Figure 6.18 presents the fundamental order value of the harmonic series associated with HSS characteristic frequency. There are 161 points in this figure and it means that only few times the sleep state, depicted by dashed lines, of AStrion-T has been used. The association with HSS is presented in Figure 6.18 and it shows the robustness of the whole proposed data-driven method for condition monitoring, since even in the case of not detecting the series to be associated with HSS characteristic frequency the tracking performed by AStrion-T is continuous.

Figure 6.19 presents another indicator computed by AStrion-H, which is the energy of the harmonic series associated with the HSS. One can observe a significant change of its value between the beginning and the end of the year 2014. The lack of data in two periods, 21^{st} June – 31^{st} July and 5^{th} September – 30^{th} October, corresponds to periods where the CMS did not record vibration data. These periods were used for maintenance actions. Among others a realignment of the gearbox and the generator has been executed on 16^{th} of July

and the change in the system performance is noticeable by observing the indicator shown in Figure 6.19. Unfortunately, there is no vibration data recorded on this WT prior to the presented period thus it is not possible to observe the augmentation of this indicator and the development of the problem.

Besides AStrion does not have any specific indicator for this type of fault, the change of energy is enough to depict it. This example shows that the AStrion methodology is capable to cope with real-world malfunction of a wind turbine case.

6.7 Case Study 5 – AStrion-K on Electrical Data

The CETIM test rig, described in section 6.1, has been also used to test the ability of a fault detection from 3-phase current and voltage measurements. The electrical signature analysis methods, referred to as SMESA and detailed in [CGB14]; [Cab+15], were successfully applied to detect a main bearing fault. Figure 6.20 shows a change of the mechanical fault detector defined as the narrow-band RMS value (see Equation (1.18)) computed around frequency 3.45 Hz which corresponds to the main bearing SKF 22210E fault of BPFI type. This indicator is evaluated by SMESA on 21 voltage signals measured during a stationary operation of the test rig. Figure 6.20 presents the test history results from the 10^{th} hour, the beginning of the high degradation test, until the 190^{th} hour while the main bearing was disassembled for an inspection. The evolution of the mechanical fault detection indicator [Cab+15], presented in Figure 6.20, is shown to depict the capabilities of SMESA method for fault detection.

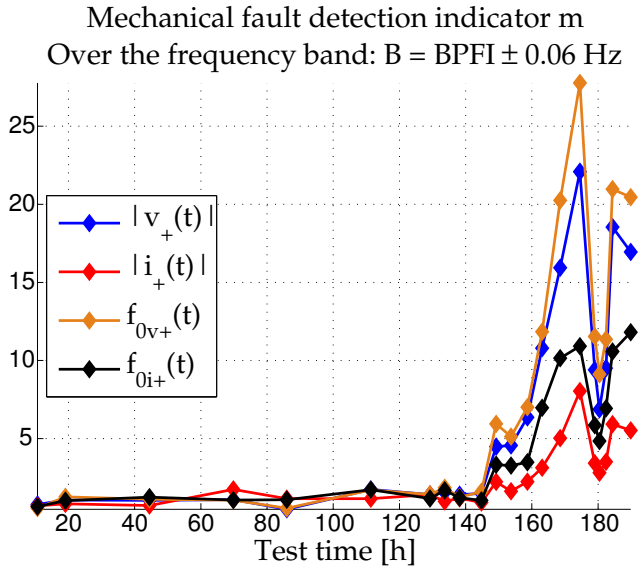

Figure 6.20: The evolution of the mechanical fault detection indicator during the main bearing degradation test for positive-sequence components of instantaneous amplitudes and frequency [Cab+15].

In this section the ability of AStrion-K usage on non-vibration data is tested. The input information is:

- Kinematic data of the CETIM test rig as presented in Table 6.1 and Table 6.2;
- Rotational speed of the HSS, which is constant during the considered measurements and equal to 2015 RPM;
- Instantaneous amplitude and frequency estimated by SMESA from the positive sequence component of the voltages, which are briefly the instantaneous amplitude and frequency [Boa92] of mono-component voltage signal obtained by filtering the three-phase signals around the fundamental frequency. For details on obtaining the signals please refer to [CGB14].

The instantaneous amplitude and frequency signals are obtained from the 3-phase voltage measurements originally sampled at 25 kHz. As a part of the signal processing executed by SMESA, the signals are down-sampled to a sampling frequency equal to 977 Hz. Among all the signals two are selected to serve as AStrion-K examples in this section. At the 158^{th} hour of the test one is the presented instantaneous amplitude and the other one the instantaneous frequency estimated from the positive sequence component of the voltages. The signals in the time domain are presented in Figure 6.21.

The two mentioned signals are processed by AStrion-DIH as explained in chapter 2. The detected harmonic and sideband series are then associated with the characteristic frequencies of the system as described in chapter 4. The results can be viewed in a web-browser based displaying tool which is presented in Figure 6.22. The highlighted series corresponds to the main bearing BPFO and BPFI characteristic fault frequencies. The mentioned series are also displayed in the spectrum representation by coloured arrows pointing out the peaks which belong to the series. The arrow colours correspond to the highlighted harmonic series.

Table 6.8 shows the full list of the associated series, both harmonic and sidebands, of the instantaneous amplitude and frequency estimated from the positive sequence component of the voltages. AStrion-K results are presented on the right-hand side of Table 6.8. In this table the column 'Theoretical freq. (Hz)' presents the result of the frequency estimation according to the speed of the investigated signal, as depicted by block 'Calculation of characteristic fault frequencies' in Figure 4.3. Employing the same colours as in Figure 6.22 the main bearing fault frequencies are highlighted in Table 6.8.

Figure 6.22 and Table 6.8 show the obtained results of the association performed by AStrion-K algorithm. Due to the signal processing done by SMESA the number of spectral components detected by AStrion-DI and then the number of patterns detected by AStrion-H is rather low. This is the reason why also a low number of the kinematic components was associated by AStrion-K and this operation is simple. In all the cases the selected candidates in the first step became the final series for the association in the second step of the AStrion-K methodology presented in chapter 4. Moreover, it is worth highlighting that for both signals,

Table 6.8: List of all the results of AStrion-K obtained on the instantaneous amplitude and the instantaneous frequency estimated from the positive sequence component of the voltages measured in 158^{th} hour of the main bearing test. Series corresponding to the damaged main bearing are highlighted using the same colors as in Figure 6.22.

Type	Freq. (Hz)	Carrier freq. (Hz)	Modulation freq. (Hz)	Number of peaks	Energy	Density	Selected component name	Theoretical freq. (Hz)	RFD_i	BSI_i
Instantaneous amplitude estimated from the positive sequence component of the voltages										
Harmonic	1	—	—	3	0.005917	0.6	Planet frequency over ring	1	0.013	—
Harmonic	2.333	—	—	3	0.041193	1	Planet stage 1 – sun shaft	2.333	0.008	—
Sideband	—	6.999	1	2 | 2	0.0077 | 0.0105	1 | 1	Planet frequency over ring	1	0.032	—
Harmonic	2.577	—	—	3	0.001179	0.75	SKF 22210E.BPFO	2.543	1.308	0.875
Harmonic	3	—	—	4	0.00986	1	SKF 21312E.BPFO	3.017	0.566	1
Sideband	—	6	0.333	3 | 4	0.0058 | 0.0111	0.75 | 0.57	Low speed shaft	0.333	0.024	—
Harmonic	3.447	—	—	3	0.010284	1	SKF 22210E.BPFI	3.457	0.29	1
Harmonic	4	—	—	3	0.009411	0.75	SKF 6307.FTF	3.958	1.075	0.875
Harmonic	4	—	—	3	0.009411	0.75	SKF 21312E.BPFI	4	0.005	0.875
Harmonic	33.584	—	—	4	0	0.8	High speed shaft	33.583	0.002	—
Harmonic	33.584	—	—	4	0	0.8	Needle 35.BPFO	34.007	1.244	0.9
Harmonic	91.552	—	—	2	0	0.667	NTN 61910.BPFI	91.76	0.226	0.833
Instantaneous frequency estimated from the positive sequence component of the voltages										
Harmonic	1	—	—	5	0.000036	0.714	Planet frequency over ring	1	0.013	—
Sideband	—	6	0.333	3 | 4	<0.0001 | <0.0001	1 | 0.5714	Low speed shaft	0.333	0.024	—
Harmonic	2.333	—	—	3	0.000127	1	Planet stage 1 – sun shaft	2.333	0.008	—
Sideband	—	7	1	2 | 2	<0.0001 | <0.0001	1 | 1	Planet frequency over ring	1	0.005	—
Harmonic	2.576	—	—	2	0.000002	0.667	SKF 22210E.BPFO	2.543	1.286	0.833
Harmonic	3	—	—	4	0.000017	1	SKF 21312E.BPFO	3.017	0.566	1
Sideband	—	6	0.333	3 | 4	<0.0001 | <0.0001	1 | 0.5714	Low speed shaft	0.333	0.024	—
Harmonic	3.446	—	—	3	0.000019	1	SKF 22210E.BPFI	3.457	0.301	1
Harmonic	4	—	—	3	0.00001	0.75	SKF 6307.FTF	3.958	1.07	0.875
Harmonic	4	—	—	3	0.00001	0.75	SKF 21312E.BPFI	4	0.001	0.875
Harmonic	7.363	—	—	2	0	1	Needle 5.BPFO	7.38	0.235	1
Harmonic	7.363	—	—	2	0	1	NTN 46790.BPFI	7.38	0.235	1

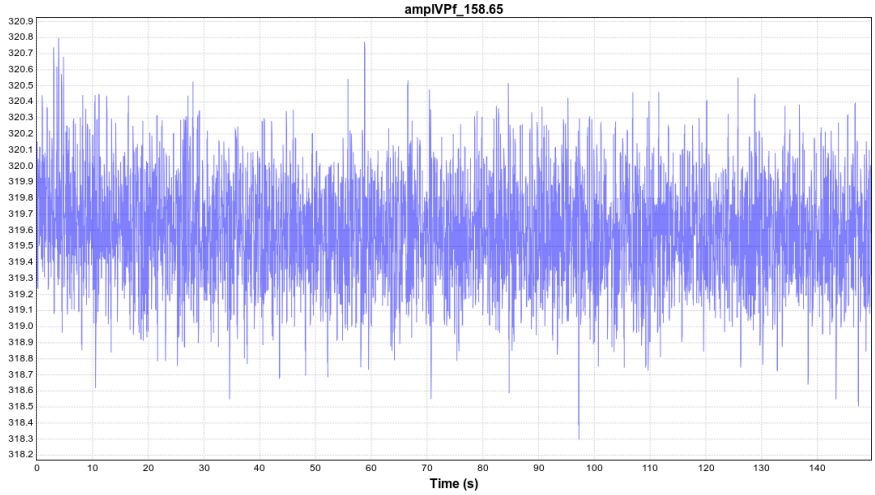

(a) Instantaneous amplitude

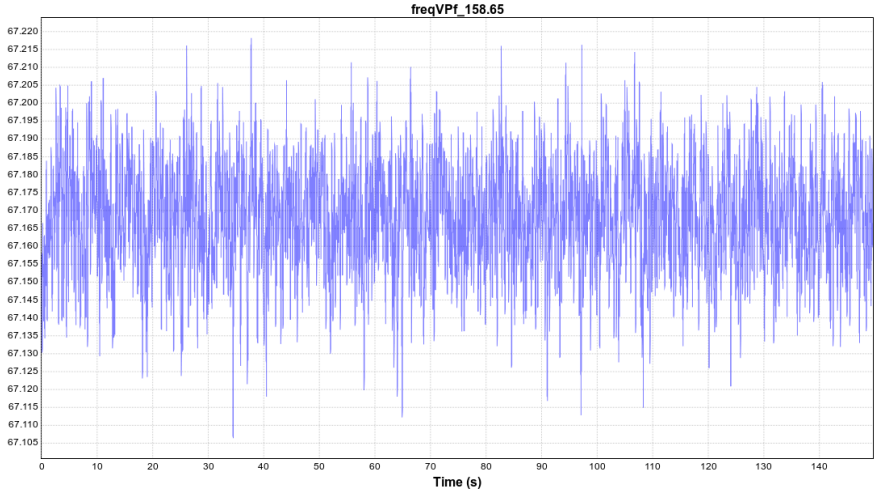

(b) Instantaneous frequency

Figure 6.21: Time domain view of (a) the instantaneous amplitude and (b) the instantaneous frequency estimated from the positive sequence component of the voltages measured in 158^{th} hour of the test. Results of SMESA method and inputs for AStrion algorithms.

instantaneous amplitude and frequency estimated by SMESA, the harmonic series corresponding to faulty rolling-element bearing are associated accordingly.

This example proves two advantages of the approach. The first one is the fact that due to the electrical analysis it is possible to detect the main bearing fault. It is important to add that the location of this mechanical defect is on the other side of the CETIM test rig compared to the generator, where the voltages are measured. This distance and the intermediate mechanical components, including the gearbox, are not a barrier for the fault detection with the usage of the electrical analysis. The second advantage is that AStrion managed to automatically

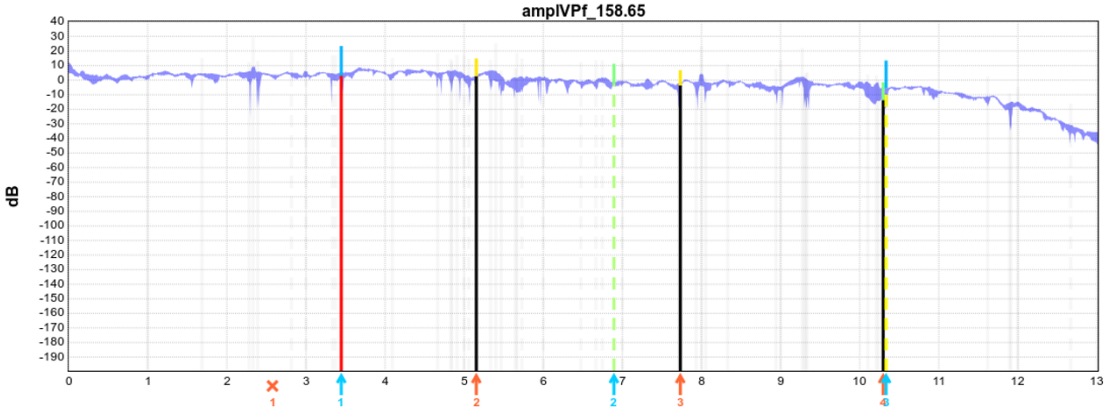

Type	Frequency/Order (Hz/Orders)	Central Frequency/Order (Hz/Orders)	Delta F (Hz/Orders)	Number	Energy	Density	Richness	THD	Kinematic component name	Model Frequency/Order (Hz/Orders)	Relative Frequency/Order difference (%)	Display
Harmonics	1.667			5	0.004867	0.454545	0.037671	-				
Harmonics	1.686			4	0.005006	1.000000	0.013841	1.552589				
Harmonics	2.333			4	0.041193	1.000000	0.019139	0.329895	Multiplicator.Shaft.1x	2.333	-0.008	
Harmonics	2.577			3	0.001179	0.750000	0.021164	-	SKF 22210E.BPFO	2.543	1.308	☑
Harmonics	2.667			3	0.010339	0.500000	0.032787	-				
Harmonics	3.000			4	0.009860	1.000000	0.024691	1.584150	SKF 21312E.BPFO	3.017	-0.566	
Harmonics	3.447			3	0.010284	1.000000	0.021277	0.385658	SKF 22210E.BPFI	3.457	-0.290	☑

(a) Instantaneous amplitude

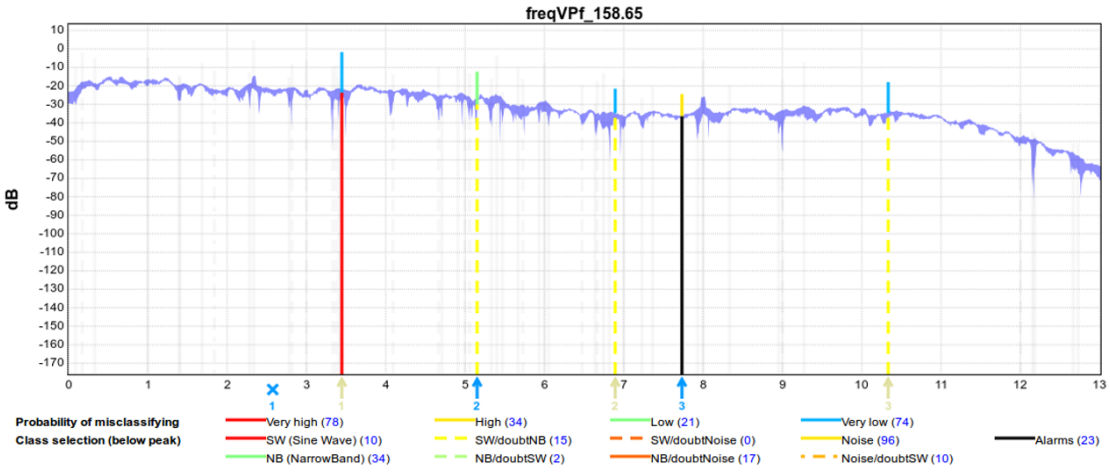

Type	Frequency/Order (Hz/Orders)	Central Frequency/Order (Hz/Orders)	Delta F (Hz/Orders)	Number	Energy	Density	Richness	THD	Kinematic component name	Model Frequency/Order (Hz/Orders)	Relative Frequency/Order difference (%)	Display
Harmonics	0.089			2	0.000031	1.000000	0.000366	3.190778				
Harmonics	0.704			5	0.000008	0.277778	0.025974	-				
Harmonics	1.000			5	0.000036	0.714286	0.014344	1.096224	PlanetaryGear.fOverR	1.000	-0.013	
Harmonics	1.395			2	0.000002	1.000000	0.005714	0.891479				
Harmonics	1.667			5	0.000009	0.454545	0.037671	-				
Harmonics	1.686			4	0.000013	1.000000	0.013841	1.099399				
Harmonics	2.333			3	0.000127	1.000000	0.014354	0.211459	Multiplicator.Shaft.1x	2.333	-0.008	
Harmonics	2.454			3	0.000004	0.500000	0.030303	-				
Harmonics	2.576			2	0.000002	0.666667	0.015873	-	SKF 22210E.BPFO	2.543	1.286	☑
Harmonics	2.667			3	0.000011	0.500000	0.032787	-				
Harmonics	3.000			4	0.000017	1.000000	0.024691	1.064110	SKF 21312E.BPFO	3.017	-0.566	
Harmonics	3.409			2	0.000001	1.000000	0.013986	0.234644				
Harmonics	3.446			3	0.000019	1.000000	0.021277	0.235169	SKF 22210E.BPFI	3.457	-0.301	☑

(b) Instantaneous frequency

Figure 6.22: Selected harmonic series corresponding to the main bearing fault frequencies in AStrion results representation for (a) the instantaneous amplitude and (b) the instantaneous frequency estimated from the positive sequence component of the voltages measured in 158^{th} hour of the test, which were computed by SMESA.

associate the BPFO and BPFI fault frequencies of the main bearing as early as in 158^{th} hour of the test with the usage of voltage signals.

6.8 Case Study 6 – AStrion-KM on Arfons Data

This section presents a detailed performance of AStrion-K and AStrion-M, which are described in chapters 4 and 5 respectively, on the real-world signal of a WT. A single signal is selected and this section does not show any evolution of the proposed health indicators.

The below described signal is measured on the WT number 6, as described in section 6.2. The selected signal is recorded with the accelerometer number 4, which is placed on the gearbox housing and more precisely close to its second parallel stage. The acquisition of the signal started 7 seconds after 11 a.m. on 31^{st} January 2015. The details on the inspected signal are given in Table 6.9, where some parameters are shown for the time domain and the angle domain signal, since angular resampling is performed with the usage of AStrion-A, as mentioned in section 2.1.

Table 6.9: Parameters of investigated signal before and after angular resampling together with the average rotational speed of HSS of WT6.

Sampling frequency	$25,000\ Hz$
Signal duration	$20\ s$
Number of samples	$500,000$
Average rotation speed	$1796.15\ RPM$
Sampling order	$835\ Orders$
Number of samples after angular resampling	$500,000$
Signal duration after angular resampling	$599.14\ rev.$

6.8.1 AStrion-K – Association of Kinematics

As in the previously presented cases using AStrion the processing begins with AStrion-A, for an angular resampling, continues with AStrion-D, for the data validation, is followed by AStrion-I, for a spectral component identification, and finishes with AStrion-H, for a spectral pattern recognition. More details about this part are presented in chapter 2. As a result 1895 spectral components are identified and AStrion-H detects 90 harmonic series and 260 sideband series. These harmonic and sideband series are used to be associated with the characteristic frequencies listed in Tables 6.4 and 6.5.

Some examples of the AStrion-K results are presented in Table 6.10. As in the previously described cases, each of the examples is separated with a double horizontal line and the series to be selected for the final association is in a highlighted row. A double vertical line divides the data available from the previous AStrion steps, on the left-hand side, and AStrion-K information on the right-hand side. The 'Theoretical order (orders)' column contains the

Table 6.10: Detailed results of AStrion-K on example of the Arfons WT6 signal recorded by accelerometer 4 on 31^{st} January 2015. Selected candidates for association, according to Equations (4.1) and (4.3), are grouped between double lines and the final series to be associated are highlighted.

Type	Order (orders)	Carrier order (orders)	Modulation order (orders)	Number of peaks	Energy	Density	Selected component name	Theoretical order (orders)	RFD_i	BSI_i
Harmonic	0.999	—	—	13	2.3^{-4}	0.812	High speed shaft	1	0.071	—
Harmonic	1.006	—	—	3	0	0.429	High speed shaft	1	0.6	—
Harmonic	2.107	—	—	3	6^{-6}	0.6	NSK HR30334.BPFI	2.073	1.621	0.8
Harmonic	2.654	—	—	3	2^{-6}	0.5	NSK HR30326.BSF2	2.64	0.53	0.286
Harmonic	2.692	—	—	3	2.8^{-5}	0.27	NSK HR30326.BSF2	2.64	1.961	0.636
Sideband	—	5.384	0.234	7 | 7	0.0004 | <0.0001	0.778 | 0.636	Intermediate shaft	0.234	0.063	—
Harmonic	25.982	—	—	5	0.18	1	GearBox17.GMF	26	0.068	—
Sideband	—	25.982	0.234	4 | 4	<0.0001 | <0.0001	0.8 | 0.4	Intermediate shaft	0.234	0.059	—
Sideband	—	25.982	0.999	3 | 5	<0.0001 | <0.0001	1 | 0.833	High speed shaft	1	0.071	—
Sideband	—	25.982	2.575	5 | 3	<0.0001 | <0.0001	0.714 | 0.75	SKF NU238.BPFI	2.541	1.314	0.866
Sideband	—	25.982	8.994	2 | 2	<0.0001 | <0.0001	1 | 1	NSK HR30326.BPFI	8.85	1.626	1
Sideband	—	51.965	0.234	8 | 4	0.0002 | 0.0001	0.727 | 0.5	Intermediate shaft	0.234	0.069	—
Sideband	—	51.965	0.702	3 | 8	0.0001 | 0.0001	1 | 0.471	SKF NJ2988.BSF2	0.701	0.173	0.867
Sideband	—	51.965	0.999	20 | 5	0.0039 | 0.0033	0.833 | 1	High speed shaft	1	0.075	—
Sideband	—	51.965	5.15	3 | 2	<0.0001 | <0.0001	0.6 | 1	SKF NU 2328.BSF2	5.100	0.973	0.9
Sideband	—	51.965	8.427	2 | 2	<0.0001 | <0.0001	0.667 | 0.667	SKF NU 2328.BPFI	8.320	1.282	0.834
Sideband	—	77.947	0.702	2 | 4	<0.0001 | <0.0001	1 | 0.667	SKF NJ2988.BSF2	0.701	0.158	0.917
Sideband	—	77.947	0.999	9 | 3	0.0013 | <0.0001	0.818 | 0.6	High speed shaft	1	0.068	—

values of the characteristic fault frequencies after taking into account the value of the rotational speed. In this case it has the same values as presented in Tables 6.4 and 6.5 as the investigated signal is resampled in order domain.

The interpretation of data presented in Table 6.10 is very similar to the ones presented in sections 4.3 and 6.5. In the investigated signal, the density of series close to characteristic orders is low. This is why only two presented examples have more than one series selected in the first step of AStrion-K as the candidates for further association.

The results presented in Table 6.10 show two groups of sideband series. The first one is associated to the intermediate shaft. Moreover, this modulation is detected around the 2^{nd} harmonic order of the harmonic series that is associated to the double value of the BSF of the bearing type NSK HR30326 characteristic order. The second group of sideband series is more interesting as it shows all the modulation series associated by AStrion-K and at the same time having the carrier order corresponding to the GMF of the second stage of parallel gearbox. Among the results there are sidebands series corresponding to the high speed shaft around the fundamental, 2^{nd}, and 3^{rd} harmonic order of GMF as well as the associations to the intermediate shaft around the fundamental and 2^{nd} harmonic order of the same GMF. The observation of changes of these modulations is crucial for gearbox fault diagnosis.

6.8.2 AStrion-M – Sideband Demodulation

This section presents the results of the demodulation method proposed in chapter 5 on a single sideband series listed in Table 6.10. For this purpose a series associated with the intermediate shaft is selected. This series has the modulation order equal to $f_\Phi = 0.234$ *orders* and having the carrier order corresponding to the 2^{nd} harmonic of the presented GMF which is equal to $f_0 = 51.965$ *orders*. The below presented results are obtained by demodulation of this sideband series only, but the AStrion-M is automatically executed on all the detected modulation series.

Similarly to the previous section, this one also takes advantage of a number of AStrion's modules and AStrion-M is performed after AStrion-ADIHK, for details see chapter 2. AStrion-K execution is not mandatory for the usage of further post-processing, but in this case it helps to select a potentially interesting series to be analyzed.

Figure 6.23 shows the AStrion spectrum representation for a view of all the peaks in the harmonic series at the top and zoom of sideband series under study only at the bottom. The investigated series has the highest sideband on the left-hand side $K_{inf} = -11$ and the highest sideband on the right-hand side $K_{sup} = 8$ identified by AStrion-H, described in section 2.2.2. Based on this information the proposed algorithm computed a target bandwidth containing components to be demodulated as $\mathbf{B} = [49.39\ ordres, 53.837\ ordres]$. Thus, the frequency bandwidth $\mathbf{B}$ is chosen as the filter bandwidth for the multi-rate filter. The multi-rate filter, as presented in section 5.2.2, accomplished the filtering, in 2 iterations constituted of automatic selection of frequency shift and signal decimation, as presented in Table 6.11. Finally, the filtered and down-sampled signal is sampled with the order equal to 23.181 *orders*. Figure 6.24

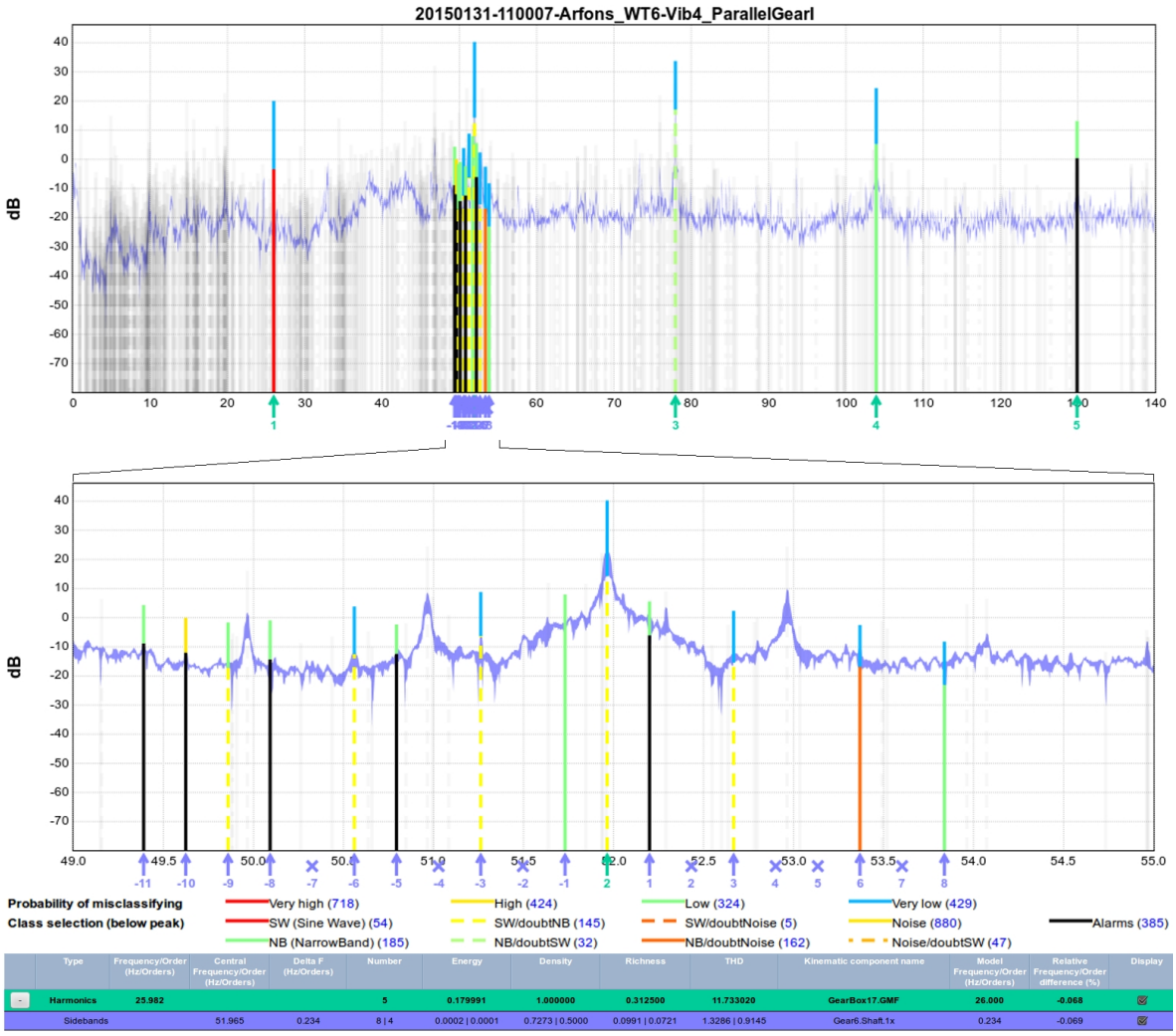

Figure 6.23: The sideband series selected to present details of the demodulation. The AStrion spectrum representation at the top shows the full harmonic series and at the bottom the zoom of signal part to be demodulated.

presents the result of the multi-rate filtering and gives a comparison with the signal before this operation.

The filtered signal is subject to further processing. Firstly, a synchronous averaging is done as specified in section 1.5.2. Secondly, a demodulation is performed as described in section 5.2.4. Finally, the features proposed in Table 5.2 are computed on the demodulated amplitude and frequency functions as defined in section 5.2.5. These results are listed in Table 6.12.

This section shows that AStrion-M is able to cope with a real-world signal measured on the WT6. The algorithms automatically computes the signal which is an advantage for CMS application. As a result, AStrion-M provides features to describe the health of the machine

Table 6.11: Iterative filtering of the signal to be demodulated.

Iteration	First	Second
Initial sampling order (*orders*)	834.527	139.088
Cut-off order of low-pass filter (*orders*)	—	4.447
Cut-off order of high-pass filter (*orders*)	−49.39	—
Freqeuncy shift (*orders*)	−49.39	—
Down-sampling rate	6	6
Final sampling order (*orders*)	139.088	23.181

Table 6.12: Features calculated from the demodulated amplitude $\hat{A}[\tau]$ and frequency $\hat{F}[\tau]$ of the investigated wind turbine signal. $\bar{A}$ – the average value, PP – peak-to-peak, $Kurt$ – kurtosis, MI modulation index of the demodulated amplitude modulation function and corresponding results of the second AStrion computation on this signal: PN – the number of peaks, and E – the energy of the harmonic series.

$\bar{A}$	PP_A	$Kurt_A$	MI_A	PN_A	E_A
0.382	0.04	2.902	0.052	3	1.8^{-5}
$\bar{F}$	PP_F	$Kurt_F$	MI_F	PN_F	E_F
51.965	0.176	2.547	0.002	3	4.6^{-4}

and enables the comparison with signals measured subsequently. An example of the evolution of AStrion-M features is presented in the next section.

6.9 Case Study 7 – AStrion-M on CETIM High Degradation Test

This section presents the results of the demodulation method proposed in chapter 5 on signals acquired on the CETIM test rig, which is described in section 6.1. Vibration signals acquired during the deterioration test of the CETIM test rig main bearing are investigated. All vibration signals are measured by one vibration sensor which is located radially on the main bearing and oriented in the horizontal direction. This sensor is marked as '*Accel2*' and the signals are acquired by the National Instrument data acquisition system. The presented results are obtained by the demodulation of the sideband series, associated to the LSS, and detected around the peaks associated with the main bearing BPFI. This characteristic fault frequency of the rolling-element bearing corresponds to SKF 22210E in Table 6.2.

This section takes advantage of a number of AStrion's modules including data validation, peak identification, harmonics and sideband detection, and kinematic association before performing the demodulation by AStrion-M module as well as the tracking module to display results computed on a sequence of measurements. All modules are referred to as AStrion-DIHKMT. For more details on these algorithms please see chapter 2.

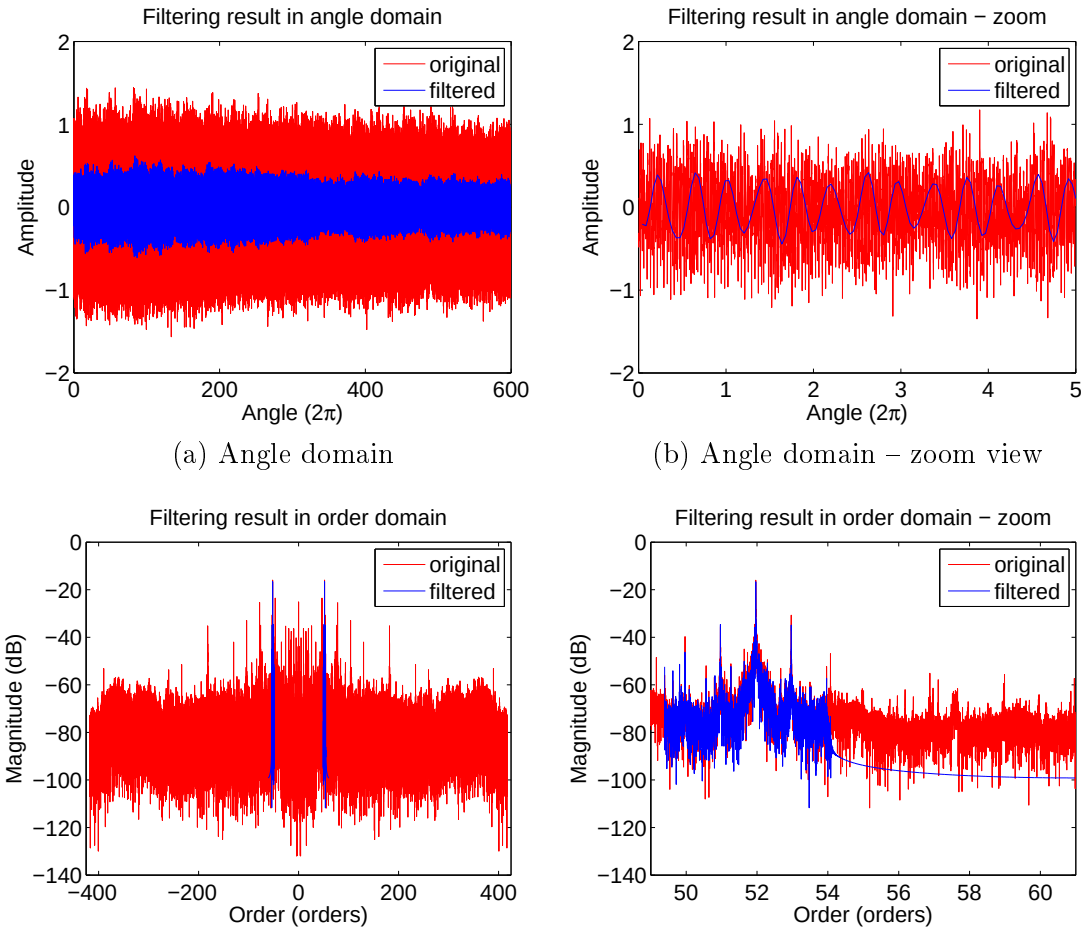

(a) Angle domain

(b) Angle domain – zoom view

(c) Order domain

(d) Order domain – zoom view

Figure 6.24: Filtering results (blue) compared with input signal (red). (a) angle domain signal and its zoom (b), (c) order domain signal with a zoom of selected frequency range (d).

6.9.1 Single Set of Features for the Sideband Demodulation

Among sixteen available vibration signals only one is selected for the purpose of an illustration. It is the 184^{th} hour of the test duration, where the damage was well developed. The proposed demodulation method automatically performs on all modulation series detected by AStrion-H. One modulation sideband series is chosen to be presented hereafter in details.

After executing AStrion-DIHK on the selected signal, the chosen sideband series has a carrier frequency $f_0 = 3.435\ Hz$ and a modulation frequency $f_\Phi = 0.334\ Hz$, which is associated to the LSS by AStrion-K. Other input data needed by the AStrion-M algorithm are the highest sideband on the left-hand side $K_{inf} = -4$ and the highest sideband on the right-hand side $K_{sup} = 6$ identified by AStrion-H, described in section 2.2.2. The investigated sideband series is shown in Figure 6.25 with the spectrum representation of AStrion.

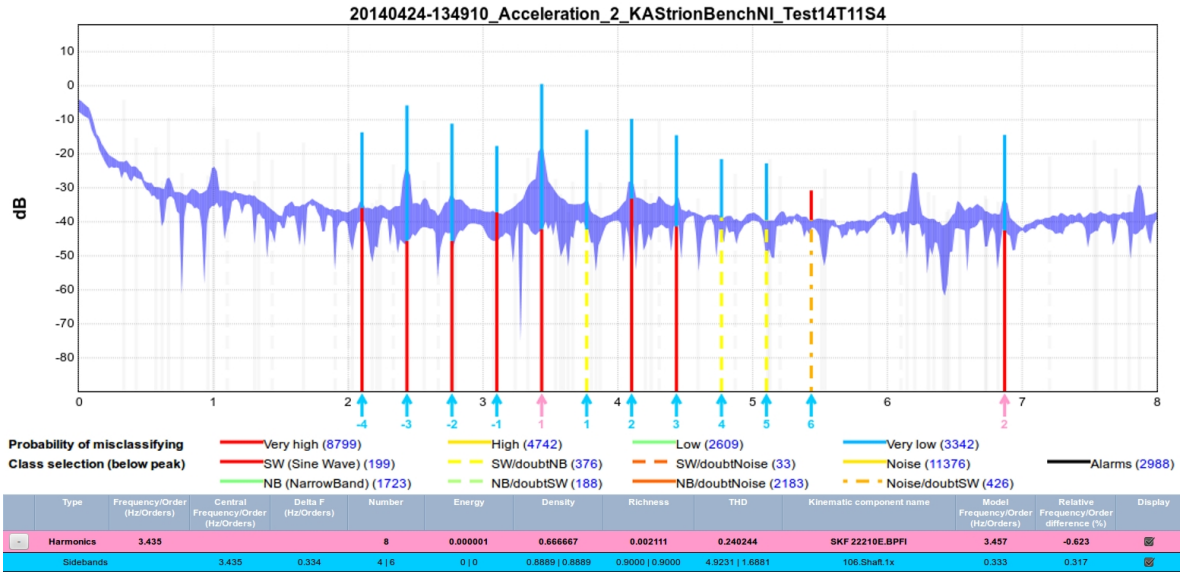

Figure 6.25: The sideband series selected to present details of the demodulation.

Table 6.13: Features calculated from the demodulated amplitude $\hat{A}[\tau]$ and frequency $\hat{F}[\tau]$ of the investigated CETIM test rig signal.

$\bar{A}$	PP_A	$Kurt_A$	MI_A
0.0013	0.0018	1.9134	0.7138
$\bar{F}$	PP_F	$Kurt_F$	MI_F
3.435	2.725	6.773	0.397

Based on the above-mentioned information AStrion-M computed a target bandwidth, see Equation (5.8), containing components to be demodulated as $\mathbf{B} = [2.099\ Hz, 5.439\ Hz]$ which is the filter bandwidth for the multi-rate filter. This bandwidth is unsymmetrical around the carrier frequency and is very narrow (the normalized bandwidth $\overline{\Delta B} = 0.017$), which implies a difficult filtering step. The multi-rate filter, as presented in section 5.2.2, accomplished the filtering in four iterations constituted of the automatic selection of the frequency shift and the signal decimation. Finally, a down-sampled signal is sampled with a frequency equal to 13.58 Hz. Figure 6.26 presents the result of the multi-rate filtering.

After a synchronous averaging done as specified in section 1.5.2 and then a demodulation as in section 5.2.4, the values of the features calculated from the demodulated amplitude and frequency as defined in section 5.2.5 are listed in Table 6.13.

The computed features give an insightful information about the demodulated part of the signal. The user can observe a change of these values over time to detect the changing condition of the mechanical components that correspond to the investigated modulation. These health indicators can be easily used in an automatic CMS. An example of such a usage of AStrion-M results is presented in the next section for the main bearing fault detection on the CETIM test rig.

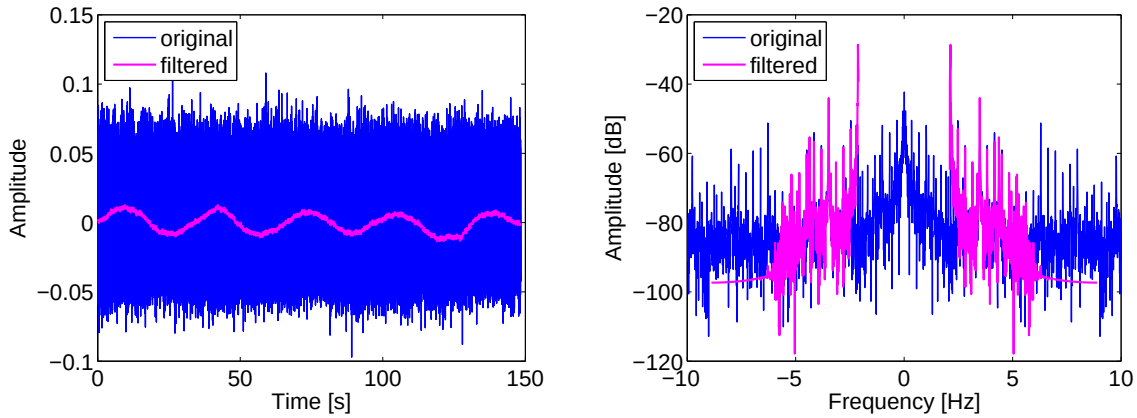

(a) Filtered signal (b) Spectrum of the signal

Figure 6.26: The *'20140424-134910 Acceleration 2 KAStrionBenchNI Test14T11S4'* signal filtered by the proposed multi-rate filter over the $\mathbf{B} = [2.099\ Hz, 5.439\ Hz]$ and compared against original signal. (a) time domain signal and (b) spectrum of the original and filtered signal – zoom of interesting range.

6.9.2 Features Tracking over Multiple Signals

The above-presented feature calculation was applied over 16 vibration measurements that covered the time span of the main bearing degradation test, from the new main bearing condition up to its spread fault in the 190^{th} hour.

For the program test, the deterioration of the main bearing has been evaluated by a narrow-band RMS value computed at the characteristic fault frequencies of the main bearing. Based on this indicator, the decision about the fault appearance has been made and the test was stopped. The energy of the harmonic series is an indicator computed by AStrion-DIHK and it can serve as a simple factor evaluated by AStrion methodology to observe the fault presence. It is shown in Figure 6.27. Although the data from the accelerometer are available since the 44^{th} hour the first value in Figure 6.27 is present in the 129^{th} hour and is consecutively present until the end of the test. Thus, there are 12 vibration signals for which harmonic series have been detected and associated with the main bearing BPFI. It informs about a change in the system. The AStrion data-driven methodology creates features only when the corresponding spectral components are detected.

As a consequence of the above-mentioned AStrion nature the modulation, we are interested in, can occur for the 12 last signals only. Figure 6.28 shows the selected features of AStrion-M and as one can notice there are 11 values per curve starting in the 134^{th} hour. It is due to the fact that the data at the 129^{th} hour have not enough energy in the sidebands corresponding to the LSS modulation to be detected by AStrion-DIHK. From the 129^{th} hour it is possible to detect harmonic series associated with the main bearing BPFI whereas from the 134^{th} hour

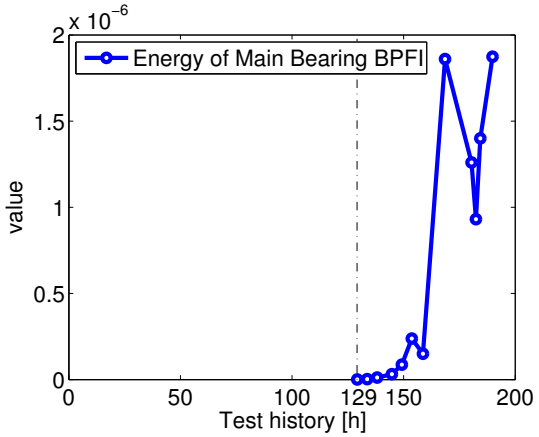

Figure 6.27: Evolution of energy of harmonic series associated with main bearing BPFI throughout the lifetime of the main bearing degradation test.

the detection of modulation associated with the LSS is possible. Thus the AStrion-M results are computed over 11 signals for test time from 134^{th} to 190^{th} hour.

Figure 6.28 presents the selected demodulation results computed on the sideband series associated with the LSS and detected around the fundamental fault frequency of BPFI as well as its second and third harmonics. Figure 6.28 (a) shows the average value of $\bar{A}$ and Figure 6.28 (b) presents the modulation index MI_A of the estimated amplitude modulation function, both defined in Table 5.2. The simultaneous interpretation of these results allows up to evaluate the severity of the investigated fault.

The average value $\bar{A}$ presented in Figure 6.28 (a) shows an abrupt increase after the 134^{th} hour above all for the fundamental frequency of the main bearing BPFI. This rapid jump corresponds to the increase of the fault size on the inner ring of the rolling-element bearing. The impact caused by the rolling elements passing the local fault on the inner race of the main bearing generates more energy from sample to sample. Most of this energy is present in the fundamental frequency and its harmonics have less and less energy, which can be also observed in Figure 6.28 (a). After the 149^{th} hour the value of the indicator fluctuates and changes more abruptly in the 182^{nd} hour.

The modulation index MI_A shown in Figure 6.28 (b) displays a steady trend of the values from the beginning of the sidebands detection. The values of MI_A are on similar level for the fundamental frequency, the 2^{nd}, and the 3^{rd} harmonic of the main bearing BPFI. In the 182^{nd} hour the indicators start to drop. The authors interpret this fact as a change of the fault nature of the bearing under investigation. The weakening of these modulations corresponds to a more and more distributed fault, since the impacts caused by the rolling elements in motion are no longer as periodic as in the case of a local fault. The fault spreads over the inner race of the main bearing.

Thanks to the interpretation of the $\bar{A}$ and MI_A indicators at the same time it is possible to trace the nature of the fault. It is confirmed by the visual inspection of the main bearing

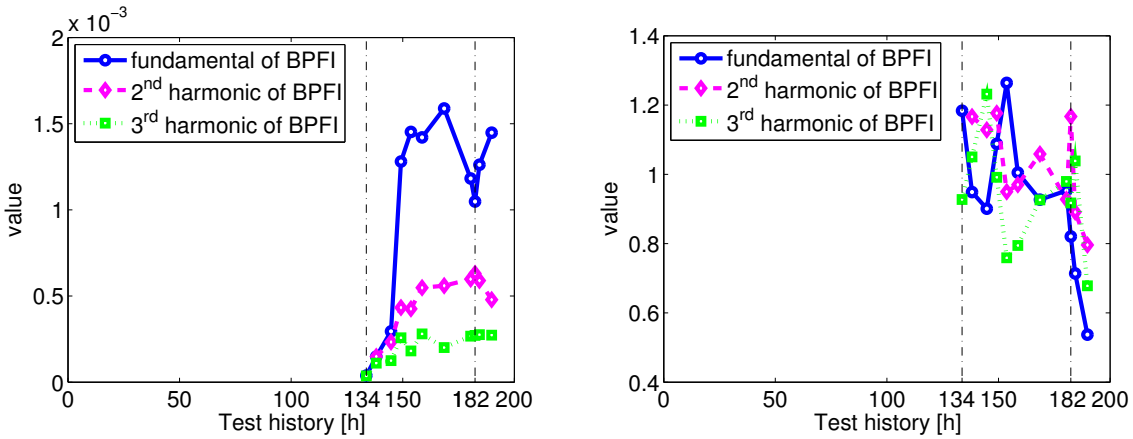

(a) $\bar{A}$ (b) MI_A

Figure 6.28: Evolution of (a) mean value of amplitude demodulation function $\bar{A}$, and (b) modulation index MI_A over detected modulation around fundamental frequency, 2^{nd} harmonic, and 3^{rd} harmonic of BPFI of the main bearing through the lifetime of the main bearing tested over CETIM test rig.

Figure 6.29: Flaking over the entire inner race of the faulty bearing.

after the end of the test proving that the entire inner race of the investigated bearing was covered with the flaking after disassembling it from the test rig. Figure 6.29 presents a photo of the bearing after the end of the deterioration test.

6.9.3 Comparison to Established CMS Techniques

Figure 6.30 presents the results of well known techniques used in CMSs applied on the same vibration signals. This is a part of fault indicators described in section 1.7. The wide-band indicators as RMS and kurtosis values, shown respectively in Figures 6.30 (a) and (b), are not sufficient for a clear detection of the fault. Among the simplest fault indicators only the crest factor, presented in Figure 6.30 (c) enables to detect the fault in the 169^{th} hour, which is much later than the proposed method. Furthermore, this indicator is incapable of identifying the faulty bearing.

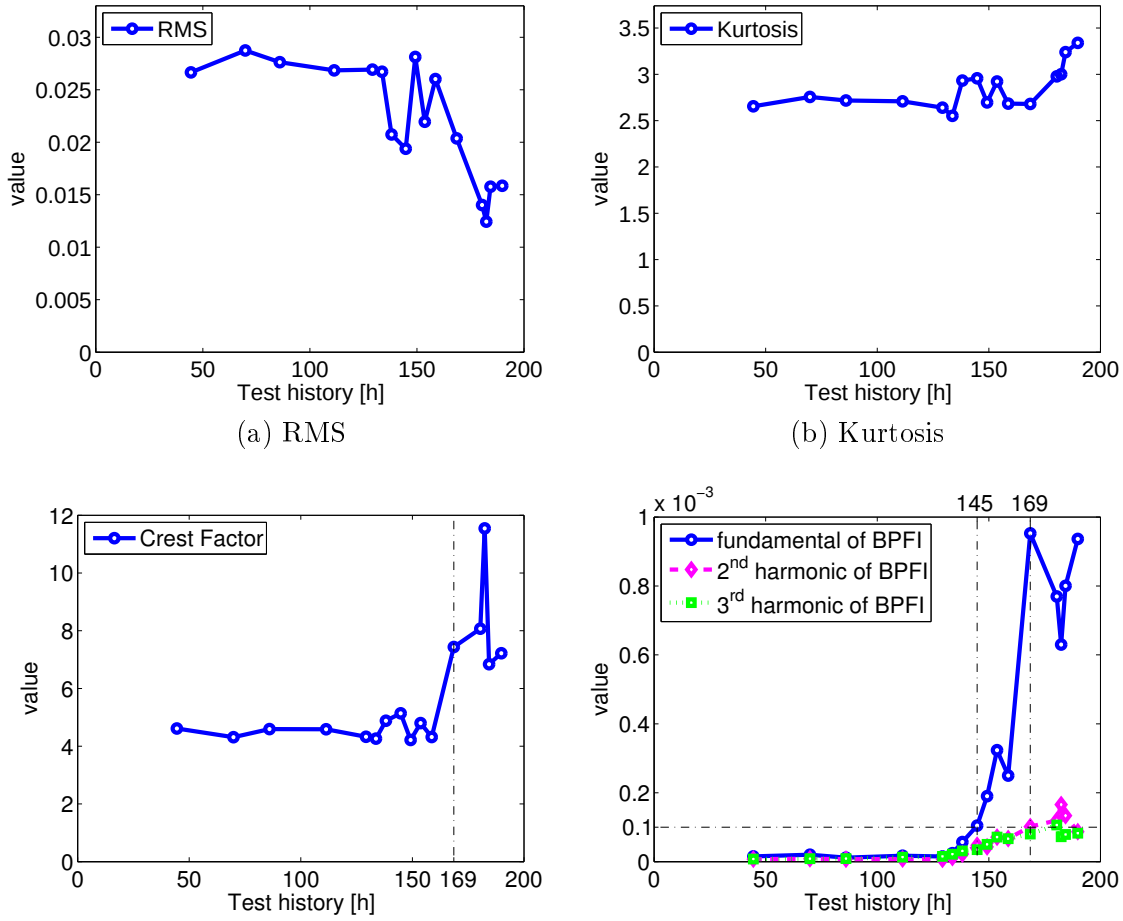

(a) RMS (b) Kurtosis

(c) Crest Factor (d) Narrow-Band RMS

Figure 6.30: Evolution of (a) RMS, (b) kurtosis, and (c) crest factor values computed on the full length signal, as well as (d) narrow-band RMS with 3% bandwidth of fundamental frequency, 2^{nd} harmonic, and 3^{rd} harmonic of BPFI of the main bearing through the main bearing lifetime.

The narrow-band RMS is the only indicator whose performance is comparable with AStrion methodology in the investigated case. Figure 6.30 (d) presents the narrow-band RMS values computed around the fundamental frequency, the 2^{nd} harmonic, and the 3^{rd} harmonic of the main bearing BPFI. The bandwidth of this feature equals 3% of the value of the investigated frequency, which is based on the generally adopted engineering practice for CMS configuration. The threshold for fault detection is selected to be equal to 0.0001. The disadvantage of this method is that the threshold depends on the user's experience and other human factors. With this selection the detection based on a narrow-band RMS of the fundamental frequency of the main bearing BPFI is in the 145^{th} hour, which is depicted with the vertical dash-dot line. It is a late detection in comparison with the proposed method, where the 134^{th} hour is achieved. The narrow-band RMS of the 2^{nd} harmonic is able to detect the fault in the 169^{th} hour. The

narrow-band RMS of the 3^{rd} harmonic is also crossing the threshold, but only for one sample in the 180^{th} hour and then drops below the threshold. This behaviour could be seen as a false alarm. Additionally, the narrow-band RMS gives no clue about the nature of the fault.

Furthermore, a try to investigate the fault with more sophisticated fault detection methods is performed. It is worth mentioning that in the investigated case a lot of well established methods of rolling-element bearing diagnosis fail because of the low rotational speed of the main bearing. There is no effect of exciting the resonance frequencies by a faulty bearing, so methods based on the envelope analysis or the cyclostationary analysis of second order are incapable of detecting the investigated fault. The examples of those methods are presented in [RA11]; [DC10].

Conclusions and Perspectives

Among different maintenance approaches CMSs gathered a considerable interest of wind turbines operators. There is a vast amount of methods which are dedicated to these machines and a lot of developments has been introduced to CMS in the recent years. This thesis proposes signal processing methods to increase the abilities of a data-driven CMS. Besides the proposed methods constitute a part of AStrion which is an automatic and adaptive signal processing approach under development in GIPSA-Lab. AStrion's objective is to interpret and evaluate a signal based on its content only and not to use the expert knowledge for each acquired data in a CMS. Moreover, AStrion constitutes a part of the KAStrion CMS.

In order to fill the identified gaps in the state of the art of CMS for rotating machinery this thesis proposes three algorithms:

- Cropping out a time-frequency representation;
- Kinematic frequency association;
- All-sideband demodulation.

Thanks to Innovation Project KAStrion the proposed methods are inspected on real-world signals. The signals originate in CETIM test rig, which is built as a smaller scale WT's drive train, and WTs located in Arfons. All the signals were made available by partners that belong to the project consortium.

The cropping out a time-frequency representation, referred to as AStrion-C, serves to select the stationary part of the vibration signal under investigation. As required by AStrion methodology, it is an automatic method. What is more the identified stationary part of the signal is cropped without filter application, but with truncation and internal manipulation of investigated signal by AStrion only.

AStrion-K is the name of the proposed technique for automatic association of characteristic frequencies of rotating machinery under investigation with previously detected spectral patterns as harmonic and sideband series. Among the biggest advantages of this method there is the proposed way of taking into account the possible slippage in the rolling-element bearings resulting in a random variation of characteristic fault frequencies.

This module opens additional possibilities for mechanical components diagnosis. Based on the results of AStrion-K, component specific fault indicators can be developed. For example there is an increase of sidebands amplitude of a gearbox with a fault occurrence correlated with diagnostic features, as noted in [Gel+05], thus, it can be incorporated in AStrion to verify wider scope of information on a mechanical component.

The last proposed technique is sideband demodulation algorithm which is called AStrion-M. This automatic signal processing method performs a full-band demodulation with auto-

matic adjustment of multiple steps based on the information obtained from the investigated signal itself. In this way all previously detected sidebands series are demodulated which brings additional feature indicators to precisely describe a condition of investigated system.

All the proposed methods are tested and validated within this thesis. Weak and strong aspects of these methods are pointed out.

The proposed method for cropping out a time-frequency representation can be successfully used for diagnosis and condition monitoring purposes. It is foreseen to incorporate the presented method within the complex AStrion strategy.

As it is shown throughout the thesis AStrion-K deals well with real-world signals. Stationary signals from CETIM test rig and non-stationary signals from Arfons wind turbine are investigated. In both cases the proposed method presents the robustness in association of previously detected spectral components pattern. Even in the cases where a vast number of approximate series is very close the theoretical characteristic frequency AStrion-K is able to select one series.

All-sideband demodulation method is validated on simulated as well as real-world signals. The results show the applicability of the AStrion-M algorithm on very difficult situations where the filter band is asymmetric and extremely narrow. It allows for a deeper insight into the modulations detected in signals. The proposed features are shown to be relative to the evolution of the fault. The proposed method is able to detect a rolling-element bearing BPFI fault in an automatic way and by a data-driven approach. The detection is very early and the proposed features characterise the nature of the investigated fault.

Moreover, AStrion does all the computation fully automatically and there is no need for any adjustment of parameters by the user. All the parameters are estimated during the processing of the investigated signal. This approach gives a well designed and robust tool, which can be used also by a non-expert in the signal processing techniques.

This thesis does not exhaust a possible application of proposed algorithms. In the author's opinion it would be interesting to apply AStrion-C for the diagnosis of signals with presence of the short-time strikes like in the case of e.g. a power press. That could allow to identify the signal parts in stationary conditions and filter the temporary excitations for further diagnosis. Moreover, an interesting scenario would be to test AStrion-M on gearbox fault data. With a support of AStrion-K, this algorithm could be a powerful tool for gearbox health diagnostic.

Since the whole algorithm is applied in a fully automatic way, it makes the proposed approach a good solution for a CMS application. It features in data-driven approach which makes AStrion valuable and smart strategy for an automatic diagnosis and monitoring of a rotating machinery especially as specific as wind turbines which are driven by constantly changing wind. Within Innovation Project KAStrion the proposed algorithms are tested in a commercial wind turbine CMS. These tests and validation are performed on on-shore wind turbines, but it is equally applicable on off-shore wind turbines.

In order to make AStrion strategy fully profitable future steps to be developed are identified. Firstly, the advancement on automatic interpretation of results is essential. This step is under development and still needs improvements in pattern recognition for fault identification over multiple signals. Secondly, an automatic summary reports generation is obligatory to meet final user requirements. AStrion is consistently able to generate enormous number of information on each investigated signal which allows for deep inspection, but for commercial application the information of higher level are expected to be sufficient for daily usage. Another way to deal with a user seeking specific type of information in the first place could be a development of specific information per each mechanical component, or set of components, to give an indicator which would be a fusion of all available AStrion data on this specific component.

In the author's opinion it is of great interest to implement the obtained features in the predictive maintenance strategy. The decision making aspect of CMSs becomes more and more important at today's developed market and among others it is valuable in wind industry. The employment of sophisticated health indicators which are part of AStrion could enhance long term productivity and limit downtime of a wind turbine, which makes proposed method economically interesting.

List of Acronyms

AM	Amplitude Modulation
BPFI	Ball Passing Frequency – Inner Race
BPFO	Ball Passing Frequency – Outer Race
BSF	Ball Spin Frequency
CF	Crest Factor
CMS	Condition Monitoring System
CPU	Central Processing Unit
Den	Density
DFT	Discrete Fourier Transform
E	Energy
FFT	Fast Fourier Transform
FM	Frequency Modulation
FTF	Fundamental Train Frequency
GMF	Gear Mesh Frequency
HT	Hilbert Transform
HSS	High Speed Shaft
ISO	International Organization for Standardization
K	Kurtosis
LSS	Low Speed Shaft
PSD	Power Spectral Density
PP	Peak to Peak
Rich	Richness
REB	Rolling Element Bearing
RMS	Root Mean Square
RPM	Revolution Per Minute

RUL	Remaining Useful Life
SNR	Signal-to-Noise Ratio
SCADA	Supervisory Control and Data Acquisition
TF	Time-Frequency
THD	Total Harmonic Distortion
VRMS	Velocity Root Mean Square
VDI	Verein Deutscher Ingenieure *(Eng. Association of German Engineers)*
WT	Wind Turbine
ZP	Zero to Peak

List of Figures

1.1 The total installed capacity of WT worldwide in the years 2011-2014 [WWE14a]. 6

1.2 The yearly installed capacity of WT worldwide [WWE14b]. 7

1.3 The total installed capacity of WT worldwide, the development and prognosis until 2020 [WWE14b]. 7

1.4 Typical configuration of a horizontal axis WT with a gearbox [Ken15]. 10

1.5 Examples of basic WT's drive train component models: (a) an one-stage planetary with two-stage parallel shaft gearbox [Hau06] and (b) a main bearing [Sch15]. 11

1.6 Spectrum of the signal before and after order tracking which is applied to avoid effect of changing operation parameters during data acquisition. 17

1.7 Procedure for envelope analysis using Hilbert transform technique [HR00]. . . . 26

1.8 The acceleration limits of WT's components according to VDI 3834 [PRÜ15]. . 29

1.9 Localization of sensors for vibration-based CMS of WT with a planetary gearbox for the Innovation Project KAStrion. 31

2.1 Flowchart of the AStrion in 2012 – Processing of a single time signal. 34

2.2 An example of (a) spectrogram computed by AStrion-D and (b) its non-stationarities detected in the signal. 36

2.3 Examples of detected series by AStrion-H. 37

2.4 Flowchart of the AStrion tracking and surveillance modules – multiple signals usage. 39

3.1 Graphical visualisation of the TF subsets. 44

3.2 Flowchart of cropping, with the frequency priority setting, the TF representation of a signal. 46

3.3 Simulated signal in the time domain. 48

3.4 Simulated signal in the frequency domain (a) spectrogram computed by AStrion-D and (b) its non-stationarities detected in the signal. The non-stationarity rate computed by AStrion-D equals to 48%. 48

3.5 Presentation of AStrion-C result represented by dashed lines; (a) spectrogram and (b) its non-stationarities detected in the signal. The non-stationarity rate for the selected part of the signal computed by AStrion-D equals to 4%. 49

3.6 Evolution of parameters during the iterative searching of the biggest area to be cropped. (a) number of time segments, (b) number of frequency segments, and (c) size of area. The vertical dashed magnet lines show the 185^{th} iteration that corresponds to the biggest area A_{max} selected by AStrion-C. 50

3.7 Evolution of the T_i during the iterative searching for the biggest area in the iteration corresponding to j equal to 2. The vertical dashed magnet line shows the 185^{th} iteration that corresponds to the biggest area A_{max} selected by AStrion-C for the investigated signal. 50

4.1 Fundamental diagnostics knowledge about gears [Ran11]. 54

4.2 A drawing of a REB with its typical faults [RA11]. 55

4.3 Flowchart of the characteristic fault frequency association algorithm. 59

4.4 Main mechanical components of the GOTIX test rig. 61

4.5 The gearbox of the GOTIX test rig. 62

5.1 Proposed demodulation algorithm. 71

5.2 Simulated signal in the time domain. 77

5.3 Detected harmonic series in the simulated signal. AStrion representation of the spectrum with peaks illustrated by two color lines: the blue part at the top corresponds to very low probability of misclassifying the class of the peak, which in this case corresponds to the pure sine wave depicted by red color. . . 77

5.4 Modulation series, detected by AStrion-H, around carrier frequency which is equal to 5000 Hz. AStrion representation of the spectrum with peaks illustrated by two color lines: the blue part at the top corresponds to very low probability of misclassifying the class of the peak, which are sine waves and sine wave / doubt narrow band classes depicted by red line and yellow dashed line respectively. The brown color arrows below the peaks indicate the modulation series and the order of the sideband is marked by the number under the arrow. 78

5.5 Filtering results (blue) compared with input simulated signal (red). (a) time domain signal and its zoom (b), (c) frequency domain signal with a zoom of selected frequency range (d). 79

5.6 Demodulation results (blue) compared with input modulation signal (red). (a) amplitude modulation and its zoom (b), (c) frequency modulation with a zoom of selected figure part (d). 80

6.1 The main mechanical components of the CETIM test rig. 84

6.2 The CETIM test rig. 85

6.3 A measurement cycle on CETIM test rig. 87

6.4 Arfons wind farm location. 89

6.5 Presentation of the wind turbines in Arfons. (a) shows two turbines on site and (b) demonstrates the kinematic configuration of the WTs drive train. 89

6.6 The time domain signal registered on 2014.04.08 at 17:13:28 by accelerometer 5 at CETIM test rig. 91

6.7 Time domain signal processed by AStrion-D which computed that the non-stationarity rate equals to 99% for the full signal; (a) spectrogram of the investigated signal and (b) detected non-stationarities on the TF plot. 92

6.8 The zoom of spectrogram and non-stationarity detection test of AStrion-D which shows the non-stationary tiles being the reason for the non-stationarity rate equal to 99%. 93

6.9 The result of AStrion-C marked by dotted lines on the (a) spectrogram of the investigated signal and (b) detected non-stationarities on the TF plot. The non-stationarity rate computed by AStrion-D equals to 0% for the selected area. 93

6.10 The investigated vibration signal in the time domain (blue line), the wind speed (green), and the mean speed of high speed shaft (pink). 95

6.11 The investigated vibration signal in the time domain (pink line) and in the angle domain (blue line). 96

6.12 The zooms (a) in the frequency domain and (b) the corresponding part of the signal in the order domain. 97

6.13 Time domain signal processed by AStrion-D with the AStrion-C result marked by dotted lines, (a) spectrogram of the investigated signal and (b) detected non-stationarities on the TF plot. The non-stationarity rate for the entire signal equals to 67%. 98

6.14 The part of the time domain signal cropped according to results of AStrion-C and processed by AStrion-D which computed the non-stationarity rate for the cropped signal equals to 56%, (a) spectrogram of the investigated signal and (b) detected non-stationarities on the TF plot. 98

6.15 Angle domain signal processed by AStrion-D with the AStrion-C result marked by dotted lines, (a) spectrogram of the investigated signal and (b) detected non-stationarities on the angle-order plot. The non-stationarity rate for the full signal equals to 88%. 99

6.16 The part of the angle domain signal cropped according to results of AStrion-C and processed by AStrion-D which computed that the non-stationarity rate equals to 24% for these area, (a) spectrogram of the investigated signal and (b) detected non-stationarities on the angle-order plot. 99

6.17 Average speed of the high speed shaft displayed for every investigated vibration signal acquired in 2014 by accelerometer located on the generator of the WT8 and during the wind turbine was operating within the range 1780 RPM – 1795 RPM of HSS. 103

6.18 Fundamental order of series associated with high speed shaft for the investigated misalignment problem. 104

6.19 Energy computed by AStrion-H of the series associated with the high speed shaft of the WT8 wind turbine. 104

6.20 The evolution of the mechanical fault detection indicator during the main bearing degradation test for positive-sequence components of instantaneous amplitudes and frequency [Cab+15]. 105

6.21 Time domain view of (a) the instantaneous amplitude and (b) the instantaneous frequency estimated from the positive sequence component of the voltages measured in 158^{th} hour of the test. Results of SMESA method and inputs for AStrion algorithms. 108

6.22 Selected harmonic series corresponding to the main bearing fault frequencies in AStrion results representation for (a) the instantaneous amplitude and (b) the instantaneous frequency estimated from the positive sequence component of the voltages measured in 158^{th} hour of the test, which were computed by SMESA. 109

6.23 The sideband series selected to present details of the demodulation. The AStrion spectrum representation at the top shows the full harmonic series and at the bottom the zoom of signal part to be demodulated. 113

6.24 Filtering results (blue) compared with input signal (red). (a) angle domain signal and its zoom (b), (c) order domain signal with a zoom of selected frequency range (d). 115

6.25 The sideband series selected to present details of the demodulation. 116

6.26 The *'20140424-134910 Acceleration 2 KAStrionBenchNI Test14T11S4'* signal filtered by the proposed multi-rate filter over the $\mathbf{B} = [2.099\ Hz, 5.439\ Hz]$ and compared against original signal. (a) time domain signal and (b) spectrum of the original and filtered signal – zoom of interesting range. 117

6.27 Evolution of energy of harmonic series associated with main bearing BPFI throughout the lifetime of the main bearing degradation test. 118

6.28 Evolution of (a) mean value of amplitude demodulation function $\bar{A}$, and (b) modulation index MI_A over detected modulation around fundamental frequency, 2^{nd} harmonic, and 3^{rd} harmonic of BPFI of the main bearing through the lifetime of the main bearing tested over CETIM test rig. 119

6.29 Flaking over the entire inner race of the faulty bearing. 119

6.30 Evolution of (a) RMS, (b) kurtosis, and (c) crest factor values computed on the full length signal, as well as (d) narrow-band RMS with 3% bandwidth of fundamental frequency, 2^{nd} harmonic, and 3^{rd} harmonic of BPFI of the main bearing through the main bearing lifetime. 120

B.1 Un example de (a) spectrogramme calculé par AStrion-D et (b) des non-stationnarités détectées dans le signal. 162

B.2 Parc éolien à Arfons. 169

B.3 Présentation des éoliennes à Arfons. (a) deux éoliennes dans le parc éolien et (b) la configuration cinematique de la transmission d'une éolienne. 169

B.4 Le signal vibratoire dans la domaine du temps (en bleu), la vitesse du vent (en vert) et la moyenne vitesse de l'arbre à grande vitesse (en rose). 171

B.5 Le signal vibratoire dans le domaine temporel (en rose) et dans le domaine angulaire (en bleu). 172

B.6 Zooms (a) dans le domaine temporel et (b) la partie correspondante du signal dans le domaine angulaire. 173

B.7 Le signal de le domaine temporel traité par AStrion-D avec le résultat d'AStrion-C marqué avec des lignes pointillées, (a) le spectrogramme du signal analysé et (b) les non-stationnarités détectés sur la représentation temps-fréquence du signal. L'index de non-stationnarité pour le signal entier est égal à 67%. 174

B.8 La partie du signal de la domaine temporel recadrée d'après les résultats d'AStrion-C et traitée par AStrion-D qui a calculé un index de non-stationnarité pour cette zone égal à 56%, (a) spectrogramme du signal analysé et (b) les non-stationnarités détectés sur la représentation temps-fréquence. 175

B.9 Le signal dans le domaine angulaire traité par AStrion-D avec le résultat d'AStrion-C marqué avec des lignes pointillées, (a) le spectrogramme du signal analysé et (b) les non-stationnarités détectées sur la représentation angle-ordre du signal. L'index de non-stationnarité pour le signal entier est égal à 88%. 175

B.10 La partie du signal de le domaine angulaire recadrée d'après les résultats d'AStrion-C et traitée par AStrion-D qui a calculé un index de non-stationnarité pour cette zone égal à 24%, (a) spectrogramme du signal analysé et (b) les non-stationnarités détectées sur la représentation angle-ordre. 176

B.11 Illustration du resultat d'AStrion-H sur une bande latérale sélectionnée. Représentation de spectre par AStrion qui montre la série harmonique entière en haut et un zoom en dessus. 180

B.12 Résultat du filtrage (bleu) comparé avec le signal original (rouge). (a) domaine angulaire du signal et le zoom (b), (c) domaine d'ordre du signal avec leur zoom de la plage de fréquence sélectionné (d) 181

List of Tables

1.1 Summary of condition monitoring techniques in WT, where a: Statistical methods; b: Time domain analysis; c: Cepstrum analysis; d: Fast Fourier Transformation (FFT); e: Amplitude demodulation; f: Wavelet transformation; g: Hidden Markov models; h: Novel techniques; i: Other. 12

3.1 Changes to perform to blocks in Figure 3.2 to obtain time priority version of AStrion-C algorithm. 47

3.2 Simulated signal parameters. 49

4.1 Selected formulae for calculating characteristic fault frequencies [Ran11]. 56

4.2 Characteristic frequencies of the GOTIX test rig gears expressed in *orders*. . . 61

4.3 Characteristic frequencies of the GOTIX test rig bearings expressed in *orders*. . 61

4.4 The GOTIX test rig signal parameters. 62

4.5 Detailed results of AStrion-K on the example of GOTIX 5797h Track 1 signal. Possible association results selected according to Equatios (4.1) and (4.3) are grouped between double lines and final series to be associated are highlighted. . 65

5.1 Specification of the digital filters used in the multi-rate filtering. 74

5.2 Features calculated from the demodulated amplitude $\hat{A}[\tau]$ and frequency $\hat{F}[\tau]$. . 76

5.3 Amplitude and frequency modulated signal parameters. 77

5.4 Comparison of features calculated from the simulated and demodulated amplitude and frequency signals. σ is the standard deviation calculated for 100 simulations. 80

6.1 Characteristic frequencies of the CETIM test rig gears expressed in *orders*. . . 86

6.2 Characteristic frequencies of the CETIM test rig bearings expressed in *orders*. . 86

6.3 CETIM test rig signal parameters. 88

6.4 Characteristic frequencies of Arfons wind turbine gears expressed in *orders*. . . 90

6.5 Characteristic frequencies of Arfons wind turbine bearings expressed in *orders*. 90

6.6 Arfons signal parameters. 90

6.7 Detailed results of AStrion-K on example of the CETIM signal recorded by accelerometer 5 on 19^{th} November 2013. Selected candidates for association, according to Equations (4.1) and (4.3), are grouped between double lines and final series to be associated are highlighted. 102

6.8 List of all the results of AStrion-K obtained on the instantaneous amplitude and the instantaneous frequency estimated from the positive sequence component of the voltages measured in 158^{th} hour of the main bearing test. Series corresponding to the damaged main bearing are highlighted using the same colors as in Figure 6.22. 107

6.9 Parameters of investigated signal before and after angular resampling together with the average rotational speed of HSS of WT6. 110

6.10 Detailed results of AStrion-K on example of the Arfons WT6 signal recorded by accelerometer 4 on 31^{st} January 2015. Selected candidates for association, according to Equations (4.1) and (4.3), are grouped between double lines and the final series to be associated are highlighted. 111

6.11 Iterative filtering of the signal to be demodulated. 114

6.12 Features calculated from the demodulated amplitude $\hat{A}[\tau]$ and frequency $\hat{F}[\tau]$ of the investigated wind turbine signal. $\bar{A}$ – the average value, PP – peak-to-peak, $Kurt$ – kurtosis, MI modulation index of the demodulated amplitude modulation function and corresponding results of the second AStrion computation on this signal: PN – the number of peaks, and E – the energy of the harmonic series. 114

6.13 Features calculated from the demodulated amplitude $\hat{A}[\tau]$ and frequency $\hat{F}[\tau]$ of the investigated CETIM test rig signal. 116

B.1 Formules pour calculer les fréquences caractéristiques de défaut [Ran11]. 164

B.2 Indicateurs de santé calculés à partir de l'amplitude $\hat{A}[\tau]$ et de la fréquence $\hat{F}[\tau]$ démodulée. 167

B.3 Paramètres des signaux à Arfons. 169

B.4 Fréquences caractéristiques des engrenages exprimées en *ordre*. 170

B.5 Fréquences caractéristique des roulements exprimées en *ordre*. La fréquence de passage des billes sur la bague externe – BPFO (*ang. Ball Pass Frequency of Outer Race*) ; la fréquence de passage des billes sur la bague interne – BPFI (*ang. Ball Pass Frequency of Inner Race*) ; la fréquence fondamentale de cage du roulement à rouleaux – FTF (*ang. Fundamental Train Frequency*) ; la double fréquence de rotation des billes – BSF2 (*ang. Double Ball Spin Frequency*). . . 170

B.6 Les paramètres du signal analysé avant et après le ré-échantillonnage angulaire, et la vitesse moyenne de l'arbre à grande vitesse de l'éolienne marqué comme WT6. 177

B.7 Résultat détaillé d'AStrion-K sur un signal enregistré le 31 janvier 2015 sur WT6. Les candidats sélectionnés pour l'association sont groupés entre deux double lignes horizontales et les séries finales à associer sont surlignées en bleu. 178

B.8 Filtrage itératif du signal démodulé. 181

B.9 Les indicateurs de santé calculés à partir de l'amplitude $\hat{A}[\tau]$ et de la fréquence $\hat{F}[\tau]$ démodulés du signal analysé. $\bar{A}$ – le valeur moyen, PP – crête-à-crête, $Kurt$ – kurtosis, MI l'indice de modulation, PN – le nombre de pics et E – l'énergie de série harmonique. 182

Bibliography

[Ana+02] A. A. Anastassopoulos, D. A. Kouroussis, V. N. Nikolaidis, A. Proust, A. G. Dutton, M. J. Blanch, L. E. Jones, P. Vionis, D. J. Lekou, D. R. V. Van Delft, P. A. Joosse, T. P. Philippidis, T. Kossivas, and G. Fernando. "Structural integrity evaluation of wind turbines blades using pattern recognition analysis on acoustic emission data". In: *Journal of Acoustic Emission* 20 (2002), pp. 229–237 (cit. on p. 12).

[ANA04] B. Al-Najjar and I. Alsyouf. "Enhancing a company's profitability and competitiveness using integrated vibration-based maintenance: A case study". In: *European Journal of Operational Research* 157.3 (Sept. 2004), pp. 643–657 (cit. on p. 14).

[Ant09] J. Antoni. "Cyclostationarity by examples". In: *Mechanical Systems and Signal Processing* 23.4 (May 2009), pp. 987–1036 (cit. on p. 12).

[APC13] K. K. Agrawal, P. G. N. Pandey, and K. Chandrasekaran. "Analysis of the Condition Based Monitoring System for Heavy Industrial Machineries". In: *Computational Intelligence and Computing Research (ICCIC), 2013 IEEE International Conference on* (2013) (cit. on p. 14).

[BB03] N. Baydar and A. Ball. "Detection of gear failures via vibration and acoustic signals using wavelet transform". In: *Mechanical Systems and Signal Processing* 17 (2003), pp. 787–804 (cit. on p. 12).

[BB83] M. Basseville and A. Benveniste. "Sequential detection of abrupt changes in spectral characteristics of digital signals". In: *IEEE Transactions on Information Theory* 29.5 (1983), pp. 709–724 (cit. on p. 42).

[BD03] M. J. Blanch and A. G. Dutton. "Acoustic emission monitoring of field Tests of an operating wind turbine". In: *Key Engineering Materials* (2003), 245–246:475–482 (cit. on p. 12).

[BJ10] T. Barszcz and A. Jabłoński. "Selected methods of finding optimal center frequency for amplitude demodulation of vibration signals". In: *Diagnostyka* 2.54 (2010), pp. 2008–2011 (cit. on p. 68).

[BJ11] T. Barszcz and A. Jabłoński. "A novel method for the optimal band selection for vibration signal demodulation and comparison with the Kurtogram". In: *Mechanical Systems and Signal Processing* 25.1 (Jan. 2011), pp. 431–451 (cit. on p. 68).

[BJB12] D. Broda, A. Jabłoński, and T. Barszcz. "Optimisation of operational state definition for wind farms – Part 1, Development of algorithms". In: *CM/MFPT: The 9th International Conference on Condition Monitoring and Machinery Failure Preventi on Technologies*. London, United Kingdom, 2012 (cit. on p. 14).

[BK09] E. Bechhoefer and M. Kingsley. "A review of time synchronous average algorithms". In: *Annual conference of the prognostics and Health Management Society 2009* (2009), pp. 1–10 (cit. on p. 75).

[BLJ06] D. Banjevic, D. Lin, and A. K. S. Jardine. "A review on machinery diagnostics and prognostics implementing condition-based maintenance". In: *Mechanical Systems and Signal Processing* 20.7 (Oct. 2006), pp. 1483–1510 (cit. on pp. 2, 27).

[BN91] M. Basseville and I. V. Nikiforov. "A unified framework for statistical change detection". In: *[1991] Proceedings of the 30th IEEE Conference on Decision and Control* (1991), pp. 2586–2591 (cit. on p. 42).

[Boa03] B. Boashash. *Time-Frequency Signal Analysis and Processing – A Comprehensive Reference*. Elsevier Science, Oxford, UK, 2003 (cit. on p. 75).

[Boa92] B. Boashash. "Estimating and interpreting the instantaneous frequency of a signal. I. Fundamentals". In: *Proceedings of the IEEE* 80.4 (Apr. 1992), pp. 520–538 (cit. on p. 106).

[Bon+05] F. Bonnardot, M. El Badaoui, R. B. Randall, J. Danière, and F. Guillet. "Use of the acceleration signal of a gearbox in order to perform angular resampling (with limited speed fluctuation)". In: *Mechanical Systems and Signal Processing* 19.4 (July 2005), pp. 766–785 (cit. on p. 14).

[Bor+10] P. Borgnat, P. Flandrin, P. Honeine, C. Richard, and J. Xiao. "Testing stationarity with surrogates: A time-frequency approach". In: *IEEE Transactions on Signal Processing* 58.7 (2010), pp. 3459–3470 (cit. on p. 42).

[BP06] E. Becker and P. Poste. "Keeping the blades turning: condition monitoring of wind turbine gears". In: *Refocus* 7.2 (2006), pp. 26–32 (cit. on p. 12).

[BR99] A. G. Beattie and M. Rumsey. "Non-destructive evaluation of wind turbine blades using an Infrared camera". In: *ASME wind energy Symposium, 18th, Aerospace Sciences Meeting and Exhibit, 37th*. Reno, NV, 1999 (cit. on pp. 12, 13).

[Bra11] S. Braun. "The synchronous (time domain) average revisited". In: *Mechanical Systems and Signal Processing* 25.4 (2011), pp. 1087–1102 (cit. on p. 17).

[Bra86] S. G. Braun. *Mechanical Signature Analysis: Theory and Applications*. San Diego: Academic Press, 1986 (cit. on p. 25).

[Bri+97] D. Brie, M. Tomczak, H. Oehlmann, and A. Richard. "GEAR CRACK DETECTION BY ADAPTIVE AMPLITUDE AND PHASE DEMODULATION". In: *Mechanical Systems and Signal Processing* 11.1 (1997), pp. 149 –167 (cit. on p. 67).

[BS12] T. Barszcz and N. Sawalhi. "Fault Detection Enhancement in Rolling Element Bearings Using the Minimum Entropy Deconvolution". In: *Archives of Acoustics* 37.2 (Jan. 2012), pp. 131–141 (cit. on p. 12).

[BS13] T. Barszcz and M. Strączkiewicz. "Novel Intuitive Hierarchical Structure for Condition Monitoring System of Wind Turbines". In: *Diagnostyka* 14.3 (2013), pp. 53–60 (cit. on p. 13).

[Bus02] R. T. Buscarello. *Practical Solutions to Machinery and Maintenance Vibration Problems*. Update International; Fourth revised edition, 2002 (cit. on p. 18).

[But73] D. E. Butler. "The shock pulse method for the detection of damaged rolling bearings". In: *NDT International* 6.2 (1973), pp. 92–95 (cit. on p. 13).

[BZ09a] W. Bartelmus and R. Zimroz. "A new feature for monitoring the condition of gearboxes in non-stationary operating conditions". In: *Mechanical Systems and Signal Processing* 23.5 (July 2009), pp. 1528–1534 (cit. on pp. 14, 41).

[BZ09b] W. Bartelmus and R. Zimroz. "Vibration condition monitoring of planetary gearbox under varying external load". In: *Mechanical Systems and Signal Processing* 23.1 (Jan. 2009), pp. 246–257 (cit. on p. 12).

[Cab+15] G. Cablea, P. Granjon, C. Bérenguer, and P. Bellemain. "Online condition monitoring of wind turbines through three-phase electrical signature analysis". In: *Tenth International Conference on Condition Monitoring and Machinery Failure Prevention Technologies. CM 2015 and MFPT 2015*. Oxford, United Kingdom, June 2015 (cit. on p. 105).

[Car22] J. R. Carson. "Notes on the theory of modulation". In: *Proc. IRE* 10.1 (1922), pp. 57–64 (cit. on p. 72).

[Cas+97] P. Caselitz, J. Giebhardt, M. Mevenkamp, and M. Reichardt. "Application of condition monitoring systems in wind energy converters". In: *Proceedings of EWEC'97*. Dublin, Ireland, 1997, pp. 579–582 (cit. on p. 12).

[Cas+98] M. Castaings, P. Cawley, R. Farlow, and G. Hayward. "Journal of Nondestructive Evaluation". In: *Single Sided inspection of composite materials using air coupled ultrasound* 17.1 (1998), pp. 37–45 (cit. on p. 12).

[CG03] P. Caselitz and J. Giebhardt. "Fault prediction techniques for offshore wind farm maintenance and repair strategies". In: *Proceedings of the EWEC2003*. Madrid, Spain, 2003 (cit. on p. 12).

[CG05] P. Caselitz and J. Giebhardt. "Rotor condition monitoring for improved operational safety of offshore wind energy converters". In: *Transactions of the ASME. Journal of Solar Energy Engineering* 127.2 (2005), pp. 253–261 (cit. on p. 12).

[CG11] F. Combet and L. Gelman. "Novel adaptation of the demodulation technology for gear damage detection to variable amplitudes of mesh harmonics". In: *Mechanical Systems and Signal Processing* 25.3 (Apr. 2011), pp. 839–845 (cit. on p. 67).

[CGB14] G. Cablea, P. Granjon, and C. Bérenguer. "Method of analysing non-stationary electrical signals". In: *4th International Conference on Condition Monitoring of Machinery in Non-Stationary Operations (CMMNO'2014)*. Lyon, France, 2014 (cit. on pp. 13, 105, 106).

[CGM94] P. Caselitz, J. Giebhardt, and M. Mevenkamp. "On-line fault detection and prediction in wind energy converters". In: *Proceedings of EWEC'94*. Thessaloniki, Greece, 1994, pp. 623–627 (cit. on p. 12).

[Cha+12] F. Chaari, W. Bartelmus, R. Zimroz, T. Fakhfakh, and M. Haddar. "Gearbox vibration signal amplitude and frequency modulation". In: *Shock and Vibration* 19.4 (2012), pp. 635–652 (cit. on pp. 14, 67).

[CR14] M. D. Coats and R. B. Randall. "Single and multi-stage phase demodulation based order-tracking". In: *Mechanical Systems and Signal Processing* 44.1-2 (2014), pp. 86–117 (cit. on p. 68).

[CW03] N. J. Cozens and S. J. Watson. *State of the art condition monitoring techniques suitable for wind turbines and wind farm applications*. Tech. rep. CONMOW project, 2003 (cit. on p. 12).

[CYY10] J. Cheng, Y. Yang, and D. Yu. "The envelope order spectrum based on generalized demodulation time—frequency analysis and its application to gear fault diagnosis". In: *Mechanical Systems and Signal Processing* 24 (2010), pp. 508–521 (cit. on p. 12).

[CZT14] C. J. Crabtree, D. Zappalá, and P. J. Tavner. *Survey of Commercially Available Condition Monitoring Systems for Wind Turbines – Revision: 05, May 2014*. Tech. rep. Durham University School of Engineering, Computing Sciences, and the SUPERGEN Wind Energy Technologies Consortium, 2014 (cit. on p. 14).

[DC10] G. M. Dong and J. Chen. "Study on cyclic energy indicator for degradation assessment of rolling element bearings". In: *Journal of Vibration and Control* 17.12 (Nov. 2010), pp. 1805–1816 (cit. on p. 121).

[DG07] M. A. Drewry and G. A. Georgiou. "A review of NDT techniques for wind turbines". In: *Insight* 49.3 (2007), pp. 137–141 (cit. on p. 13).

[Dju+12] S. Djurovic, C. J. Crabtree, P. J. Tavner, and A. C. Smith. "Condition monitoring of wind turbine induction generators with rotor electrical asymmetry". In: *IET Renewable Power Generation* 6.4 (2012), p. 207 (cit. on p. 13).

[DL03] H. J. Decker and D. G. Lewicki. "Spiral Bevel Pinion Crack Detection in a Helicopter Gearbox". In: *59th Annual Forum of the American Helicopter Society*. June. Phoenix, AZ, USA, 2003 (cit. on pp. 24–26).

[DL05] D. S. L. Dolan and P. W. Lehn. "Real-time wind turbine emulator suitable for power quality and dynamic control Studies". In: *Proceedings of international conference on power systems transients*. Montreal, Canada, 2005, pp. 1–6 (cit. on p. 13).

[DRR00] G. Dalpiaz, A. Rivola, and R. Rubini. "Effectiveness and Sensitivity of Vibration Processing Techniques for Local Fault Detection in Gears". In: *Mechanical Systems and Signal Processing* 14.3 (May 2000), pp. 387–412 (cit. on p. 12).

[DS78] D. Dyer and R. M. Stewart. "Detection of rolling element bearing damage by statistical vibration analysis". In: *ASME Journal of Mechanical Design* 100 (1978), pp. 229–235 (cit. on p. 12).

[Dur99] M. Durnerin. "A strategy for interpretation in spectral analysis – Detection and characterization of spectral components (in French)". PhD thesis. Grenoble INP, 1999 (cit. on pp. 34, 161).

[Dut+01] A. G. Dutton, M. J. Blanch, P. Vionis, D. Lekou, D. R. V. van Delft, P. A. Joosse, A. Anastassopoulos, D. Kouroussis, T. Kossivas, T. P. Philippidis, T. T. Assimakopoulou, G. Fernando, C. Doyle, and A. Proust. "Acoustic emission condition monitoring of wind turbine rotor blades: laboratory certification testing to large scale in-service deployment". In: *Proceedings of the 2001 European wind energy conference*. Copenhagen, Denmark, 2001 (cit. on p. 12).

[Egu+15] E. Egusquiza, C. Valero, D. Valentin, A. Presas, and C. G. Rodriguez. "Condition monitoring of pump-turbines. New challenges". In: *Measurement* 67 (2015), pp. 151–163 (cit. on p. 14).

[EM10] M. Elforjani and D. Mba. "Accelerated natural fault diagnosis in slow speed bearings with Acoustic Emission". In: *Engineering Fracture Mechanics* 77.1 (Jan. 2010), pp. 112–127 (cit. on p. 12).

[ES08] W. Ecke and K. Schröder. "Fiber Bragg grating sensor system for operational load monitoring of wind turbine blades". In: *Proceedings of SPIE*. Vol. 6933. 2008 (cit. on p. 12).

[Fel11] M. Feldman. "Hilbert transform in vibration analysis". In: *Mechanical Systems and Signal Processing* 25.3 (2011), pp. 735–802 (cit. on p. 76).

[Fen+12] Z. Feng, M. Liang, Y. Zhang, and S. Hou. "Fault diagnosis for wind turbine planetary gearboxes via demodulation analysis based on ensemble empirical mode decomposition and energy separation". In: *Renewable Energy* 47 (Nov. 2012), pp. 112–126 (cit. on p. 68).

[Fen+15] Z. Feng, X. Chen, M. Liang, and F. Ma. "Time–frequency demodulation analysis based on iterative generalized demodulation for fault diagnosis of planetary gearbox under nonstationary conditions". In: *Mechanical Systems and Signal Processing* 62–63 (2015), pp. 54 –74 (cit. on p. 68).

[Fir+14] M. Firla, Z.-Y. Li, N. Martin, and T. Barszcz. "Automatic and Full-band Demodulation for Fault Detection – Validation on a Wind Turbine Test Rig". In: *4th International Conference on Condition Monitoring of Machinery in Non-Stationary Operations (CMMNO'2014)*. Lyon, France, 2014 (cit. on pp. 38, 56, 81, 161).

[FM97] K. R. Fyfe and E. D. S. Munck. "Analysis of computed order tracking". In: *Mechanical Systems and Signal Processing* 11.2 (1997), pp. 187–205 (cit. on pp. 14, 16, 41, 56).

[FPB11] J. G. Fantidis, C. Potolias, and D. V. Bandekas. "Wind turbine blade nondestructive testing with a transportable Radiography system". In: *Science and Technology of Nuclear Installations* ID 347320 (2011) (cit. on p. 13).

[Fut95] D. N. Futter. "Vibration monitoring of industrial gearboxes using time domain averaging". In: *IMechE 2nd International conference on gearbox noise, vibration and diagnostics. Mechanical Engineering Publications*. 1995 (cit. on p. 12).

[Gel+00] L. M. Gelman, D. A. Kripak, V. V. Fedorov, and L. N. Udovenko. "Condition Monitoring Diagnosis Methods of Helicopter Units". In: *Mechanical Systems and Signal Processing* 14.4 (2000), pp. 613–624 (cit. on p. 58).

[Gel+05] L. M. Gelman, R. Zimroz, J. Birkel, H. Leigh-Firbank, D. Simms, B. Waterland, and G. Whitehurst. "Adaptive vibration condition monitoring technology for local tooth damage in gearboxes". In: *Insight: Non-Destructive Testing and Condition Monitoring* 47.8 (2005), pp. 461–464 (cit. on p. 123).

[Ger15] T. Gerber. "Dynamic tracking of modulated components. Application to automatic condition monitoring of failures in wind farms. (in French)". PhD thesis. Grenoble INP, 2015 (cit. on pp. 38, 72).

[Gho+00] A. Ghoshal, M. J. Sundaresan, M. J. Schulz, and P. F. Pai. "Structural health monitoring techniques for wind turbines blades". In: *Journal of Wind Engineering and Industrial Aerodynamics* 85 (2000), pp. 309–324 (cit. on p. 12).

[Gie+06] G. Giebel, G. Oliver, M. Malcolm, and B. Kaj. "Common Access to wind turbines data for condition monitoring". In: *Riso National Laboratory. In: Proceedings of the 27th Riso International Symposium on Material Science.* Denmark, 2006, pp. 157–164 (cit. on p. 12).

[GM+12] F. P. García Márquez, A. M. Tobias, J. M. Pinar Pérez, and M. Papaelias. "Condition monitoring of wind turbines: Techniques and methods". In: *Renewable Energy* 46 (Oct. 2012), pp. 169–178 (cit. on pp. 11, 13).

[GMM13] T. Gerber, N. Martin, and C. Mailhes. "Identification of harmonics and sidebands in a finite set of spectral components". In: *Tenth International Conference on Condition Monitoring and Machinery Failure Prevention Technologies. CM 2013 and MFPT 2013.* Kraków, Poland, 2013 (cit. on pp. 34, 36, 72, 76, 161).

[GMM14] T. Gerber, N. Martin, and C. Mailhes. "Monitoring based on time-frequency tracking of estimated harmonic series and modulation sidebands." In: *4th International Conference on Condition Monitoring of Machinery in Non-Stationary Operations (CMMNO'2014).* Lyon, France, 2014 (cit. on p. 38).

[GMM15] T. Gerber, N. Martin, and C. Mailhes. "Time-Frequency Tracking of Spectral Structures Estimated by a Data-Driven Method". In: *Industrial Electronics, IEEE Transactions on* 62.10 (Oct. 2015), pp. 6616–6626 (cit. on p. 38).

[GMRT10] F. P. García Márquez, C. Roberts, and A. M. Tobias. "Railway point mechanisms: condition monitoring and fault detection". In: *Proceedings of the Institution of Mechanical Engineers, Part F, Journal of Rail and Rapid Transit* 224.1 (2010), pp. 35–44 (cit. on p. 13).

[GR97a] J. H. Gieske and M. A. Rumsey. "Acoustic emission monitoring of a wind turbines blade during a fatigue test". In: *Musial W, Berg DE, editors. ASME Wind Energy Symposium. AIAA ASME.* Denmark, 1997, pp. 239–248 (cit. on p. 12).

[GR97b] J. H. Gieske and M. A. Rumsey. "Nondestructive evaluation (NDE) of composite-metal bond interface of a wind turbines blade using an acousto-ultrasonic technique". In: *Musial W, Berg DE, editors. ASME Wind Energy Symposium. AIAA ASME.* Denmark, 1997, pp. 249–254 (cit. on p. 12).

[Han+] J. Hanna, C. Hatch, M. Kalb, A. Weiss, and H. Luo. *Detection of Wind Turbine Gear Tooth Defects Using Sideband Energy Ratio™, Wind energy resource assessment and forecasting – GE Energy.* `http://www.ge-mcs.com/download/monitoring/SER-Technical-Paper.pdf`. [Online; accessed 12-Aug-2015] (cit. on p. 25).

[Hat04] C. Hatch. "Improved wind turbines condition monitoring using acceleration enveloping". In: *Orbit* (2004), pp. 58–61 (cit. on p. 13).

[Hau06] E. Hau. *Wind Turbines: Fundamentals, Technologies, Application, Economics.* Springer, 2006 (cit. on pp. 10, 11, 13, 30).

[Hen+09] A. Heng, S. Zhang, A. C. C. Tan, and J. Mathew. "Rotating machinery prognostics: State of the art, challenges and opportunities". In: *Mechanical Systems and Signal Processing* 23.3 (2009), pp. 724–739 (cit. on p. 27).

[HM06] J. Huillery and N. Martin. "Time-Frequency Modeling and Detection of random non-stationary signals for Monitoring Purposes". In: *47th AIAA/ASME/ASCE/AHS/ASC Structures, Structural Dynamics, and Materials Conference; Structures, Structural Dynamics, and Materials and Co-located Conferences* (May 2006), pp. 1–6 (cit. on pp. 14, 35).

[HM96] R. B. Heng and M. J. Mohd. "Condition monitoring using acoustic signals". In: *Proceedings of the Fifth International Conference on Profitable Condition Monitoring Fluids and Machinery Performance Monitoring. UK: Mechanical Engineering Publications Limited.* 1996, pp. 145–158 (cit. on p. 12).

[Hon+02] J.-C. Hong, Y. Y. Kim, H. C. Lee, and Y. W. Lee. "Damage detection using the Lipschitz exponent estimated by the wavelet transform: application to vibration modes of a Beam". In: *International Journal of Solids and Structures* 39 (2002), pp. 1803–1816 (cit. on p. 12).

[HR00] D. Ho and R. B. Randall. "Optimisation of Bearing Diagnostic Techniques Using Simulated and Actual Bearing Fault Signals". In: *Mechanical Systems and Signal Processing* 14.5 (Sept. 2000), pp. 763–788 (cit. on pp. 12, 26, 75, 167).

[IH82] T. Igarashi and H. Hamada. "Studies on the vibration and sound of defective roller bearings (First report: vibration of ball bearing with one defect)". In: *Bulletin of JSME* 25.204 (1982), pp. 994–1001 (cit. on pp. 12, 13).

[IY83] T. Igarashi and S. Yabe. "Studies on the Vibration and Sound of Defective Rolling Bearings: First Report: Vibration of Ball Bearings with One Defect". In: *Bulletin of JSME* 26.220 (1983), pp. 1791–1798 (cit. on pp. 12, 13).

[Jab12] A. Jabłoński. "Methods of automatized monitoring and diagnosis of wind turbines". PhD thesis. AGH University of Science and Technology, Faculty of Mechanical Engineering and Robotics, Department of Robotics and Mechatronics, 2012 (cit. on p. 31).

[Jas+08] E. Jasiūnienė, R. Raišutis, R. Šliteris, A. Voleišis, and M. Jakas. "Ultrasonic NDT of wind turbine blades using contact pulse-echo immersion testing with moving water container". In: *Ultragarsas (Ultrasound)* 63.3 (2008), pp. 28–32 (cit. on p. 12).

[Jas+09] E. Jasiūnienė, R. Raišutis, R. Šliteris, A. Voleišis, A. Vladišauskas, D. Mitchard, and M. Amos. "NDT of wind turbine blades using adapted ultrasonic and radiographic techniques". In: *Insight- Non-Destructive Testing and Condition Monitoring* 51.9 (2009), pp. 477–483 (cit. on pp. 12, 13).

[JB12] A. Jabłoński and T. Barszcz. "Optimisation of operational state definition for wind farms – Part 2, Integration of Matlab environment with web-enabled database system". In: *CM/MFPT: The 9th International Conference on Condition Monitoring and Machinery Failure Preventi on Technologies*. London, United Kingdom, 2012 (cit. on p. 14).

[JB13] A. Jabłoński and T. Barszcz. "Validation of vibration measurements for heavy duty machinery diagnostics". In: *Mechanical Systems and Signal Processing* 38.1 (July 2013), pp. 248–263 (cit. on pp. 14, 41).

[JBB11] A. Jabłoński, T. Barszcz, and M. Bielecka. "Automatic validation of vibration signals in wind farm distributed monitoring systems". In: *Measurement* 44.10 (Dec. 2011), pp. 1954–1967 (cit. on p. 14).

[JL95] C. James Li and S. Y. Li. "Acoustic emission analysis for bearing condition monitoring". In: *Wear* 185.1-2 (1995), pp. 67–74 (cit. on p. 12).

[Joo+02] P. A. Joosse, M. J. Blanch, A. G. Dutton, D. A. Kouroussis, T. P. Philippidis, and P. S. Vionis. "Acoustic emission monitoring of small wind turbine blades". In: *Journal of Solar energy Engineering* 124.4 (2002), pp. 446–455 (cit. on p. 12).

[Jun08] A. Jungert. "Damage detection in wind turbine blades using two different acoustic techniques". In: *The e-Journal of Nondestructive Testing* 25 (2008) (cit. on p. 12).

[Kim+99] J. S. Kim, M. C. Kang, B. J. Yyu, and Y. K. Ji. "Development of an online tool-life monitoring system using acoustic emission signals in gear shaping". In: *International Journal of Machine Tools and Manufacture* 39.11 (1999), pp. 1761–1777 (cit. on p. 12).

[LCB14] T. T. Le, F. Chatelain, and C. Berenguer. "Hidden Markov Models for diagnostics and prognostics of systems under multiple deterioration modes". In: *European Safety and Reliability Conference - ESREL 2014*. Wrocław, Poland: Taylor & Francis - CRC Press/Balkema, 2014, pp. 1197–1204 (cit. on pp. 14, 27).

[LD98a] H. Laurent and C. Doncarli. "Stationarity index for abrupt changes detection in the time-frequency plane". In: *IEEE Signal Processing Letters* 5.2 (1998), pp. 43–45 (cit. on p. 42).

[LD98b] H. Laurent and C. Doncarli. "Stationarity index for abrupt changes detection in the time-frequency plane". In: *IEEE Signal Processing Letters* 5.2 (1998), pp. 43–45 (cit. on p. 42).

[Liu+15] W. Y. Liu, B. P. Tang, J. G. Han, X. N. Lu, N. N. Hu, and Z. Z. He. "The structure healthy condition monitoring and fault diagnosis methods in wind turbines: A review". In: *Renewable and Sustainable Energy Reviews* 44 (2015), pp. 466–472 (cit. on p. 11).

[LK06] S. Leske and D. Kitaljevich. "Managing gearbox failure, Dewek". In: *Dewi Magazine* 26 (2006) (cit. on p. 12).

[LL95] C. J. Li and S. Y. Li. "Acoustic emission analysis for bearing condition monitoring". In: *Wear* 185 (1995), pp. 64–74 (cit. on p. 12).

[LLW15] C. Li, M. Liang, and T. Wang. "Criterion fusion for spectral segmentation and its application to optimal demodulation of bearing vibration signals". In: *Mechanical Systems and Signal Processing* 64–65 (2015), pp. 132–148 (cit. on p. 68).

[LM95] S. T. Lin and P. D. McFadden. "Vibration analysis of gearboxes by the linear wavelet transform". In: *IMechE 2nd International conference on gearbox noise, vibration and diagnostics. Mechanical Engineering Publications.* 1995 (cit. on p. 12).

[LOI03] G. Y. Luo, D. Osypiw, and M. Irle. "On-Line vibration analysis with fast continuous wavelet algorithm for condition monitoring of bearing". In: *Journal of Vibration and Control* 9 (2003), pp. 931–947 (cit. on p. 12).

[LS10] M. Liang and I. Soltani Bozchalooi. "An energy operator approach to joint application of amplitude and frequency-demodulations for bearing fault detection". In: *Mechanical Systems and Signal Processing* 24.5 (2010), pp. 1473–1494 (cit. on p. 68).

[MA08] D. McMillan and G. W. Ault. "Condition monitoring benefit for onshore wind turbines: sensitivity to operational parameters". In: *Renewable Power Generation, IET* 2.1 (2008), pp. 60–72 (cit. on p. 14).

[Mai+06] C. Mailhes, N. Martin, K. Sahli, and G. Lejeune. "A spectral identity card". In: *EUropean SIgnal Processing Conference, EUSIPCO 06.* Florence, Italy, 2006 (cit. on pp. 56, 76).

[Mar05] N. Martin. "A Criterion for Detecting Nonstationary Events". In: *Twelfth International Congress on Sound and Vibration, ICSV12, Jul 2005.* Lisbon, Portugal, 2005 (cit. on pp. 35, 42, 43, 162).

[Mar07] N. Martin. "Advanced signal processing and condition monitoring". In: *Insight - Non-Destructive Testing and Condition Monitoring* 49.8 (Aug. 2007), pp. 459–464 (cit. on p. 14).

[MB76] R. Meyer and C. S. Burrus. "Design and implementation of multirate digital filters". In: *Acoustics, Speech and Signal Processing, IEEE Transactions on* 24.1 (1976), pp. 55–58 (cit. on p. 70).

[MB96] D. U. Mba and R. H. Bannister. "Profitable condition monitoring of low speed rotating machinery using stress waves". In: *Proceedings of the Fifth International Conference on Profitable Condition Monitoring Fluids and Machinery Performance Monitoring. UK: Mechanical Engineering Publications Limited.* 1996, pp. 159–168 (cit. on p. 12).

[MBM12] R. F. Mesquita Brandão, J. A. Beleza Carvalho, and F. P. MacIel Barbosa. "Forecast of faults in a wind turbine gearbox". In: *Proceedings of 9th International Conference, ELEKTRO 2012* (2012), pp. 170–173 (cit. on p. 13).

[McF86] P. D. McFadden. "Detecting fatigue cracks in gears by amplitude and phase demodulation of the meshing vibration". In: *Journal of Vibration, Acoustics, Stress, and Reliability in Design* 108 (1986), pp. 165–170 (cit. on pp. 12, 67).

[McF87a] P. D. McFadden. "A revised model for the extraction of periodic waveforms by time domain averaging". In: *Mechanical Systems and Signal Processing* 1.1 (1987), pp. 83–95 (cit. on pp. 17, 18, 75, 167).

[McF87b] P. D. McFadden. "Examination of a technique for the early detection of failure in gears by signal processing of the time domain average of the meshing vibration". In: *Mechanical Systems and Signal Processing* 1.2 (1987), pp. 173–183 (cit. on p. 12).

[McF94] P. D. McFadden. "Window Functions for the Calculation of the Time Domain Averages of the Vibration of the Individual Planet Gears and Sun Gear in an Epicyclic Gearbox". In: *Journal of Vibration and Acoustics* 116.2 (1994), p. 179 (cit. on p. 18).

[MD03] S. A. McInerny and Y. Dai. "Basic vibration signal processing for bearing fault detection". In: *IEEE Transactions on Education* 46.1 (2003), pp. 149–156 (cit. on p. 68).

[Mei12] A. Meisingseth. "Demodulation Techniques in Gearbox Diagnostics". MA thesis. Upsala Universitet, 2012 (cit. on p. 68).

[Men+00] S. Menon, J. N. Schoess, R. Hamza, and D. Busch. "Wavelet-Based acoustic emission detection method with adaptive thresholding". In: *Proceedings of the SPIE 3986*. 2000, pp. 71–77 (cit. on p. 12).

[MHB04] M. Mosher, E. M. Huff, and E. Barszcz. "Analysis of in-flight measurements from helicopter transmissions". In: *American Helicopter Society 60th Annual Forum*. Baltimore, MD, USA, 2004 (cit. on p. 15).

[Mil99] A. J. Miller. "A New wavelet basis for the decomposition of gear motion error signals and its application to gearbox diagnostics". MA thesis. The Pennsylvania State University, 1999 (cit. on p. 12).

[MK06] A. R. Mohanty and C. Kar. "Fault Detection in a Multistage Gearbox by Demodulation of Motor Current Waveform". In: *IEEE Transactions on Industrial Electronics* 53.4 (June 2006), pp. 1285–1297 (cit. on p. 68).

[ML96] J. Ma and C. J. Li. "GEAR DEFECT DETECTION THROUGH MODEL-BASED WIDEBAND DEMODULATION OF VIBRATIONS". In: *Mechanical Systems and Signal Processing* 10.5 (1996), pp. 653 –665 (cit. on p. 67).

[MM07] Q. Miaoa and V. Makis. "Condition monitoring and classification of rotating machinery using wavelets and Hidden Markov models". In: *Mechanical Systems and Signal Processing* 21 (2007), pp. 840–855 (cit. on p. 12).

[MM09] N. Martin and C. Mailhes. "A non-stationary index resulting from time and frequency domains". In: *Sixth International Conference on Condition Monitoring and Machinery Failure Prevention Technologies. CM 2009 and MFPT 2009*. Dublin, Ireland, 2009 (cit. on pp. 14, 33, 35, 43, 45, 161–163).

[MM10] N. Martin and C. Mailhes. "About periodicity and signal to noise ratio – The strength of the autocorrelation function." In: *CM 2010 and MFPT 2010*. 2010 (cit. on pp. 33, 35, 161).

[MMG13] N. Martin, C. Mailhes, and T. Gerber. *Anomaly detection system.* Patent no. FR N°13/53860. 2013 (cit. on pp. 34, 36, 161).

[MPP00] E. Morfiadakis, K. Papadopoulos, and T. P. Philippidis. "Assessment of the strain gauge technique for measurement of wind turbine blade loads". In: *Wind Energy* 3.1 (2000), pp. 35–65 (cit. on p. 12).

[MS84] P. D. McFadden and J. D. Smith. "Vibration monitoring of rolling element bearings by the high-frequency resonance technique — a review". In: *Tribology International* 17.1 (1984), pp. 3–10 (cit. on p. 12).

[MT06] R. Matsuzaki and A. Todoroki. "Wireless detection of internal delamination cracks in CFRP laminates using oscillating frequency changes". In: *Composites Science and Technology* 66 (2006), pp. 407–416 (cit. on p. 13).

[MZ11] R. A. Makowski and R. Zimroz. "Adaptive Bearings Vibration Modelling for Diagnosis". In: *Adaptive and Intelligent Systems*. Ed. by A. Bouchachia. Vol. 6943. Lecture Notes in Computer Science. Springer Berlin Heidelberg, 2011, pp. 248–259 (cit. on p. 42).

[Mü+06] H. Müller, M. Pöller, A. Basteck, M. Tilscher, and J. Pfister. "Grid compatibility of variable speed wind turbines with directly coupled synchronous generator and hydro-dynamically controlled gearbox". In: *Sixth International Workshop on Large-Scale integration of wind power and transmission networks for offshore wind farms*. Delft, NL, 2006, pp. 307–315 (cit. on p. 13).

[NA02] N. G. Nikolaou and I. A. Antoniadis. "Rolling element bearing fault diagnosis using wavelet packets". In: *NDT & E International* 35.3 (2002), pp. 197–205 (cit. on p. 12).

[NH92] B. Najafi and H. Hakim. "A comparative study of non-parametric spectral estimators for application in machine vibration analysis". In: *Mechanical Systems and Signal Processing* 6.6 (1992), pp. 551–574 (cit. on p. 1).

[NK03] M. P. Norton and D. G. Karczub. *Fundamentals of Noise and Vibration Analysis for Engineers*. 2nd ed. Vol. 55. 2. Cambridge University Press; 2 edition, 2003, p. 275 (cit. on pp. 9, 42).

[NPLAFK] G. de Novaes Pires Leite, E. Alencar Feitosa, and A. G. Kraj. *Remote conditioning monitoring system for a hybrid wind-diesel system – Application at Fernando de Naronha Island, Brasil*. `http://www.ontario-sea.org/`. [Online; accessed 2-June-2015] (cit. on p. 12).

[NS96] S. Ness and C. N. Sherlock. *Nondestructive Testing Handbook*. Columbus, Ohio: Nondestructive Testing Overview, vol. 10. American Society for Nondestructive Testing, 1996 (cit. on p. 13).

[OL01] H. Ocak and K. A. Loparo. "A New bearing fault detection and diagnosis Scheme based on Hidden Markov modeling of vibration signals". In: *Acoustics, Speech, and Signal Processing, 2001 Vol 5. Proceedings. (ICASSP '01). 2001 IEEE International Conference on*. Salt Lake City, UT, USA: IEEE, May 2001, pp. 3141–3144 (cit. on p. 12).

[Oli+90] C. Olivier, P. Courtellemont, D. D. Brucq, and O. Colot. "Algorithms for treatment of locally stationary multichannel signals –proposition of a method for change detection based on histograms". In: *[Proceedings] IECON '90: 16th Annual Conference of IEEE Industrial Electronics Society* (1990) (cit. on p. 42).

[OSB98] A. V. Oppenheim, R. W. Schafer, and J. R. Buck. *Discrete-Time Signal Processing*. 2nd ed. New Yersey, USA: Prentice-Hall, Inc., 1998 (cit. on pp. 16, 42).

[OWZ14] J. Obuchowski, A. Wyłomańska, and R. Zimroz. "Selection of informative frequency band in local damage detection in rotating machinery". In: *Mechanical Systems and Signal Processing* 48.1-2 (Oct. 2014), pp. 138–152 (cit. on p. 68).

[Pac+13] C. Pachaud, T. Gerber, M. Firla, N. Martin, and C. Mailhes. "Consequences of non-respect of the Bedrosian theorem when demodulating". In: *Tenth International Conference on Condition Monitoring and Machinery Failure Prevention Technologies. CM 2013 and MFPT 2013*. Kraków, Poland, 2013 (cit. on p. 69).

[PCT07] Z. K. Peng, F. L. Chu, and P. W. Tse. "Singularity analysis of the vibration signals by means of wavelet Modulus Maximal method". In: *Mechanical Systems and Signal Processing* 21.2 (2007), pp. 780–794 (cit. on p. 12).

[PJ99] A. Prabhakaran and C. R. Jagga. "Condition monitoring of Steam turbine-generator through contamination analysis of used lubricating oil". In: *Tribology International* 32 (1999), pp. 145–152 (cit. on p. 12).

[PKC05] Z. Peng, N. J. Kessissoglou, and M. Cox. "A study of the effect of contaminant particles in lubricants using wear debris and vibration condition monitoring techniques". In: *Wear* 258.11-12 (June 2005), pp. 1651–1662 (cit. on p. 12).

[Pop99] T. D. Popescu. "Change detection in signals using linear regression models". In: *Proceedings of the 1999 IEEE International Symposium on Computer Aided Control System Design (Cat. No.99TH8404)* (1999), pp. 182–187 (cit. on p. 42).

[PRÜ15] PRÜFTECHNIK. *VDI 3834 – Acceptance criteria for vibration levels*. `http://www2.pruftechnik.com`. [Online; accessed 22-May-2015]. 2015 (cit. on p. 29).

[RA11] R. B. Randall and J. Antoni. "Rolling element bearing diagnostics—A tutorial". In: *Mechanical Systems and Signal Processing* 25.2 (Feb. 2011), pp. 485–520 (cit. on pp. 54, 55, 57, 68, 70, 121, 179).

[Raf+07] J. Rafiee, F. Arvani, A. Harifi, and M. H. Sadeghi. "Intelligent condition monitoring of a gearbox using artificial neural network". In: *Mechanical Systems and Signal Processing* 21.4 (May 2007), pp. 1746–1754 (cit. on p. 12).

[Rai+08] R. Raišutis, E. Jasiūnienė, R. Šliteris, and A. Vladišauskas. "The review of non-destructive testing techniques suitable for inspection of the wind turbines blades". In: *Ultragarsas (Ultrasound)* 63.1 (2008), pp. 26–30 (cit. on p. 12).

[Ran11] R. B. Randall. *Vibration-based Condition Monitoring*. Chichester, UK: John Wiley & Sons, Ltd, Jan. 2011 (cit. on pp. 1, 9, 15–18, 54, 56, 164).

[RCP96] J. C. Robinson, R. G. Canada, and K. R. Piety. "Vibration monitoring on slow speed machinery: new methodologies covering machinery from 0.5 to 600 RPM". In: *Proceedings of the Fifth International Conference on Profitable Condition Monitoring Fluids and Machinery Performance Monitoring. UK: Mechanical Engineering Publications Limited*. 1996, pp. 169–181 (cit. on p. 12).

[RCS14a] R. B. Randall, M. Coats, and W. Smith. "Bearing diagnostics under widely varying speed conditions". In: *4th International Conference on Condition Monitoring of Machinery in Non-Stationary Operations (CMMNO'2014)*. Lyon, France, 2014 (cit. on p. 68).

[RCS14b] R. B. Randall, M. Coats, and W. Smith. "Gear diagnostics under widely varying speed conditions". In: *4th International Conference on Condition Monitoring of Machinery in Non-Stationary Operations (CMMNO'2014)*. Lyon, France, 2014 (cit. on p. 68).

[RJv08] R. Raišutis, E. Jasiūnienė, and E. Žukauskas. "Ultrasonic NDT of wind turbines blades using guided waves". In: *Ultrasound, Technologija, Kaunas* 63 (2008), pp. 7–11 (cit. on p. 12).

[RM01] M. A. Rumsey and W. Musial. "Application of infrared thermography nondestructive testing during wind turbine blade Tests". In: *Journal of Solar Energy Engineering* 123.4 (2001), p. 271 (cit. on p. 13).

[RSC12] R. B. Randall, N. Sawalhi, and M. D. Coats. "Separation of Gear and Bearing Fault Signals from a Wind Turbine Transmission under Varying Speed and Load". In: *Proceedings of the Second International Conference "Condition Monitoring of Machinery in Non-Stationnary Operations" CMMNO'2012*. Hammamet, Tunisia: Springer Berlin Heidelberg, 2012, pp. 3–12 (cit. on pp. 12, 14).

[Sch15] Schaeffler. *Performance, efficiency, intelligence – rolling bearings are at the heart of new trends in technology and products*. `http://www.schaeffler.de/`. [Online; accessed 19-June-2015]. 2015 (cit. on p. 11).

[SF84] N. S. Swansson and S. C. Favaloro. *Applications of Vibration Analysis to the Condition Monitoring of Rolling Element Bearings, Volume 163 of Aero propulsion report*. Aeronautical Research Laboratories, 1984 (cit. on p. 22).

[SL99] D. C. Seo and J. J. Lee. "Damage detection of CFRP laminates using electrical resistance measurement and neural network". In: *Composite Structures* 47 (1999), pp. 525–530 (cit. on p. 13).

[Slo01] G. R. Slone. *The audiophile's project sourcebook*. McGraw-Hill/TAB Electronics, Jan. 2001 (cit. on p. 38).

[Smi+93] G. M. Smith, B. R. Clayton, A. G. Dutton, and A. D. Irving. "Infra-red thermography for condition monitoring of composite wind turbine blades feasibility studies using cyclic loading tests". In: *15th British Wind Energy Association Conference (BWEA15)*. York, UK, 1993 (cit. on p. 13).

[Sor+02] B. F. Sorensen, L. Lading, P. Sendrup, M. McGugan, C. Debel, O. J. D. Kristensen, G. Larsen, A. M. Hansen, J. Rheinländer, J. Rusborg, and J. D. Vestergaard. "Fundamentals for remote structural health monitoring of wind turbines blades - A Preproject". In: *Riso-R-1336(EN)* (2002) (cit. on pp. 12, 13).

[Sou+12] D. B. de Souza, J. Chanussot, A. Favre, and P. Borgnat. "A modified time-frequency method for testing wide-sense stationarity". In: *Acoustics, Speech and Signal Processing (ICASSP), 2012 IEEE International Conference on*. Mar. 2012, pp. 3409–3412 (cit. on p. 42).

[SP05] P. D. Samuel and D. J. Pines. "A review of vibration-based techniques for helicopter transmission diagnostics". In: *Journal of Sound and Vibration* 282.1–2 (2005), pp. 475 –508 (cit. on pp. 24, 68).

[SSE11] A. S. Sait and Y. I. Sharaf-Eldeen. "A Review of Gearbox Condition Monitoring Based on vibration Analysis Techniques Diagnostics and Prognostics". English. In: *Rotating Machinery, Structural Health Monitoring, Shock and Vibration, Volume 5*. Ed. by T. Proulx. Conference Proceedings of the Society for Experimental Mechanics Series. Springer New York, 2011, pp. 307–324 (cit. on pp. 24, 25).

[ST02] Q. Sun and Y. Tang. "Singularity analysis using continuous wavelet transform for bearing fault diagnosis". In: *Mechanical Systems and Signal Processing* 16.6 (2002), pp. 1025–1041 (cit. on p. 12).

[Str+15] M. Strączkiewicz, P. Wiciak, A. Jabłoński, and T. Barszcz. "Machinery in highly changing working conditions: on designation of operational modes". In: *The Twelfth International Conference on Condition Monitoring and Machinery Failure Prevention Technologies, from sensors through diagnostics and prognostics to maintenance. CM 2015 and MFPT 2015*. Oxford, United Kingdom, June 2015 (cit. on p. 14).

[Sun+05] Q. Sun, Y. Tang, W. Yang, and Y. Ji. "Feature extraction with discrete wavelet transform for drill wear monitoring". In: *Journal of Vibration and Control* 11 (2005), pp. 1375–1396 (cit. on p. 12).

[SZB15] S. Sieg-Zieba and N. Bédouin. "Endurance testing on a wind turbine testbench. A focus on slow rotating bearing monitoring". In: *Tenth International Conference on Condition Monitoring and Machinery Failure Prevention Technologies. CM 2015 and MFPT 2015*. Oxford, United Kingdom, June 2015 (cit. on p. 83).

[Szc89] A. Szczepanik. "Time synchronous averaging of ball mill vibrations". In: *Mechanical Systems and Signal Processing* 3.1 (1989), pp. 99–107 (cit. on p. 25).

[Tch+13] P. Tchakoua, R. Wamkeue, T. A. Tameghe, and G. Ekemb. "A review of concepts and methods for wind turbines condition monitoring". In: *2013 World Congress on Computer and Information Technology (WCCIT)* 2.1 (2013), pp. 1–9 (cit. on p. 13).

[TJ11] Z. Tian and T. Jin. "Maintenance of wind turbine systems under continuous monitoring". In: *2011 Proceedings - Annual Reliability and Maintainability Symposium* (2011) (cit. on p. 13).

[TN90] N. Tandon and B. C. Nakra. "Defect detection in rolling element bearings by acoustic emission method". In: *Journal of Acoustic Emission* 9.1 (1990), pp. 25–28 (cit. on p. 12).

[TN92] N. Tandon and B. C. Nakra. "Comparison of vibration and acoustic measurement techniques for the condition monitoring of rolling element bearings". In: *Tribology International* 25.3 (1992), pp. 205–212 (cit. on pp. 12, 13).

[Tom98] L. A. Toms. "Machinery oil analysis: methods, automation and benefits". In: *Coastal* (1998) (cit. on p. 12).

[Tow97] D. P. Townsend. "Gear and Transmission Research at NASA Lewis Research Center". In: *Congresso Internazionale della Trasmissione di Potenza '97*. Milano, Italy, June 1997 (cit. on pp. 24, 68).

[TPY01] P. W. Tse, Y. H. Peng, and R. Yam. "Wavelet analysis and envelope detection for rolling element bearing fault diagnosis-their effectiveness and Flexibilities". In: *ASME Journal of Vibration and Acoustics* 123 (2001), pp. 303–310 (cit. on p. 12).

[TT02] A. Todoroki and Y. Tanaka. "Delamination identification of cross-ply graphiteeepoxy composite beams using electric resistance change method". In: *Composites Science and Technology* 62 (2002), pp. 629–639 (cit. on p. 13).

[TTM05] T. Toutountzakis, C. K. Tan, and D. Mba. "Application of acoustic emission to seeded gear fault detection". In: *NDT and E International* 38.1 (Jan. 2005), pp. 27–36 (cit. on p. 12).

[UBA13] J. Urbanek, T. Barszcz, and J. Antoni. "A two-step procedure for estimation of instantaneous rotational speed with large fluctuations". In: *Mechanical Systems and Signal Processing* 38.1 (July 2013), pp. 96–102 (cit. on p. 14).

[VKŠ05] P. Večeř, M. Kreidl, and R. Šmíd. "Condition Indicators for Gearbox Condition Monitoring Systems". In: *Acta Polytechnica* 45.6 (2005), pp. 35–43 (cit. on pp. 24, 25).

[VPD05] W. Van Paepegem and J. Degrieck. "Simulating damage and permanent strain in composites under in-plane fatigue loading". In: *Computers and Structures* 83 (2005), pp. 1930–1942 (cit. on p. 12).

[Wer+04] J. Wernicke, J. Shadden, S. Kuhnt, R. Byars, P. Rhead, and M. Damaschke. "Field experience of fibre optical strain sensors for providing real time load information from wind turbine blades during operation". In: *Paper presented at the European wind energy conference*. November, London, UK, 2004, pp. 22–25 (cit. on p. 12).

[Wis94] N. J. Wismer. *Gearbox analysis using cepstrum analysis and comb liftering*. `http://www.bruelkjaer.de/doc/bo0440.pdf`. Application Note Brüel & Kjaer. Denmark, 1994 (cit. on p. 12).

[WM93] J. Wei and J. McCarty. "Acoustic emission evaluation of composite wind turbine blades during fatigue testing". In: *Wind Engineering* 17.6 (1993), pp. 266–274 (cit. on p. 12).

[WM96] W. J. Wang and P. D. McFadden. "Application of wavelets to gearbox vibration signals for fault detection". In: *Journal of Sound and Vibration* 192 (1996), pp. 927–939 (cit. on p. 12).

[WST07] M. R. Wilkinson, F. Spinato, and P. J. Tavner. "Condition monitoring of generators & other subassemblies in wind turbine drive trains". In: *2007 IEEE International Symposium on Diagnostics for Electric Machines, Power Electronics and Drives, SDEMPED*. IEEE, Sept. 2007, pp. 388–392 (cit. on p. 12).

[Wu+09] J.-D. Wu, M. R. Bai, F.-C. Su, and C.-W. Huang. "An expert system for the diagnosis of faults in rotating machinery using adaptive order-tracking algorithm". In: *Expert Systems with Applications* 36.3 (Apr. 2009), pp. 5424–5431 (cit. on p. 14).

[WW04] Z. J. Wang and P. Willett. "Joint Segmentation and Classification of Time Series Using Class-Specific Features". In: *IEEE Transactions on Systems, Man, and Cybernetics, Part B: Cybernetics* 34.2 (2004), pp. 1056–1067 (cit. on p. 42).

[Yan+08] W. Yang, P. J. Tavner, C. J. Crabtree, and M. Wilkinson. "Research on a simple, cheap but globally effective condition monitoring technique for wind turbines". In: *Proceedings of the 2008 International Conference on Electrical Machines, ICEM'08* (2008) (cit. on p. 13).

[YCJ13] W. Yang, R. Court, and J. Jiang. "Wind turbine condition monitoring by the approach of SCADA data analysis". In: *Renewable Energy* 53 (May 2013), pp. 365–376 (cit. on p. 13).

[YSM03] D.-M. Yang, A. F. Stronach, and P. Macconnell. "The Application of Advanced Signal Processing Techniques to Induction Motor Bearing Condition Diagnosis". In: *Meccanica* 38 (2003), pp. 297–308 (cit. on p. 12).

[YT09] W. Yang and P. J. Tavner. "Empirical mode decomposition, an adaptive approach for interpreting shaft vibratory signals of large rotating machinery". In: *Journal of Sound and Vibration* 321.3-5 (Apr. 2009), pp. 1144–1170 (cit. on p. 12).

[YTC13] W. Yang, P. J. Tavner, and R. Court. "An online technique for condition monitoring the induction generators used in wind and marine turbines". In: *Mechanical Systems and Signal Processing* 38.1 (July 2013), pp. 103–112 (cit. on p. 13).

[Zha+14] M. Zhao, J. Lin, X. Xu, and X. Li. "Multi-Fault Detection of Rolling Element Bearings under Harsh Working Condition Using IMF-Based Adaptive Envelope Order Analysis". In: *Sensors* 14.11 (2014), pp. 20320–20346 (cit. on p. 12).

[Zhe+08] L. Zhen, H. Zhengjia, Z. Yanyang, and C. Xuefeng. "Bearing condition monitoring based on shock pulse method and improved redundant lifting scheme". In: *Mathematics and Compuers in Simulation* 79.3 (2008), pp. 318–338 (cit. on p. 13).

[Zhu+14] J. Zhu, T. Nostrand, C. Spiegel, and B. Morton. "Survey of Condition Indicators for Condition Monitoring Systems". In: *Annual Conference of the Prognostics and Health Management Society* 5 (2014) (cit. on p. 68).

[Zil06] E. R. Zilberman. "Autonomous time-frequency cropping and feature-extraction algorithms for classification of LPI radar modulations". MA thesis. 2006 (cit. on p. 42).

[Zim+14] R. Zimroz, W. Bartelmus, T. Barszcz, and J. Urbanek. "Diagnostics of bearings in presence of strong operating conditions non-stationarity - A procedure of load-dependent features processing with application to wind turbine bearings". In: *Mechanical Systems and Signal Processing* 46.1 (2014), pp. 16–27 (cit. on p. 12).

[ZM07] A. S. Zaher and S. D. J. McArthur. "A multi-agent fault detection system for wind turbines defect recognition and diagnosis". In: *Proceedings IEEE Lausanne POWERTECH 2007*. Lausanne, Switzerland, 2007, pp. 22–27 (cit. on p. 13).

[ZW01] G. T. Zheng and W. J. Wang. "A new cepstral analysis procedure of recovering excitations for transient components of vibration signals and applications to rotating machinery condition monitoring". In: *ASME Journal of Vibration and Acoustics* 123 (2001), pp. 222–229 (cit. on p. 12).

[EWE15] EWEA – European Wind Energy Association. *Wind in power: 2014 European statistics*. `http://www.ewea.org/statistics/`. [Online; accessed 22-May-2015]. 2015 (cit. on p. 6).

[GWE14] GWEC – Global Wing Energy Council. *Global Wind Report. Annual Market Update 2013*. `http://www.gwec.net/`. [Online; accessed 22-May-2015]. 2014 (cit. on p. 14).

[GWE15] GWEC – Global Wind Energy Council. *Wind in numbers, Global Offshore*. `http://www.gwec.net/`. [Online; accessed 22-May-2015]. 2015 (cit. on pp. 6, 8).

[Goo15] Google Maps. *Arfons*. `https://goo.gl/maps/tXcP8pYAur12`. [Online; accessed 12-October-2015]. 2015 (cit. on pp. 89, 169).

[ISO b] ISO – International Organization for Standardization. *Condition monitoring and diagnostics of wind turbines – Part 1: General guidelines*. ISO 16079-1. to be published (cit. on p. 29).

[ISO02] ISO – International Organization for Standardization. *Condition monitoring and diagnostics of machines – Vibration condition monitoring – Part 1: General procedures*. ISO 13373-1:2002. Feb. 2002 (cit. on p. 29).

[ISO04] ISO – International Organization for Standardization. *Rolling bearings – Damage and failures – Terms, characteristics and causes*. ISO 15243. 2004 (cit. on p. 19).

[ISO05] ISO – International Organization for Standardization. *Condition monitoring and diagnostics of machines – Vibration condition monitoring – Part 2: Processing, analysis and presentation of vibration data*. ISO 13373-2:2005. July 2005 (cit. on p. 29).

[ISO11] ISO – International Organization for Standardization. *Condition monitoring and diagnostics of machines – General guidelines*. ISO 17359:2011. Apr. 2011 (cit. on p. 30).

[ISO12] ISO – International Organization for Standardization. *Condition monitoring and diagnostics of machines – Data interpretation and diagnostics techniques – Part 1: General guidelines*. ISO 13379-1:2012. May 2012 (cit. on p. 30).

[ISO15a] ISO – International Organization for Standardization. *Condition monitoring and diagnostics of machines – Data interpretation and diagnostics techniques – Part 2: Data-driven applications*. ISO 13379-2:2015. Apr. 2015 (cit. on p. 30).

[ISO15b] ISO – International Organization for Standardization. *Mechanical vibration – Evaluation of machine vibration by measurements on non-rotating parts – Part 21: Horizontal axis wind turbines with gearbox*. ISO 10816-21:2015. May 2015 (cit. on p. 27).

[ISO95] ISO – International Organization for Standardization. *Gears – Wear and damage to gear teeth – Terminology*. ISO 10825. 1995 (cit. on p. 21).

[Ken15] Kent Wind Energy. *Building an offshore wind farm*. `http://www.kentwindenergy.co.uk/`. [Online; accessed 19-June-2015]. 2015 (cit. on p. 10).

[The15] The U.S. Energy Department. *Wind Turbine Basics*. `http://energy.gov`. [Online; accessed 22-May-2015]. 2015 (cit. on p. 30).

[VDI14] VDI – Fachbereich Schwingungstechnik. *Measurement and evaluation of the mechanical vibration of wind turbines and their components – Part 1: Wind turbines with gearbox*. VDI 3844. Sept. 2014 (cit. on pp. 27, 28).

[WWE14a] WWEA – World Wind Energy Association. *Half-year Report 2014*. `http://www.wwindea.org/wwea-publishes-half-year-report-2014/`. [Online; accessed 22-May-2015]. 2014 (cit. on pp. 5, 6).

[WWE14b] WWEA – World Wind Energy Association. *World Wind Energy Report 2013*. `http://www.wwindea.org/wwec2014-key-statistics-of-world-wind-energy-report-published/`. [Online; accessed 22-May-2015]. 2014 (cit. on p. 7).

Appendix A

List of Publications

Conference papers:

[1] C. Pachaud, T. Gerber, M. Firla, N. Martin, C. Mailhes (2013). "Consequences of non-respect of the Bedrosian theorem when demodulating", The Tenth International Conference on Condition Monitoring and Machinery Failure Prevention Technologies. CM 2013, Jun 2013, Kraków, Poland.

[2] M. Firla, Z.-Y. Li, N. Martin, T. Barszcz (2014). "Automatic and Full-band Demodulation for Fault Detection – Validation on a Wind Turbine Test Rig", 4th International Conference on Condition Monitoring of Machinery in Non-Stationary Operations (CMMN0'2014), Dec 2014, Lyon, France.

[3] Z.-Y. Li, T. Gerber, M. Firla, P. Bellemain, N. Martin, C. Mailhes (2015). "AStrion strategy: from acquisition to diagnosis. Application to wind turbine monitoring", The Twelve International Conference on Condition Monitoring and Machinery Failure Prevention Technologies. CM 2015, Jun 2015, Oxford, United Kingdom.

Journal papers:

[1] Z.-Y. Li, T. Gerber, M. Firla, P. Bellemain, N. Martin, C. Mailhes (2015). "AStrion strategy: from acquisition to diagnosis. Application to wind turbine monitoring", Insight – Non-Destructive Testing and Condition Monitoring, Volume 57, Number 8, August 2015, pp. 442-447(6).

[2] M. Firla, T. Gerber, P. Bellemain, N. Martin (2015). "Automatic Method for Spectral Pattern Association with Characteristic Frequencies", Diagnostyka, Vol. 16, No.4.

[3] M. Firla, Z.-Y. Li, N. Martin, C. Pachaud, and T. Barszcz (2015). "Automatic Characteristic Frequency Association and All-Sideband Demodulation for Detection of a Bearing Fault of a Wind Turbine Test Rig", submitted to Mechanical Systems and Signal Processing (MSSP).

Appendix B

French Summary – Résumé en français (French)

B.1 Introduction

Le développement rapide des technologies de l'information est omniprésent. L'utilisation des méthodes numériques de traitement du signal a permis d'introduire des techniques complexes post-traitement. L'état de la technologie actuelle permet d'utiliser des composés et CPU exigeants des algorithmes dans des systèmes de traitement du signal en temps réel. Ces circonstances ouvrent la possibilité pour la mise en œuvre de méthodes avancées de traitement du signal. Cette thèse présente une tentative d'utiliser des algorithmes avancés de traitement du signal pour la surveillance de la santé des machines.

Cette thèse propose une nouvelle approche pour le traitement de signal vibratoire dans le but d'aider les opérateurs de machines à la surveillance des composants mécaniques cruciales dans une usine. Parfois, il est nécessaire de surveiller des nombreux systèmes ou composants comme c'est le cas des grands parcs éoliens. Ce contexte requiert un haut niveau d'automatisation des systèmes de surveillance. Cette automatisation est déjà mise en œuvre à un niveau simple de contrôle et d'acquisition des données SCADA (*ang. supervisory control and data acquisition*) des systèmes ou des systèmes de surveillance d'état, mais en général seulement des simples méthodes de diagnostic sont adoptées. L'objectif de cette thèse est de proposer une extension des capacités des systèmes de surveillance actuelles en les combinant avec des méthodes de traitement de signal avancées. Le but est de pouvoir effectuer un diagnostic vibratoire précis sans l'aide d'expert en vibrations. La mise en œuvre d'algorithmes complexes et adaptatifs de traitement du signal dans les systèmes actuels de surveillance ouvre la possibilité d'effectuer une analyse sophistiquée sans augmenter la charge de travail pour les opérateurs et les équipes de maintenance.

L'objectif principal de cette thèse est de proposer des algorithmes pour l'étape de traitement des données de la stratégie de maintenance conditionnelle. Le lien entre l'industrie et l'académie révèle la nécessité d'une amélioration des systèmes de surveillance. Cette recherche est axée sur un cas particulier de système de surveillance d'état, c'est-à-dire les éoliennes. L'industrie éolienne a des marges financières très faibles, de sorte qu'elle est en constant besoin de diminuer le coût de la production d'énergie. L'un des aspects à améliorer est le coût

d'exploitation et d'entretien des éoliennes. Grâce aux possibilités techniques et à des algorithmes de traitement du signal avancés, il est maintenant possible de détecter les premiers symptômes des défauts, principalement les défauts de composants mécaniques tels que les roulements et boîtes de vitesses. Plus tôt les informations sur les défauts à venir sont fournies aux opérateurs d'éoliennes, la meilleure est la réparation. Cette situation apporte des avantages économiques, d'où son intérêt dans le développement de la technologie de l'industrie. Le monde universitaire est en mesure de proposer des solutions pour ce problème et cette thèse propose une réponse aux besoins de l'industrie.

Cette thèse propose le développement de techniques avancées de traitement du signal sur trois aspects, tous dédiés, mais non limités à la surveillance et le diagnostic de l'état des systèmes mécaniques. Le fonctionnement automatique et guidés par les données sont les points communs des méthodes proposées. Chaque algorithme a été conçu comme un outil convivial et auto-configure avec un paramétrage minimum, de sorte que chaque méthode peut être utilisé même par un non-expert en traitement du signal.

La première méthode proposée vise à faciliter le diagnostic et la surveillance de l'état des machines qui travaillent dans des conditions non-stationnaires. C'est nécessaire pour les machines fonctionnant avec des conditions variables. La solution consiste à "rogner" une représentation temps-fréquence en utilisant un détecteur des non-stationnarités. L'approche est fondée sur une recherche itérative à travers la représentation temps-fréquence du signal et elle est adaptée pour des signaux vibratoires. Cette méthode permet de sélectionner la partie stationnaire des signaux vibratoires et peut être appliquée dans des systèmes de surveillance et de diagnostic.

Une connaissance des fréquences caractéristiques d'un système analysé est toujours un avantage dans la surveillance et le diagnostic d'un système. Par conséquent, il existe un besoin pour une utilisation automatique de ces informations. Le deuxième algorithme proposé est l'association automatique des fréquences caractéristiques de défaut selon une configuration cinématique de la machine analysée avec les pics détectés précédemment. L'approche proposée est adaptative et dispose d'une association unique de données cinématiques avec les structures spectrales identifiées dans un signal. En outre, l'avantage de la méthode consiste à prendre en compte le glissement dans les roulements, une question qui n'a pas encore été abordée dans les systèmes de surveillance.

La démodulation est une technique puissante pour le diagnostic de la santé de la machine. Cependant, les solutions existantes pour son utilisation dans les systèmes de surveillance n'adaptent pas au contenu du signal. C'est pour cette raison que cette thèse propose une troisième technique de traitement du signal qui est un processus de démodulation de toutes les bandes latérales. Pour chaque série de bandes latérales détectée dans le signal étudié, une procédure automatique de démodulation est proposée et le signal est démodulée sur toute sa bande spectrale. Cette méthode consiste en un processus de filtrage à plusieurs cadences d'échantillonnage, un moyennage synchrone et le calcul des fonctions de modulation d'amplitude et de fréquence ainsi que le calcul des indicateurs de santé qui décrivent l'état du système étudié qui a pour but de détecter les défauts.

La thèse commence, dans le chapitre 1, avec un aperçu général des sujets liés à la surveillance des systèmes et le diagnostic de machines. Ce chapitre est concentré principalement sur l'application aux composants mécaniques des éoliennes comme les roulements, les boîtes de vitesses et les arbres. La description des dysfonctionnements et des défauts les plus courantes est donnée. Par la suite, une description exhaustive des méthodes de détection de défaut est présentée. Elle donne une liste des indicateurs populaires utilisés dans les systèmes de surveillance. Ce chapitre comprend également la description des normes utilisées dans l'industrie. Le chapitre 1 finit par la description des approches de détection de défaut utilisées dans les système de surveillance et la description la plus populaire des installations existantes de la configuration des éoliennes.

Le chapitre 2 présente l'approche de traitement du signal en cours de développement à GIPSA-Lab. Denommée AStrion elle est caractérisée par les algorithmes guidés directement par les données. Elle consiste en une l'interprétation du signal en fonction de son contenu spectral. Les résultats d'interprétation de signaux sont utilisés pour un traitement ultérieur. Ceci est la raison pour laquelle les résultats des étapes précédemment développés d'AStrion sont une partie importante de ce travail et sont utilisés comme une entrée pour les méthodes proposées. AStrion est composé d'une ètage de validation du signal [MM09]; [MM10], puis d'une interpretation [Dur99] et d'une identification des structures spectrales [GMM13]; [MMG13]. En plus, un ré-échantillonnage angulaire [Fir+14] est intégré à AStrion pour faciliter l'interprétation et le suivi des données acquises dans différentes conditions opérationnelles. Ce chapitre met l'accent sur les résultats de l'interprétation des signaux qui sont utilisés comme entrée pour les techniques de traitement du signal proposées.

Le premier algorithme proposé, le "rognage" de la représentation temps-fréquence, est présenté dans le chapitre 3. Le deuxième algorithm, l'association de cinématique, est détaillé dans le chapitre 4. La dernière méthode de traitement du signal, la démodulation de toutes les bandes de modulation, est proposée dans le chapitre 5. Toutes les méthodes de traitement du signal proposées sont validées sur les signaux réels provenant de sources diverses. Ces validations sont présentés dans le chapitre 6. La thèse finit avec un résumé présenté dans le chapitre "Conclusions and Perspectives". Les avantages des algorithmes proposés sont énumérés avec les perspectives pour l'avenir.

B.2 Proposition des 3 méthodes automatiques pour le traitement du signal

Cette section résume brièvement l'idée principale des trois méthodes proposées. Cette description est simplifiée et vise à donner une vue d'ensemble des techniques proposées. Les chapitres correspondants dans le manuscrit fournissent une description détaillée de ces méthodes.

B.2.1 AStrion-C

Les signaux non-stationnaires sont toujours présents dans les applications réelles. Certaines non-stationnarités peuvent être causées par l'état de fonctionnement ou la présence d'un défaut. Cependant, une non-stationnarité du signal trop élevée peut rendre l'interprétation automatique impossible. Il est aussi nécessaire de sélectionner une zone du signal qui est stationnaire. Une nouvelle approche pour le "rognage" de la représentation temps-fréquence est appelée AStrion-C. Tous les détails sont décrits dans le chapitre 3.

La méthode proposée recherche de une manière itérative une zone de la représentation temps-fréquence grâce aux resulatats de la détection de non-stationnarités dans un spectrogramme, partie des résultats d'AStrion-D [MM09]; [Mar05].

Un exemple des non-stationnarités détectés par AStrion-D est représenté sur la figure B.1.

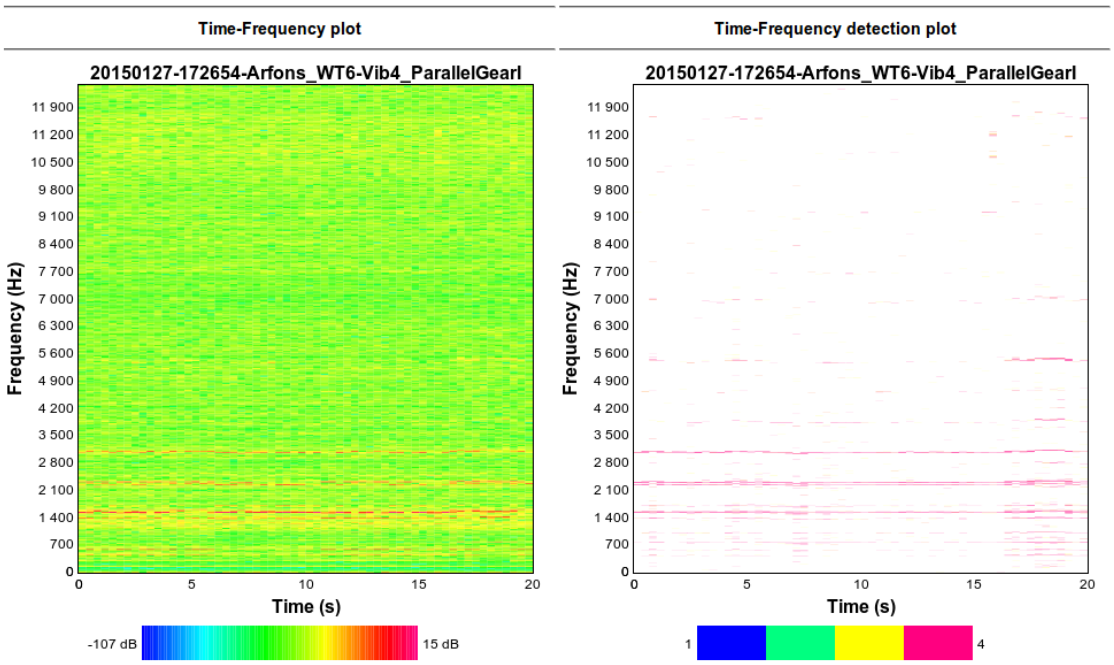

(a) Spectrogramme (b) Des non-stationnarités détectées

Figure B.1: Un example de (a) spectrogramme calculé par AStrion-D et (b) des non-stationnarités détectées dans le signal.

Tous les parties correspondants à des événements non-stationnaires dans la représentation temps-fréquence du signal sont détectés par AStrion-D, comme cela est illustré sur la figure B.1 (b). Cette thèse propose un traitement supplémentaire afin d'en extraire une zone temps-fréquence qui a un indice de stationnarité inférieur. Cet indice est défini par AStrion-D pour décrire le niveau de stationnarité de signal.

Pour assurer un temps de calcul raisonnable des hypothèses sur le signal à l'étude ont été faites. Tout d'abord, les segments de fréquence sélectionnées commencent toujours à partir de la fréquence minimale égale à 0 Hz. Cette sélection est faite en raison de la nature des signaux vibratoires, qui sont l'objet de cet étude. En outre, cette restriction assure que le temps de calcul est fortement réduit par la méthode itérative proposée. En plus, la zone sélectionnée doit être rectangulaire. Troisièmement, le nombre minimal de segments temporel doit être fixé. Cette valeur dépend de la résolution spectrale requise Δf du signal, qui dépend du système mécanique analysé. Enfin, le nombre minimal de segments fréquentiel doit être fixé. En règle générale, nous proposons d'utiliser au moins 10% du longueur du signal original et 5% de la plage de fréquences disponible (fréquence de Nyquist divisée par deux), mais ces valeurs peuvent être modifiées en fonction des besoins des utilisateurs.

L'objectif de la méthode proposée consiste à sélectionner la plus grande partie possible de la représentation temps-fréquence qui est stationnaire jusqu'à un certain niveau. La quantité T_i est utilisée comme mesure de la stationnarité de la région et elle est inspirée par la définition de l'indice de stationnarité proposé pour AStrion-D [MM09]. Selon le besoin de l'utilisateur le niveau acceptable de non-stationnarité, seuil T_S, peut être adapté et seule la zone qui répond à la condition

$$T_i \leq T_S \tag{B.1}$$

est considérée comme un résultat acceptable pour le "rognage". A la base des exemples testés le valeur de seuil T_S est fixé à 4%, ce qui permet de réduire la non-stationnarité du signal après l'opération de "rognage", ainsi que de préserver une durée suffisante du signal analysé.

L'algorithme itératif de sélection de la zone stationnaire du signal comporte deux boucles. La première sert à effectuer une itération à partir du temps pour la sélection de la zone du signal. La deuxième boucle est exécutée dans le cadre de la première et une itération à travers la représentation temps-fréquence pour sélectionner la plus grande zone qui remplit la condition d'un seuil T_S. Enfin, l'algorithme sélectionne la plus grande zone du signal entre tous les résultats sauvegardés de l'itération dans la première boucle. Ce résultat est utilisé pour le "rognage" du signal.

L'opération de "rognage" sur le signal est exécutée sans aucune application de filtre. Dans l'approche proposée, la première étape consiste à tronquer le signal dans la domaine temporel en fonction de la zone sélectionnée. L'étape suivante consiste à utiliser la bande de fréquence sélectionnée et d'analyser le signal seulement jusqu'à la fréquence évaluée, ce qui est possible dans AStrion.

Dans le chapitre 3 la validation de la méthode proposée sur un signal simulé est présentée. Cet exemple montre que l'algorithme proposé est capable de sélectionner une zone stationnaire d'un signal. En outre, la validation de l'algorithme proposée nous permet de l'intégrer dans l'ensemble de la méthodologie d'AStrion. AStrion-C peut donc être considéré comme un moyen de traiter automatiquement les signaux non-stationnaires, ce qui est une nécessité pour une utilisation dans un système automatique de surveillance.

B.2.2 AStrion-K

Une partie importante des systèmes de surveillance présents sur le marché est l'utilisation de l'information cinématique du système analysé. Les machines tournantes génèrent des modes de vibration qui sont liés à leur géométrie, il est donc possible de calculer une valeur théorique de la fréquence caractéristique de défaut d'un composant tournant. Les équations pour calculer ces valeurs sont présentés dans le tableau B.1, où f_r est la vitesse de l'arbre exprimée en Hz, z est le nombre de dents d'un engrenage, n_r est le nombre d'éléments roulants dans le roulement, d_r est le diamètre des éléments roulants, d_p est le diamètre primitif et ϕ est l'angle de la charge par rapport au plan radial.

Table B.1: Formules pour calculer les fréquences caractéristiques de défaut [Ran11].

Nom de fréquence de défaut	**Formule**
Arbre	
Vitesse fréquentielle de l'arbre	$SSF = f_r$
Boîte de vitesses	
Fréquence d'engrènement	$GMF = f_r \cdot z$
Roulement	
Fréquence du passage des billes sur la bague externe	$BPFO = \frac{n_r f_r}{2}\left\{1 - \frac{d_r}{d_p}cos(\phi)\right\}$
Fréquence du passage des billes sur la bague interne	$BPFI = \frac{n_r f_r}{2}\left\{1 + \frac{d_r}{d_p}cos(\phi)\right\}$
Fréquence fondamentale de la cage du roulement	$FTF = \frac{f_r}{2}\left\{1 - \frac{d_r}{d_p}cos(\phi)\right\}$
Fréquence de vitesse de rotation des billes	$BSF = \frac{f_r \cdot d_p}{2d_r}\left\{1 - \left(\frac{d_r}{d_p}cos(\phi)\right)^2\right\}$

Une approche standard dans le système de surveillance est d'utiliser directement les fréquences caractéristiques pour calculer les indicateurs de santé. Il n'y a pas de méthode qui applique les informations cinématiques seulement pour ajouter des informations à la série harmonique et la bande de modulation obtenue précédemment telle qu'elle est présentée dans la partie suivante.

Donc une méthode automatique d'associer des structures spectrales détectées précédemment dans un signal avec des fréquences caractéristiques de défaut est proposée et elle est appelée AStrion-K. Les détails de cette technique sont présentées au chapitre 4.

La méthode proposée pour l'utilisation de la cinématique est une approche guidée par les données. Elle nécessite une interprétation *a-priori* d'un contenu spectral d'un signal, ainsi qu'une identification des harmonique et des bandes latérales qui sont fournies par AStrion-IH effectué dans une étape précédente. L'algorithme proposé fait l'association des fréquences caractéristiques de défaut avec les séries harmoniques et les bandes latérales détectées précédemment. C'est un processus itératif, qui effectue une liaison avec chaque fréquence caractéristique fournies par la cinématique du système.

Dans l'étape préliminaire de cette méthode, les fréquences caractéristiques doivent être calculées pour chaque composant mécanique comme indiqué dans le tableau B.1. La vitesse de rotation et la liste des fréquences caractéristiques exprimées en ordre sont nécessaires. Les valeurs d'ordre proviennent de la méthode de ré-échantillonnage angulaire. Elles sont équivalentes aux fréquences caractéristiques calculées pour une vitesse de rotation égale à $1\ Hz$. Les valeurs d'ordre sont exprimées en *ordres*.

L'association des fréquences caractéristiques de défauts est effectuée en deux étapes. Premièrement, les séries harmoniques qui répondent à un critère sont identifiées comme candidats pour l'association. La seconde étape est la sélection d'un candidat final. Ces deux étapes sont exécutées de façon itérative pour la série harmonique et par la suite le même ensemble des opérations est effectuée sur la série des bandes de modulation.

Les détails de l'association sont différents pour les roulements et les autres composants. Dans tous les cas, l'étape d'identification des candidats est basée sur une différence relative entre la fréquence théorique f_t et la fréquence détectée f_d définie comme :

$$RFD_i = \left| \frac{f_{d,i} - f_{t,j}}{f_{t,j}} \right| \cdot 100\% < \eta, \tag{B.2}$$

où i est l'indice d'une série, j est l'indice d'une fréquence caractéristique calculée pour la configuration cinématique analysée, $f_{d,i}$ est la fréquence fondamentale de la série détectée, $f_{t,j}$ est la fréquence théorique basée sur la cinématique du système. Seulement les séries avec une valeur de RFD_i inférieure à un seuil η sont conservées. Dans le cas des arbres et des boîtes de vitesses η est égal à 1% de la fréquence théorique $f_{t,j}$, cependant pour les roulements, η est égal à 2%. Cette différence est due au phénomène de glissement dans le roulement et la justification détaillée est donnée dans le manuscrit.

Dans la deuxième étape de l'algorithme proposé la seule série parmi les candidats issus de l'étape précédent est sélectionnée. Dans le cas des fréquences des arbres et des boîtes de vitesse cette sélection est effectuée en fonction de la valeur du RFD. La série avec la valeur RFD la plus faible est sélectionnée. Cela ne suffit pas dans le cas de roulement et c'est pour cette raison que l'indice BSI (*ang. Bearing Selection Index*) est proposé dans la section 4.2. La série avec la valeur la plus grand de BSI est choisie. La série sélectionnée est associée à la fréquence caractéristique de défaut.

B.2.3 AStrion-M

La démodulation est appliquée avec succès dans la diagnostic de défaut des boîtes de vitesses et des roulements depuis des années. Les techniques de démodulation permettent pour la diagnostic précoce de défauts d'obtenir des informations utiles sur le contenu du signal. Ceci est une raison d'appliquer une telle technique dans les systèmes automatiques de surveillance. Ainsi, cette thèse propose une méthode de démodulation dérivée directement à partir des données.

Une fois les conditions sur le signal satisfaites, la modulation d'amplitude $A[n]$ et la modulation de phase $\Phi[n]$ peuvent être récupérées à partir du signal en utilisant la transformée de Hilbert. La fréquence instantanée de la modulation $F[n]$ peut être obtenue à partir du signal de phase $\Phi[n]$. Ainsi, la démodulation proposée effectue la démodulation d'amplitude et de fréquence .

Sur cette base, cette thèse propose l'algorithme de démodulation qui peut être décomposé en deux étapes. Dans la première étape, le signal est filtré avec une bande passante centrée sur la fréquence porteuse f_0, afin d'isoler les composantes spectrales pertinentes pour les phénomènes à analyser. Dans la deuxième étape, les fonctions de modulation d'amplitude et de modulation de fréquence sont calculés après moyennage synchrone. Enfin, certains indicateurs de santé sont proposés. Cette méthode de démodulation est appelée AStrion-M.

Afin d'obtenir la meilleure précision possible de la démodulation, un filtrage à plusieurs cadences d'échantillonnage est proposé dans AStrion-M. La méthode de filtrage vise à préserver l'ensemble de l'information spectrale dans une bande de fréquence $\mathbf{B}$

$$\mathbf{B} = [f_{inf}, f_{sup}], \tag{B.3}$$

où f_{inf} et f_{sup} sont les limites de fréquence inférieure et supérieure du filtre, respectivement, positives et en dessous de la fréquence de Shannon. La bande passante du filtre est définie comme $\Delta B = f_{sup} - f_{inf}$.

Le défi apparaît si la bande passante est très faible ou si la bande de filtre est très proche des fréquence extrêmes dans le spectre. La conception d'un filtre stable qui satisfait la performance souhaitée est difficile. Donc, nous proposons une nouvelle technique de filtrage qui décompose automatiquement une tâche de filtrage difficile en N_q itérations. Le filtre à plusieurs cadences d'échantillonnage se compose de trois opérations de base :

- un décalage de fréquence ;
- un filtre qui filtre sur la bande de filtre cible $\mathbf{B}_q$;
- un sous-échantillonnage qui décime le signal.

La méthode proposée est également un algorithme guidé directement à partir des données et les résultats des étapes précédentes d'AStrion sont utilisés. La bande passante du

Table B.2: Indicateurs de santé calculés à partir de l'amplitude $\hat{A}[\tau]$ et de la fréquence $\hat{F}[\tau]$ démodulée.

Moyenne	$\bar{A} = \frac{\sum_{\tau=1}^{T} \hat{A}[\tau]}{T}$	$\bar{F} = \frac{\sum_{\tau=1}^{T} \hat{F}[\tau]}{T}$
Crête-à-crête	$PP_A = max\hat{A}[\tau] - min\hat{A}[\tau]$	$PP_F = max\hat{F}[\tau] - min\hat{F}[\tau]$
Kurtosis	$Kurt_A = \frac{\left(\sum_{\tau=1}^{T} \hat{A}^4[\tau]\right)/T}{\left[\left(\sum_{\tau=1}^{T} \hat{A}^2[\tau]\right)/T\right]^2}$	$Kurt_F = \frac{\left(\sum_{\tau=1}^{T} \hat{F}^4[\tau]\right)/T}{\left[\left(\sum_{\tau=1}^{T} \hat{F}^2[\tau]\right)/T\right]^2}$
Indice de modulation	$MI_A = \frac{\max\{\hat{A}[\tau]\} - min\{\hat{A}[\tau]\}}{\bar{A}}$	$MI_F = \frac{\max\{\hat{F}[\tau]\} - min\{\hat{F}[\tau]\}}{\bar{F}}$

filtre est sélectionnée à partir de l'identification de bandes de modulation par AStrion-H. Par conséquent, la bande passante du filtre peut être choisie comme

$$\begin{aligned} f_{inf} &= f_0 + K_{inf} \times f_\Phi, \qquad K_{inf} \in \mathbb{Z}, K_{inf} < 0, \\ f_{sup} &= f_0 + K_{sup} \times f_\Phi, \qquad K_{sup} \in \mathbb{Z}, K_{sup} > 0, \end{aligned} \tag{B.4}$$

où K_{inf} est l'ordre le plus bas de bande latérale, et K_{sup} est l'ordre le plus élevé de bande latérale. La bande passante du filtre est proportionnelle à $(|K_{sup}|-|K_{inf}|)$. Le filtre à plusieurs cadences d'échantillonnage peut choisir automatiquement le nombre optimal d'itérations et les configurations optimales des opérations, ce qui est une avantage significatif.

Après l'opération de filtrage la moyenne synchrone est exécutée. En général, la période du signal obtenu par le filtre n'est pas un nombre entier de points par période. Par conséquent, le signal doit être ré-échantillonné avec une interpolation pour contenir un nombre entier de points par période, ce qui est une méthode classique [McF87a]. Le signal interpolé est ensuite traité par le algorithme de moyenne synchrone.

Le signal moyenné obtenu après filtrage peut être considéré comme à bande limitée et mono-composant, car il ne contient qu'une seule porteuse et ses bandes latérales associées. Par conséquent, une transformation d'Hilbert peut être appliquée pour donner un signal analytique [HR00]. Cette opération est effectuée pour obtenir l'amplitude $A[\tau]$ et la fréquence $F[\tau]$ démodulée.

Il est proposé d'utiliser les signaux démodulés dans le domaine temporel pour calculer les statistiques des indicateurs de santé. Le tableau B.2 montre les caractéristiques scalaires qui sont dérivés des fonctions démodulés $\hat{A}[\tau]$ et $\hat{F}[\tau]$. Ces valeurs constituent des indicateurs de défaut mécanique sachant qu'une modulation détectée dans un signal vibratoire a souvent une origine dans la détérioration des composants mécaniques.

Une autre étape exécute AStrion sur $\hat{A}[\tau]$ et $\hat{F}[\tau]$ est calcule le nombre de pics (PN_A et PN_F respectivement) et l'énergie (E_A et E_F respectivement) de la série harmonique, qui pos-

sède une fréquence fondamentale égale à la fréquence de modulation de la série de modulation analysée. Ces valeurs contribuent à deux indices de santé supplémentaires pour $\hat{A}[\tau]$ et $\hat{F}[\tau]$.

L'algorithme proposé est validé sur un signal simulé. AStrion-M est capable d'ajuster automatiquement plusieurs paramètres afin d'effectuer la démodulation et ensuite calculer les indices de santé. La méthode proposée a la capacité de gérer la démodulation de toutes les séries de modulation détectées quelle que soit un bande et malgré leur nombre important, ce qui pourrait être le cas pour les signaux réels. En plus, dans cette thèse la performance d'AStrion-M est illustrée sur des signaux réels.

B.3 Présentation des résultats

Cette section présente des résultats sélectionnés pour les méthodes proposées dans la thèse. Le choix a été fait pour se concentrer seulement sur les résultats obtenus à partir des signaux éoliens. Après une description d'une éolienne et une présentation des signaux sont discutés des résultats des méthodes proposées.

B.3.1 Données des éoliennes – Arfons

Arfons est une petite ville au sud de la France où se trouve un parc éolien Arfons-Sor. Ce parc appartient à Valorem et est sous la maintenance de Valemo, un partenaire du consortium de Projet d'Innovation KAStrion. Il y a 11 éoliennes à Arfons. La figure B.2 présente la situation du village et des éoliennes. Un prototype du système KAStrion est installé sur 2 éoliennes nommées WT6 et WT8 sur la figure B.2 (b).

Un exemple des éoliennes à Arfons est présenté sur la figure B.3 (a). Toutes les éoliennes installées à Arfons sont de type 80 2.0 ALSTOM Ecotècnia. Ces éoliennes sont capables de générer jusqu'à 2 MW, elles ont 80 m de diamètre du rotor, mesurent 70 m de haut et fonctionnent avec une vitesse du vent entre 3 m/s et 25 m/s. Ce type d'éolienne possède trois pâles avec la boîte de vitesse en ligne avec générateur. La boîte de vitesse des éoliennes à Arfons contient un train parallèle et deux engrenages parallèles. Les éléments mécaniques principaux de la transmission sont présentés sur la figure B.3 (b).

Toutes les données provenant des éoliennes à Arfons sont enregistrées par un prototype du système de surveillance KAStrion. Les paramètres des signaux vibratoires sont présentés dans le tableau B.3.

Le liste des fréquences caractéristiques provenant de la boîte de vitesse est présentée dans le tableau B.4 et celles provenant des roulements dans le tableau B.5. Ces deux tableaux contiennent des valeurs théorétiques calculés d'après le tableau B.1. Les valeurs sont relatives à la vitesse de l'arbre à grande vitesse égal à 1 Hz.

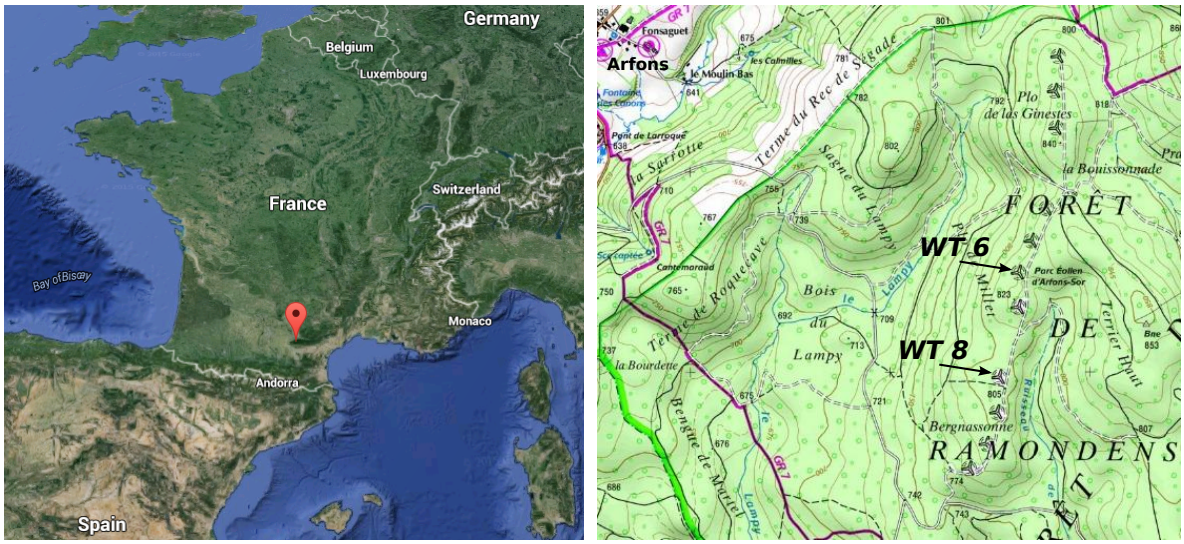

(a) Situation d'Arfons [Goo15] (b) Situation du parc éolien à Arfons

Figure B.2: Parc éolien à Arfons.

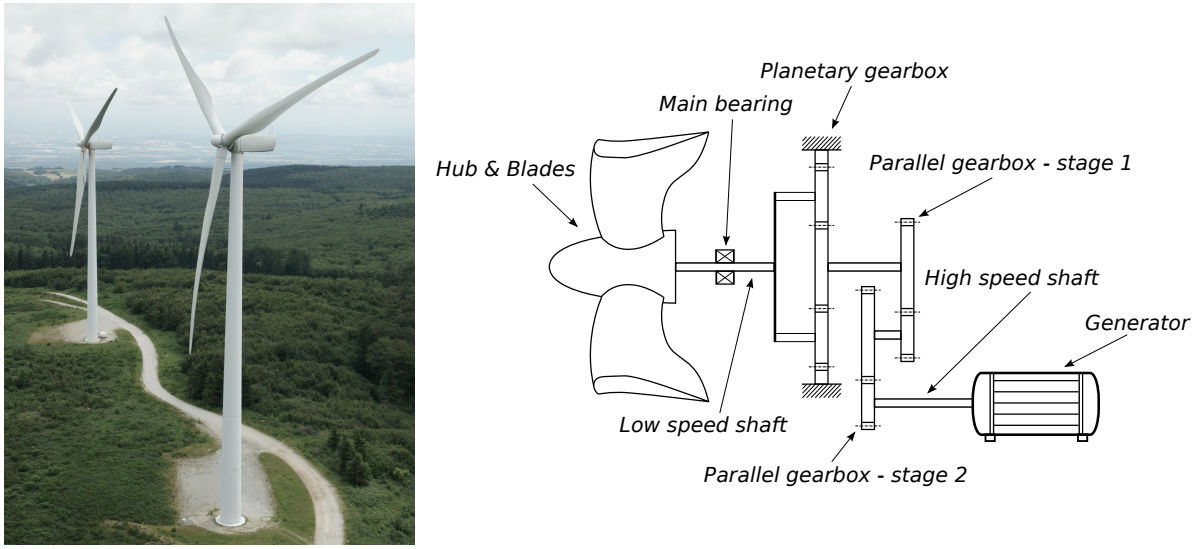

(a) Éoliennes à Arfons. (b) Les éléments mécaniques principaux de la transmission d'une éolienne à Arfons.

Figure B.3: Présentation des éoliennes à Arfons. (a) deux éoliennes dans le parc éolien et (b) la configuration cinematique de la transmission d'une éolienne.

Table B.3: Paramètres des signaux à Arfons.

Fréquence d'échantillonnage	$25,000\ Hz$
Durée du signal (dépend du capteur)	$10\ s - 60\ s$
Nombre d'échantillons	$250,000 - 1,500,000$

Table B.4: Fréquences caractéristiques des engrenages exprimées en *ordre*.

Nom d'élément	**Ordre**
Deux engrenages parallèles	
Fréquence d'engrènement – GMF (*ang. Gear Mesh Frequency*) – étage 2	26
Arbre à grande vitesse	1
Arbre intermédiaire	0.234234
Fréquence d'engrènement – GMF – étage 1	4.918919
Arbre coaxial	0.056539
Train parallèle	
Fréquence d'engrènement – GMF	0.885259
Engrenage satellite	0.015346
Arbre à petite vitesse	0.009947

Table B.5: Fréquences caractéristique des roulements exprimées en *ordre*. La fréquence de passage des billes sur la bague externe – BPFO (*ang. Ball Pass Frequency of Outer Race*) ; la fréquence de passage des billes sur la bague interne – BPFI (*ang. Ball Pass Frequency of Inner Race*) ; la fréquence fondamentale de cage du roulement à rouleaux – FTF (*ang. Fundamental Train Frequency*) ; la double fréquence de rotation des billes – BSF2 (*ang. Double Ball Spin Frequency*).

Nom de roulement	**BPFO**	**BPFI**	**FTF**	**BSF2**
Roulement de l'arbre générateur				
6330-MC3	3.57	5.43	0.4	2.32
Roulement de l'arbre à grande vitesse				
(59) NSK HR30326	6.15	8.85	0.41	2.64
Engrenage parallèle – étage 2				
(58) SKF NU 2328	5.68	8.32	0.405	5.1
(56) SKF NU238	1.909009	2.541441	0.100486	0.810496
Engrenage parallèle – étage 1				
(57) NSK HR30334	1.440541	2.072973	0.096036	0.618378
(55) SKF 6026	0.370954	0.477079	0.024708	0.444908
(53) SKF NJ2988	0.830904	0.978130	0.026008	0.701087
Train parallèle				
(51) SKF EE243190	1.334327	1.492637	0.972476	0.026687
(52) LB 3U240	0.001048	0.001509	0.000104	0.000686
Roulement de l'arbre à petite vitesse				
TIMKEN XC25695C	0.290721	0.316046	0.004765	0.113525
TIMKEN XC2364CA	0.215343	0.242219	0.004685	0.082162

B.3.2 Résultats d'AStrion-C

Cette section présente les résultats d'AStrion-C, une méthode pour le traitement du signal détaillée dans le chapitre 3, sur un signal réel acquis sur une éolienne à Arfons.

Les données vibratoires sont enregistrées par un accéléromètre situé sur le roulement principal de l'éolienne marquée comme WT6. Le signal dure 60 s avec une fréquence d'échantillonnage égale à $25,000$ Hz. A cause du temps de mesure, le signal a été enregistré avec une vitesse du vent variable. Ainsi, la vitesse de l'arbre à grande vitesse diminue. Le changement de la vitesse est significatif et diminue de 1800 RPM à 1550 RPM pendant 60 s. Ces signaux sont présentés sur la figure B.4.

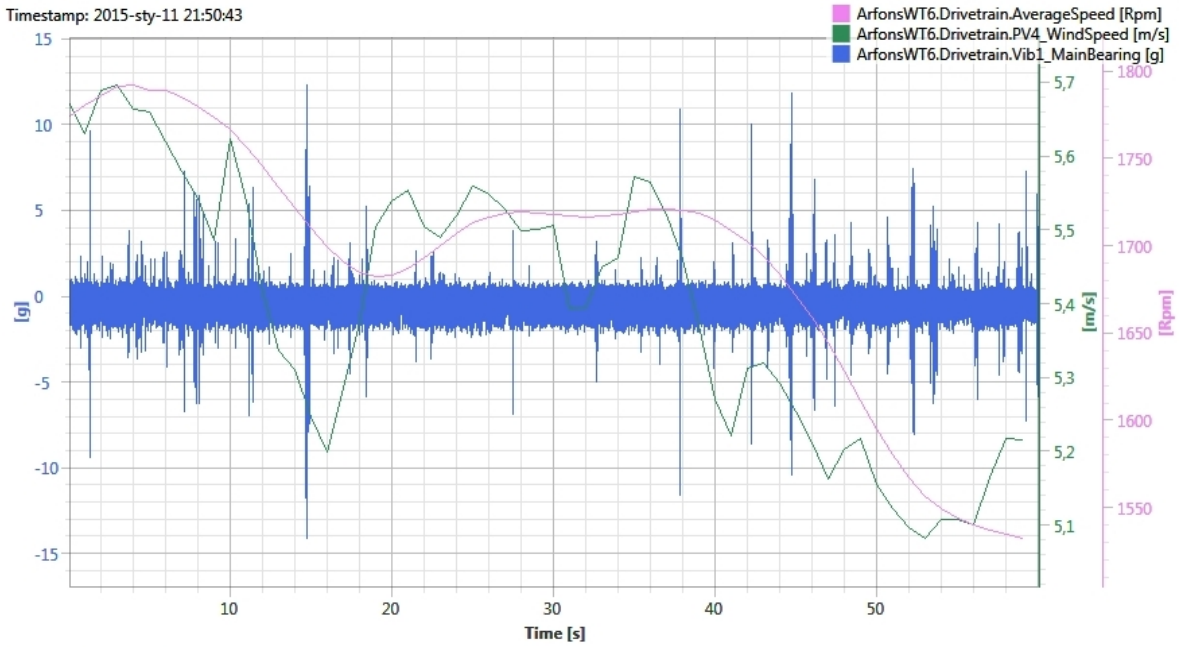

Figure B.4: Le signal vibratoire dans la domaine du temps (en bleu), la vitesse du vent (en vert) et la moyenne vitesse de l'arbre à grande vitesse (en rose).

Le signal est analysé deux fois, la première fois dans la domaine temporel et la deuxième fois dans le domaine angulaire après un ré-échantillonnage angulaire. La figure B.5 présente une superposition des signaux dans le domaine temporel et le domaine angulaire. Le ré-échantillonnage angulaire est réalisé avec le module AStrion-A (voir chapitre 2) et le signal obtenu est échantillonné avec 890 *ordres* et dure 1685 *rev.*.

La comparaison des spectres en basse fréquence et pour les ordres correspondants est présentée sur la figure B.6. Il est important de souligner qu'après le ré-échantillonnage angulaire du signal, certains éléments deviennent stationnaires. Par exemple, le tableau B.4 montre que c'est le cas pour la fréquence caractéristique correspondant au deuxième étage de l'engrenage parallèle égal à l'ordre 26, ce qui correspond à 780 Hz. La deuxième harmonique de cette GMF est plus facile à voir sur la figure B.6 et on peut voir le changement de fréquence

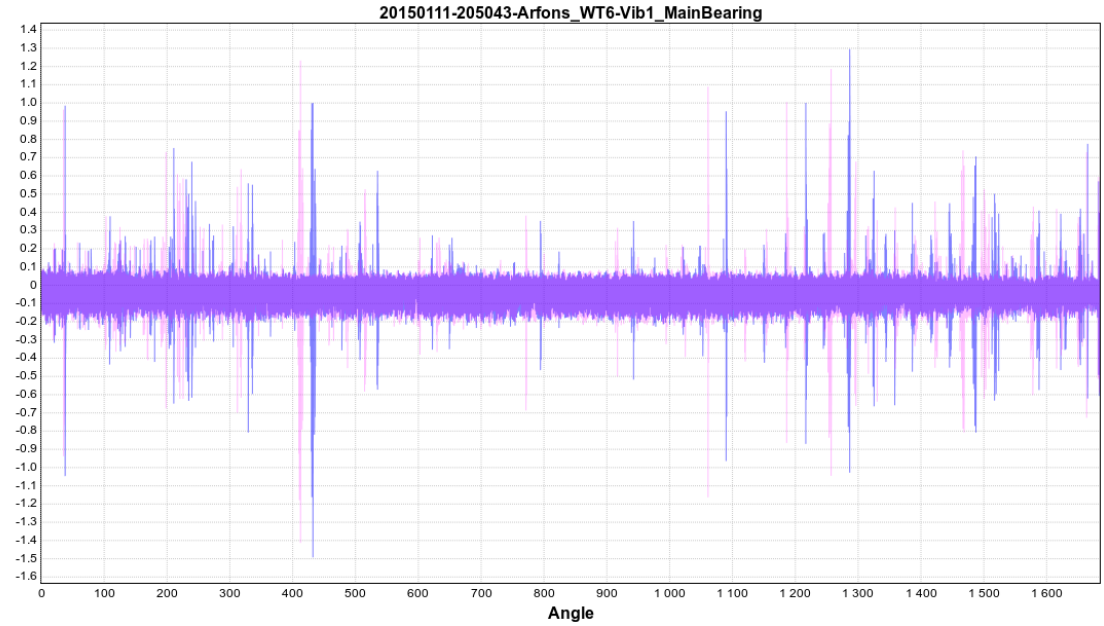

(a) Signaux temporels

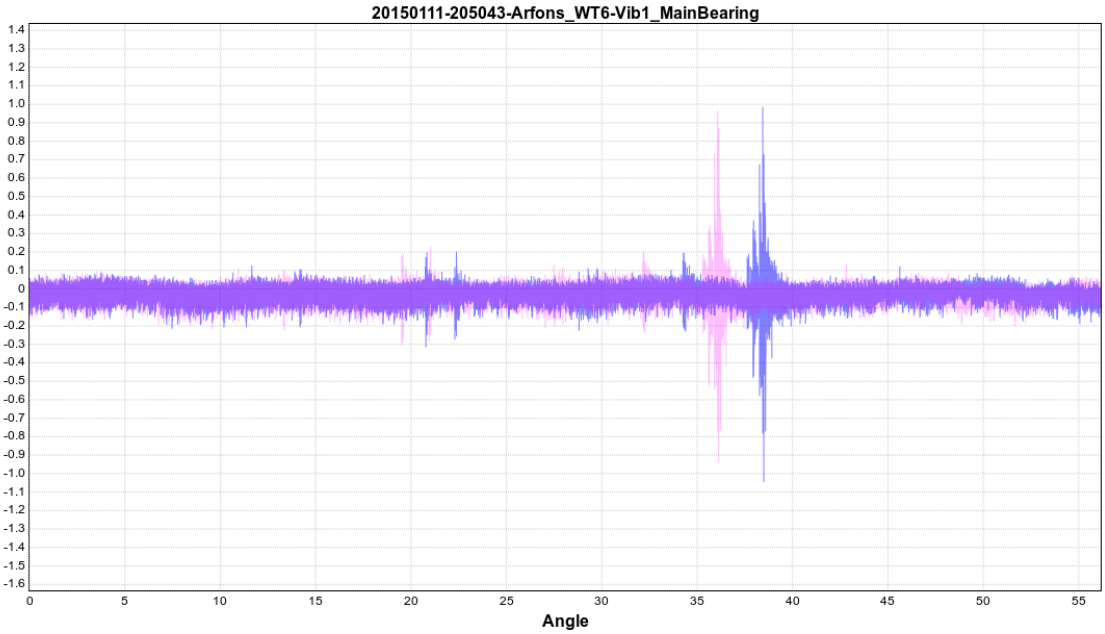

(b) Zoom des signaux dans la plage $0\ s - 2\ s$ correspondants à $0\ rev. - \sim 56\ rev.$

Figure B.5: Le signal vibratoire dans le domaine temporel (en rose) et dans le domaine angulaire (en bleu).

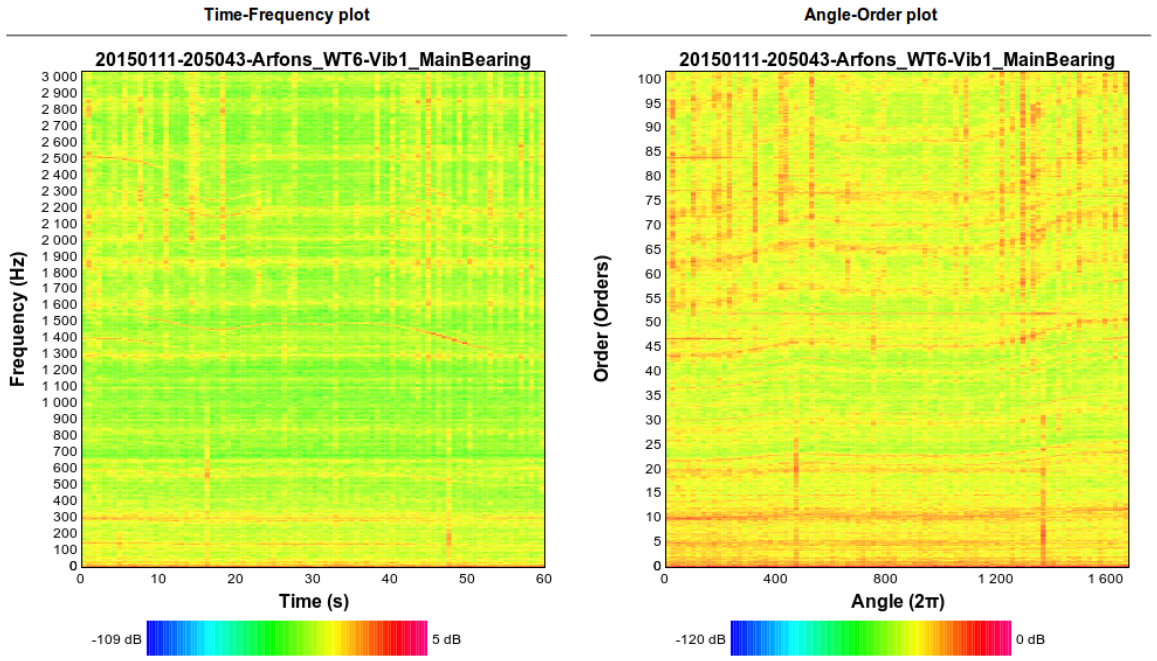

(a) Signal dans le domaine temporel (b) Signal dans le domaine angulaire

Figure B.6: Zooms (a) dans le domaine temporel et (b) la partie correspondante du signal dans le domaine angulaire.

sur la figure B.6 (a) commençant à environ 1600 Hz. Sur la figure B.6 (b) cette fréquence est une ligne horizontale égale à l'ordre 52.

Sur la figure B.4 les impulsions sont visibles sur le signal temporel. Ils correspondent à des non-stationnarités large bande détectées dans le signal et sont aussi visibles sur la figure B.7 (b) comme des lignes verticales rouges. L'origine de ces chocs reste inconnu. La fréquence de leur apparition ne correspond à aucun élément mécanique détaillé dans les tableaux B.4 et B.5. Ce phénomène est ignoré dans cet thèse.

La première étape consiste à obtenir des zones non-stationnaires du signal en appliquant AStrion-D, comme décrit dans la section 2.2.1. Dans cet exemple le spectrogramme obtenu a 90 segments temporels et 32769 segments fréquentiels. L'index de non-stationnarité calculé par AStrion-D est égal à 67%, ce résultat étant considéré comme un indice de non-stationnarité élevé, sachant que 0% correspond à un signal stationnaire. À partir de ce résultat, l'algorithme recherche une partie stationnaire du signal.

La zone la plus grande qui répond à la condition définie pour AStrion-C à T_S égal à 4% a été identifiée à l'itération 43. Cette zone est définie par 16 segments temporels sur 32769 segments fréquentiels. Ce résultat correspond à un signal de 10 s qui commence à la 28^{ieme} seconde. La figure B.7 affiche ce résultat grâce à une courbe pointillée sur le spectrogramme et sur le résultat de détection temps-fréquence. Cette partie du signal est traitée par AStrion-D encore une fois. La figure B.8 présente ce résultat sur la représentation temps-fréquence du

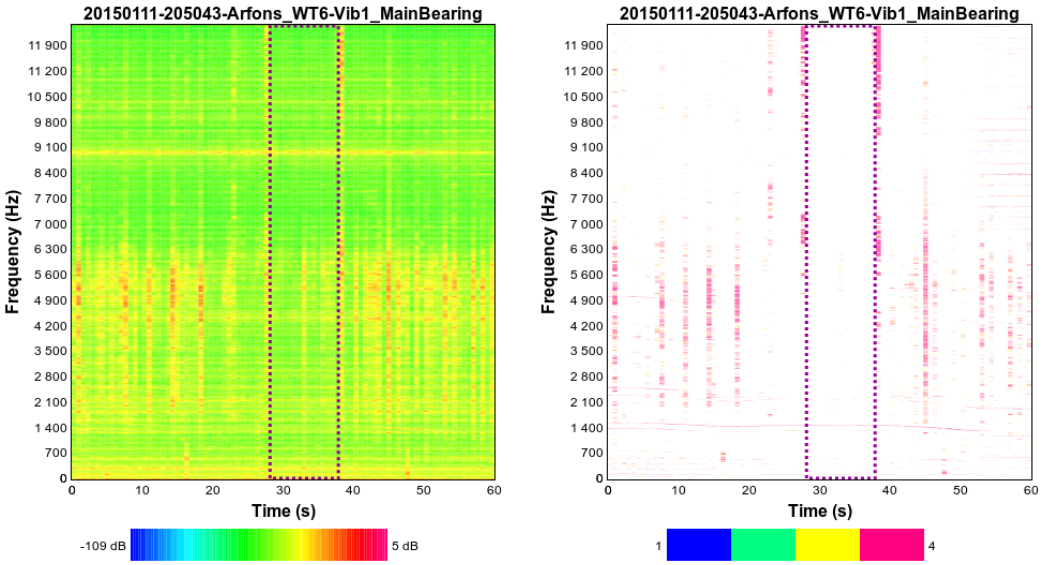

(a) Spectrogramme (b) Non-stationnarités

Figure B.7: Le signal de le domaine temporel traité par AStrion-D avec le résultat d'AStrion-C marqué avec des lignes pointillées, (a) le spectrogramme du signal analysé et (b) les non-stationnarités détectés sur la représentation temps-fréquence du signal. L'index de non-stationnarité pour le signal entier est égal à 67%.

signal. L'index de non-stationnarité calculé par AStrion-D est égal à 56%, valeur inférieur eau résultat obtenu pour le signal entier. Cette zone temps-fréquence est définie par 60 segments temporels et 8193 segments fréquentiels.

Maintenant, l'idée est de tester AStrion-C après un ré-échantillonnage angulaire effectué par le module AStrion-A. Ce signal est traité par AStrion-D pour détecter les non-stationnarités. La représentation angle-ordre de signal est calculé et contient 90 segments angulaires et 32769 segments en *ordre*. L'index de non-stationnarité calculé par AStrion-D est égal à 88%. Cet index de non-stationnarité est supérieur au résultat dans le domaine temporel du signal à cause des composants important aux *ordres* 160 et 300 environ. Le changement de ces composants spectraux est associé directement à un changement de vitesse de l'arbre à grande vitesse. Dans le domaine temporel ces composants spectrales sont visibles au niveau de 4500 Hz et 9000 Hz respectivement et peuvent être liés à la fréquence de variateur.

L'algorithme AStrion-C trouve la zone stationnaire de signal la plus grande à l'itération 44. La zone sélectionnée est définie par 10 segments en angle sur 22298 segments en ordre. La zone sélectionnée correspond à un signal de durée $168,45\ 2\pi$ qui commence à la 805^{ieme} $rev.$ du signal angulaire. Sur l'axe vertical le signal est limité à l'ordre $605,6$. La figure B.9 présente le résultat de l'algorithme pour le "rognage" marqué avec des lignes pointillées sur le spectogramme et sur les non-stationnarités détectés sur la représentation angle-ordre du signal entier. L'index de non-stationnarité calculé par AStrion-D pour la zone d'AStrion-C

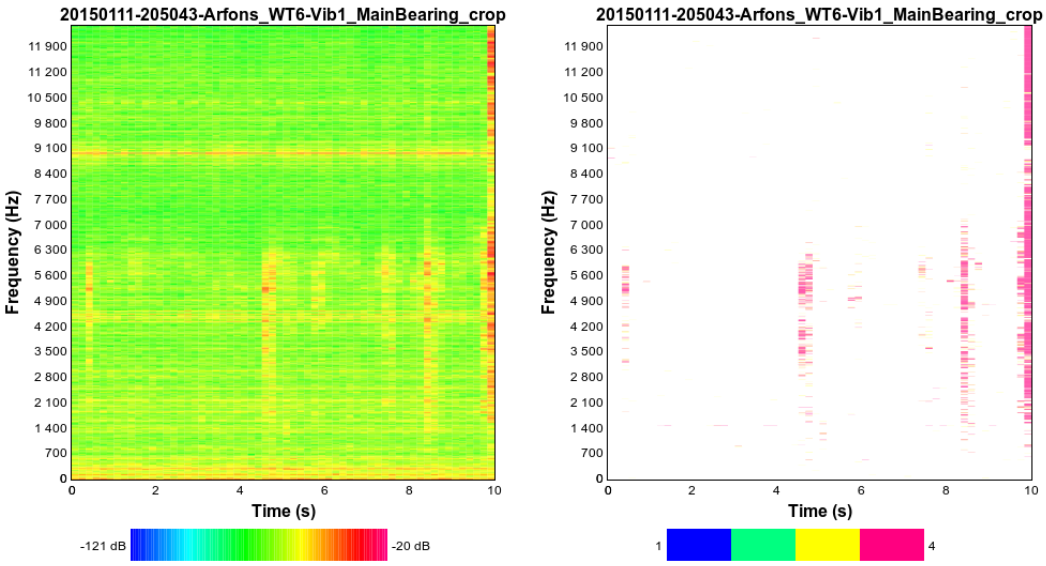

(a) Spectrogramme (b) Non-stationnarités

Figure B.8: La partie du signal de la domaine temporel recadrée d'après les résultats d'AStrion-C et traitée par AStrion-D qui a calculé un index de non-stationnarité pour cette zone égal à 56%, (a) spectrogramme du signal analysé et (b) les non-stationnarités détectés sur la représentation temps-fréquence.

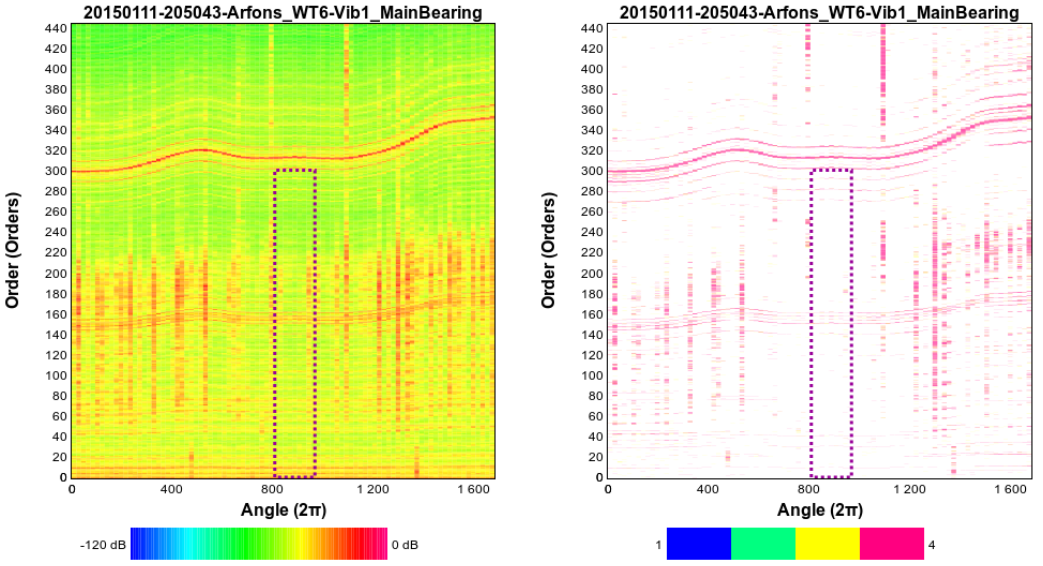

(a) Spectrogramme (b) Non-stationnarités

Figure B.9: Le signal dans le domaine angulaire traité par AStrion-D avec le résultat d'AStrion-C marqué avec des lignes pointillées, (a) le spectrogramme du signal analysé et (b) les non-stationnarités détectées sur la représentation angle-ordre du signal. L'index de non-stationnarité pour le signal entier est égal à 88%.

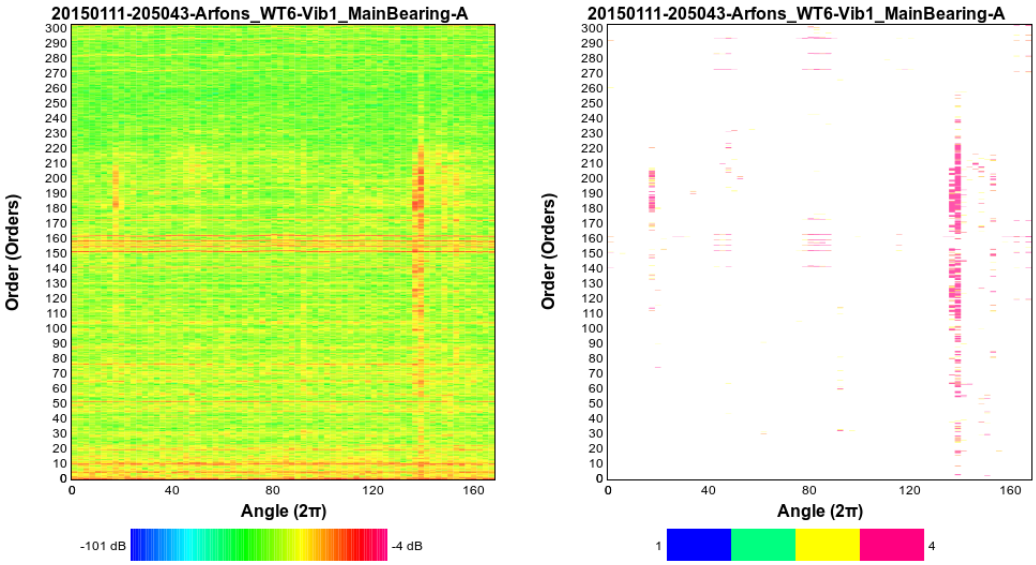

(a) Spectrogramme (b) Non-stationnarités

Figure B.10: La partie du signal de le domaine angulaire recadrée d'après les résultats d'AStrion-C et traitée par AStrion-D qui a calculé un index de non-stationnarité pour cette zone égal à 24%, (a) spectrogramme du signal analysé et (b) les non-stationnarités détectées sur la représentation angle-ordre.

est égal à 24%. C'est une diminution de non-stationnarité considérable par rapport au signal entier.

La figure B.10 présente la détection des non-stationnarités par AStrion-D sur le signal récadré d'après l'analyse par AStrion-C. Cette nouvelle représentation angle-ordre d'un signal contient 72 segments angulaires et 4097 segments en ordre.

Vu que le signal sélectionné est très non-stationnaire et difficile à interpréter du point de vue du diagnostic, cette section présente une bonne performance de la méthode proposée. AStrion-C a réussi à sélectionner des parties raisonnables des signaux dans le domaine temporel et angulaire.

B.3.3 Résultats d'AStrion-KM

La section ci-dessous présente une performance d'AStrion-K et AStrion-M, décrits dans les chapitres 4 et 5 respectivement, sur le signal réel d'une éolienne. Un signal individuel est sélectionné et décrit de façon très détaillée, par contre cette section ne montre aucune évolution des indicateurs de santé proposés.

Le signal décrit ci-dessous est mesuré sur l'éolienne marquée comme WT6 dans la section B.3.1. Le signal sélectionné est enregistré avec l'accéléromètre numéro 4 qui est situé sur

le boîtier d'engrenage. L'acquisition du signal a commencé à 11:00:07 h le 31 janvier 2015. Les paramètres du signal sont présentés dans le tableau B.6 où certains d'entre eux sont exprimés dans le domaine temporel et d'autres dans le domaine angulaire, le ré-échantillonnage angulaire étant fait à l'aide d'AStrion-A.

Table B.6: Les paramètres du signal analysé avant et après le ré-échantillonnage angulaire, et la vitesse moyenne de l'arbre à grande vitesse de l'éolienne marqué comme WT6.

Fréquence d'échantillonnage	25000 Hz
Duré du signal	20 s
Nombre d'échantillons	500000
Vitesse moyenne	1796, 15 RPM
Ordre d'échantillonnage	835 $Orders$
Nombre d'échantillons après le ré-échantillonnage angulaire	500000
Duré du signal après le ré-échantillonnage angulaire	599, 14 $rev.$

B.3.3.1 AStrion-K – association cinématique

Le traitement du signal est fait par AStrion et commence avec AStrion-A pour le ré-échantillonnage angulaire, continue avec AStrion-D pour la validation des données, et est suivi par AStrion-I pour l'identification des composants spectraux et finit avec AStrion-H pour la reconnaissance des structures spectrales. Les détails de cette partie se trouvent dans le chapitre 2.

Après l'application d'AStrion-ADIH, 1895 composants spectraux sont identifiés par AStrion-I, AStrion-H détecte 90 séries harmoniques et 260 bandes de modulation. Ces séries harmoniques et bandes de modulation sont utilisées pour l'association avec les fréquences caractéristiques détaillées dans les tableaux B.4 et B.5.

Certains exemples des résultats d'AStrion-K sont présentés dans le tableau B.7. Chaque exemple est séparé avec une double ligne horizontale et la série à sélectionner pour l'association finale est surlignée en bleu. Une double ligne verticale divise les données calculées par les étapes précédentes d'AStrion à gauche et les informations d'AStrion-K à droite. La colonne "Ordre théorétique (ordres)" contient les valeurs des fréquences caractéristiques de défaut après ré-échantillonnage angulaire.

Dans le premier exemple deux séries sont sélectionnées comme candidates possible pour l'association avec le composant de l'arbre à grande vitesse. La série finale pour l'association est choisie par la valeur de RFD (*ang. Relative Frequency Difference*) qui est la plus faible. Les détails se trouvent dans la section 4.2. Le deuxième exemple de l'association des séries harmoniques détectées par AStrion-H avec la fréquence caractéristique de défaut correspondant à la fréquence de passage des billes sur la bague intérieure (BPFI) est facile. Dans la première étape de l'algorithme une seule série est sélectionnée comme candidat potentiel pour l'association et donc dans la deuxième étape cette série est associée avec la fréquence de roulement. Dans le troisième exemple deux séries harmoniques sont identifiées comme des candidats potentiels pour l'association grâce à une valeur de RFD inférieure à 2%. A cause du

Table B.7: Résultat détaillé d'AStrion-K sur un signal enregistré le 31 janvier 2015 sur WT6. Les candidats sélectionnés pour l'association sont groupés entre deux double lignes horizontales et les séries finales à associer sont surlignées en bleu.

Type	Ordre (ordres)	Ordre de porteuse (ordres)	Ordre de modulation (ordres)	Nombre de pics	Énergie	Densité	Nom de composant sélectionné	Ordre théorétique (ordres)	RFD	BSI
Harmonique	0,999	—	—	13	$2,3^{-4}$	0,812	Arbre à grande vitesse	1	0,071	—
Harmonique	1,006	—	—	3	0	0,429	Arbre à grande vitesse	1	0,6	—
Harmonique	2,107	—	—	3	6^{-6}	0,6	NSK HR30334.BPFI	2,073	1,621	0,8
Harmonique	2,654	—	—	3	2^{-6}	0,5	NSK HR30326.BSF2	2,64	0,53	0,286
Harmonique	2,692	—	—	3	$2,8^{-5}$	0,27	NSK HR30326.BSF2	2,64	1,961	0,636
Modulation	—	5,384	0,234	7 | 7	0,0004 | <0,0001	0,778 | 0,636	Arbre intermédiaire	0,234	0,063	—
Harmonique	25,982	—	—	5	$0,18$	1	Engrenage17.GMF	26	0,068	—
Modulation	—	25,982	0,234	4 | 4	<0,0001 | <0,0001	0,8 | 0,4	Arbre intermédiaire	0,234	0,059	—
Modulation	—	25,982	0,999	3 | 5	<0,0001 | <0,0001	1 | 0,833	Arbre à grande vitesse	1	0,071	—
Modulation	—	25,982	2,575	5 | 3	<0,0001 | <0,0001	0,714 | 0,75	SKF NU238.BPFI	2,541	1,314	0,866
Modulation	—	25,982	8,994	2 | 2	<0,0001 | <0,0001	1 | 1	NSK HR30326.BPFI	8,85	1,626	1
Modulation	—	51,965	0,234	8 | 4	0,0002 | 0,0001	0,727 | 0,5	Arbre intermédiaire	0,234	0,069	—
Modulation	—	51,965	0,702	3 | 8	0,0001 | 0,0001	1 | 0,471	SKF NJ2988.BSF2	0,701	0,173	0,867
Modulation	—	51,965	0,999	20 | 5	0,0039 | 0,0033	0,833 | 1	Arbre à grande vitesse	1	0,075	—
Modulation	—	51,965	5,15	3 | 2	<0,0001 | <0,0001	0,6 | 1	SKF NU 2328.BSF2	5,100	0,973	0,9
Modulation	—	51,965	8,427	2 | 2	<0,0001 | <0,0001	0,667 | 0,667	SKF NU 2328.BPFI	8,320	1,282	0,834
Modulation	—	77,947	0,702	2 | 4	<0,0001 | <0,0001	1 | 0,667	SKF NJ2988.BSF2	0,701	0,158	0,917
Modulation	—	77,947	0,999	9 | 3	0,0013 | <0,0001	0,818 | 0,6	Arbre à grande vitesse	1	0,068	—

phénomène de glissement dans le roulement [RA11] cette plage est plus large que dans le cas d'autres composants mécaniques comme des arbres ou engrenages. Le phénomène de glissement est aussi la cause d'une condition différente pour l'association finale. Dans la deuxième étape de l'algorithme, l'association avec la fréquence NSK HR30326.BSF2 est effectuée grâce à un valeur de BSI (*ang. Bearing Selection Index*) la plus élevée, la série harmonique associée est surlignée.

Dans le signal analysé, la densité des séries proches aux ordres caractéristiques est faible. C'est la raison pour laquelle seulement deux exemples ont plus qu'une série sélectionnée comme candidats potentiels.

Les résultats présentés dans le tableau B.7 montrent deux groupes de bandes latérales. Le premier est associé à l'arbre intermédiaire. En plus, cette modulation est détectée au 2^{ieme} ordre de l'harmonique associé au double de la fréquence de vitesse de rotation des billes BSF pour le roulement du type NSK HR30326. Le deuxième groupe de bandes latérales est plus intéressant car il montre toutes les séries de modulation associées par AStrion-K à une même porteuse correspondant à la fréquence d'engrènement (GMF) du deuxième étage d'engrenages parallèles. Parmi les résultats il y a des bandes latérales qui correspondent à l'arbre à grande vitesse qui apparait autour de la fréquence fondamentale, de l'*ordre* 2 et 3 de la GMF. Il y a aussi une association avec l'arbre intermédiaire autour de la fréquence fondamentale et de l'*ordre* 2 de la même GMF. Le suivi de changement de ces modulations est crucial pour la diagnostic des défauts d'engrenage.

B.3.3.2 AStrion-M – démodulation de bande latérale

Cette section présente le résultat de la méthode de démodulation proposée dans le chapitre 5 sur une série individuelle de bande latérale mentionnée dans le tableau B.7. Pour cette raison la série associée avec l'arbre intermédiaire est sélectionnée. Cette série a un ordre de modulation égal à $f_\Phi = 0,234$ *ordres* et un ordre de porteuse égal à $f_0 = 51,965$ *ordres* qui correspond à la deuxième fréquence harmonique de l'engrenage (GMF). Les résultats présentés ci-dessous correspondent à la démodulation d'une série individuelle, mais AStrion-M est exécuté automatiquement sur toutes les bandes latérales détectées dans le signal.

Comme la méthode précédente, AStrion-M utilisent les résultats de modules antérieurs, soient les étapes AStrion-ADIHK. AStrion-K n'est pas obligatoire, mais dans ce cas il aide à la sélection d'une série potentiellement intéressante pour l'analyse.

La figure B.11 montre la représentation de spectre par AStrion. La série analysée a la bande latérale la plus haute sur le côté gauche K_{inf} égal à -11 et la bande latérale la plus haute sur le côté droit K_{sup} égal à 8 qui sont identifiée par AStrion-H. Avec ces informations l'algorithme calcule la bande passante $\mathbf{B} = [49,39\ ordres, 53,837\ ordres]$. Ainsi $\mathbf{B}$ est sélectionnée comme la bande passante du filtre à plusieurs cadences d'échantillonnage. Le signal après filtrage et décimation a un ordre d'échantillonnage égal à $23,181$. La figure B.12 présente le résultat du filtrage et la comparaison avec le signal avant cette opération.

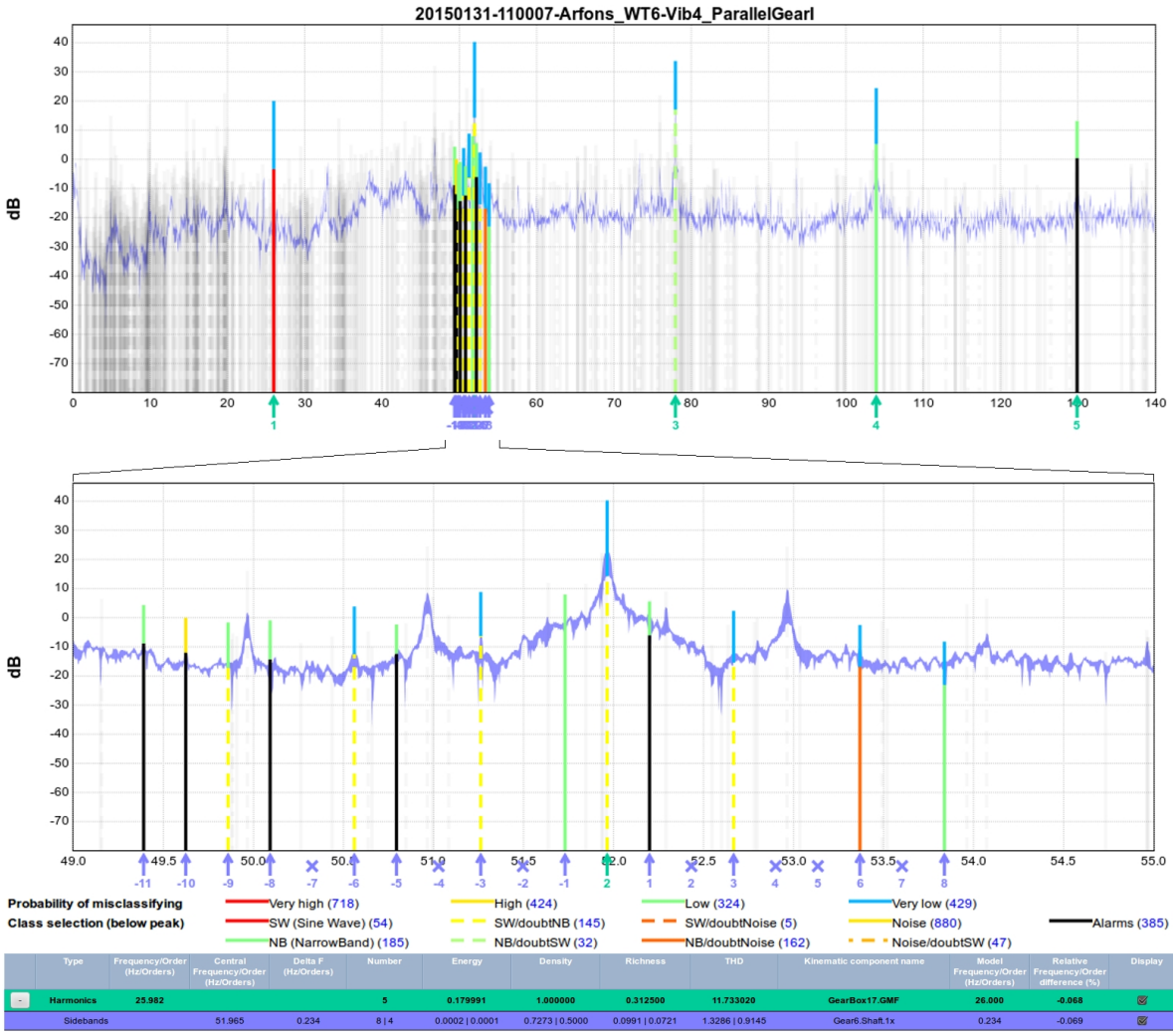

Figure B.11: Illustration du resultat d'AStrion-H sur une bande latérale sélectionnée. Représentation de spectre par AStrion qui montre la série harmonique entière en haut et un zoom en dessus.

Le signal filtré est ensuite traité. Tout d'abord la moyenne synchrone est calculée. Deuxièmement la démodulation est faite. Finalement les indicateurs de santé proposés dans le tableau B.2 sont calculés pour l'amplitude et la fréquence démodulés. Ces résultats sont présentés dans le tableau B.9.

Cette section montre qu'AStrion-M est capable d'analyser un signal réel mesuré sur l'éolienne WT6. L'algorithme proposé calcule automatiquement un analyse du signal, ce qui est un avantage pour un système de surveillance. Par conséquence AStrion-M fournit les indicateurs de santé de la machine et permet la comparaison avec les signaux mesurés par la suite.

Table B.8: Filtrage itératif du signal démodulé.

Itération	Première	Deuxième
Ordre d'échantillonnage initial (*ordre*)	$834,527$	$139,088$
Ordre de coupure du filtre passe-bas (*ordre*)	—	$4,447$
Ordre de coupure du filtre passe-haut (*ordre*)	$-49,39$	—
Décalage de fréquence (*ordre*)	$-49,39$	—
Taux de décimation	6	6
Oordre d'échantillonnage final (*ordre*)	$139,088$	$23,181$

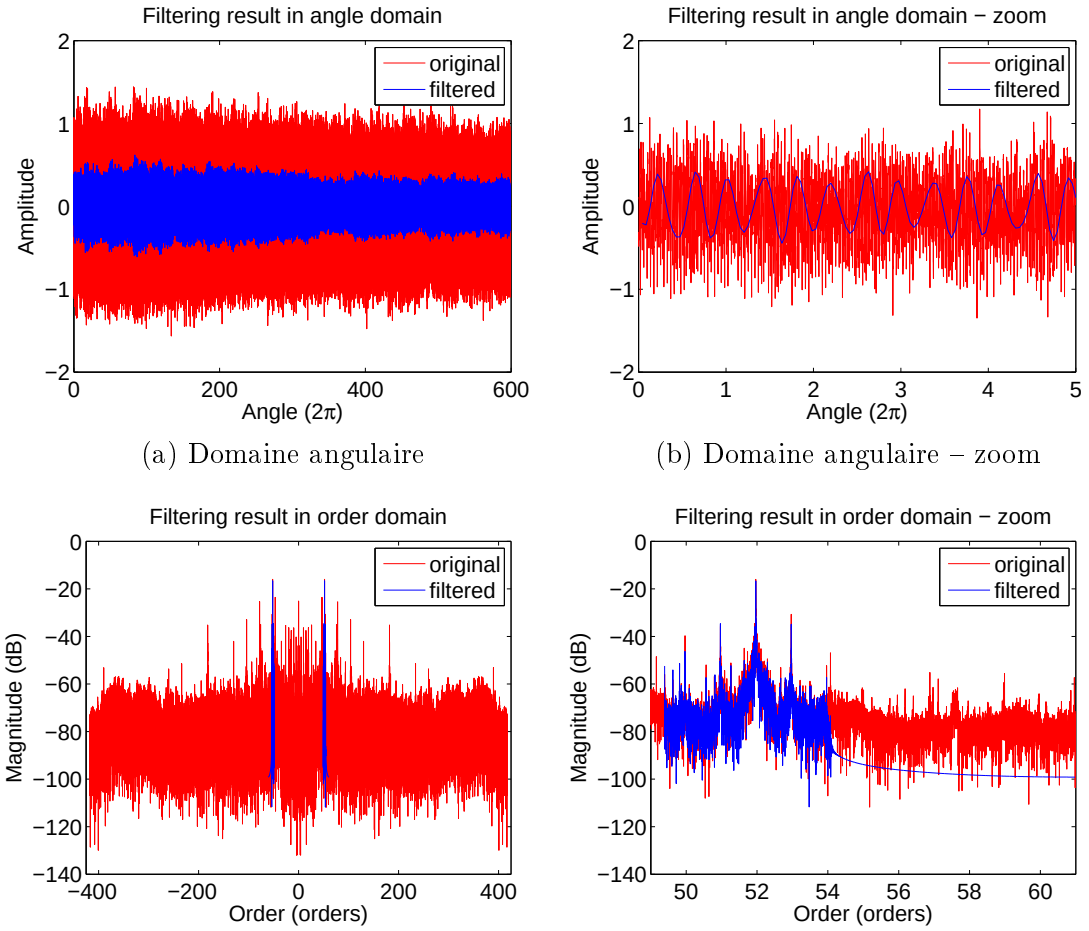

(a) Domaine angulaire

(b) Domaine angulaire – zoom

(c) Domaine d'ordre

(d) Domaine d'ordre – zoom

Figure B.12: Résultat du filtrage (bleu) comparé avec le signal original (rouge). (a) domaine angulaire du signal et le zoom (b), (c) domaine d'ordre du signal avec leur zoom de la plage de fréquence sélectionné (d)

Table B.9: Les indicateurs de santé calculés à partir de l'amplitude $\hat{A}[\tau]$ et de la fréquence $\hat{F}[\tau]$ démodulés du signal analysé. $\bar{A}$ – le valeur moyen, PP – crête-à-crête, $Kurt$ – kurtosis, MI l'indice de modulation, PN – le nombre de pics et E – l'énergie de série harmonique.

$\bar{A}$	PP_A	$Kurt_A$	MI_A	PN_A	E_A
$0,382$	$0,04$	$2,902$	$0,052$	3	$1,8^{-5}$
$\bar{F}$	PP_F	$Kurt_F$	MI_F	PN_F	E_F
$51,965$	$0,176$	$2,547$	$0,002$	3	$4,6^{-4}$

B.4 Conclusions et perspectives

L'industrie éolienne est très intéressée par les systèmes de surveillance. Il y a beaucoup de méthodes dédiées à l'éolien et beaucoup de développement ont été proposés récemment. Cette thèse propose une méthode du traitement de signal pour améliorer les capacités de système de surveillance guidés directement à partir des données. En plus, les méthodes proposées font partie d'AStrion qui est un analyseur de spectre automatique en développement à GIPSA-Lab.

Après l'identification des besoins dans l'état de l'art du système de surveillance des machines tournantes cette thèse propose trois algorithmes :

- "Rognage" de la représentation de temps-fréquence ;
- Association cinématique ;
- Démodulation de chacune des bandes de modulation.

Grâce au Projet d'Innovation KAStrion les méthodes proposées sont évaluées sur des signaux réels. Les signaux utilisés dans cette thèse sont issue d'un banc d'essai simulant le fonctionnement d'une éolienne construit au CETIM et des éoliennes situées à Arfons.

L'algorithme pour le "rognage" de la représentation de temps-fréquence s'appelle AStrion-C et il sert à sélectionner la plage stationnaire du signal vibratoire analysé. Conformément avec la méthodologie d'AStrion, c'est une méthode entièrement automatique. En plus, le "rognage" est possible sans l'utilisation de filtre mais avec une troncature et une manipulation interne du signal analysé par AStrion.

AStrion-K est le nom de la méthode proposée pour l'association automatique de fréquences caractéristiques de défaut avec des structures spectrales détectées précédemment. Parmi les plus grands avantages de cette méthode, il y a la possibilité de prendre en compte le glissement possible dans les roulements résultant d'une variation aléatoire des fréquences de défaut caractéristiques.

La dernière méthode proposée est la démodulation de chacune des bandes de modulation qui s'appelle AStrion-M. Ce traitement automatique du signal effectue une démodulation pleine bande avec un réglage automatique de plusieurs étapes basés sur les informations

obtenues à partir du signal lui-même. De cette manière toutes les bandes de modulation détectées auparavant sont démodulées et des indicateurs supplémentaires de santé de la machine surveillée sont fournis pour arriver à une description plus détaillée.

Cette thèse n'épuise pas les applications possibles des algorithmes proposés. Dans l'opinion de l'auteur ça serait intéressant d'appliquer d'AStrion-C pour la diagnostic sur les signaux avec la présence de chocs de courte durée comme dans le cas par example d'une presse plieuse hydraulique. En plus, il serait vraiment intéressant d'utiliser AStrion-M sur les signaux d'engrenage avec un défaut. Avec le support d'AStrion-K, cet algorithm pourrait être un outil puissant pour la diagnostic de la santé de la boîte de vitesse.

Résumé — Cette thèse propose trois méthodes de traitement du signal orientées vers la surveillance d'état et le diagnostic. Les techniques proposées sont surtout adaptées pour la surveillance d'état, effectuée à la base de vibrations, des machines tournantes qui fonctionnent dans des conditions d'opération non-stationnaires comme par exemple les éoliennes mais elles ne sont pas limitées à un tel usage. Toutes les méthodes proposées sont des algorithmes automatiques et gérés par les données. La première technique proposée permet de sélectionner la partie la plus stationnaire d'un signal en cadrant la représentation temps-fréquence d'un signal. La deuxième méthode est un algorithme pour l'association des dispositions spectrales, des séries harmoniques et des séries à bandes latérales avec des fréquences caractéristiques provennant du cinématique d'un système analysé. Cette méthode propose une approche unique dédiée à l'élément roulant du roulement qui permet de surmonter les difficultés causées par le phénomène de glissement. La troisième technique est un algorithme de démodulation de bande latérale entière. Elle fonctionne à la base d'un filtre multiple et propose des indicateurs de santé pour faciliter une évaluation d'état du système sous l'analyse. Dans cette thèse, les méthodes proposées sont validées sur les signaux simulés et réels. Les résultats présentés montrent une bonne performance de toutes les méthodes.
Mots clés : Traitement du signal, Surveillance d'état, Signaux de vibration, Signaux non stationnaires, Cinématique, Démodulation, Machines tournantes, Détection de défaillances

Abstract — This thesis proposes a three signal-processing methods oriented towards the condition monitoring and diagnosis. In particular the proposed techniques are suited for vibration-based condition monitoring of rotating machinery which works under highly non-stationary operational condition as wind turbines, but it is not limited to such a usage. All the proposed methods are automatic and data-driven algorithms. The first proposed technique enables a selection of the most stationary part of signal by cropping time-frequency representation of the signal. The second method is an algorithm for association of spectral patterns, harmonics and sidebands series, with characteristic frequencies arising from kinematic of a system under inspection. This method features in a unique approach dedicated for rolling-element bearing which enables to overcome difficulties caused by a slippage phenomenon. The third technique is an all-sideband demodulation algorithm. It features in a multi-rate filter and proposes health indicators to facilitate an evaluation of the condition of the investigated system. In this thesis the proposed methods are validated on both, simulated and real-world signals. The presented results show good performance of all the methods.
Keywords: Signal processing, Condition monitoring, Vibration signals, Non-stationary signals, Kinematics, Demodulation, Rotating machinery, Fault detection

GIPSA-lab, Grenoble Campus, BP 46 - 11 rue des Mathématiques
F-38402 Saint Martin d'Hères - FRANCE